Atomic Processes in Nova Shells

By

Derck Peter Smits

Submitted in partial fulfilment of the
requirements for the degree of
Doctor of Philosophy
in the
Department of Astronomy,
University of Cape Town
February, 1990.

To Ellen who, in spite of everything,
has seen this through to the end.

ACKNOWLEDGEMENTS

I would like to thank my supervisor, Prof. Brian Warner, for suggesting this subject and taking me on as a student. His insight into the problems has been a source of inspiration. Dr. R.E. Williams provided a lot of encouragement at the beginning of this project, and suggested calculating the recombination coefficients. Both B.W. and R.E.W made funds available for an observing trip to CTIO, Chile, for which I am extremely grateful. It was a most rewarding experience. I am grateful to Penny Dobbie for typing most of the references and sorting out many of the administrative hassles, and to the users of the Apollo for their cooperation in allowing me to consume many hours of computer time. Ellen has provided moral support through the years and has kept me overfed. The Foundation for Research Development of the Council for Scientific and Industrial Research is thanked for the financial assistance they provided in the form of a postgraduate student bursary.

I, **Derck Smits**, hereby declare that the work on which this thesis is based is original (except where acknowledgements indicate otherwise) and that neither the whole work nor any part of it has been, is being, or is to be submitted for another degree in this or any other University.

I empower the University to reproduce for the purpose of research either the whole or any portion of the contents in any manner whatsoever.

Signed by candidate

16 February 1990

(Date)

Abstract

The unusual spectra of the spatially-resolved nova shells of DQ Her, T Aur, and CP Pup, interpretted as being due to lines formed by recombination in low temperature ($T_e < 1000$ K) plasmas, are reviewed. Because calculations for these conditions have not been made, we have constructed recombination models of HI, HeI, and CNO from a neutral to a doubly ionized state. The models, which rely heavily on hydrogenic calculations and follow the method of Brocklehurst (1970, 1971), are described, and results presented for densities of 10^6, 10^4, and 10^2 cm^{-3} at temperatures of 2500, 1250, 625, and 312.5 K. The HI calculations supplement those of Martin (1988) and Brocklehurst (1971) by providing results for non-zero densities at low temperatures. The HeI results extend the calculations of Brocklehurst (1972) to low temperatures. The flux of forbidden CNO lines formed by recombination have also been determined. These data are then used to check the line identifications in the spectra of the three nova shells, and to determine the abundances in these gases. We confirm that the cool nova shells are metal-enriched and, in some cases, have helium excesses. The [NII] $\lambda\lambda$6584, 6550 and [OII] λ3727 lines do not appear to be due to recombination, which suggests that these lines are formed in a warm component of gas, and hence that temperature and density inhomogeneities exist within the shells.

A photoionization model, developed to investigate the behaviour of metal-enriched gases over a broad range of temperatures, is described. Our low temperature recombination rates have been included in the codes so that accurate calculations can be made at $T_e < 1000$ K. The process of K-shell photoionization by X-radiation is taken into account. CNO enrichment is shown to increase the radiative cooling rate in the gas so that low temperature, high ionization plasmas can be achieved. The effects of non-uniform density distributions in nova shells have been investigated and the observational consequences discussed.

A model of the CP Pup shell is described and the evolution of this plasma during the nova's constant luminosity phase traced. A theoretical continuum source produced by accretion onto a $1M_\odot$ white dwarf was used to ionize the gas. In our model the NIII 57 μm fine-structure transition produces the largest line flux and is responsible for most of the cooling in the gas.

The properties of neon novae are summarized and compared with the features seen in the optical spectra of old classical novae. Photoionization models of nova shells are used to trace how the ejecta from neon novae should evolve, and to predict what old neon nova shells should look like. Enhanced neon abundances are used in the model of the CP Pup shell to investigate its effect on the evolution of the shell.

Finally, the results of some near-infrared observations we made on the shells of CP Pup, RR Pic and T Pyx are reported. Unfortunately the surface brightness of these nebulae was too faint for any detections to be made.

Contents

List of Figures

List of Tables

Chapter 1

An Overview of Novae

1.1 Introduction

The occasional sudden appearance of new stars in the night sky had been noticed by astronomers even before the invention of the telescope. These "nova stella" or "guest stars" as they were then known are believed to belong to either the class of objects now called cataclysmic variables (CVs), sometimes also called eruptive binaries, or to the quite distinct category supernovae. The cataclysmic variable systems are seen to brighten temporarily, sometimes creating naked eye stars, before fading back to a quiescent state which is believed to be much like their pre-outburst state. Unlike CVs, supernovae are totally disrupted by their outburst and as such can be considered catastrophic variables. It is thought that some CV systems do end up becoming supernovae (type 1) if the mass of one of the stars is forced over the Chandrasekhar limit. We shall be examining the shell of material ejected by novae during outburst in more detail, but first we present a brief background on these systems and some of their properties so that we can get some perspective of our problem in the context of the nova phenomenon.

1.2 Classification

Cataclysmic variables can be further subdivided into the following four categories: classical novae, nova-like variables (UX UMa stars), recurrent novae and dwarf novae. This classification is based on the nature of the outburst, which shows great diversity in the range of magnitudes by which the star can brighten and the time scale between events. Note, however, that the inclination of the system with respect to the observer is responsible for some of the variation in range of magnitude (Warner 1986b). No classical nova has ever been observed (by definition) to erupt more than once, a situation thought to be due to their long quiescent period of $10^3 - 10^4$ years. The star brightens by between 8 and 15 magnitudes and is estimated to reach a maximum absolute magnitude of $-10 < M_v < -3.9$, depending on its speed class (Warner 1987). An extensive nebular shell, having a mass of $\approx 10^{-4} - 10^{-5}\ M_\odot$ and a radial velocity of $250 < v < 2500$ km/s, is ejected by the outburst. The nova-like variables are believed to be classical novae whose eruptions have not been recorded previously. Recurrent novae undergo outbursts on a timescale of 20 – 80 years, displaying smaller outburst amplitudes than classical nova. Their peak visual magnitudes are typically between 4 – 9 with absolute magnitudes between 0.8 and -0.8. As in the case of classical novae, a shell of material is ejected by the outburst. Similarities between classical novae and recurrent novae suggest that some of the latter class might just be the short-period

tail of the distribution of novae (e.g. T Pyx), but Webbink et al. (1987), who have defined some specific criteria to distinguish recurrent novae from other objects, regard them as distinct phenomena. Dwarf novae exhibit irregular, repetitive eruptions with outburst intervals of ten to thousands of days. Their outbursts last a few days to a few weeks. Optical amplitudes of between 1.5 – 8 magnitudes are observed, which translate to an optical luminosity of $\sim 10^{34}$ erg/s. No substantial mass loss due to the outburst has ever been observed in dwarf novae, but a stellar wind is always present.

1.3 Canonical Model

The basic model of CVs has evolved over the years following Walker's classic paper (Walker 1954) in which DQ Her was recognized to be an eclipsing binary system. It is now generally accepted that all CVs are semi-detached binary star systems consisting of a degenerate primary, a white dwarf, and a secondary that overflows its Roche lobe and accretes matter through the inner Lagrangian point into an accretion disc around the primary. If the orbital period of the system is less than about 2 hours it is difficult to observe the secondary, and therefore not much is known about these stars. However, when it has been detected, the secondary is normally a dwarf of lower mass than the primary and of spectral type G, K or M. These cool dwarfs appear to be hydrogen-burning main sequence stars. The matter accreted on to the primary from these stars is, therefore, hydrogen-rich. Conservation of angular momentum causes the infalling matter to form the disc around the primary. The disc, in turn, interacts with the infalling matter, producing a hot spot on the disc. In most cases almost all the observed visible light comes from the accretion disc. It is conceivable that a nova could be caused by accretion of matter directly onto an isolated degenerate star from the interstellar medium, but no conclusive evidence for such an event has yet been found.

There are other systems that are closely related to CVs: examples include symbiotic variables and some X-ray sources. The symbiotic variables consist of a red giant and a close, compact companion surrounded by an ionized gas. A substantial transfer of matter from the larger partner to the smaller leads to outbursts with mass ejection, but the characteristics of the outburst differ from those of novae. The X-ray sources Sco X1 and Cyg X2 are thought to be binary stars with a neutron star rather than a white dwarf as their primary. The intense gravitational fields of these degenerate stars is responsible for accelerating matter to energies in the X-ray region.

Variations on the basic model presented above produce a variety of systems each with their own idiosyncratic light curves. For example, the secondary could be a red giant as in the recurrent nova T CrB, or another white dwarf as in AM CVn. A subclass of nova-like variables is the AM Her stars, or polars, whose primaries have very strong magnetic fields ($B_{surface} \sim 10^7 G$).

The presence of this strong magnetic field causes the spin period of the white dwarf to be phase-locked to the orbital period. Furthermore, the accreting material is frozen onto the field and, guided by the lines of force, falls onto the magnetic poles of the primary emitting optical cyclotron radiation as it drops into the gravitational well. This highly polarized radiation, together with intense soft and hard X-ray emission, identifies these systems. Clearly no accretion disc can form so all the angular momentum of the infalling matter is transferred to the primary, thereby spinning it up much more efficiently than when an accretion disc is present. Another class of CVs, with DQ Her as their prototype, have weaker magnetic fields than the polars which allows a partial accretion disc to be formed. Inside a certain radius known as the Alfven radius, the magnetic field energy density is higher than the particle kinetic energy density so the plasma becomes frozen to the field lines. As in the polars, the material accretes onto the magnetic poles of the primary. These systems, however, do not have any hard X-ray emission or polarized radiation. They are also characterized by having a rapidly rotating white dwarf which has a very short period compared to the orbital period. Between the polars and the DQ Her systems are the intermediate polars, which have asynchronous, but very similar, orbital and spin periods. The rotational and optical modulation of intermediate polars is at least an order of magnitude larger than for the DQ Her systems, in addition to which they have observable hard X-ray fluxes. DQ Her systems might be the short period tail of the intermediate polars, but to date no systems with properties between these two extremes have been found.

Pre-outburst behaviour of classical novae is not well documented but it appears from the few cases for which observations are available that the preeruption and posteruption magnitudes are the same, and only a few systems (5 out of $\sim$ 20) show any changes in their light curves in the 1 – 15 years prior to their outburst (Robinson 1975). All novae show a rapid rise to maximum light (1 – 3 days) followed by a slower decline to pre-outburst magnitude. The timescale and behaviour of the decline, however, can vary significantly from one system to another. The overall timescale of a classical or recurrent nova outburst is often defined in terms of its "speed class" introduced by McLaughlin (1945) but modified by Cecilia Payne-Gaposchkin (1957). Her definitions depend on the time taken for the nova to fall by two magnitudes from maximum light, or, equivalently, the rate of decline during that time. There are 5 speed classes in this scheme ranging from very fast to very slow, and covering a time period of less than 10 days to 250 days. The speed class has been found to be related to absolute magnitude at maximum light — the fastest novae are the brightest. Novae in other galaxies can therefore be used as distance indicators.

1.4 The Outburst

The characteristics of dwarf nova and classical nova outbursts indicate a distinctly different mechanism in each case. Dwarf nova oubursts are best explained as being due to a variable accretion rate which leads to instabilities in the disc. These instabilities cause the whole disc to brighten temporarily, thereby creating the dwarf nova. The outburst mechanism in classical novae, on the other hand, is thought to be due to thermonuclear runaway (TNR) of the hydrogen-rich material accreted onto the surface of the degenerate primary. Most novae studied so far are believed to have a carbon-oxygen white dwarf, but recently a new class of novae, which occurs on O-Ne-Mg white dwarfs, has been identified (Starrfield & Sparks 1987). Although the physics is similar on both types of white dwarf, we shall discuss the outburst as it occurs on C-O primaries. The spatially-resolved nova shells which have been analysed thus far appear to have been ejected from this type of star, and their properties are therefore of more interest to us at this stage. However, in Chp. 10 we shall look in more detail at neon novae and the shells they give rise to.

As the layer of accreted material builds up, the pressure and temperature at the base of the envelope gradually rise until hydrogen fusion reactions (proton-proton chain) are initiated. This occurs when about $10^{-5} - 10^{-4} M_{\odot}$ (or $10^{28} - 10^{29}$ g) of matter has been accreted. As this material is partially degenerate it does not expand as the temperature rises, and therefore cannot cool. The thermonuclear energy generated causes a rise in temperature which increases the rate of energy generation, leading to the thermal runaway. The increasing temperature makes it possible for the CNO cycle to become operative, thereby adding further fuel to the TNR. Finally, when the temperature reaches about 10^8 K the electron degeneracy is lifted and the material starts to expand.

A convective region develops in the envelope, due to the energy generation at its base, which mixes the contents of the shell. The half-lives of the β^+-decay nuclei produced in the CNO cycle are very long compared to the dynamical time scales of the convective processes in the envelope, and are carried to the surface before decaying and releasing their energy. In the mean time, fresh, unburned CNO is brought into the hot shell source, thus keeping the nuclear reactions far from equilibrium. Under normal stellar conditions the β^+-unstable nuclei decay rates greatly exceed the proton capture rates of the other nuclei in the cycle and thus the abundance of these β^+-nuclei can be neglected. At temperatures of 10^8 K, however, the proton capture rates are comparable with (or larger than) the β^+-decay rates and, since the nuclei must decay before continuing the cycle, the rate of energy generation is limited by the decay rate. At the peak of the outburst most of the CNO nuclei in the envelope will be β^+-unstable nuclei. Calculations show that once peak temperature is reached and the envelope starts to expand, the enhanced

CNO nuclei release more than 10^{47} erg into the envelope, thereby aiding the ejection of the shell (Starrfield & Sparks 1987). The energy released during the runaway stage is insufficient to give rise to rapid mass ejection, but H burning on a longer time scale can lead to radiation pressure-driven mass loss.

The character of the outburst depends on the initial amounts of CNO nuclei present in the envelope. Theoretical simulations (cf. Starrfield & Sparks 1987 for references) demanded enhanced CNO abundances in the envelopes to produce fast novae, a prediction now amply supported by observations of novae during outburst and old nova shells (Tylenda 1978; Ferland & Shields 1978; Williams et al. 1978; Williams & Gallagher 1979; Gallagher et al. 1980; Williams 1982). A general conclusion seems to be that not only are nova shells enhanced in CNO, but there is also a correlation between the degree of enhancement and nova speed class — an increase in CNO abundances leads to an increase in speed class. There are some exceptions, however. DQ Her has large CNO over-abundances but was a slow nova, and the recurrent nova U Sco is another maverick. If the primary of DQ Her has an anomalously low mass ($< 0.5 M_{\odot}$) then a slow evolution can be expected even for high concentrations of CNO. Such an explanation for U Sco is confusing, though, particularly in the light of its recent (1987) outburst. Note also that another critical parameter determining the speed class of a nova outburst is the pressure at the base of the accreted envelope. The pressure is related to the accretion rate and the mass of the degenerate star accreting the matter. Sparks et al. (1978) found that all degrees of CNO enhancement could lead to nova outbursts provided the primary mass was large enough.

1.5 Shell Ejection

There are a number of processes that could eject mass from the primary. They are: 1) the rapid release of energy in the envelope produces shock ejection of material, 2) the gradual release of energy in the envelope produces pressure ejection, and 3) radiation pressure-driven mass loss. All three processes occur; however the first two are more important during the early stages of fast novae, while the third mechanism is more important in slow novae. A constant luminosity model has been proposed by Bath & Shaviv (1976) to explain the outbursts of slow novae such as HR Del, RR Tel and RT Ser. In these systems the outburst occurs over a time scale of years. The constant luminosity and continuous ejection can reproduce many of the features of slow novae and, in addition, some of the later stages of fast novae. The luminosity increases to the Eddington limit so that material on the surface of the primary is driven radially outwards by the radiation pressure. Modelling in which a variable opacity was incorporated (Sparks et al. 1978) found that the envelope obtains a quasi-equilibrium condition where expansion is just fast enough to keep the opacity at a value needed to absorb enough radiation

energy for the expansion. Enhanced CNO abundances in the shell increase its opacity and lead to faster ejection velocities. Starrfield et al. (1978) found that if envelopes of $\sim 10^{-4} M_{\odot}$ were used rather than $10^{-3} M_{\odot}$ in their models on a 1.00 $M_{\odot}$ white dwarf that shells having a mass of $\sim 10^{-5} - 5 \times 10^{-5} M_{\odot}$ were ejected. This is a larger fraction of the shell than for the bigger mass envelope, but for ejection to occur the initial composition must have high abundances of CNO relative to solar values. Fast novae models require an enrichment in carbon to produce the observed rapid light curve development and burst ejection of matter at high velocities.

The mechanism for the CNO enrichment in the envelope is not settled, but it seems that the secondary is too close to the main sequence to be supplying non-solar abundance matter to the primary. The mass of the white dwarf, the mass of the envelope and the CNO enhancement have all been found to have an influence on the nova outburst. Clearly nova shell analyses can provide useful information regarding properties of the outburst, such as the mass of the shell and its chemical composition, while the temperature and state of ionization of the nebula should reveal some characteristics of the UV radiation coming from the central stellar components.

Chapter 2

Nova Shells

2.1 Introduction

Classical novae outbursts cause the outer layer of material on the surface of the white dwarf to be ejected. The ejected material has a mass of $10^{-5} - 10^{-4}$ $M_{\odot}$ and a velocity of $250 < v[\mathrm{km/s}] < 2500$ (Cohen 1985). It forms an expanding shell of gas in the medium around the central star and can sometimes be spatially resolved a few years after the eruption. The rapid expansions and small masses involved cause the emissivity of the shells to decline rapidly with time, so that the extended envelopes can only be observed for time periods of 10 - 100 years. If a nova is too distant, by the time the shell becomes spatially resolvable the surface brightness has decreased to the extent that it cannot be detected against the sky background. Past interest in nova shells has mainly concerned their angular rates of expansion, which have been used together with expansion velocities to derive distances to the novae (e.g. Cohen 1985).

Nova shells provide a potentially useful source of information about the eruption since the ejected mass consists of material from the surface of the primary that has been processed by, and participated in, the outburst. Some contamination of the ejected gas may occur from material in the accretion disc or the interstellar medium which is swept up by the expanding envelope. A comparison of the composition of the pre-outburst accreted gas with that of the post-outburst ejecta should reveal something about the nature of the outburst. Of the known novae, relatively few have spatially resolvable shells, although many novae have been studied spectroscopically while still in the nebular stage. The problem with these observations is that if the shell is optically thick only the outer layers can be seen, while if it is optically thin the emission from the central stellar source is also present and it is not possible to determine which emission is from the shell and which from the star. Clearly, spectroscopy of spatially resolved nova shells provides the best method of determing their chemical composition, as well as other properties such as the density and hence the mass of the ejected envelope.

In this chapter we review the observations that have been made on nova shells and discuss their similarities and differences. We shall use the notation $F(\lambda)$ to denote the observed flux of a line with a wavelength λ in Å. In the last section we summarise the infrared (IR) observations that have been made on novae, which are particularly useful for revealing the presence of dust in the shells.

2.2 Observations

The structure of a few shells has been studied independently by Hutchings (1972), Weaver (1974) and Soderblom (1976) by means of analysis of high dispersion spectra with different slit orientations. This has made it possible to reconstruct the geometry of the shells. More recently, CCDs are being used to image the faint nebulosity by combining several frames, and abundance inhomogeneities can be mapped by combining pictures taken through narrow band interference filters (Duerbeck 1987b). It appears that a number of shells show a moderate degree of symmetry with gas concentrated in equatorial rings and polar condensations. There is some indication of different chemical composition in the two regions. The origin of the spherical asymmetry and chemical inhomogeneity is still unknown, although the presence of a stellar magnetic field might be responsible in some way.

A wealth of data exists on the nebular phase of novae during decline. Abundance analyses of the nebula can be made if its contribution to the spectrum can be identified, but unambiguous results are seldom obtained. The identification of emission lines in nova shells, however, is also problematic since the lines are intrinsically very broad. Conditions in novae show such extremes of variation that it is risky to anticipate the presence of specific lines, even though the spectra in the period of late decline are generally similar to those of gaseous nebulae.

We present a summary of the extended shells that have been analysed so far, together with details regarding the stellar components and the outburst. The year of the outburst and the time t_3 taken by the nova to decline by three magnitudes from maximum are included in parentheses after the name. The data, unless otherwise specified, come from Duerbeck (1987a).

DQ Her (1934, $t_3 = 94$ days) is a spectroscopic and eclipsing binary star with an orbital period $P_{orb} = 0.193621$ days at a distance of 310 pc (Cohen & Rosenthal 1983) to 420 pc (Ferland 1980a). The secondary is a K or M dwarf. Flickering in the visual light with a period of 71 s has been shown (by observing the phase changes of the flickering before and after eclipse (Warner et al. 1972; Patterson et al. 1978)) to come from the disc. A model that explains these observations has UV or X-ray radiation beamed from the accretion column(s) of the rapidly spinning magnetic primary being re-processed by the disc. No X-ray flux has been observed from DQ Her even though it has a dipole field strength of about 10^6 G. This may, however, be due to absorption of the radiation by the accretion disc, since the system has an inclination of nearly 90°. During outburst the light curve at maximum showed small variations in visual brightness, while a sudden dimming by 3 magnitudes during decline indicated pronounced dust formation in the shell.

Williams et al. (1978) obtained spectra from 4 regions of the shell, which has an ellipsoidal shape of angular size $15'' \times 20''$ in the light of Hα. The

salient features of the spectra are (a) heavy element permitted line strengths are much greater, relative to the Balmer lines, than normally seen in HII regions or planetary nebulae; (b) a broad emission feature peaking at λ3644 is attributed to the Balmer continuum formed in a cold gas ($T_e \leq 500$ K); (c) the presence of forbidden lines of NII and OII as well as allowed CII, NII and OII lines indicates a hot component of gas (recombination in a cold gas is excluded because of the absence of other ions of CNO); and (d) the spectra along the major axis differ from those on the minor axis. The Balmer, [OII] and [NII] lines are similar throughout the shell but CII, NII and OII lines found along the major axis are absent or weak along the minor axis. The Hβ flux was measured by Ferland et al. (1984) to be 6.2×10^{-14} erg/cm^2/s.

Abundance analyses were made using the shell spectra (Williams et al. 1978) and indicate that CNO is enhanced by 2 orders of magnitude above solar values. Ferland & Truran (1980) used data from the nebular phase to estimate the carbon and He composition of the shell, and compared it with the analysis by Williams et al. (1978). They found that the He abundance has decreased slightly while the carbon abundance has increased by a factor of more than 3. The earlier observations seem more secure, but even so give an unusually high carbon abundance that is twice that of the fast nova V1500 Cyg. UV observations of the shell were made by Ferland et al. (1984) using the *IUE* satellite. The only emission detected was that of CII λ1335. The ratio of the CII lines, F(1335) and F(4267), confirmed that the shell temperature is low and showed that most of the carbon in the shell is in the form of CIII.

T Aur (1891, $t_3 = 100$ days) has characteristics very similar to those of DQ Her. It displayed virtually identical outburst behaviour and was subsequently also found to be an eclipsing and spectroscopic binary, with an orbital period $P_{orb} = 0.204380$ days. Its minimum light properties are also very similar to DQ Her's, except that it does not show the periodic variability in visual light with a modulation period of 71 s that DQ Her has (Robinson & Nather 1977). The shell of T Aur is ring shaped and slightly ellipsoidal, but much fainter and hence more difficult to observe than that of DQ Her.

Only four lines, [OII] λ3727, Hβ, Hα and [NII] λ6584, were definitely identified from long slit photographic spectra, while reticon data revealed a feature at λ5876, probably due to HeI, and lines of NII at λ5680 and λ5005, as well as a possible OII λ4651 line (Gallagher et al. 1980). The T Aur and DQ Her shells are very similar spectroscopically: recombination lines dominate over forbidden line emissions, N and O appear overabundant by large factors and a low T_e, high ionization plasma seems to be responsible for the observed line spectrum. One difference, however, is that T Aur's shell appears to have an enhancement of He by a factor of 3, whereas DQ Her has He/H $\approx$ 0.14. The measured flux ratio F(Hα)/F(Hβ) was $\sim$ 7, which

is much larger than recombination theory predicts and suggests that T Aur suffers substantial extinction. This makes the interpretation of the spectrum more difficult.

CP Pup (1942, t_3 = 8 days), lying about 800 pc away, was a very fast nova reaching an absolute magnitude of $M_v \approx -9.4$, making it the brightest known nova. The pre-nova had $M_v > 7.4$ (Gaposchkin 1946) while the post-nova has remained at $M_v \approx 5$ for the last two decades (Warner 1985). The central stellar system has photometric and spectroscopic variations of the same frequency — the modulation period is 0.06143 days (O'Donoghue et al. 1989). If this is the orbital period, then CP Pup is the only known classical nova with an orbital period shorter than the period gap. An X-ray luminosity of $\approx 9.5 \times 10^{31}$ erg/s was reported by Becker & Marshall (1981). The outburst characteristics of the polar, V1500 Cyg, and CP Pup were similar and led Warner (1985) to suggested that CP Pup is an intermediate polar. Thus far, there is no compelling evidence to indicate the presence of a magnetic field in this system. Post-outburst spectra indicated gas ejection velocities of about 700 km/s for the shell, although there also appeared to be a transient ejection in the early phase of the outburst which had velocities up to 1500 km/s (see chapter 10 for a discussion of these points and the references). The spectrum was normal and the decline was smooth and fast without major disturbances.

The shell is nearly circular with the matter distributed in clumps around the rim. A stronger inner nebulosity has also been reported (Duerbeck 1987b). Williams (1982) has given a spectroscopic analysis of the shell. A broad line peaking at λ3640 has been identified as the Balmer continuum due to an electron temperature of $T_e \approx 800$ K, while the measured Hβ flux was 5.8×10^{-15} erg/cm^2/s. The presence of both allowed and forbidden lines of NII in the spectra are attributed to recombination since the gas temperature is too low for collisional excitation to be occurring. Lines from higher stages of ionization of nitrogen were also identified, in particular NIII λ4379 and λ4640 and NIV λ4606. The HeII λ4686 line is strong (F(4686) $\approx$ F(Hβ)) but HeI lines are only marginally detectable. The HeII, NIII, and NIV lines are characteristic of high excitation planetary nebulae, but in these objects OIII is usually present and increases the NIII emissions via resonance fluorescence. A line due to [OII] λ3727 was quite strong but was narrower than the other lines and therefore attributed to diffuse emission of [OII] from the interstellar medium. The nitrogen abundance must be very high to account for the line intensities, crude analysis indicating N/H $\approx$ 0.1 by number. Oxygen and carbon lines are not seen and these elements must therefore have abundances of less than 0.1 that of nitrogen.

Intense forbidden lines, which can only be formed at high temperatures, were reported in the spectrum after the outburst (Gratton 1953) so there has

been considerable cooling since then. The presence of high excitation lines in the spectra indicates a strong far-UV ionizing radiation field that would normally heat the gas. The observed low temperature of the shell must be due to an efficient cooling mechanism within the gas. Williams (1982) suggested that the current ionization could be either fossil ionization from the outburst or else possibly due to an X-ray flux which can ionize, but not effectively heat the shell (cf. Ferland & Truran 1981). However, neither model has been succesful in explaining the DQ Her shell (Ferland et al. 1984).

It is of interest to note that the outburst characteristics of V1500 Cyg (Nova Cyg 1975), also a very fast nova with an exceptionally large range, were very similar to those of CP Pup (Warner 1985). If the shells develop along similar lines then it may be possible to observe the time dependence of the shell parameters, in particular the electron temperature T_e. Reports of strong polarization in the visual output from this nova remnant point towards it being a polar (Stockman et al. 1988; Kaluzny & Chlebowski 1988), and considering its similarity to CP Pup, strengthens the case for the latter being an intermediate polar. However, O'Donoghue et al. (1989) found no evidence for a magnetic field, nor has any polarization been found in the optical light curve (Stockman et al. 1988; Kaluzny & Chlebowski 1988).

RR Pic (1925, $t_3 = 150$ days) is a spectroscopic binary with an orbital period $P_{orb} = 0.1450255$ days, displaying shallow or absent eclipses and lying at a distance of about 480 pc. The pre-nova was observed on several occasions, always at $m_v \approx 12.75$ (Robinson 1975) while in 1986 it was at $m_v \approx 12.3$ and dropping in brightness (Warner 1986a). Flickering has been observed in the system but it is not modulated by the orbital phase and it therefore appears to arise in the disc as a whole and not from a bright spot. The proposed model of Haefner & Metz (1982) explains the polarimetry, photometry and spectroscopy, but precise details of the system are still uncertain. Structural changes have taken place in the central binary system, resulting in a more isotropic distribution of the radiation. A substantial part of the decline in system brightness is attributable to this structural rearrangement (Warner 1986a). The most notable feature of its spectrum during decline was the prominence of numerous lines of iron in a number of different ionization stages. There is evidence to suggest that the progenitor of this nova could be an iron white dwarf (Shara 1989).

The ejecta now appears as a ring of material around the central star with two pairs of condensations at right angles to the ring which have higher velocities and are moving in opposite directions to each other. There are some filaments extending from the central nebulosity to the condensations. The strongest lines in the spectra of the condensations (Williams & Gallagher 1979) were due to Hα, [NII] λ6584, [OIII] $\lambda\lambda$5007, 4959, Hβ, and HeII λ4686. Five lines of [FeV] were identified and two lines of NeIII. Unfortunately no

flux calibrations have been reported. The filaments have spectra very similar to those of high excitation planetary nebulae. Satellite UV observations by Gallagher & Holm (1974) found the central star to be very hot ($T_* > 35000$ K), so that it seems likely that the shell is photoionized by UV radiation from this star. The spectrum of the central star is peculiar in that it seems to be H-deficient (Wykoff & Wehinger 1977).

T Pyx (1890, 1902, 1944, 1966, $t_3 = 88$ days), is a recurrent nova lying somewhere between 1 – 1.9 kpc away, which has undergone four observed outbursts. All maxima have exhibited fluctuations near peak brightness and the declines have been remarkably similar from one event to the next. T Pyx is the slowest of the recurrent novae, and the most regular. The slow rise of T Pyx to maximum is reminiscent of that of very slow novae such as HR Del and RR Pic. Absorption spectra following outbursts have shown ejection velocities of around 850 km/s, while some absorptions indicate velocities up to 2000 km/s. Catchpole (1969) has noted that its spectral development is different to that of classical novae.

The observed shell was originally thought to be that from the 1966 outburst (Williams 1982), although the 1944 outburst was not entirely ruled out. A more recent photograph of the shell, however, shows no significant expansion of the shell since Williams's 1980 observations so that Webbink et al. (1987) and Shara et al. (1988) conclude that the ejecta is from an event earlier than 1966. The spectra obtained by Williams (1982) were dominated by [OIII] $\lambda\lambda$5007, 4959 and [OII] λ3727 and [NII] λ6584 as well as the Balmer lines of HI. The [NII] line is even stronger than Hα. HeII λ4686 was present but rather weak, as was HeI λ5876 and [OIII] λ4363. The Hβ flux was 3.5×10^{-15} erg/cm^2/s. The shell spectrum is similar to that of a normal gaseous nebula and is presumably formed in the same manner as a planetary nebula: the shell is photoionized by the UV radiation from the stellar nova remnant. Abundance and temperature determinations are more difficult to do in this case, but if they are similar to planetary nebulae them we get roughly solar CNO abundances with moderate N/O enhancement and $T_e \sim$ 15000 K (Peimbert 1978). These characteristics are very similar to another recurrent nova, U Sco, which was analysed by Williams et al. (1981) during its nebular phase. This is in distinct contrast to classical nova shells which have all so far shown marked over-abundance of CNO and often also low electron temperatures. The apparent lack of CNO or He enhancements in the shell of T Pyx does not, however, exclude a nuclear runaway model for its outbursts. The dredge up and mixing processes that give classical novae their unusual abundances may be too slow to compete with the recurrence timescale.

2.3 Discussion

Five old, spatially resolvable nova shells have been studied spectroscopically thus far. One of the progenitors, T Pyx, is a recurrent nova while the other four are classical novae. All show some degree of enhancement (with respect to solar values) of at least one of He, C, N or O. The spectral development of the 1966 outburst of T Pyx was different to that of classical novae (Catchpole 1969), although its eruptions are believed to be caused by a mechanism similar to that of classical novae (Webbink et al. 1987). Both T Pyx and RR Pic have planetary nebula type spectra, with $T_e \sim 15000$ K, while the other three classical novae have low temperatures but a fairly high state of ionization. The characteristics of T Aur are somewhat speculative in that only four lines were definitely identified in the optical spectrum. The temperature of this plasma is inferred to be low ($T_e < 3000$ K) as no [OIII] λ4959 emission was seen but recombination lines of OII were present (Gallagher et al. 1980). Unfortunately, T Aur suffers from such large extinction and is so faint that any Balmer continuum signal it might have is undetectable.

The shells surrounding DQ Her and CP Pup show many similarities but also have some striking differences. The temperatures of both are unusually low and the spectra are believed to be produced by recombination. The densities are similar if we accept the estimated distances of 420 pc and 800 pc and the measured Hβ fluxes of 6.2×10^{-14} and 5.8×10^{-15} erg/cm^2/s respectively. Both show enhancements of heavy elements, but abundance inhomogeneities within the shells do exist (Duerbeck 1987b).

The nature of the outbursts were very different. DQ Her was a slow nova and is the protoype of nova systems with a rapidly spinning white dwarf. Typical of slow novae it underwent a phase of rapid grain formation during its decline. CP Pup, on the other hand, was a very fast nova which had a large range of magnitudes, and its orbital period of P $\sim$ 1.5 hrs is the only one of the classical novae to lie below the period gap.

The heavy element abundances are quite different. CP Pup had lines of NII, NIII, NIV and strong HeII, while the DQ Her shell had lines of CII, NII, OII and weak HeII along the major axis but only CII along the minor axis. The HI Balmer lines were visible in all spectra as was [OII] λ3727, although this emission was attributed to the ISM in the case of CP Pup. The lines λ4041, λ4239 and λ5005 of NII were seen along the major axis of DQ Her while only λ5005 and λ5678 were seen in the CP Pup spectra and yet nitrogen is supposedly enhanced quite drastically in the latter nebula. The ratio of the NII lines F(5005) to F(6584) was about 4:3 in DQ Her (Ferland et al. 1984) while 4:1 in CP Pup (Williams 1982). A hot component in the DQ Her plasma was proposed by Williams et al. (1978) to explain some of the forbidden lines. This could be the explanation for the different N spectra but the source of the hot component of gas has not been explained yet. The different spectra observed on the major and minor axes of the DQ Her shell

could be due partly to differences in the illuminating continuum.

Heavy element enhancements, oxygen in particular (Ferland et al. 1984), appear to be capable of producing the required cooling to create the low temperature plasmas found in nova shells. However, the observations are not completely consistent with this explanation. In the DQ Her shell, for example, the Balmer continuum feature indicated a uniformly low temperature of 500 K, but the heavy element enhancements differed along the major and minor axes. If fine-structure lines of OIII are responsible for maintaining the low temperatures, then we would expect to see recombination lines of OII throughout the nebula. Likewise, in the CP Pup shell we expect to see lines from oxygen ions, and yet only nitrogen lines were found. It may be that the optical emission from oxygen is too weak for it to be detected, but there is still sufficient OIII present to cool the nebula. The constraint these observations provide on the oxygen abundance has been used in a photoionization model of the shell and is described in Chp. 10. The possibility of observing oxygen lines in the IR or UV has also been investigated, as they provide a more sensitive indicator of the presence of this element.

2.4 Infrared Observations of Nova Shells

In this section we review the IR observations made from the ground and from satellites on novae in all stages of their evolution and discuss these results in the context of nova shells. The IR sky survey carried out by IRAS made observations in four bands between 12μm and 100μm. This latter region of the spectrum is particularly important in that blackbody emission with $T < 1000$ K peaks here, so the presence of cool dust can be detected. Not all IR radiation is due to the re-radiation of energy from heated dust grains though. There are fine-structure lines from heavy ions which can be significant sources of IR emission. A case in point is the 12.8μm line of NeII which was seen in nova Vul 1984 number 2 (Gehrz et al. 1985). It has been suggested that in old nova shells the far IR fine-structure lines are responsible for most of the radiative energy output of the shells, thereby maintaining them at low temperatures (Ferland et al. 1984).

The first IR observations of a nova were made by Geisel et al. (1970) who looked at FH Ser 1970 about three months after maximum. Their observations, made at wavelengths between 1μm and 22μm, showed an IR excess and coincided with a steep decline in the visual light curve. The IR emission had a spectral distribution very similar to that of a blackbody and for a while dominated the energy output of the nova. Over a period of sixty days the blackbody temperature dropped from ~1300 K to ~900 K. Since then many novae have been found to show thermal IR components characteristic of blackbody radiation at a temperature of ~1000 K which appear about sixty days after the visual maximum. The onset of the IR emission often occurs simultaneously with a sudden decline in the visual

light curve.

The IRAS survey is relatively insensitive compared to ground based observations at shorter wavelengths, but these data are the only IR results available to date in this spectral region. Schaefer (1986) looked at 260 binary systems containing compact objects, including many known CVs, but only 32 of these objects were found in the IRAS point source catalogue. Included in this list are two recurrent novae and five classical novae, one of which, RR Pic, was incorrectly identified (Dinerstein 1986), and two of which were in eruption. Sixty seven classical novae with well-determined positions were looked for in the IRAS point source catalogue by Dinerstein (1986), but only four correspondences were found. Seven novae were studied using IRAS data obtained as additional observations which went deeper than the general survey. This was achieved by longer integrations which improved the signal to noise ratio by between 4.4 and 7.7 (Callus et al. 1987). In total, two recurrent novae, T CrB and RS Oph, have been found to have IR excesses and so also have five classical novae: DQ Her 1934, HR Del 1967, FH Ser 1970, V4077 Sgr 1982 and GQ Mus 1983. Of these, V4077 Sgr 1982 was undergoing a phase of optical extinction about three months after its maximum. On the whole, novae and their shells do not seem to feature significantly at IR wavelengths.

The slow nova V4077 Sgr 1982 was observed by IRAS on day 368 after outburst and using JHKL photometery from SAAO 390 days after outburst during a deep ($\sim$ 2 magnitudes) minimum in its optical light curve (Callus et al. 1987). Both sets of data are consistent with the observed emission being due to a blackbody at 800 K. The only reasonable explanation seems to be that an optically thick dust shell formed, with the thermal emission being produced by the heated grains. The mass of dust in the ejecta has been estimated from the temperature and observed fluxes as $\sim 10^{-6} M_{\odot}$ (Dinerstein 1986). In all, three observations of V4077 were made by IRAS with the amplitude decreasing with time. It turned out to be one of the largest amplitude variable IR sources seen in the survey. From its amplitude variations Callus et al. (1987) have estimated a grain destruction time of $\sim$ 200 days.

No evidence of dust was found in the fast nova GQ Mus 1983 from near-IR observations (Whitelock et al. 1984; Krautter et al. 1984), but the nova was detected as an X-ray source about 1.3 years after outburst (Ögelman et al. 1984). If the X-rays came from shock heated circumstellar gas, then shock heated dust should also have been present. IR fluxes were determined for this model and compared with the IRAS data (Callus et al. 1987). While Band I of IRAS data agreed with the shock heated dust scenario, Band II did not and therefore the far IR emission cannot be caused by dust grains. The spectra obtained on the ground and from the satellite can be explained in terms of an optically thin gas in which the IR emission is caused by bound-

free and free-free processes in a gas with $T_e \sim 2.5 \times 10^4$ K. During its early stages this outburst had the characteristics of a fast nova. The behaviour of this nova was unusual, however, in that its later development was slower than for typical objects of this class (Whitelock et al. 1984).

The recurrent novae T CrB and RS Oph are unusual amongst CVs in that they have red giant secondaries, but their long wavelength spectra (i.e. in the region "seen" by IRAS) do not fall off as a Rayleigh-Jeans spectrum, even though single stars of similar spectral type do (Schaefer 1986). This could be due to mass ejection (possibly associated with their frequent outbursts) which forms dust with a wide range of temperatures and distances. Coadded IRAS data for T CrB were used by Dinerstein (1986) to find that the IR spectrum corresponds to a colour temperature of ~900 K. The presence of such hot dust at detectable levels is unlikely to be a remnant of the 1958 outburst, but rather indicates continuing dust-rich mass loss.

The well-studied old nova DQ Her 1934 showed up in the IRAS data from which a colour temperature of ~35 K was determined (Callus et al. 1987). This is close to the temperature of the IR cirrus with which it could be confused, but DQ Her's position is far enough above the galactic plane that it seems more plausible that the IR emission is intrinsic to the system. The visual minimum in 1935 had an optical depth $\tau \sim 9$ which would now, after expansion and cooling, be $\sim 5.8 \times 10^{-4}$ if it was due to dust. The measured optical depth at 60μm, if it is assumed that the IR emission is due to thermal radiation from dust, is ~ 0.08 (Callus et al. 1987), which would mean there was more dust in 1983 than needed for the minimum in 1935. This discrepancy can be resolved if (i) the extrapolation based on uniform outflow is unreasonable, (ii) the dust is not being heated by the remnant, or (iii) the emission detected by IRAS in bands III and IV is not due to dust.

Neither T Aur 1890 nor CK Vul 1670 were detected to low levels (Dinerstein 1986) and the identification of RR Pic as an IR source by Schaefer (1986) appears to be incorrect (Dinerstein 1986). Other novae specifically mentioned as being below detection threshold are V1370 Aql 1982, MU Ser 1983 and V1668 Cyg 1978 (Callus et al. 1987).

One of the slowest novae in recent years was HR Del 1967 which, surprisingly, showed no minimum in its optical light curve. Likewise, IR monitoring of the post-maximum phase of the nova did not show any evidence for dust formation. This is unusual behaviour for a slow nova and casts doubts on the dust creation model. However, observations obtained three years after outburst (Geisel et al. 1970) showed an IR excess with a colour temperature of $\sim$ 300 K. HR Del was only detected by IRAS in band II which led Dinerstein (1986) to rule out thermal emission by dust, suggesting instead that fine-structure lines of [SIII], [NeV], [OIV] or [SiII] might be responsible for the observed radiation. Callus et al. (1987) point out that several sulphides have strong features in the 20 – 30 μm window and that sulphide condensates

would not necessarily have blackbody emission characteristics. They suggest looking for spectral lines from these compounds.

McLaughlin (1935) was the first to suggest the formation of dust in novae ejecta after observing a sudden dimming in the light curve of nova DQ Her 1934. Grotrian (1937) found that a more satisfactory explanation of all transition-related phenomena lay in the abrupt cessation of mass loss and the consequent thinning out of the ejecta. The application of the dust model to the light curve and spectral changes at transition of novae of other speed classes met with difficulties (McLaughlin 1960), so the dust model fell from favour. However, the obvious candidate for the source of the IR emission in FH Ser was circumstellar dust, and Geisel et al. (1970) concluded that the dust was carbon in the form of graphite that had condensed out of the nova ejecta. As the material continued to move away from the centre of the eruption it cooled. Dusty shells were back in vogue. The rapid grain formation model has further support in that it explains the suppression of the red wings of emission lines relative to the blue which has been observed in many novae with pronounced light curve breaks (Bode & Evans 1983).

An alternative model for the IR excess is for pre-existing grains to be heated by the radiation from the outburst after a delay, in the same way that light echoes are formed. The grains would only effectively be heated well after the eruption if their absorption efficiency peaked in the far ultraviolet. Most of the properties of nova eruptions can be explained in terms of this model (Bode & Evans 1983). In the end it may turn out that both models have a domain of validity at various stages of the eruption.

The dust grains are assumed, by default, to be composed predominantly of graphite. The lack of any CO lines in the spectra implies that $C/O > 1$, while there is also not much evidence (e.g. no spectral emission lines) that the grains are silicates. The temperature of the dust in NQ Vul was higher than in other novae, which could suggest that something other than pure graphite was present. A feature at 5μm was proposed as being due to C_3 molecules (Ney & Hatfield 1978) that would have acted as nucleation centres for grain formation, but this feature disappeared as the IR emission rose. Fine-structure lines could be responsible for the band II emission seen in HR Del 1967, but Callus et al. (1987) point out that condensates need not have blackbody emission characteristics if, for example, sulphides are formed.

The mass and optical thickness of dust in novae ejecta varies widely. However, there is some correlation between the speed class of the nova and the presence of dust. It appears that the slower a nova is, the more dust it produces. An exception was the slow nova HR Del 1967 which showed no signs of any dust formation. Gallagher (1977) suggested that the ionization of the gas by the higher luminosities of faster novae inhibits the formation of condensation nuclei which are necessary to start the growth of grains.

As far as old nova shells are concerned, the IR observations have not been

very illuminating. If dust is formed in the ejecta during its decline and is the cause of the observed dip in the light curve of many slow novae, then the dust density will be so low by the time the shell is spatially resolvable that IR characteristics of the dust will be below the threshold of all existing detectors. If the dust is formed in the outer layers of the novae ejecta which are optically thick to the central stars then it is possible that the grains are destroyed when the shell becomes optically thin. Evidence for this occurring is provided by the IR observations of V4077 Sgr 1982. This mechanism could also be used to explain the differences in the carbon abundances found in the shell of DQ Her at different times (Ferland & Truran 1980). Higher resolution spectra with a lower detection threshold are needed to determine which fine-structure lines, if any, are present.

Chapter 3

Modelling of Nova Shells

3.1 Introduction

Abundance analyses and knowledge of the ionization states of nova shells are based on comparison of the observed fluxes of spectral lines with model calculations. Because nova shells have such unusual characteristics, exhaustive calculations are not available for their range of parameters and it has been necessary to extrapolate existing models into the regime believed to exist in the shells. We examine the assumptions that have been made in deriving the parameters of nova shells, and discuss the validity of these results.

As an example of the uncertainty in the methods employed we can quote the determinations of the carbon abundance in the DQ Her shell. Plates taken during the 1930s and 1940s were used by Ferland & Truran (1980) to estimate the nova shell's carbon composition during its nebular phase, and compared them with the abundance determined by Williams et al. (1978) from spectroscopic observations of the spatially resolved nova shell. The results indicated a time dependence in the nebular composition, which does not seem physically realistic. A heavy element stratification could possibly exist, but this is not understandable in terms of thermonuclear runaway models for the outburst. Ferland & Truran suggest instead that the carbon abundance has been over-estimated in the more recent observations.

3.2 Effective Recombination Rates

Abundance determinations are based on the relative intensities between observed spectral lines and some standard, usually Hβ, together with some knowledge of the effective recombination rate for the transitions involved. The effective recombination rate is a measure of the rate at which transitions occur to produce the line, expressed in terms of the ion and electron density, N_i and N_e respectively, i.e.

$$N_e N_i \alpha_{mn}^{eff} = N_m A_{mn}.$$

The spontaneous transition rate A_{mn} is determined from either laboratory measurements or theoretical calculations, while N_m must be determined using a model. The relationship between relative densities and relative fluxes is then given by

$$\frac{F_j}{F_{H\beta}} = \frac{N_{j+1}\,\alpha_j^{eff}\,\nu_j}{N_{HII}\,\alpha_{H\beta}^{eff}\,\nu_{H\beta}}$$

where F_j is the observed flux, ν_j, the frequency of the transition, is known from laboratory measurements and α_j^{eff} is calculated using an appropriate

model. This method determines abundances relative to $H\beta$, but if the distance to the object is known then absolute fluxes can be determined, and hence also the absolute densities. Note that even if individual lines are fairly temperature dependent, it appears that ratios of effective recombination coefficients have a relatively weak temperature dependence, something like $T^{0.1} - T^{0.2}$.

Clearly, it is necessary to determine α_{nl}^{eff} for all atoms or ions of interest. The simplest models, involving only radiative processes, are called capture-cascade models, while the more realistic models include collisional processes as well and will henceforth be referred to as capture-collision-cascade, or C^3, models. Stimulated emission and most absorption processes are not important in the densities found in nebulae and so are not included. Lyman reabsorption has the highest probability of occurring and can be crudely treated in an approximation, originally introduced by Baker & Menzel (1938), as being optically thick. All transitions to the groundstate are ignored since the photons emitted by Lyman transitions are assumed to be immediately reabsorbed (on-the-spot approximation). This is referred to as case B, the optically thin situation being case A. If the Balmer lines as well as the Lyman lines are taken to be optically thick, the models are referred to as case C.

The first capture-cascade model for HI (Seaton 1959b) treated the radiative processes in terms of the atom's principal quantum numbers only. This treatment is called the n-method, and is appropriate when the orbitals are all populated according to their statistical weights. The alternate situation, in which each l-shell has to be considered separately, is called the nl-method and was solved for HI by Pengelly (1964) using a capture-cascade model. This model is applicable under conditions of very low density and/or temperature when collisional processes between sublevels are unimportant. Note that as the radiative terms are proportional to (T/Z^2), where Z is the ionic charge and T the electron temperature, the results of capture-cascade models can be scaled to apply to any hydrogenic ion at the appropriate temperature, without having to redo the calculations.

Low temperature calculations for HI were made by Ferland (1980b) using digitized values of the bound-free Gaunt factors from the graphs presented by Karzas & Latter (1961). His recombination rates are accurate to $\sim 1\%$ compared to the exact calculations, but he only treats levels up to n = 13. A capture-cascade nl-model has been used by Martin (1988) to calculate α_{nl}^{eff} for hydrogenic atoms over a range of temperatures from 78.13 K to 20000 K. His model treats levels up to n = 60 and represents a vast improvement over Pengelly's treatment which terminated at n = 20. Both case A and case B results are presented.

For hydrogen atoms and both the singlet and triplet states of neutral helium the definitive effective recombination rates have been from the work of Brocklehurst (1970, 1971, 1972). He used a capture-collision-cascade model

to calculate the population levels up to $n = 300$ in the atoms. The hydrogen calculations tabulated by Brocklehurst (1971) are all for case B, although case A results are available in the library of the Royal Astronomical Society. The gas is assumed to be pure hydrogen, with any abundance changes being catered for in a variation of N_e. The lowest temperature for which tabulated values are available is 5000 K. The helium computations (Brocklehurst 1972) treat triplets in case B and the singlets as either case A or case B. Helium triplet lines must be calculated under case B conditions since there are no allowed transitions to the groundstate, but the singlet lines can be either case A or case B depending on the density of helium. Electron, proton and He impacts are included in the helium model which uses $N(He^+) = 0.1\ N_e$ and $N_e = N(H^+) + N(He^+)$. The largest uncertainties in these models lie in the collision reaction cross sections and in the neglect of collisions with $|\Delta n| = |n' - n| > 1$. The metastable levels of HeI can lead to radiative transfer effects in lines produced by transitions which cascade into these levels. Any effects of dust have also been completely ignored.

Recently Hummer & Storey (1987) have revived Brocklehurst's programs and used them to calculate relative intensities of HI and HeII recombination lines in case B over a considerably larger range of temperature, density and principal quantum number than before. They made improvements to some of the collision rates but the overall effect produced changes of less than 5% in the relative line strengths with respect to Brocklehurst's values. However, at the higher temperatures and densities that they consider, these rates are much more important. Effective recombination rates for the hydrogenic atoms CVI, NVII and OVIII have also been calculated (Storey & Hummer 1988).

C^3 models for calculating the effective recombination rates of transitions in complex atoms (other than He) have not been attempted. Hydrogenic approximations are usually used together with suitable weighting functions for the excited states, while empirical data are usually available for levels in the groundstate configuration. For levels of complex atoms above the groundstate Grandi (1976) used the recombination rates for hydrogen tabulated in Osterbrock (1974) for each principal quantum number, which he then divided up among the terms with the same n according to their statistical weights. He introduced an arbitrary factor of 1/2 to account for recombinations to higher levels that cascaded to lower levels bypassing the line under consideration. Applying this method to the Orion nebula, it was found that certain lines over-estimated and others under-estimated the elemental abundances in the gas.

3.3 Total Recombination Rates

Total recombination rates are required for the study of the ionization structure of a nebula and the thermal balance within a plasma. The state of ion-

ization of the various components of a plasma can be determined from the intensity of the lines of the components and a knowledge of their effective recombination rates, which we defined above in terms of the ionic density. In complex atoms recombination rates are determined by two processes, namely radiative and dielectronic recombination, the total rate being a sum of these two quantities. Aldrovandi & Pequignot (1973) treated the radiative term by using empirical rates for the ground state and taking excited states to be hydrogenic. They then fitted a formula of the form

$$\alpha_{rad} = A_{rad} \left(\frac{T_e}{10^4} \right)^{-\eta}$$

to their values, and tabulated A_{rad} and η. They claim an agreement to $\sim 10\%$ over a range $T_{max} \geq T_e \geq T_{max}/10$ where T_{max} has also been tabulated and is around 10^5 K.

For dielectronic recombination rates a four-term parametric fit to data based on the Burgess (1965b) formula was adopted by Aldrovandi & Pequignot (1973). The process described by Burgess involves excitation to optically allowed states and is only operative at high temperatures (T $\sim 10^6$ K) in CNO ions. At lower temperatures a process in which excitation occurs via optically forbidden transitions becomes important in these ions. At sufficiently low temperatures, typically < 1000 K, even this process becomes insignificant. The authors claim an overall accuracy for their total recombination rate (which is a sum of the radiative and dielectronic rate) of at least 15% over the specified temperature range, but since they have not included the optically forbidden dielectronic process, these rates must be a lower limit.

The calculation of the radiative recombination rates of complex atoms was improved by Gould (1978) who pointed out that the nonhydrogenic character of the excited states cannot be neglected. Captures to levels other than the groundstate are evaluated using hydrogenic formulae but with a correction factor for their nonhydrogenic nature. The correction factor is due to incomplete shielding of the nuclear charge by the inner electrons and represents an effective charge for the recombining ion which can be determined semi-empirically. Suitable weighting factors according to the level structure are also included in the prescription. In some cases recombination rates were altered by as much as 50% from their hydrogenic value. Although the recombination rate for individual levels might be incorrect, the total rate is believed to be fairly accurate as over- and under-estimates for the separate levels tend to cancel when added together (Gould 1978).

3.4 Heavy Element Abundance Determinations

Abundance determinations in the spatially resolved shell around DQ Her were initially made by Williams et al. (1978), who also determined the temperature of the gas as ~ 500 K from the width of a broad emission line which

they identified as the Balmer continuum. The abundances of CNO are based on the observed fluxes of CII λ4267, NII λ4239 and OII λ4651 with respect to Hβ. It was assumed that the heavy element lines are formed in the same region of the gas as the Balmer lines. Effective recombination rates for the heavy ions are based on Grandi's (1976) method but have been scaled according to the observations he made on the Orion nebula, and as such are semi-empirical values.

Ferland et al. (1984) made observations of DQ Her in UV using the IUE satellite, but only detected the CII λ1335 line in emission. This line originated in the shell, so they used the ratio F(1335)/F(4267) of CII lines to estimate the temperature of the shell. They assumed that both lines are formed purely by recombination (i.e. no cascade contributions were included), λ4267 by radiative recombination only while λ1335 has a contribution from dielectronic recombination as well. Hydrogenic values were used throughout, giving a temperature for the shell of $\sim$ 700 K, which is higher than the value of $\sim$ 500 K determined by Williams et al. (1978). The lack of detection of λ1656 and λ1909 allowed them to set limits on the ratio of C^{+2}/C^{+3}. Both these lines were assumed to be formed by radiative recombination alone and showed that most of the carbon is in the form of C^{+2}.

The CP Pup shell was found to contain both permitted and forbidden lines of NII (Williams 1982). Forbidden lines can be formed in a pure recombination spectrum, as Williams points out, and he believes that this is how [NII] λ6584 is produced. The nitrogen abundance was estimated from permitted lines using the procedure outlined by Grandi (1976), and from [NII] using the Aldrovandi & Pequignot (1973) recombination coefficients with the assumption that 1/3 of all recombinations gave rise to a λ6584 photon. This gave a high nitrogen abundance: N/H $>$ 0.1 by number. Assuming that all lines are formed by recombination and that case A prevails, the abundance of He relative to H was determined using extrapolated effective recombination coefficients from Brocklehurst (1972) and Pengelly (1964) for HeI and HI respectively.

Of the nova shells studied, that surrounding T Aur is the faintest and has the fewest features and is, therefore, also the most difficult to interpret. The presence of the OII λ4651 recombination line strengthened the case for a cool plasma while the absence of [OIII] λ5007 was used to set an upper limit on T_e of $\sim$ 3000 K. The abundances of N^{+2} and O^{+2} were estimated by using Gould's (1978) total recombination rates and assuming that all recombinations lead to the production of photons of the observed line. Brocklehurst's (1971, 1972) calculations were used to determine that He is overabundant by a factor of 2 to 3. These abundances were determined using very small line intensities, though, so large errors could easily have been introduced into the determinations.

The spectrum of the T Pyx shell resembles that of a moderate excitation

planetary nebula and is most likely formed in the same way: the shell is photoionized by UV radiation from the nova remnant (Williams 1982). Only forbidden lines from the heavy elements were found, and these are presumed to be formed by collisional excitation. The intensities of [OIII] λ5007 and λ4363 gave a value of $T_e \approx 29000$ K using standard nebular theory (Osterbrock 1974), although the weakness of λ4363 leads to large uncertainties in this result. The He/H ratio was determined using the same method as outlined for CP Pup but adjusted for higher temperatures, and yielded a value of ~ 0.06. This means that He is deficient with respect to solar values. Not enough lines of CNO were observed to enable reliable abundance determinations to be made. However, if it is assumed that this nebula is similar to that of a planetary nebula, then CNO have roughly solar abundances.

The shell of RR Pic was modelled using a number of ionization models at various temperatures and luminosities under the assumption that the gas is photoionized by Planckian radiation and has solar abundances (Williams & Gallagher 1979). Parameters which produced the best fit to the observed data were found, and indicated the need for nonsolar abundances in certain elements. In particular, the observed λ4686/Hβ flux ratio required N(He)/N(H) ≈ 0.2 in the model. Both N and Ne needed to be enhanced to match observations, the N calculations showing the largest discrepancy with respect to the observations. Another model was constructed using the modified abundances indicated by their first attempts, which, due to increased cooling, led to a lower electron temperature than found in the first model. The computed line fluxes of this model showed general agreement with the observed spectra. However, this model is not necessarily unique, particularly since abundances can be adjusted to fit the observations exactly if only one line for an element is observed.

3.5 Models for Nova Shells

It was suggested by Mustel & Boyarchuk (1970) that a nova shell's expansion rate could be faster than its recombination rate so that the state of ionization becomes frozen-in to the plasma. To test this hypothesis, Williams et al. (1978) constructed a time dependent ionization model to see whether it was possible for CNO to remain doubly ionized in the time that H became essentially neutral. This would explain why recombination lines of CII, NII and OII were seen in the nova shell's spectra, even though it had such a low temperature that, under normal circumstances, it would have totally recombined. Furthermore, if most of the hydrogen was neutral it would not show up in the spectra and the CNO abundances derived from the intensity of the recombination lines would be more nearly solar. It is perhaps worth noting at this stage that Williams et al. were somewhat sceptical of the CNO excess they had found in the nova shell from their initial analysis, and were looking for ways to interpret their observations in terms of more conventional

abundances.

In their model they used the $\alpha_i(T_e)$ of Aldrovandi & Pequignot (1973), and neglected charge exchange reactions on the grounds that these are important primarily only for the lower ionization stages of CNO. The initial conditions for their model were that all elements were completely ionized, and they then traced the evolution of the model from temperatures of 10^4 K down to 10^2 K. The results showed that, regardless of the parameters used, the CNO always recombined from their highest ionization state to C^{+2}, N^{+2} and O^{+2} before hydrogen had been substantially reduced in ionization. These models are hence incapable of explaining the observations.

Frozen-in ionization models can also be discarded on the grounds that the thermal energy of the nebula would take less than three years to be radiated away (Ferland et al. 1984). The only way for the shell still to have a temperature of 500 K after several decades is that a heating source exist. Furthermore, the nova shell of DQ Her has emitted HeII λ4868 radiation for virtually its entire history (see summary in Ferland & Truran 1981) and yet the recombination time scale for the He^{+2} ion is among the shortest of the observed components. This also points to there being an ionizing source of radiation present.

An X-ray model for the nebula surrounding DQ Her was proposed (Ferland & Truran 1981), but has been rejected in light of further observations. The proposed X-ray emission was supposed to arise from radial accretion onto the poles of a magnetic white dwarf, but *Einstein* observations have established that DQ Her is not a detectable X-ray source (Cordova et al. 1981). It can be argued that, because we are viewing the system from near the orbital plane, the X-ray source is significantly obscured by interactions with the disc. The UV carbon spectrum (Ferland et al. 1984) indicates that the gas is fairly highly ionized, having $N(C^{+2})/N(C^{+}) > 1.5$, but the X-ray model relied on Auger production of C^{+2} from neutral C, requiring that the gas be quite neutral. Detailed agreement with all line strengths was not obtained. In particular, CII and NII should be weaker and HeI λ4771 stronger than observed, while no OII recombination lines should be seen due to rapid neutralization of the oxygen ions by charge exchange with HI. No [NII] lines were predicted in the model unless the temperature was increased, but then [OI] λ6300 should be found, which it is not. Finally, it has become apparent that low temperatures characterize nebulae surrounding other novae (Williams 1982; Gallagher et al. 1980), so an explanation for the DQ Her nebula cannot rely on features unique to DQ Her itself.

Further photoionization calculations for DQ Her were reported by Ferland et al. (1984). The atomic data used in this model, vastly different to previous calculations, were taken from Mendoza (1983), while the radiative recombination rates for $T_e = 10^4$ K from Gould (1978) were used with the temperature scaling laws of Aldrovandi & Pequignot (1973). The charge ex-

change reaction rates had to be extrapolated below 5000 K, and could well be in error.

They included an ionizing continuum in their model based on theoretical estimates of the flux emitted by accretion discs at various rates of mass transfer. They found that to achieve low T_e requires a low density and enhanced oxygen abundances. The fine-structure lines of [OIII] at 88μm and 52μm are extremely efficient coolants and easily cool the gas to 500 K. Enhancements of other elements, particularly He and C, tended to raise the temperature by adding to the opacity without contributing to the cooling efficiency.

3.6 Discussion

Some difficulties have been experienced in trying to fit observed Balmer decrements to model calculations. The calculations made by Martin (1988) cover the temperature range found in nova shells and should be applicable to their plasmas. The low densities found in these nebulae result in the collisional processes, even those involving transitions from nl to nl$\pm$1, being unimportant compared to radiative reaction rates, particularly for n $<$ 10. However, Martin has noted problems in trying to match the Balmer decrement found in the DQ Her shell (Ferland et al. 1984) with his calculations. A further constraint, which Martin has not considered, is the ratio of the integrated Balmer continuum flux to the Hβ flux $F_{Bac}/F_{H\beta}$. The measured value for DQ Her was 2.5 (Williams et al. 1978), whereas extrapolation of Brocklehurst's (1971) tables predicts a value of 1.2. If these differences represent errors of observation then the abundance determinations of CNO, which are also based on relative line strengths, could be equally uncertain. Alternatively, if the errors arise from incorrect physics applied to HI, we can have little faith in the results for complex atoms.

The Balmer decrement in the old shell of CP Pup was measured by Williams (1982) and agrees reasonably with case A calculations at T = 800 K (Martin 1988). A high Hα/Hβ ratio of 7 was measured in the shell of T Aur which suggests that it suffers substantial extinction. A value of 3.3 was adopted for F(Hα)/F(Hβ), corresponding to case B with $T_e = 10^4$ K (Brocklehurst 1971), although no independent temperature determination is available either from forbidden line intensities or the Balmer continuum. In the RR Pic shell, after dereddening, the ratio of Hα to Hβ was found to be $\sim$ 10, which is considerably steeper than the calculated radiative decrement. The relative intensities of Hβ/Hγ/Hδ were in fair agreement with the radiative decrement, so it may be that the calibration of the red scan (which included Hα) and the blue scan (which included the other Balmer lines) was inaccurate. However, an unusually large $F_{H\alpha}/F_{H\beta}$ was also found in T Aur but was dismissed as being due to reddening. Although Balmer self-absorption is not expected to occur in such low density gases, it would

have the effect of steepening the Hα/Hβ decrement (Netzer 1975).

Effective recombination rates for hydrogen can be modelled with good accuracy because all processes can be analytically determined to high precision. It is therefore disturbing to find that the measured Balmer line fluxes in nova shells do not agree with these calculations. The intrinsic faintness of nova shells does make their observation difficult, but the disagreement between theory and measurement could be due to incomplete modelling of the physics. Clearly this problem needs to be given some attention.

The heavy element abundances determined thus far should be treated with caution considering the large uncertainties found for HI. Not only have the values been extrapolated to low temperatures, which was inaccurate in the case of hydrogen, but the methods used to estimate metal abundances are themselves subject to much larger uncertainties than the HI calculations. For example, Grandi's (1976) method has its limitations because of the arbitrariness of some of the factors he used, and the assumptions he made regarding the formation of the lines. Even the empirical effective recombination rates determined at T $\sim 10^4$ K could contain significant errors because they are model dependent. Furthermore, their extrapolation to low temperatures is suspect as processes such as dielectronic recombination are significant at T $= 10^4$ K but not at T < 1000 K.

Ferland et al. (1984) have pointed out that there is no way known to estimate the extinction due to dust in a nebula. The effects of any dust in the DQ Her shell at present could be magnified by resonant scattering of λ1335 from CII. The observations of this line show great variety — Hartmann & Raymond (1981) found the flux of CII λ1335 to be half that measured by Ferland et al. (1984).

The results are understandably tentative in view of the sparsity of the data. More observational data would be helpful but realistic modelling could be used to direct observations to features that will help to tie down the conditions in nova shells. An atomic model that makes predictions about all the lines is preferrable to the situation where an effective recombination rate is estimated for one line only.

Chapter 4

Atomic Model for HI

4.1 Introduction

The first few lines of the Balmer series of HI have been seen in the optical spectra of all spatially resolved nova shells. Balmer intensities observed in the cold nova shells were initially compared to values of α^{eff} extrapolated from Brocklehurst's (1971) tables, but nothing definite was concluded because of large uncertainties in the extrapolations. More recently, values of α^{eff} for low temperatures have been calculated by Martin (1988) using a capture-cascade model, but problems still exist in trying to match the modelled results to observations. As is to be expected, the shells consist predominantly of hydrogen, most of which is believed to be in its ionized form. Note, though, that while HI is certainly the most abundant constituent of the gas by number, it is not always so by mass if we accept the number abundance for nitrogen of N(N)/N(H) = 0.1 determined by Williams (1982) for CP Pup.

Hydrogenic models are important not only because of the large abundance of HI, but also because of their wide field of application. Low Z atoms, such as C, N and O, with only one excited electron tend to behave more like hydrogenic systems as either the principal or orbital quantum number of the valence electron increases. Modelling of these atoms relies heavily on hydrogenic models for this reason. An added feature of hydrogenic atoms is the computational ease and precision with which the various atomic properties and processes can be calculated. For example, hydrogenic radiative transition rates can be calculated exactly to four significant figures, whereas for atoms with more than one electron these same processes can only be determined subject to a number of approximations. This obviously limits their accuracy, and can only be improved with a lot more labour. The recombination spectrum of hydrogenic atoms is, hence, well determined by models, and should be able to be used to establish the properties of a gas by suitable selection of the parameters of the model.

We have used various methods to model the conditions in nova shells. Initially, n-method and nl-method capture-cascade calculations were made for case A and case B. The n-method fluxes differed quite drastically from those of the nl-method at low temperatures and comparison of these results with the observed fluxes from nova shells showed that the observations lay between the n- and nl-method values. This led to the development of C^3 models to see if better agreement between observations and modelling could be obtained. In this chapter we first describe the methods used to calculate the rates for the various atomic processes and then describe the models that have been constructed using these rates.

4.2 Atomic Data

4.2.1 Spontaneous Transitions

Only electric dipole transitions were used in the hydrogenic model. A-values calculated with the quantum mechanical expression of Gordon (1929) were used between all levels in the nl-model and for transitions with upper levels ≤ 50 in the n-model. In the n-method model the A-values were averaged over the orbital quantum number. For levels above $m = 50$ the transition rates were calculated using

$$A_{mn} = \frac{1.574 \times 10^{10} Z^4 g_1}{m^3 n(m^2 - n^2)}$$

where g_1 is the bound-bound Gaunt factor and Z is the ionic charge. We used the semi-empirical approximation to g_1 given by Johnson (1972) rather than the more complicated forms given by Brocklehurst (1970) or Burgess & Summers (1976). Tests indicated that these rates are accurate to better than 1%. Furthermore, at these high values of the principal quantum number, collisional effects start to become important and since the rates for these reactions are relatively poorly known there is no need to calculate the A-values to high accuracy.

4.2.2 Radiative Recombination

We used the quantum mechanical expression of Karzas & Latter (1961) for determining α_{nl} and $\alpha_n = \sum \alpha_{nl}$. The computations were performed using the method outlined by Burgess (1964) and Brocklehurst (1971). For the n-method we also determined α_n using Kramers's semiclassical expression multiplied by g_2, the bound-free Gaunt factor. We have used Seaton's (1959a) asymptotic expression for g_2 which gives values that are accurate to better than 1%. The two values of α_n converge as n increases, so when they agreed to better than 0.2% we used only the formula of Kramers which is much faster to compute for the higher levels.

4.2.3 Inelastic bound-bound collisions

These rates are very poorly known with uncertainties in the theoretical values of 20% and very little experimental data to constrain them. The compilation of Giovanardi et al. (1987) gives the most complete tabulation of calculations of electron impact transition coefficients for atomic hydrogen but unfortunately their temperature range only covers 5000K $\leq T \leq 5 \times 10^5$ K. Their collisional transitions between levels with large n are based largely on the results of Johnson (1972). Gee et al. (1976) claim that Johnson's cross sections are adequate at $1/n <$ E [Ryd] < 1 but underestimate the cross sections for other energies.

We used the cross sections of Percival & Richards (1978) which are based on a classical treatment and the correspondence principle whenever the condition $1.6 \times 10^5 Z^2/T < n$ is met. We have integrated the cross sections over a Maxwellian distribution using a 10 point Gauss-Laguerre quadrature scheme. For other values of n we used the results of Johnson (1972), which have been extensively used in astrophysical modelling. At the low temperatures and densities that concern us collisional processes are not very important for small n so that accurate values are not crucial.

We used the same expressions in the nl-model, but a way of distributing these rates between the individual l-states was needed. We used the Bethe approximation suggested by Hummer & Storey (1987), in which it is assumed that the collision rates are proportional to the A-values. We therefore set

$$C_{ml',nl} = \frac{A_{ml',nl} C_{mn}}{A_{mn}}$$

so that only transitions to levels with $l' = l \pm 1$ are non-zero. Hummer & Storey (1987) used this approximation only if $m - n = \Delta n = 1$. For $\Delta n > 1$ they used the simpler approximation $C_{ml',nl} = C_{m,n}$. We have used the Bethe approximation for all Δn but since the $\Delta n = 1$ transitions are the most important our results should be very similar to those of Hummer & Storey.

4.2.4 Bound-free collisional processes

We used Johnson's (1972) formula, which takes into account collective plasma effects that effectively lower the ionization energy of each level. The continuum is regarded as starting at a finite value n_c of the principal quantum number, determined by the condition that the size of the Bohr orbit of n_c equals the smaller of the Debye length or the inter-particle spacing. The binary encounter results of Percival & Richards (1975) were tested and found to have a noticeable but only slight effect on the level populations around $n = 100$. Once again experimental data are very sparse so it is difficult to know which values are better.

For the nl-method we took $C_{nl,i} = C_{n,i}$ for all l on any given level n. When collisional ionization is important the distribution of particles between the l-shells is such that the total rate of collisional ionization from any level is just $C_{n,i}$.

4.2.5 Angular momentum changing collisions

The impact parameter method developed by Pengelly & Seaton (1964) was used by Brocklehurst (1971). We followed his treatment but included the modifications suggested by Hummer & Storey (1987) to get the collision rates to vary smoothly with the orbital quantum number. The method is

similar to the Bethe approximation used above for inelastic collisions in that the rates are distributed between the sublevels according to the oscillator strengths. We first calculated Q_{nl} following Brocklehurst (1971), then used the oscillator strengths to determine $Q_{nl,nl+1}$ from

$$Q_{nl,nl+1} = \frac{f_{nl,nl+1} Q_{nl}}{\sum_{l'} f_{nl,nl'}}$$

where the sum is over $l' = l + 1$ and $l - 1$. The rates for the reverse process were calculated using detailed balance.

4.3 Capture-Cascade Models

These models are constructed from radiative processes only. Descriptions of the method can be found in Seaton (1959b), Pengelly (1964) and Osterbrock (1974). The main difference between our work and other calculations is in the method we have used to sum the series to infinity. The number of terms on which the extrapolation is based greatly exceeds those of previous computations.

In capture-cascade models the effective recombination rate to a level n is a measure of the total rate at which electrons arrive at this level, either by direct recombination or by recombinations to higher levels followed by cascades to the lower level. Hence

$$\alpha_n^{eff} = \sum_{m=n}^{\infty} \alpha_m C_{m,n}$$

where $C_{n,n} = 1$ and $C_{m,n}$ is the probability for an electron initially in upper level m to cascade down to level n, via all possible channels. We calculated the quantities α_m and $C_{m,n}$ up to $m = 50$ and extrapolated these results to $m = \infty$. This greatly extends the upper limit of $m = 10$ used by Seaton (1959b) and $m = 20$ used by Pengelly (1964). The sum to infinity was approximated by calculating the quantity

$$f_n^j = \sum_{m=n}^{j} \alpha_m C_{m,n}$$

and least squares fitting f_n^j to $1/j$ on the interval $31 < j < 50$. The y-intercept, corresponding to $j = \infty$, is the desired quantity. The errors introduced by this fitting procedure increased as either n or l increased and as the temperature decreased. The value of α^{eff} also changed slightly if we summed f^j over a different range of j. Our nl-method results are very similar to Martin's (1988), however.

4.4 Capture-Collision-Cascade Models

Our C^3 models are similar to those used by Brocklehurst (1970, 1971), Burgess & Summers (1976) and Summers (1977). Brocklehurst's results are regarded as the definitive treatment (Osterbrock 1974) for hydrogenic atoms although the collisional rates are somewhat uncertain. It has been pointed out by Brocklehurst that the departure of the gas from equilibrium is very dependent upon the form of the electron-hydrogen atom cross section used. Hummer & Storey (1987) have used Brocklehurst's models over different ranges of temperature and density but have made some modifications to some of the earlier rates. Their results differ from the previous computations by a couple of percent at most.

It is usual practice in determing the occupation numbers to solve the equations in terms of a quantity b_{nl} or b_n, where the b factors represent the deviation of N_{nl} or N_n from their thermodynamic value as defined by the Saha-Boltzmann equation. A two-stage process is used to solve for b_{nl}. In the first stage, values of b_n are calculated assuming that the l-sublevels have statistical distributions, i.e. proportional to (2l+1), so that $b_{nl} = b_n$. This is an n-method model. In the second stage of the calculation, the values of b_n from stage one are used to start an iterative solution for the b_{nl}. We assume that above some level, n_c say, $b_{nl} = b_n$ and solve for b_{nl} for $n < n_c$ explicitly including $l \rightarrow l \pm 1$ collisions. This assumption is physically justified in that at sufficiently high n the dominant mechanisms populating and depopulating sublevels are angular momentum changing collisions, which set up Boltzmann distributions between the l-states. We also require that the differences between the b_n's and b_{nl}'s at $n < n_c$ do not significantly modify the values of b_n when $n > n_c$. Computations have confirmed that this is the case (Brocklehurst 1971). The value of $n = n_c$ necessary to ensure that $b_{nl} = b_n$ depends on system parameters such as ion charge, particle density and electron temperature. The iteration begins at $n = n_c$ and ends at $n = 3$ for Baker & Menzel Case B. A few such iterations are normally sufficient to ensure adequate convergence.

4.5 Numerical methods

The equilibrium equation for level n that has to be satisfied in the n-method is

$$N_e N_i(\alpha_n + N_e C_{i,n}) + \sum_{m>n} N_m(A_{mn} + N_e C_{mn}) + \sum_{k<n} N_e C_{kn}$$
$$= N_n \left[\sum_{k<n} (A_{nk} + N_e C_{nk}) + N_e C_{n,i} + \sum_{m>n} N_e C_{nm} \right].$$

In terms of deviations from Boltzmann distributions this equation can be written as

$$\left(\frac{2\pi mkT}{h^2}\right)^{3/2}(\alpha_n + N_e C_{i,n}) + \sum b_m m^2 e^{\chi_m/kT}(A_{mn} + N_e C_{mn}) + N_e \sum b_k k^2 e^{\chi_k/kT} C_{kn} = b_n n^2 e^{\chi_n/kT}\left[\sum(A_{nk} + N_e C_{nk}) + N_e C_{n,i} + \sum N_e C_{nm}\right].$$

As mentioned earlier, we introduced an upper cutoff to n so we had a finite (but large, $O(10^3)$) number of simultaneous equations to be solved. For large values of n, collisional transitions between the levels dominate and the various levels become statistically populated, which means that $b_n = 1$. Tests indicated that for the range of parameters that we were interested in, $b_n = 1$ always occurred above $n = 496$. We therefore wrote the above equation as

$$\left(\frac{2\pi mkT}{h^2}\right)^{3/2}(\alpha_n + N_e C_{i,n}) + \sum_{m=497} m^2 e^{\chi_m/kT}(A_{mn} + N_e C_{mn}) = -\sum b_m m^2 e^{\chi_m/kT}(A_{mn} + N_e C_{mn}) - N_e \sum b_k k^2 e^{\chi_k/kT} C_{kn} + b_n n^2 e^{\chi_n/kT}\left[\sum(A_{nk} + N_e C_{nk}) + N_e C_{n,i} + \sum N_e C_{nm}\right].$$

In matrix form this equation becomes

$$\mathbf{a} = \mathbf{b} \cdot \mathbf{X}$$

where the row vector $\mathbf{a}$ has components

$$a_n = \left(\frac{2\pi mkT}{h^2}\right)^{3/2}(\alpha_n + N_e C_{i,n}) + \sum_{m=497} m^2 e^{\chi_m/kT}(A_{mn} + N_e C_{mn})$$

and row vector $\mathbf{b}$ has components b_n, the deviation factors. Matrix $\mathbf{X}$ has diagonal elements

$$X_{nn} = n^2 e^{\chi_n/kT}\left[\sum_k(A_{nk} + N_e C_{nk}) + N_e C_{n,i} + \sum_m N_e C_{nm}\right]$$

which are the depopulation rates for level n, while below the diagonal we have

$$X_{mn} = m^2 e^{\chi_n/kT}(A_{mn} + N_e C_{mn}) \qquad (\text{where } m > n)$$

and above the diagonal we have

$$X_{kn} = N_e k^2 e^{\chi_n/kT} C_{kn} \qquad (k < n).$$

We can solve for b_n by matrix inversion i.e.

$$\mathbf{b} = \mathbf{a} \cdot \mathbf{X}^{-1}$$

where $\mathbf{X}^{-1}$ is the inverse of $\mathbf{X}$. We have used the matrix condensation technique of Burgess & Summers (1969) to solve for b_n by matrix inversion, which is the same method that Brocklehurst (1970) used. A variable step length was used between the pivotal points starting with a step length of 1 for the first 20 levels (i.e. no interpolation required) and ending with a step length of 9. A 496 × 496 matrix was reduced to a 100 × 100 matrix. Level 1 (and level 2 in case B) required a different treatment, so we set the diagonal element equal to unity, while row 1 and column 1 (and 2 for case B) were set to zero.

To calculate $\sum(A_{mn} + N_e C_{mn})$ from $m = 497$ to the ionization limit we used a numerical integration technique. First we converted the sum to an integral using the trapezoidal rule, then the integral was evaluated using a 20 point Gaussian quadrature. The A-values and collision rates required in the numerical integration were determined by linear interpolation of the upper quantum number from the nearest integral values.

If the temperature that we used was very low and/or highly charged ions were considered then the Boltzmann factors, $e^{\chi_n/kT}$, became too large for evaluation on the computer. For example, a hydrogenic ion with a charge Z = 1 (a proton) at a temperature of 500 K has a Boltzmann factor for level 2 of $e^{78.9} \approx 1.85 \times 10^{34}$. For HeII this factor would be too large for single precision computations. The program has been set up so that it only calculates values of b_n for levels n whose Boltzmann factors are less than 10^{30}.

The major differences between our model and that used by Brocklehurst (1971) and Hummer & Storey (1987) are 1) we used the collisional ionization formula of Johnson rather than a binary encounter formula, 2) we have introduced a finite cutoff in our upper quantum number, 3) for small n we have used Johnson's collisional transition rates.

The equations that had to be solved in the nl-method were essentially the same as those we had for the n-method, except that each sub-orbital had to be considered separately. We included a collisional term that caused shifts of angular momentum between degenerate energy states. As before, we used a formulation in terms of deviations from a Boltzmann distribution using the Saha-Boltzmann equation

$$N_{nl} = N_e N_i \left(\frac{h^2}{2\pi m k T}\right)^{3/2} (2l+1) e^{\chi_{nl}/kT} b_{nl}$$

giving equilibrium equations of the form

$$\left(\frac{2\pi\bar{m}kT}{h^2}\right)^{3/2}(\alpha_n + N_e C_{i,n}) + \sum_m \sum_{l'} b_{ml'}(2l'+1)e^{\chi_{ml'}/kT}(A_{ml',nl} + N_e C_{ml',nl}) + N_e \sum_k \sum_{l''} b_{kl''}(2l''+1)e^{\chi_{kl''}/kT} C_{kl'',nl}$$

$$= b_{nl}(2l+1)e^{\chi_{nl}/kT}\left[\sum (A_{nl,kl''} + N_e C_{nl,kl''}) + N_e C_{nl,i} + N_e \sum_m \sum_{l'} C_{nl,ml'} + N_p \sum_{l'} Q_{nl,nl'}\right].$$

These equations were solved iteratively, using the b_n's from the n-method as the first step in the iteration, i.e. we set $b_{nl} = b_n$ initially and then solved for b_{nl} using the above equations, replacing the old value with the new at each step. The highest level determined in the nl-method was $n = 50$.

The results and comparisons with other calculations will be discussed in Chp. 7.

Chapter 5

Atomic Model for HeI

5.1 Introduction

Helium, the second most abundant element, accounts for about 27% of the total mass of the Universe. While most of the observable helium is primordial, having been synthesised in the first few minutes of the Big Bang, it is also generated by nucleosynthesis in the centre of stars, and possibly in white dwarf envelopes during novae outbursts. Its presence in nova shells was not unexpected, but its abundance is not known accurately yet and hence it is not possible to determine how much, if any, helium is produced by the outburst.

Some of the emission lines observed in nova shell spectra have been attributed to the recombination spectrum of atomic helium. Model calculations are required to determine the HeI abundance from the observed line intensities, and can also be used to confirm the line identifications and establish the physical conditions in the gas. For example, the presence of HeII lines has been shown by Ferland et al. (1984) to indicate that a source of UV radiation must be responsible for keeping the shell of DQ Her ionized. Models of HeI are important in that calculations of the rates of the atomic processes, while not as accurate as HI, are reasonably uncomplicated but nevertheless accurate enough to produce reliable results. The calculations of Brocklehurst (1972) are regarded as the definitive treatment of HeI (previous computations are reviewed in his paper), but, unfortunately, do not extend to the low temperatures discovered in some nova shells. We have therefore developed a model for HeI to investigate the low temperature recombination spectrum.

The spectrum of HeI is much richer in lines than HI. Electron-electron interactions lift the energy-degeneracy occuring in hydrogenic atoms between levels with the same principal quantum number. Transitions between the individual angular momentum states of helium are, therefore, observed as distinct lines. Further diversity is produced by the presence of two multiplicities, the singlets and triplets, each with its own set of levels.

5.2 The Model

The capture-collision-cascade model we have developed is similar to that of Brocklehurst (1972). Some changes have been introduced to the collision rates following the suggestions of Hummer & Storey (1987) for HI, and we have used new atomic data to investigate the populations of the metastable levels, 2^1S and 2^3S, more thoroughly. The calculations make extensive use of the level population calculations of hydrogen and in many instances hydrogenic rates have been used. This procedure is a reasonable approximation since, as either n or l increases, the helium wave functions and term values

become better approximations to their hydrogenic counterparts. The basic method of solution is similar to that used in the hydrogenic model.

LS coupling is a good approximation for the HeI atom and has been used throughout the calculations. LS-forbidden transitions and collisional transitions between triplets and singlets have been included in the $n = 2$ level only. The triplet series has been treated as case B as there is no 1^3S state and transitions to 1^1S are forbidden. The singlet series, however, can be either case B or case A depending on whether the HeI Lyman lines are optically thick or thin. Angular momentum-changing collisions of the type $nl \rightarrow nl \pm 1$ are affected by the small energy differences between the levels and are noticeably different from those of hydrogenic atoms. The atomic processes relevant to HeI in nebular shells and their implementation in a model are described below.

5.3 Atomic Data

5.3.1 Spontaneous Transitions

The effective principal quantum of the states of HeI with $l \geq 3$ differ from integral values by $< 0.1\%$ so that hydrogen rate coefficients are sufficiently accurate. Their calculation has been fully described in Chp. 4. For $l \leq 2$ the A-values tabulated in Wiese et al. (1966) have been used. The remaining transition rates were calculated using the Coulomb approximation method of Bates & Damgaard (1949) for $n \leq 3$, and that of Van Regemorter et al. (1979) for $n > 3$, where n is the lower level principal quantum number. The effective principal quantum number, n^*, needed in the Coulomb approximation calculations, was determined from the term value listings of Moore (1949). Values up to and including $n = 50$ were required, which exceeds the listings in Moore. An extrapolated quantum defect was used to extend the values up to the limit. Brocklehurst (1972) used scaled hydrogenic values for the higher levels in his calculation, which is most probably less accurate than our method, but this change should not have much effect on the results. An extra factor of 2.35 was required to bring the calculated A-values to 1^1S in line with the values tabulated in Wiese et al. (1966).

5.3.2 Radiative Recombination

For $l \geq 3$ the term values are effectively hydrogenic. Hydrogen recombination coefficients with the appropriate spin statistical weights have been used. Recombination rates for $l \leq 2$ are calculated using the quantum defect method (Burgess & Seaton 1960), the data from Moore (1949) being used to determine the necessary quantum defects. The values we used for the quantum defects of HeI were in good agreement with the values quoted by Peach (1965). If $n > 12$ computational problems arise so we used the scaled

hydrogenic approximation employed by Brocklehurst (1972) for s, p and d states, namely

$$\alpha_{He}(n,l) = \alpha_H(n,l)\frac{\alpha_{He}(n=12,l)}{\alpha_H(n=12,l)}$$

where α_{He} and α_H are the respective HeI and HI recombination rates.

It has been pointed out by Peach (1967) that there are some errors due to extrapolation in the values quoted by Burgess & Seaton (1960), and the expressions have been recalculated using numerical integrations. The tables produced by Peach (1967) list an amplitude and a phase factor versus the energy E of the free electron. These tables, however, provide insufficient coverage of the low energy region. For example, at a temperature of 500 K most of the contribution to α comes from the region between 0.0 and 0.02 Ry, for which Peach gives only two values. For the purposes of calculating α it is far more convenient to have an analytical expression as a function of E for the cross section, such as that given by Burgess & Seaton (1960), even though we perform a numerical integration. We tested the Burgess & Seaton formula against the values given by Peach at low temperatures and found that the differences between α calculated using the two methods varied from 5% in the worst case to less than 1% in most cases. At temperatures above $\sim$ 2000 K the differences between the two methods can start to become important, but for low temperatures the Burgess & Seaton results appear satisfactory.

Recombination coefficients for the triplet series of HeI up to $n = 10$, calculated using the tables of Peach (1967), have been listed by Robbins (1968, 1970). We have compared these rates against our quantum defect calculations for the s, p and d levels, the other l-level rates being hydrogenic are the same in both cases. There are a few spurious large deviations in Robbins' tables, probably due to printing errors, since some of the errors occur in the hydrogenic values. We found differences between the s levels increased as temperature decreased but they were always less than 6%. The p levels agreed to within 2% at all temperatures except for the 3p level which had a difference of $\sim$ 20% at 5000 K and $\sim$ 40% at 2500 K. The d levels showed the largest deviations with differences of up to 13% except for 8d at 5000 K which had a difference of 27.5%. There is at least one error in Robbins' tables, namely $n = 6$ $l = 5$ at 2500 K, so some of the other large differences could also be due to errors in the tables. Brocklehurst (1972) reported values of α 20% smaller for $n > 8$ $l = 0$ when using Peach's data rather than the data of Burgess & Seaton (1960). However, even if we allow for changes in the extrapolated quantum defect we do not get differences as large as this. The source of these conflicting results remains a mystery.

5.3.3 Collisional Ionization

The rates which we used for ionization by collisions with electrons and the inverse process, three body recombination, were identical to those used for

hydrogen. The approximation $C_{nl,i} = C_{n,i}$ has been used throughout, even though the s, p and d states show deviations from hydrogenic behaviour. The collisional ionization rates were never the dominant process affecting a level and therefore errors in their values will not significantly influence the population levels.

5.3.4 Collisional Transitions with $\Delta n \neq 0$

Collisional rates for transitions causing n to change are largest by orders of magnitude for electrons when compared to rates for protons or HeII, so only the electron rates are considered. Hydrogenic collision rates have been used for all $l \geq 3$ (see chapter 4.2.3 for a description of the method). For $l \leq 2$ the quantum defects are sufficiently different from integer values that a separate treatment is required. We have used the impact parameter treatment of Seaton (1962) to determine the collision rates. The impact parameter cross sections have been numerically integrated over a Maxwellian velocity distribution using the trapezoidal rule. The integration is terminated when the integration increment becomes less than 1 part in 10^5 of the total rate.

5.3.5 Collisional Transitions with $\Delta n = 0$

Rates are calculated for collisions with electrons, protons and HeII ions when n does not change. If other ions are present in sufficiently large numbers they too should be included, but tests indicated that the expected abundances of CNO would not have much effect on the total angular momentum collision rates. In HeI the energy gap between the nl and $nl+1$ levels for $l \geq 3$ can be evaluated using the polarization formula for hydrogen-like terms (Edlén 1964). For hydrogenic ions we have (Dalgarno 1962)

$$\Delta E\ [\mathrm{cm}^{-1}] = \frac{740327(5n^2 - l(l-2))}{n^5(l-\frac{1}{2})l(l+\frac{1}{2})(l+\frac{3}{2})(l+2)(l+\frac{5}{2})}$$

The impact parameter method of Seaton (1962) can be used, but the values become unreliable as $\Delta E \rightarrow 0$ since the cross sections diverge. Pengelly & Seaton (1964) (hereafter PS) developed an impact parameter formulation for transitions between energy degenerate levels which can be applied to non-degenerate levels if ΔE is much less than unity. This method was used by Brocklehurst (1972) for $l > 5$. As temperature decreases or the mass or charge of the incident particle increases, however, the conditions under which this method can be applied change, and so a criterion is needed for determining which formula to use. We address this problem in the next section.

5.3.6 Impact Parameter Cross Sections

Seaton (1962) introduced a lower cutoff ρ_0 to the impact parameter b, where ρ_0 is determined so that in the case of weak coupling the cross sections agree with the Born cross sections at high energies, while for strong coupling $P_{if}(\rho_0) = \frac{1}{2}$, where P_{if} is the probability of a transition occuring. If b is less than ρ_0 then the probability P_{if} oscillates rapidly between 0 and 1 as the wave packets of the two particles interfere, resulting in an average value for P_{if} of $\frac{1}{2}$. The cross section for a collision to take place is then given by

$$\sigma_{if} = \frac{1}{2}\pi\rho_0^2 + \int_{\rho_0}^{+\infty} P_{if}\, 2\pi b\, db.$$

The procedure for calculating the cross section is to take the smaller of the weak and strong coupling cross sections. The cross sections thus obtained often contain discontinuities in their first derivative (with respect to energy) but, in general, the cross sections agree well with experimental results (Seaton 1962). Impact parameter calculations of dipole, quadrupole and octopole transitions at high energies have been made using a classical Coulomb trajectory and have been found to give reliable results compared to experimental data (Walling & Weisheit 1988). These authors point out that at velocities near threshold any semiclassical method fails because the same trajectory is incorrectly used for all scattering channels. However, the use of Coulomb trajectories at low energies is unnecessary since the incident particle does not have enough kinetic energy to penetrate very deeply into the Coulomb potential of the target ion. Note also that in Seaton's treatment the reciprocity condition for the forward and reverse processes was introduced in such a manner that near threshold the results will be most affected.

In the case of transitions between energy degenerate levels, the perturbation acts for a time τ only, so an upper cutoff ρ_1 was introduced by PS such that $\tau \sim \rho_1/v$, where v is the relative velocity of the particles. If τ is taken to be the time it takes for the atom to radiate, then a numerical integration shows that $\rho_1 = 0.72/\sum A$ where $\sum A$ is a sum of all spontaneous transitions out of the level. An alternative value for ρ_1 is the Debye length. In practice the smaller of these two values for each velocity should be adopted. PS obtained an analytical form for the collision rate by integrating the cross sections over a Maxwellian velocity distribution. However, they calculated the rate using each value of ρ_1 separately and then chose the smaller of these two rates. Furthermore, they did not properly take into account the lower cutoff ρ_0. This latter neglect allows ρ_1 to become less than ρ_0 so that, in certain situations, the collision rates become negative. This is physically incorrect.

We derived the collision rate using the smaller cross section at all velocities and with

$$\sigma_{if} = \frac{1}{2}\pi\rho_1^2 \qquad \text{when } \rho_1 < \rho_0.$$

This gives a collision rate which is always positive. We compared the rates from this formula against that of PS over a wide range of temperature and electron density and found that the largest differences occurred for low T_e and high N_e. However, the difference in the values at $T = 10^2$ K and $N_e = 10^5$ cm^{-3} was below 20% for all levels up to $n = 30$, and $\sim 2\%$ below $n = 10$. Increased differences between the two values were found if the mass or charge of the incident particle was increased, or if the charge of the target ion was increased. The values obtained from our formula were larger than the values from the PS formula which seems surprising considering that we always used the smaller cross section. The reason for this behaviour, however, is due to the incorrect treatment of the cross sections by PS at low velocities which allows their value to become negative. Although the Maxwellian averaged value is positive the negative contribution reduces the overall rate. The effect of these collision rate changes on the behaviour of the recombination spectrum was not noticeable to 4 significant figures. It appears that the PS formula is suitable in most situations, the exception being when ρ_1 becomes too small. To quantify this consideration we look at transitons involving very small energy gaps.

If the energy gap between two levels is sufficiently small then it seems reasonable that the energy-degenerate formula can be employed provided an upper cutoff can be found that is related to the energy gap. Such a relationship has been discussed by PS, and was used by Brocklehurst (1972) for calculating the collision rates between the nearly degenerate l-shells in HeI. However, at low temperatures if l is too small then rates using the PS formula turn out negative. Using the expression for ΔE given in §5.3.5 and the upper cutoff of PS, the values calculated from our formula were compared with computations using the PS formula and the Seaton formula. Although the values from our formula are always positive they differed from the Seaton values by up to an order of magnitude when the PS values were negative. It appears then that the use of $\sigma_{if} = \frac{1}{2}\pi\rho_1^2$ is unreasonable, at least for non-degenerate levels, although in most cases that this approximation is required the collisional reactions are unimportant compared to other processes. As the energy gap decreased there was an improvement in the agreement between the PS and Seaton values, while our formula was always found to be smaller than the other two values, sometimes by up to 20%. Storey & Hummer (1988) also used $\sigma_{if} = \frac{1}{2}\pi\rho_1^2$ when $\rho_1 < \rho_0$ for the l-changing collision rate between the degenerate energy levels of the hydrogenic ions CVI, NVII and OVIII. They commented that other methods would probably provide a better description of this mechanism, but also pointed out that the tabulated intensities were rather insensitive to density changes, and hence also to a change in collision cross section.

Computationally the PS method is much faster to implement than the Seaton formula when calculating collision coefficients between non-degener-

ate energy levels. We needed some criterion to decide when to switch over from one formula to the other. Since, at a fixed n, the two sets of values converge as l increases, we have changed to the PS method when the agreement was within 6%. This automatically ensured that when changing to the PS formula the rates were always positive.

For degenerate energy levels we need to determine a reliable lower limit to the collision rates. In the impact parameter approximation one of the requirements of the PS formulation was that $\rho_1/\rho_0 \gg 1$. While this condition might be valid over most of the velocity range, it always breaks down as $v \rightarrow 0$. We calculated the mean value of ρ_1/ρ_0 by integrating it over a Maxwellian velocity distribution, getting

$$\rho_m = < \rho_1/\rho_0 > = 3.929 \times 10^{11} \frac{m_e T \rho_c}{m \sqrt{DNL}}$$

with $\rho_c = 0.72/\sum A$ and DNL is the function defined in PS. Comparisons between our formula, the PS formula and the Seaton formula have shown that provided $\rho_m > 10$ the PS formula can be used. If $\rho_m < 10$ we used our formula, but the rates were so small that they were unimportant anyway. Note that another condition required in the impact approximation, namely $L/\hbar \gg 1$, automatically holds if $\rho_m \geq 10$ since $< L/\hbar >= \rho_m \times \frac{m}{m_e}$.

5.4 The Metastable Levels

The 2^1S and 2^3S levels of HeI are metastable. Collisional processes help to depopulate these levels but these rates are quite small and hence large populations build up. Collisional excitation by electrons out of the 2S levels into the 2P and higher levels becomes important because of these large populations, even though the collisional cross sections are fairly small. Similarly, the flux of forbidden spontaneous transitions out of these levels becomes significant.

The collisional processes and the forbidden spontaneous transitions couple the singlet and triplet series and the populations of these levels need to be solved simultaneously. We have employed matrix inversion techniques to solve for the populations of the four $n = 2$ levels. We have treated them as being populated by (1) allowed spontaneous transitions from levels with $n \geq 3$, (2) direct radiative recombination and (3) collisional processes (excitation and deexcitation) within the $n = 2$ level. At nebular temperatures and densities collisional deexcitation from $n \geq 3$ into $n = 2$ is negligible compared to the spontaneous transition rate, but collisional excitation from the metastable levels into n ≥ 3 is an important depopulating mechanism under certain conditions. The excitation rates from 1^1S could be neglected at the temperatures that concerned us, but collisional deexcitation by electrons from the metastable levels to the groundstate is an important source of

temperature drops collisional deexcitation to 1^1S becomes more important. At $\sim$ 2500 K the rates for these two processes are the same. At very low temperatures ($<$ 500 K) the collision deexcitation rate is poorly determined so it is difficult to make any conclusive statements regarding behaviour of the gas under these conditions.

The case B condition for singlets assumes that any Lyman photon emitted is immediately reabsorbed so that transitions to 1^1S can be ignored. Forbidden transitions were treated differently, however. The ratio of the A-values for allowed and forbidden transitions from the $n = 2$ level is larger than 10^7, so that photons produced by forbidden transitions have a much longer mean free path than those produced by allowed transitions, and the gas can hence be regarded as optically thin to these photons. The case B treatment of the metastable levels was carried out as previously described except that the allowed transition from 2^1P to 1^1S was excluded from the matrix equations. The singlets then all cascade down to the 2^1S level, which is emptied mainly via the forbidden transition to 1^1S. The triplet levels were affected very little by by this change, because the 2^1S level has a much lower population than 2^3S even in case B conditions. The filling rate for singlets (excluding the groundstate) is $\sim 1/3$ of that for triplets and the spontaneous transition rate from 2^1S to 1^1S is 51 s^{-1} compared to 1.13×10^{-4} s^{-1} for the 2^3S to 1^1S transition, so that it is emptied at a much faster rate.

Photoionization cross sections for the $n = 2$ level of HeI were calculated using the QDM. The results obtained agreed reasonably well ($\sim$ 10%) with the more accurate calculations of Jacobs (1974) and Stewart (1979) and are certainly accurate enough for our purposes considering the large uncertainty that exists in the ionizing fluxes. The transition rates from 2^1S and the P states are much larger than from 2^3S and this level can therefore be used to set a lower limit on all the calculations. Using I_ν = constant (see Ferland et al. 1984, for example), we calculated a photoionization rate of $\leq 10^9$ I_ν for all the $n = 2$ levels, so provided $I_\nu < 10^{-13}$ erg/cm^2/s/Hz the depopulation rate of 2^3S will not be affected by photoionizations. Ferland et al. (1984) suggest fluxes of $\sim 10^{-17}$ erg/cm^2/s/Hz from the central stellar system of DQ Her based on observations and theoretical models, and similar values can presumably also be applied to other novae.

The high concentrations of He(2^3S) that can be formed have led to several theoretical and experimental investigations into reaction rates of this atom with various other reactants. The combined rate of associative ionization and Penning ionization of He(2^3S) with HI is $\sim 5 \times 10^{-10}$ cm^3/s (Roberge & Dalgarno 1982). A density of 10^6 HI atoms/cm^3 would be required for this process to be comparable to the spontaneous transition rate. This is an upper limit on the particle density that is expected in nova shells, on top of which most of the hydrogen present in the gas should be in the form of HII rather than HI, so we have ignored this process. Molecular H_2 and heavy

element reaction rates for these same processes are similar to that for HI (Roberge & Dalgarno 1982) but because of the much lower abundances of these reactants anticipated in nova shells we excluded these processes from further consideration as well.

Reaction rates for charge transfers of the type $He(2^3S) + X^+ \rightarrow He^+ + X^0$ were looked for in the literature but nothing was found. In particular, the reaction with protons is not known. However, the fastest charge exchange rates that we did find have values of $\sim 10^{-9}$ /cm^3/s and occur with the more highly charged ions. Once again large number densities ($\sim 10^5$ cm^{-3}) of suitable ions would be required for these reaction rates to compete with the processes in our formulation.

The results of this model for a range of parameters are presented in Chp. 7.

Chapter 6

Complex Atoms

6.1 Introduction

Cool nova shells have displayed both allowed and forbidden lines of CNO in their optical spectra. It has been suggested (Williams 1982) that all these lines are formed by recombination in the low temperature, low density environment of the shells. The line identifications are somewhat tentative in many cases as only one or two lines of each ionic species are seen and no quantitative measure of their expected relative intensities is currently available. Line emissions from PN have been used as a guide, but the conditions in these plasmas are quite different to those found in the cool nova shell gases and so are not directly applicable. In this chapter we describe the atomic models of CNO atoms and ions that we have constructed in an attempt to identify and quantify the line emissions observed in nova shells.

6.2 The Model

Capture-collision-cascade models for many electron atoms are complicated to construct. Not only are there more atomic processes that can occur than in HI or HeI, but there is also a larger number of terms that need to be considered in these atoms, leading to a vast number of possible transitions between the various terms. Coupling the angular momentum of the valence electrons to the ionic core can be done in a number of different ways, none of which is perfect. This leads to a source of uncertainty in any calculations. The empirical transition rate and term value data sets for these atoms are, in general, smaller than for either HI or HeI, which is a serious constraint to the accuracy that can be achieved by any model. Accurate calculations of the various atomic rates are complicated and hence not many have been made. The lack of experimental data to check the computations has made it difficult to assess their validity in any case.

Fortunately there are a number of simplifying procedures that can be applied in the calculation of the various rates so that a tractable model is possible. The accuracy that can be achieved by these models will be discussed later. The first simplification we made was to regard the atom as having only one valence electron. As either the n or l quantum number of the valence electron increased, we assumed that the ions behaviour tended towards that of a hydrogenic atom, and used the rates from a hydrogenic model with an ionic charge appropriate to the ion under consideration. For atoms and ions with low atomic numbers, such as CNO, it appears that LS coupling is a reasonably good approximation in most cases. We therefore adopted this coupling scheme for determining allowed transitions, although

for small n we were able to add in transitions allowed by other coupling schemes. Our model has used atomic terms only, rather than all the possible levels, even though some of the energy level data and some of the transition rates are available. This approximation makes the modelling easier in that the number of equilibrium equations that need to be solved is drastically reduced. In practice blends of lines are often observed if the resolution is limited, which is particularly true when observing low surface brightness objects such as nova shells. The level populations can be recovered from the term populations if it is assumed that the levels are statistically distributed, a reasonable approximation if the energy separations are small.

In all cases we adjusted the rates so that they had the correct statistical weight according to an LS coupling scheme. When term values were not available and we had to resort to hydrogenic rates, we summed over L, assuming that the individual levels were statistically populated. The justification for this is the same as that for the models of HI and HeI where similar procedures were applied.

In the sections that follow we describe the general methods we used to determine the various atomic rates. We then briefly discuss the modelling of each atom or ion individually.

6.3 Atomic Data

6.3.1 Spontaneous Transitions

When available we have used tabulated values of spontaneous transition rates which have been determined either from theoretical calculations or laboratory experiments (see §6.6 for details). The listings in Wiese et al. (1966) are the most comprehensive but rather limited and by no means definitive. Very often more than one value for a given transition was found in the literature, depending on the method of calculation or experimental arrangement used. It was sometimes a subjective choice as to which was the best value to use, although generally the most recent value represented an improvement over previous estimates and was therefore the one chosen. All the important optical lines as well as lines involving transitions to the groundstate (including the fine-structure, nebular and auroral lines) have been well studied both theoretically and experimentally. The compendium of Mendoza (1983) has been used as a guide to work prior to 1983. These values were put into the model "by hand" and we have therefore been able to include LS-forbidden transitions such as intercombination lines and 2-electron transitions. Unfortunately intercombination lines could not be included interactively in the model since we solved for only one multiplicity at a time. However, the inclusion of intercombination lines in the depopulation rates of levels was possible, and, by using the level populations from previous calculations, their rate of filling a level also.

When term values were available effective principal quantum numbers were determined and, provided $l \leq 3$, the A-values were calculated using the Coulomb approximation method of Bates & Damgaard (1949) for $n \leq 3$ or Van Regemorter et al. (1979) for $n > 3$. Levels up to $n = 50$ were determined with integer values for the upper level effective principal quantum number for those levels for which term values were not available. When neither the upper nor lower level term values were known, or if $l > 3$, hydrogenic transition rates were used. The Coulomb approximation is unreliable for many series, particularly those involving an excited core configuration. For example, transitions into the $2s2p^2$ states of CII, determined using the Coulomb approximation, differed radically from the A-values of Nussbaumer & Storey (1983). Spontaneous transition rates for these levels were based entirely on values in the literature, which meant that transitions from $n > 4$ into these excited core configurations were not included in the model.

In the model for HeI, quantum defects were extrapolated up to $n = 50$ to obtain effective principal quantum numbers for terms with $l < 3$. When modelling the ions of CNO this procedure could not be reliably applied. Firstly, the number of known term values is usually quite small for any particular series — sometimes only one or two values are known. Secondly, the series often displays anomalous values due to the presence of nearby resonances from other series which cause a shift in the energy eigenvalues, and hence also the quantum defects. It is therefore difficult to extrapolate many of the series, a problem also for the calculation of recombination coefficients by the quantum defect method.

It was difficult to judge the accuracy of most of our calculated transition rates since few other determinations exist. Besides the listing in Wiese et al. (1966), which contains relatively few lines, there is the list of semi-empirical gf values calculated by Kurucz & Peytremann (1975), from which A-values could be obtained and against which we were able to check our values. The method of computation used by these authors is slightly different in that they used scaled Thomas-Fermi-Dirac wavefunctions to fit the observed energy levels. When the two sets of results differed there was no way of knowing which set was more reliable (if either). However, it was comforting to find general agreement between the Kurucz & Peytremann results and ours to within an order of magnitude at least, but often much better. We also found that the calculated A-values from the two different Coulomb approximation algorithms converged as n increased, and agreed to within a couple of percent for $n = 4$. In some cases, usually involving the groundstate, we found that Coulomb approximation calculations for a Rydberg series could be fitted to the alternative data by the use of a multiplicative factor.

6.3.2 Recombination Rates

Recombination rates were obtained by integrating free-bound cross sections, derived from the photoionization cross section using the Einstein-Milne relations, over a Maxwellian velocity distribution. We used the semi-empirical photoionization cross sections of Henry (1970) when available, which included the groundstate configurations of all atoms and some of the metastable levels. The quantum defect method (Burgess & Seaton 1960) was used for the other levels for which term values were available. For most ions extrapolated quantum defects could not be determined from the available data so we used the values calculated by Theodosiou et al. (1986). These quantum defects agreed quite well with the values we could determine and seemed to be reasonable extrapolations of the relevant Rydberg series. The values, however, do not make allowance for differences in the L quantum number; they are listed only with respect to the l-shell quantum number. Levels having an excited core configuration, such as $2s2p^3$, did not yield reliable A-values when using the Coulomb approximation, so we felt it unlikely that the quantum defect method (which is a Coulomb approximation method for bound-free transitions) would be applicable to these terms either. Instead, we used the effective-charge method of Gould (1978) to determine the recombination rates. No other calculations of these rates could be found in the literature so we have no idea as to their accuracy. Hydrogenic recombination rates were used for all other levels.

6.3.3 Collisional Processes

Hydrogenic rates have been used when nothing else was available. Collision rates between terms for which non-hydrogenic A-values occur, have been calculated using the impact parameter method (Seaton 1962). For collisional transitions with $\Delta n \neq 0$, or if one level had $l \leq 3$, we have only determined rates due to collisions with electrons. For the $\Delta n = 0$ transitions between levels with hydrogenic term values we have used the helium angular momentum collision rates and included rates due to electrons, protons and ions. The hydrogenic formula (Pengelly & Seaton 1964) applies to degenerate energy levels only and overestimates the rates when the energy difference is non-zero. The helium rates on the other hand are likely to underestimate the collision rates slightly for CNO ions.

Collisional ionization and three-body recombination rates were the same, and were implemented in the same way, as in the hydrogen model.

In our model for HI we used the electron collision rates of Johnson (1972) for $n \leq n_c$ and Percival & Richards (1978) for $n > n_c$, where n_c is a lower limit of applicability for the latter rates. Johnson's results have been widely used in astrophysical calculations but are restrictive in that they apply only to the HI atom. For hydrogenic calculations with an ionic charge greater

than unity we needed another formula. We tested impact parameter cross sections (Seaton 1962) but found that only transitions from $n \rightarrow n+1$ compared reasonably (at least within a factor of 2, but typically only a few percent different) with either the Johnson (1972) or Percival & Richards (1978) values. Impact parameter rates were smaller, sometimes by orders of magnitude, for all other transitions, the difference increasing as $\Delta n = n' - n$ increased and as n increased. Seaton (1962) suggested taking the smaller of the weak and strong coupling cross sections to determine the rates. We found that if we used the strong coupling condition only, the collision rates thus obtained were in much better agreement with the hydrogenic rates of Johnson (1972) and Percival & Richards (1978) for ionic charges of one. This was also true for ionic charges of 2 and more, although in these cases we only had the Percival & Richards (1978) rates to compare with. The impact parameter rates were still smaller than the Percival & Richards rates but the differences were much smaller. Computationally it was better to calculate deexcitation rates rather than excitation rates to circumvent problems with small number arithmetic. This had the effect of increasing the rates slightly so that the agreement with the Percival & Richards' rates improved.

The impact parameter collision rates from level m to level n were computed using two methods. We used the shell-averaged A-value A_{mn} to calculate C_{mn} in one method, and the individual A-values $A_{ml \rightarrow nl\mp1}$ in the other to determine $C_{ml \rightarrow nl\mp1}$ which was then averaged over l to get C_{mn}. The two methods differed by a few percent only, so we chose to use the first method as it is computationally faster. This same conclusion was reached by Saraph (1964) who looked only at $n \rightarrow n+1$ transitions.

6.4 Method of Solution

The equilibrium equations for each level were formulated in terms of b_{nlL} if term values were available, or b_{nl} when hydrogenic values were used. If only nl was specified it was assumed that L had been summed over. The procedure for solving the equations was similar to that employed in solving the HI and HeI models. First we solved for b_n using a hydrogenic model with the appropriate ionic charge and the lowest level corresponding to the groundstate of the atom under consideration. The atoms and ions that we considered have mainly 2p groundstates, but 2s and 3s also occur. The b_n values were then used as a first approximation in solving the b_{nlL} and b_{nl} values by iteration.

6.5 Accuracy Estimates

The accuracy of the model was assessed by running it with the HeI data, and comparing the results with the HeI model described in Chp. 5. Term values for $n \leq 11$ and $l \leq 3$ were prepared as input for the program. This

model differed from the HeI model in that the recombination coefficients for $n > 11$ were pure hydrogenic rather than scaled rates, while extrapolated quantum defects were not used to calculate A-values for these higher levels. In fact we did try scaling both the A-values and the radiative recombination coefficients but these changes made very little difference to the end results.

A much larger difference was produced by reducing to 6 the number of empirical levels entered into the model. Under these conditions the b_{nl} values were under/over estimated by $\sim 10\%$ for the $n = 3$ levels, but the deviations decreased as n increased.

6.6 Atomic Data for Individual Ions

CI Radiative transition rates between the six energetically lowest configurations of CI have been taken from the multiconfiguration, intermediate-coupling calculations of Nussbaumer & Storey (1984a). We used their values but averaged over the j quantum number. In general, an LS coupling scheme is well fulfilled (Tozzi et al. 1983), although some UV multiplets, in particular those involving the 4s and 3d configurations which all lie very close energetically, have been found to show significant deviations from this coupling scheme. The calculations are in good agreement with measurements (Goldbach & Nollez 1987).

Photoionization cross sections for the groundstate configuration of CI (^{3}P, ^{1}D and ^{1}S) have been calculated by Hofmann et al. (1983) for photon energies between the ionization threshold ($2s^22p\ ^2P^0$) and 2.2 Ry. Large resonances are present which makes the curve of the cross section versus energy complicated to describe by means of a simple formula. We have instead used rates determined from the data of Henry (1970) for these levels, which do not take into account these resonances.

CI has 3 terms with the configuration $2s^22p^2$, namely ^{3}P, ^{1}S and ^{1}D, the ^{3}P term being the groundstate. Decays from the singlet terms to the groundstate and from $^1D \rightarrow {}^1S$ occur via magnetic dipole and electric quadrupole transitions which lead to these levels having very long lifetimes. The ^{1}S and ^{1}D levels are therefore metastable and, like the helium 2s levels, develop large populations. The situation for CI is different to HeI however, in that these metastable levels are singlets rather than triplets. The singlet levels only aquire about 1/4 of all recombinations and these are then divided between the two singlet states. Intercombination transitions complicate matters but LS allowed transitions are stronger in almost all cases, and transition from singlets to triplets balance those acting in the other direction to an extent. Collisional transitions from 2^3S and to a lesser extent 2^1S in HeI were shown to be important in populating higher levels, thereby enhancing the fluxes of lines from these levels. In CI the energy gaps between the $2s^22p^2$ configurations and the $2s^22p3s$ configurations, which lie energetically next, are much larger than the equivalent levels in HeI. The HeI metastable levels are

separated from higher levels by energies that give rise to optical photons, whereas the CI lines that cascade into the metastable states are all shorter than λ2582. Furthermore, the CI metastable levels are much closer to the groundstate than to the higher levels so that collisions between the terms of $2s^22p^2$ are more important than collisions to $n \geq 3$. Collisional depopulation of ^{1}D and ^{1}S is likely to be an important mechanism for these levels since A-values for these states are 0.5 s^{-1} ($^1S \rightarrow {}^1D$), 3.60×10^{-4} s^{-1} ($^1S \rightarrow {}^3P$) and 3.09×10^{-4} s^{-1} ($^1D \rightarrow {}^3P$).

Analyses of most of the Rydberg series only go up to $n = 10$ so we used this as our cutoff for looking at individual terms. A few of the series had to be extrapolated by one or two terms. The np ^{3}S series only have term energies for $n = 3$ and 4, which suggests that transitions from these terms are too weak for them to be detected in the laboratory. We left out the higher terms in our calculations as there were not enough data to use for an extrapolation. Data for the f-shell term values were not available either so we used hydrogenic values.

Collisional processes were not included in the intercombination transitions because at low n the spontaneous transitions are usually the dominant processes. Unfortunately, we did not have spontaneous radiative rates or collision cross sections for intercombination transitions between the 4s and 3d levels. Electron collision rates, in particular, could be quite important between these levels since their energy separations are quite small.

NI Neutral nitrogen has a rich spectrum of transitions, many of which lie in the optical region, but unfortunately modelling calculations are hampered by a lack of reliable data for these lines. Both experimental and theoretical determinations of the A-values are very limited so we have had to rely predominantly on Coulomb approximation calculations. The accuracy of these computations is difficult to assess since alternative values only overlap one or two members of each Rydberg series. The only correction factor we included in our Coulomb approximation calculations was on the ns $^2P \rightarrow 2p^3$ ^{2}D series where we multiplied the calculated values by 2.5. A-values for the series nd $^2L \rightarrow 2p^3$ ^{2}D might also be grossly underestimated if we consider that the only comparison value we have for each L series is about an order of magnitude greater than the Coulomb approximation calculation.

The groundstate configuration of NI is $1s^22s^22p^3$ $^4S^0$ which is formed from the NII groundstate $2s^22p^2$ $^3P^0$ with an added p electron. This core configuration also produces a set of NI doublet states starting with the metastable levels $2p^2$ ^{2}D and $2p^2$ ^{2}P. The quartet lines should dominate the spectrum since about 2/3 of all recombinations from NII $^3P^0$ will be to these states and only 1/3 to the doublets. However, NII has two metastable singlet levels, namely $2s^22p^2$ ^{1}D and ^{1}S, which can also form a core for doublets. There are some strong transitions (of order 10^8 s^{-1}) from configurations involving

these cores to the groundstate and possibly other important two-electron transitions exist as well. Unfortunately, our routines cannot calculate reliable values for this type of transition and no alternative data sources are available as yet.

Note that the recombination rate for doublets should take the NII singlets $2p^2\ ^1D$ and ^1S as well as $2p^2\ ^3P^0$ into account. We have data for the NI groundstate configuration doublets from Henry (1970), but for other levels we have no way of determing the recombination rate from the NII singlet levels.

OI A-values for OI came from the compilations of Hey (1987) and Zeippen et al. (1977). The latter results are theoretical while the former are based on the best theoretical or experimental value. Extrapolated quantum defects of 1.150, 0.714 and 0.020 were used for the triplet S, P and D terms respectively, and 1.225, 0.790 and 0.040 for the quintet terms. We also used the extrapolated quantum defect to calculate an effective principal quantum number for the purposes of determining the A-values of the s and p levels for which term energies were not available. Transitions to the groundstate, $2p^4\ ^3P^0$, were corrected by a factor of 220 and 1880 for upper states ns ^3S and nd ^3D respectively. Calculations of spontaneous transitions using the Bates & Damgaard (1949) and Van Regemorter et al. (1979) algorithms converged above $n = 4$ and showed deviations of less than 25% for $n = 3$.

CII The groundstate of CII has the configuration $1s^22s^22p\ ^2P^0$ and has a lowest-energy core configuration of $1s^22s^2$ (^1S). The first excited state of the core configuration is $1s^22s2p$ ($^3P^0$) which gives rise to both doublets and quartets of CII when a valence electron is added. The 2s2p ($^3P^0$) core terms are important in the CII doublet spectrum because, as shown by Nussbaumer & Storey (1981), two-electron decays with large transition probabilities occur which couple this core to the $2s^2$ (^1S) core configuration. For the doublets Nussbaumer & Storey (1981) have calculated all the strongest transitions between levels below 4f, including the two-electron transitions which involve the $2s2p^2\ ^2D$, ^2S, ^2P and $2p^3\ ^2D^0$ levels. We used all these values in our model.

The quartet series has an excited core and so reliable A-values can not be calculated using the Coulomb approximation. We have no alternative routines to use and as tabulated values for this series are in short supply we have had to neglect it for the present.

Hofmann et al. (1983) investigated the effects of the groundstate terms of CI being photoionized such that the CII ion was left in an excited state. They calculated photoionization rates to the ground and excited states of CII using two different solar spectra at a distance of 1 A.U. The rate from the CI ^3P term to the CII groundstate dominated the rate to excited states by more

than two orders of magnitude, while from the ^{1}S and ^{1}D terms there were more than three orders of magnitude difference between the ground and excited states. This mechanism does not seem to be a strong contributor to the excited states of CII, although this does depend on the energy distribution of the ionizing flux. We did not include contributions from the photoionization of CI into the excited states of CII in our model.

NII Spontaneous transition rates for NII are, in general, poorly known. We used the theoretical values of Fawcett (1987) for transition into the groundstate configuration. The highest level in these computations was 4d. The large uncertainty in these values can be seen by comparing them with the beam foil measurements of Chang (1977) and the listings in Wiese et al. (1966). Transitions listed in Wiese et al. (1966) but not involving the groundstate were also used. In all cases only term averages were used. The only two-electron transitions included in the model were from $2p^3$ into the groundstate configuration, and the only way these levels were filled was by direct recombination. The transition rates from these levels to the groundstate configuration are quite large according to Fawcett's values but most of these transitions lie above the HI ionization limit, and are hence of little interest from an observational point of view. There is, however, one line that should be observable, namely the triplet line $2p^3\ ^3D \rightarrow 2p^2\ ^3P$ at λ1084.

The coloumb approximation results mostly showed agreement to $< 10\%$ for $n = 3$ and 4, the exceptions with larger differences only occurring when the A-values were small. Empirical data for term energies up to $n = 5$ were available, except for 5p levels which were missing, so we estimated values by extrapolation of the quantum defect for 5p and the $n = 6$ levels.

OII Spontaneous transitions to the groundstate configuration of the doublets were taken from Ho & Henry (1984), and all other transitions listed in Wiese et (1966) which have a ^{3}P core. None of the transitions involving either ^{1}S or ^{1}D cores were used unless they had a $2p^4$ configuration. Intercombination lines were also excluded because all those listed had branching ratios of ~ 0.01 compared to LS allowed transitions and their effect would therefore be quite small.

CIII A-values for transitions within the $n = 2$ level of CIII were taken from Nussbaumer & Storey (1978), while transitions from $n = 3$ came from Hummer & Norcross (1974), and transitions from 2s4p ^{1}P from Mühlethaler & Nussbaumer (1976). We adopted a value of 1.30×10^9 s^{-1} for $2p^2\ ^3P \rightarrow 2s2p\ ^3P^0$ from Chang (1977) which agrees with most theoretical and experimental determinations (Hummer & Norcross 1974). The $2p^2$ levels have been included in the prescription but data for transitions from 2s4p ^{1}P and 2s3p to $2p^2$ only were available. Intercombination transitions from $2p^2$ to 2s2p were

not included, even though A-values are available in Nussbaumer & Storey (1978), because the LS allowed transitions out of $2p^2$ are at least 4 orders of magnitude larger than these transitions, and they are hence not important as either depopulators of $2p^2$ or fillers of 2s2p. At higher temperatures collisional processes would make these levels play a more dominant role but the term energy gaps are too large for thermal excitation at low temperatures. The only relevant intercombination line is that from the metastable 2s2p ^{3}P level to the groundstate which produces λ1909 photons. The electric quadrupole and magnetic dipole transitions listed by Nussbaumer & Storey (1978) have also been left out because, as with the intercombination lines, their rates are too low compared to transition rates via other channels.

Recombination rates for the $2p^2$ levels could not be found in the literature, and only the calculations of Drew & Storey (1982) were found for the 2s2p $^3P^0$ level. These authors have shown that there are a number of resonances near the photoionization threshold of the $2s^2$ level which are not incorporated in the quantum defect method formulation of the photoionization cross section which we used.

NIII Only the doublets with a ^{1}S core were modelled, because, as in the case of the isoelectronic CII ion, the quartets are formed from an excited core configuration which we do not expect to find with any significant population in a low temperature plasma. Alternative sources of A-values to our coloumb approximation calculations were available in Wiese et al. (1966) and Nussbaumer (1971). We used the Nussbaumer calculations and any additional transitions in Wiese et al. (1966). There are quite large discrepancies between some of these A-values and, as Nussbaumer has pointed out, some of the calculations are very sensitive to the method of evaluation.

OIII Values for the spontaneous transition rates of OIII can be found in Fawcett (1987), Bhattia et al. (1979), Nussbaumer & Storey (1981), Chang (1977) Wiese et al. (1966) and Westhaus & Sinanoğlu (1969). Transitions for which comparisons were possible had differences of up to factors of 2 or 3 in some cases, although in general the agreement was not unreasonable. We used the level-averaged values of Fawcett (1987) and supplemented them by any additional lines listed by Wiese et al. (1966) and Bhatia et al. (1979).

The results of these calculations are presented in chapter 7.

Chapter 7

Results and Comparisons

7.1 Introduction

In this chapter we present the results of the calculations performed using the models described in the previous three chapters. Where possible we also compare our results with other model calculations. The most convenient way of presenting the results for comparison with observed spectra is to tabulate modelled line fluxes for each atom. Only the strongest lines from each atom that are of astronomical interest have been tabulated. Lines of little interest to us include those with weak fluxes, which will be unobservable in faint objects, and those with wavelengths that lie in unobservable regions of the spectrum. The UV band shortward of 1200Å falls in the latter category, with the result that many of the strongest line fluxes produced by recombination in astronomical plasmas cannot be detected. The interstellar medium (ISM) is responsible for absorbing most of the UV radiation with wavelengths shorter than the threshold of the hydrogen Lyman continuum, and since the column density of the ISM is so high, the flux at these wavelengths get severly attenuated.

An economical way of storing the results of model calculations is to tabulate the level populations N_{nl} for a representative set of terms. Effective recombination coefficients and emissivities can then be determined for any transition originating on one of these terms. Tables of level populations have been made and are available. They contain the necessary information for calculating effective recombination coefficients or line fluxes for many transitions, including all the UV lines. Some of these lines are important in fluorescence processes and in determining the ionization conditions in the gas.

The emission coefficient of a line, j_λ, is often expressed in terms of the effective recombination coefficient α_{eff}, defined by

$$4\pi j_\lambda = N_{nl} A_{nl,n'l'} \frac{hc}{\lambda} = N_e N_i \alpha_{eff} \frac{hc}{\lambda}.$$

Observed line fluxes, very often only expressed relative to another line, will be written as $F(\lambda)$, where λ in Å is the wavelength of the line under consideration. If we set $j_{eff}\ (\lambda) = \alpha_{eff} \frac{hc}{\lambda}$, the measured flux of a line is obtained from

$$F(\lambda) = N_e N_i\, j_{eff}(\lambda) \times \frac{V}{4\pi R^2}$$

where V is the volume of the emitting gas and R its distance from the observer. This quantity is convenient in that it can be used to determine abundances directly from observed integrated line fluxes. Henceforth j_{eff}

shall be referred to as the effective flux of a line (although the term *effective emission coefficient* might be more appropriate). Abundances are often expressed relative to $N(H^+)$ which is determined from the measured Hβ flux in case B conditions. The abundance of a species X is given by

$$\frac{N(X)}{N(HII)} = \frac{j_{eff}(H\beta)F(X)}{j_{eff}(X)F(H\beta)}$$

where j_{eff} are our temperature-dependent modelled values.

We first briefly discuss the HI capture-cascade models and their limitation and then go on to look at the C^3 results for hydrogen in low temperature conditions. Extensive results for the capture-cascade models are not necessary since we provide detailed C^3 model calculations. The results for HeI are discussed in some detail because they should be quite accurate and are used as a testing ground for the other complex atom calculations. Finally, we consider the modelled spectra of the complex atoms CNO in three stages of ionization. In most of the tables we present results for electron densities N_e of 10^6, 10^4, and 10^2 cm^{-3}, and temperatures T of 2500, 1250, 625, and 312 K. This makes it possible to determine trends in the data as either N_e or T is varied.

7.2 Hydrogen

Our n-method calculations are similar to those of Brocklehurst (1970) and Burgess & Summers (1976), and the nl-method to those of Brocklehurst (1971) and Summers (1977). We have compared our results with all of the above and also with Hummer & Storey (1987). In the calculation of b_n and b_{nl} for hydrogenic ions the rate coefficients for radiative processes are known extremely well. Numerical inaccuracy might creep in at large values of n but this is still likely to give errors less than 1%. The rates for collisional processes, however, are very poorly known and introduce uncertainties of up to a few percent in our values of b_n and b_{nl}. Fortunately most of the transitions producing photons in the visible range are not too sensitive to these uncertainties since Δb_n and Δb_{nl} are largest around n = 50.

Results using the n-method have been published by Brocklehurst (1970) for case B and Burgess & Summers (1976) for case A and case B over restricted ranges. Hummer & Storey (1987) calculate b_n factors to use in their case B nl calculations, but only quote percentage deviations from Brocklehurst (1970). Our method is very similar to theirs, differing mainly in the values we used for some collisional terms and in the pivotal points used in the matrix condensation scheme. Using a combination n/nl method Summers (1977) has calculated b_{nl} for $T = 10^4$ and 2×10^4 at N_e of 10^4 and 10^5 in case B conditions. These latter results are slightly larger than his pure n-method calculations. The model of Burgess & Summers contains a

weak blackbody background radiation which affects the low n levels via the inclusion of stimulated and absorption terms in the equilibrium equations.

Brocklehurst (1970) has presented results for $\log N_e$ between 1.0 and 5.0 at temperatures from 2500 K – 2×10^4 K. At T = 2500 K our results differ most when $N_e = 10^5$ with errors of 6.5%. When $N_e = 10^1$ the maximum error is < 3%. At $T = 2 \times 10^4$ K the maximum error is 0.7% for $N_e = 10^5$ dropping to 0.3% when $N_e = 10^1$. The value of n at which the maximum deviation occured shifted downwards as N_e increased. Our b_n factors for case B, like those of Hummer & Storey, are bigger than those of Summers (1977) by $\sim 2\%$. The agreement between our results and those of Hummer & Storey was excellent. The variations can all be attributed to the different expressions used for the collisional reaction rates.

Intensity ratios for the HI Lyman, Balmer, and Paschen lines relative to $H\beta$ for n-method and nl-method capture-cascade models are presented in Table 7.1. Both case A and case B conditions are considered. These results serve mainly to illustrate the large differences between these two methods. All of these values can be scaled in T/Z^2 to apply to any other hydrogenic ion, where T is the gas temperature and Z the ionic charge. Extensive listings of nl-method calculations have been produced by Martin (1988). The nl-method is essentially a zero-density model since no collisional effects are included in the formulation. As such these results should be applicable to the low temperature, low density plasmas found in cool nova shells. However, there is a significant difference between the n-method and nl-method results, and we need to know under what conditions each model is applicable.

Table 7.1a: Capture-cascade n-method models for case A and case B. The intensities are all listed relative to Hβ. The first row of each series is the total integrated continuum flux.

	CASE A N-METHOD				CASE B N-METHOD			
	Temperature in K							
	2500	1250	625	312.5	2500	1250	625	312.5
LINES TO LEVEL 1								
1	41.074	35.199	30.876	27.599				
2	39.078	37.783	37.051	36.702				
3	14.501	14.229	14.073	13.998				
4	7.593	7.593	7.593	7.593				
5	4.652	4.748	4.811	4.851				
6	3.122	3.250	3.341	3.402				
7	2.224	2.360	2.463	2.534				
8	1.650	1.788	1.892	1.967				
9	1.268	1.393	1.500	1.575				
10	0.996	1.113	1.216	1.291				
LINES TO LEVEL 2								
2	5.438	4.743	4.200	3.772	2.337	1.989	1.716	1.504
3	1.792	1.759	1.739	1.730	2.574	2.542	2.521	2.507
4	1.000	1.000	1.000	1.000	1.000	1.000	1.000	1.000
5	0.624	0.637	0.646	0.651	0.530	0.540	0.546	0.549
6	0.422	0.440	0.452	0.460	0.327	0.338	0.346	0.351
7	0.302	0.321	0.335	0.344	0.219	0.231	0.240	0.245
8	0.225	0.244	0.258	0.268	0.156	0.168	0.176	0.182
9	0.173	0.190	0.205	0.215	0.116	0.127	0.135	0.140
10	0.136	0.152	0.166	0.176	0.089	0.098	0.106	0.112
LINES TO LEVEL 3								
3	1.576	1.411	1.268	1.148	0.678	0.591	0.518	0.457
4	0.277	0.277	0.277	0.277	0.277	0.277	0.277	0.277
5	0.184	0.188	0.190	0.192	0.156	0.159	0.161	0.162
6	0.127	0.132	0.136	0.138	0.098	0.101	0.104	0.105
7	0.091	0.097	0.101	0.104	0.066	0.070	0.072	0.074
8	0.068	0.074	0.078	0.081	0.047	0.051	0.053	0.055
9	0.053	0.058	0.062	0.065	0.035	0.039	0.041	0.043
10	0.042	0.046	0.051	0.054	0.027	0.030	0.032	0.034

Table 7.1b: Capture-cascade nl-method models for case A and case B. The intensities are all listed relative to Hβ. The first row of each series is the total integrated continuum flux.

	CASE A NL-METHOD				CASE B NL-METHOD			
	Temperature in K							
	2500	1250	625	312.5	2500	1250	625	312.5
LINES TO LEVEL 1								
1	26.447	22.588	20.110	18.465				
2	33.267	34.669	36.917	39.766				
3	6.058	5.598	5.278	5.033				
4	2.233	2.010	1.854	1.740				
5	1.094	0.980	0.898	0.840				
6	0.627	0.561	0.514	0.480				
7	0.395	0.355	0.326	0.305				
8	0.267	0.240	0.221	0.207				
9	0.190	0.171	0.158	0.149				
LINES TO LEVEL 2								
2	3.501	3.044	2.735	2.524	2.534	2.265	2.075	1.945
3	3.478	3.922	4.467	5.095	3.365	3.722	4.155	4.665
4	1.000	1.000	1.000	1.000	1.000	1.000	1.000	1.000
5	0.442	0.424	0.409	0.397	0.444	0.431	0.419	0.408
6	0.239	0.227	0.216	0.207	0.241	0.231	0.223	0.215
7	0.146	0.138	0.130	0.124	0.147	0.141	0.135	0.130
8	0.096	0.091	0.086	0.082	0.097	0.093	0.089	0.086
9	0.067	0.063	0.060	0.057	0.068	0.065	0.062	0.060
LINES TO LEVEL 3								
3	1.015	0.905	0.826	0.768	0.735	0.674	0.626	0.592
4	0.696	0.853	1.044	1.264	0.531	0.660	0.817	0.997
5	0.266	0.290	0.312	0.330	0.209	0.231	0.251	0.268
6	0.134	0.140	0.143	0.145	0.107	0.113	0.117	0.119
7	0.079	0.080	0.080	0.080	0.063	0.065	0.066	0.067
8	0.051	0.051	0.051	0.050	0.041	0.042	0.042	0.042
9	0.035	0.035	0.034	0.034	0.028	0.029	0.029	0.028

The n-method models implicitly contain l-changing collisions because the angular momenta of the valence electrons are assumed to be statistically distributed between the energy-degenerate orbitals. Pengelly & Seaton (1964) showed that these l-changing collisions are a function of 1/v where v is the relative velocity between the target and incident particle. Hence, they are caused predominantly by the slow moving ionic components of the gas. However, the importance of these collisions in determining the equilibrium populations in an orbital depend on the abundances of the colliding particles and on the total spontaneous transition rate out of the orbital. For small principal quantum numbers ionic densities have to be very large for collisions to be important. In low density plasmas the equilibrium populations of the lower levels, with the exception of the metastable 2s level in HI, are determined almost exclusively by the spontaneous transition rates.

Energy-changing collisions shift valence electrons from one level to another and are produced predominantly by collisions of atoms with electrons. These collisions, whose rates are smaller than the l-changing rates, tend to set up Boltzmann distributions between the various levels. For large principal quantum numbers neither an nl- nor an n-method model is appropriate, although usually lines from these levels are so weak that they cannot be detected anyway. Our C^3 model has been used to investigate all of these collisional effects quantitatively.

Table 7.2 contains the flux ratios calculated using our C^3 model for the Lyman (case A only), Balmer and Paschen series, all expressed relative to the value for Hβ. These models were run assuming a pure hydrogen plasma, i.e. $N_e = N_H$. Tests have shown that altering the electron density by 50% leads to line flux changes of less than two percent. Effective fluxes for the Hβ line of each model are also listed in Table 7.2. Results for higher temperatures and higher densities can be found in Brocklehurst (1971) and Hummer & Storey (1987).

Comparison of Tables 7.1 and 7.2 show that the collisional processes produce a smooth change in the fluxes as the density is increased from the zero-density nl-method capture-cascade model. The effects of collisions on the level populations, and hence also the effective flux, increase rapidly as n increases. We can see from the tables that increasing the density flattens the Balmer decrement, although even at $N_e = 10^6$ cm^{-3} the modelled decrement is still much steeper than the n-method decrement. However, nova shells are reported to have large abundances of heavy ions and their effect on the hydrogen spectrum has not been considered yet.

Table 7.2a: Fluxes of HI lines relative to Hβ calculated using a capture-collision-cascade model (upper) and the effective flux [erg cm^3/s] of the Hβ line (lower). The first row of each series is the total integrated continuum flux. An electron density of 10^6 cm^{-3} was used, and $N_e = N_H$.

	CASE A				CASE B			
	Temperature in K							
	2500	1250	625	312.5	2500	1250	625	312.5
LINES TO LEVEL 1								
1	25.646	20.341	15.665	11.204				
2	36.211	35.646	35.273	0.000				
3	6.434	6.102	5.912	5.843				
4	2.406	2.248	2.157	2.124				
5	1.191	1.110	1.065	1.051				
6	0.700	0.658	0.636	0.632				
7	0.471	0.449	0.441	0.446				
8	0.353	0.345	0.347	0.359				
9	0.289	0.293	0.306	0.328				
10	0.255	0.270	0.295	0.323				
LINES TO LEVEL 2								
2	3.395	2.741	2.131	1.531	2.307	1.866	1.432	0.998
3	3.021	3.161	3.258	3.288	3.040	3.151	3.227	3.257
4	1.000	1.000	1.000	1.000	1.000	1.000	1.000	1.000
5	0.459	0.451	0.446	0.445	0.458	0.452	0.448	0.447
6	0.253	0.248	0.245	0.244	0.253	0.249	0.248	0.248
7	0.158	0.155	0.154	0.156	0.159	0.158	0.158	0.159
8	0.107	0.107	0.109	0.111	0.110	0.111	0.113	0.116
9	0.079	0.081	0.085	0.088	0.082	0.085	0.088	0.092
10	0.063	0.067	0.071	0.075	0.065	0.069	0.075	0.079
LINES TO LEVEL 3								
3	0.984	0.815	0.643	0.466	0.669	0.555	0.432	0.304
4	0.535	0.586	0.620	0.632	0.414	0.457	0.486	0.497
5	0.241	0.254	0.262	0.265	0.189	0.201	0.208	0.211
6	0.129	0.134	0.137	0.138	0.102	0.107	0.110	0.111
7	0.078	0.080	0.082	0.083	0.062	0.065	0.067	0.068
8	0.051	0.053	0.055	0.056	0.042	0.044	0.046	0.047
9	0.036	0.038	0.040	0.041	0.030	0.032	0.034	0.036
10	0.027	0.029	0.031	0.032	0.023	0.025	0.027	0.029

	Temperature in K			
	2500	1250	625	312.5
CASE A	2.768-25	4.961-25	9.134-25	1.809-24
CASE B	4.074-25	7.287-25	1.359-24	2.775-24

Table 7.2b: Same as Table 7.2a but for $N_e = 10^4$ cm^{-3}.

	CASE A				CASE B			
	Temperature in K							
	2500	1250	625	312.5	2500	1250	625	312.5
LINES TO LEVEL 1								
1	26.126	21.692	18.202	15.019				
2	36.429	36.275	36.403	0.000				
3	6.182	5.767	5.485	5.310				
4	2.289	2.089	1.953	1.868				
5	1.123	1.019	0.948	0.903				
6	0.642	0.583	0.542	0.516				
7	0.405	0.369	0.343	0.327				
8	0.274	0.250	0.234	0.224				
9	0.195	0.179	0.168	0.161				
10	0.145	0.134	0.127	0.122				
LINES TO LEVEL 2								
2	3.459	2.923	2.476	2.053	2.455	2.113	1.804	1.491
3	3.235	3.500	3.748	3.941	3.196	3.410	3.613	3.771
4	1.000	1.000	1.000	1.000	1.000	1.000	1.000	1.000
5	0.448	0.435	0.424	0.417	0.449	0.439	0.430	0.424
6	0.244	0.234	0.226	0.221	0.245	0.237	0.231	0.226
7	0.150	0.143	0.137	0.134	0.150	0.144	0.140	0.137
8	0.099	0.094	0.091	0.088	0.099	0.096	0.093	0.091
9	0.069	0.066	0.064	0.062	0.069	0.067	0.065	0.064
10	0.051	0.049	0.047	0.046	0.051	0.049	0.048	0.047
LINES TO LEVEL 3								
3	1.003	0.869	0.747	0.625	0.712	0.629	0.544	0.454
4	0.611	0.705	0.793	0.861	0.471	0.550	0.624	0.681
5	0.256	0.276	0.291	0.301	0.201	0.219	0.233	0.243
6	0.133	0.138	0.142	0.144	0.105	0.111	0.115	0.117
7	0.079	0.081	0.081	0.082	0.063	0.065	0.067	0.067
8	0.051	0.052	0.052	0.052	0.041	0.042	0.043	0.043
9	0.035	0.035	0.036	0.035	0.028	0.029	0.029	0.029
10	0.025	0.026	0.026	0.026	0.020	0.021	0.021	0.021

	Temperature in K			
	2500	1250	625	312.5
CASE A	2.717-25	4.652-25	7.861-25	1.349-24
CASE B	3.828-25	6.434-25	1.079-24	1.858-24

Table 7.2c: Same as Table 7.2a but for $N_e = 10^2$ cm^{-3}.

	CASE A				CASE B			
	Temperature in K							
	2500	1250	625	312.5	2500	1250	625	312.5
LINES TO LEVEL 1								
1	26.378	22.321	19.434	17.114				
2	36.809	37.098	37.955	0.000				
3	6.108	5.666	5.353	5.139				
4	2.255	2.043	1.892	1.788				
5	1.106	0.996	0.917	0.864				
6	0.633	0.570	0.525	0.494				
7	0.400	0.360	0.332	0.313				
8	0.270	0.244	0.226	0.213				
9	0.191	0.174	0.161	0.153				
10	0.141	0.129	0.120	0.114				
LINES TO LEVEL 2								
2	3.492	3.008	2.644	2.339	2.511	2.216	1.979	1.765
3	3.342	3.692	4.072	4.444	3.272	3.554	3.864	4.170
4	1.000	1.000	1.000	1.000	1.000	1.000	1.000	1.000
5	0.444	0.429	0.416	0.405	0.447	0.435	0.424	0.415
6	0.241	0.230	0.220	0.212	0.243	0.234	0.226	0.219
7	0.147	0.140	0.133	0.128	0.148	0.142	0.137	0.133
8	0.097	0.092	0.088	0.084	0.098	0.094	0.090	0.088
9	0.068	0.064	0.061	0.059	0.068	0.066	0.063	0.061
10	0.050	0.047	0.045	0.043	0.050	0.048	0.046	0.045
LINES TO LEVEL 3								
3	1.012	0.895	0.798	0.712	0.728	0.659	0.597	0.537
4	0.648	0.772	0.906	1.037	0.498	0.602	0.713	0.822
5	0.262	0.284	0.303	0.318	0.205	0.226	0.244	0.257
6	0.134	0.139	0.143	0.145	0.106	0.112	0.116	0.119
7	0.079	0.080	0.081	0.081	0.063	0.065	0.067	0.067
8	0.051	0.051	0.051	0.051	0.041	0.042	0.042	0.042
9	0.035	0.035	0.035	0.034	0.028	0.029	0.029	0.029
10	0.025	0.025	0.025	0.025	0.020	0.021	0.021	0.021

	Temperature in K			
	2500	1250	625	312.5
CASE A	2.691-25	4.521-25	7.363-25	1.184-24
CASE B	3.743-25	6.137-25	9.837-25	1.569-24

The l-changing collision rate for a target ion increases as the charge and mass of the incident particle increase. A doubly ionized atom is therefore more effective than a proton, for example, in producing an angular momentum-changing transition. Increasing the ionic density or state of ionization also increases the electron density which, in turn, enhances the effects of processes involving electrons. We pointed out earlier that the level populations, particularly for the lower principal quantum numbers, are insensitive to changes in the electron density. Similarly, the mass and charge of the incident particle do not produce large changes in the l-changing collision rates so that large abundances of heavy ions are needed to produce any major changes in the HI spectrum . To illustrate these points we have run the model with the following parameters; $N_e = 10^6$, $N_H = 10^6$, $N_I = 10^5$, $m_I = 14m_p$ and $Z_I = 2$, where m_I and m_p are the ion and proton mass respectively and Z_I is the ionic charge of the incident ion. The ions contribute to the model only through their effect on the angular momentum-changing collision rates. The results are shown in Table 7.3. Once again the higher levels are most affected by these changes, but even so the differences amount to only a few percent.

The case A results for HI should be very accurate for an optically thin plasma. The collision rates have the largest uncertainties of all the atomic rates but, as we have discussed, the model is not very sensitive to changes in these values at the densities that are of interest to us. Radiative rates for Lyman transitions are larger than for any other series and they, therefore, also have the largest radiative absorption cross sections. Furthermore, a large fraction of HI is in the groundstate compared to the exited states. Lyman lines should become optically thick before any substantial absorption occurs to lines in other series. Case B calculations are supposed to apply to HI regions which have optically thick Lyman lines but use the additional approximation that the Lyman photons are absorbed "on-the-spot". These calculations are used extensively in the literature, although a proper radiative transfer treatment which includes diffuse and stellar radiation fields would be far more suitable. In low density plasmas there are further complications in that the metastable 2s level can build up a large population because collisional processes are not very efficient at emptying it. This could lead to substantial radiative absorption of the Balmer lines.

Table 7.3: Relative intensities of the Lyman, Balmer, and Paschen series of HI for a plasma with $N_e = 10^6$ cm^{-3}, $N_H = 10^6$ cm^{-3}, and $N_I = 10^5$ cm^{-3} where the heavy atoms are in a doubly ionized state.

	CASE A				CASE B			
	Temperature in K							
	2500	1250	625	312.5	2500	1250	625	312.5
LINES TO LEVEL 1								
1	25.817	20.496	15.808	11.322				
2	36.231	35.635	35.232	0.000				
3	6.481	6.161	5.981	5.922				
4	2.429	2.277	2.192	2.164				
5	1.207	1.130	1.089	1.077				
6	0.717	0.678	0.659	0.658				
7	0.491	0.472	0.467	0.475				
8	0.376	0.372	0.379	0.396				
9	0.316	0.327	0.347	0.373				
10	0.287	0.311	0.344	0.372				
LINES TO LEVEL 2								
2	3.418	2.762	2.150	1.548	2.305	1.863	1.429	0.995
3	2.993	3.121	3.205	3.228	3.019	3.120	3.186	3.209
4	1.000	1.000	1.000	1.000	1.000	1.000	1.000	1.000
5	0.461	0.454	0.449	0.448	0.459	0.454	0.451	0.450
6	0.255	0.250	0.248	0.248	0.255	0.252	0.251	0.252
7	0.160	0.158	0.158	0.160	0.161	0.161	0.162	0.164
8	0.110	0.111	0.114	0.117	0.113	0.115	0.118	0.121
9	0.082	0.086	0.090	0.094	0.085	0.089	0.094	0.098
10	0.066	0.071	0.077	0.079	0.068	0.074	0.080	0.084
LINES TO LEVEL 3								
3	0.991	0.821	0.649	0.471	0.668	0.554	0.431	0.303
4	0.524	0.571	0.602	0.610	0.407	0.446	0.471	0.480
5	0.239	0.251	0.258	0.260	0.187	0.198	0.205	0.207
6	0.128	0.133	0.136	0.137	0.102	0.106	0.109	0.110
7	0.078	0.080	0.082	0.083	0.063	0.065	0.067	0.069
8	0.052	0.054	0.056	0.057	0.042	0.045	0.047	0.048
9	0.037	0.039	0.041	0.042	0.031	0.033	0.035	0.037
10	0.028	0.030	0.032	0.033	0.024	0.026	0.029	0.030

	Temperature in K			
	2500	1250	625	312.5
CASE A	2.750-25	4.924-25	9.052-25	1.790-24
CASE B	4.078-25	7.301-25	1.362-24	2.783-24

7.3 Helium

We have listed relative fluxes of some of the strongest, astronomically important recombination lines of HeI with respect to F(4472) in Table 7.4. Effective fluxes of the λ4472 line for the models in Table 7.4 are listed in Table 7.5. In Table 7.6 we have listed perturbative corrections to the fluxes of some of the lines with upper state $n \leq 3$, once again relative to F(4472). These corrections arise from collisional excitations out of 2^3S and into the $n = 3$ levels. Below 2500 K the collisional rate becomes too small to have any noticeable effect. Since they depend critically on the population of the metastable level and can be affected by external conditions, we have not included them directly into Table 7.4. If, for example, a suitable ionizing source was present, the 2^3S population could be reduced sufficiently that the collisional excitations become insignificant even at high temperatures. The HeI Lyman lines, even though they have much larger fluxes than the listed lines, can ionize HI and, therefore, will most probably be scattered to undetectable limits by the ISM. They are of no observational interest, although the diffuse radiation they produce can influence the ionization structure within the nebula. We used a mixture similar to that of Brocklehurst (1972), namely a plasma consisting of electrons and singly ionized hydrogen and helium only, with abundances of $N_{HII} = 0.9N_e$ and $N_{HeII} = 0.1N_e$. The inclusion of ions of CNO in the plasma will mainly affect the angular momentum collision rates, but the level populations are not very sensitive to changes in these coefficients. The results presented should apply satisfactorily to the interpretation of nova shell spectra.

The model calculations of Brocklehurst (1972) are regarded as the definitive treatment for HeI (Osterbrock 1974) and so were used for comparison with our computations. We expect some differences between our results because we have treated more levels, included more collision terms and added the process of collisional ionization. Also, the various atomic rates have been calculated using slightly different algorithms. In some instances the Coulomb approximation algorithms are very sensitive to the effective principal quantum n that is used, and significantly different A-values can be generated from small changes in n. The non-degenerate nature of the l-levels leads (in principle) to a set of n Rydberg series per principal quantum number n. These series are much more sensitive to the rates of the atomic processes than the Rydberg series of HI because the latter rates are averages over the l-levels. Brocklehurst tabulates the effective recombination coefficients, α_{eff}, for the reference lines λ4472.7 (triplets) and λ4923.2 (singlets) but only relative intensities with respect to these for all the other lines. Differences in the α_{eff} of the reference lines between Brocklehurst's results and ours increase as N_e increases. At $N_e = 10^6$ cm^{-3} differences of $\sim 3\%$ were found. Brocklehurst (1972) listed relative intensities for 2P – nS, 2S – nP and 2P – nD series for both triplets and singlets. All series except 2^3P – n^3S had deviations

of < 3%, with the exception of one or two lines which had deviations of $\sim$ 7%. These differences were present at all temperatures and densities and are most probably the result of differences between the values used for the spontaneous transition rate. The 2^3P - n^3S series had differences of 50% for n = 3, decreasing to $\sim$ 15 - 10% as n increased. This was a source of grave concern considering the excellent agreement found for all the other series. We checked the capture-cascade results of Robbins (1968, 1970) and Robbins & Robinson (1971) and found that our results agreed with theirs to within a few percent. Our results have been carefully checked and we feel confident that they are correct. This points to an error in Brocklehurst's calculations. We ran tests on our model to see if a possible source of error could be identified. We found that we could reproduce Brocklehurst's results to within a couple of percent if, in populating level n^3S, we left out the transition $n^3P \rightarrow n^3S$. This omission has a small effect on the level populations of other l shells.

Table 7.4a: Relative fluxes for the strongest lines in the HeI spectrum with wavelengths above the hydrogen ionization limit. The model used 10% HeII and 90% HII by number and an electron densities of 10^6 cm^{-3}. The columns, from left to right, are the n and l quantum numbers of the lower and upper levels, the multiplicity M with B representing singlets in case B conditions, the wavelength in Angstroms, and the fluxes for temperatures from 20,000 K to 312.5 K as listed.

					λ	Temperature in K						
n_l	l_l	n_u	l_u	M	[Å]	20000	10000	5000	2500	1250	625	312.5
2	0	2	1	3	10830	73.106	39.328	15.918	5.881	3.919	3.894	3.921
2	1	3	2	3	5876	2.462	2.650	2.881	3.129	3.372	3.553	3.685
2	0	3	1	3	3889	2.886	2.146	1.713	1.462	1.319	1.243	1.204
2	1	3	2	B	6681	0.697	0.759	0.831	0.906	0.980	1.032	1.075
2	1	4	2	3	4472	1.000	1.000	1.000	1.000	1.000	1.000	1.000
2	1	3	2	1	6681	0.671	0.733	0.802	0.869	0.928	0.957	0.974
3	2	4	3	3	18686	0.303	0.352	0.417	0.492	0.570	0.632	0.687
2	0	2	1	B	20581	1.654	1.264	0.846	0.645	0.621	0.628	0.637
2	0	4	1	3	3188	1.174	0.927	0.757	0.643	0.566	0.517	0.484
2	1	5	2	3	4027	0.509	0.487	0.467	0.450	0.436	0.426	0.419
2	0	3	1	B	5017	0.688	0.586	0.511	0.457	0.420	0.393	0.376
2	1	4	2	B	4923	0.267	0.271	0.273	0.275	0.276	0.277	0.278
2	1	4	2	1	4923	0.257	0.261	0.264	0.264	0.262	0.258	0.253
3	2	5	3	3	12785	0.138	0.155	0.174	0.194	0.213	0.228	0.240
3	2	4	3	B	18696	0.101	0.117	0.138	0.163	0.189	0.209	0.229
2	0	5	1	3	2945	0.557	0.437	0.355	0.299	0.262	0.238	0.222
2	1	3	0	3	7067	0.661	0.463	0.352	0.288	0.250	0.229	0.215
2	1	6	2	3	3820	0.286	0.267	0.251	0.237	0.226	0.219	0.214
3	2	4	3	1	18696	0.098	0.113	0.134	0.156	0.179	0.193	0.206
4	3	5	4	3	40512	0.060	0.073	0.091	0.114	0.139	0.159	0.176

Table 7.4b: Same as Table 7.4a but for $N_e = 10^4$ cm^{-3}.

					λ	Temperature in K						
n_l	l_l	n_u	l_u	M	[Å]	20000	10000	5000	2500	1250	625	312.5
2	0	2	1	3	10830	62.025	31.084	11.420	4.643	3.968	4.012	4.074
2	1	3	2	3	5876	2.476	2.680	2.935	3.232	3.553	3.860	4.066
2	0	3	1	3	3889	2.873	2.128	1.689	1.429	1.274	1.179	1.122
2	1	3	2	B	6681	0.700	0.767	0.846	0.936	1.031	1.123	1.185
2	1	4	2	3	4472	1.000	1.000	1.000	1.000	1.000	1.000	1.000
2	1	3	2	1	6681	0.682	0.749	0.828	0.915	1.004	1.085	1.127
3	2	4	3	3	18686	0.308	0.362	0.434	0.524	0.627	0.731	0.812
2	0	2	1	B	20581	1.412	1.075	0.754	0.633	0.632	0.648	0.665
2	0	4	1	3	3188	1.168	0.919	0.747	0.632	0.554	0.502	0.467
2	1	5	2	3	4027	0.508	0.486	0.465	0.447	0.430	0.416	0.407
2	0	3	1	B	5017	0.685	0.582	0.506	0.451	0.412	0.385	0.366
2	1	4	2	B	4923	0.267	0.270	0.273	0.275	0.276	0.277	0.277
2	1	4	2	1	4923	0.259	0.263	0.266	0.268	0.269	0.269	0.266
3	2	5	3	3	12785	0.139	0.156	0.177	0.199	0.221	0.240	0.255
3	2	4	3	B	18696	0.102	0.120	0.144	0.174	0.208	0.242	0.269
2	0	5	1	3	2945	0.554	0.433	0.350	0.293	0.256	0.231	0.215
2	1	3	0	3	7067	0.662	0.464	0.351	0.286	0.247	0.224	0.211
2	1	6	2	3	3820	0.285	0.266	0.249	0.235	0.223	0.213	0.206
3	2	4	3	1	18696	0.101	0.118	0.141	0.170	0.202	0.234	0.255
4	3	5	4	3	40512	0.062	0.076	0.098	0.126	0.160	0.197	0.225

Table 7.4c: Same as Table 7.4a but for $N_e = 10^2$ cm^{-3}.

					λ	Temperature in K						
n_l	l_l	n_u	l_u	M	[Å]	20000	10000	5000	2500	1250	625	312.5
2	0	2	1	3	10830	8.193	5.558	4.344	4.030	4.022	4.117	4.268
2	1	3	2	3	5876	2.484	2.695	2.968	3.290	3.658	4.050	4.405
2	0	3	1	3	3889	2.870	2.125	1.685	1.423	1.266	1.169	1.107
2	1	3	2	B	6681	0.703	0.771	0.856	0.952	1.062	1.177	1.282
2	1	4	2	3	4472	1.000	1.000	1.000	1.000	1.000	1.000	1.000
2	1	3	2	1	6681	0.687	0.757	0.842	0.937	1.045	1.156	1.251
3	2	4	3	3	18686	0.311	0.367	0.444	0.543	0.661	0.792	0.922
2	0	2	1	B	20581	0.753	0.679	0.639	0.630	0.641	0.665	0.696
2	0	4	1	3	3188	1.167	0.917	0.746	0.630	0.553	0.502	0.468
2	1	5	2	3	4027	0.508	0.485	0.465	0.445	0.428	0.414	0.403
2	0	3	1	B	5017	0.684	0.581	0.505	0.450	0.411	0.384	0.366
2	1	4	2	B	4923	0.266	0.270	0.273	0.274	0.276	0.276	0.277
2	1	4	2	1	4923	0.259	0.264	0.267	0.269	0.270	0.271	0.270
3	2	5	3	3	12785	0.139	0.157	0.178	0.201	0.223	0.243	0.260
3	2	4	3	B	18696	0.103	0.122	0.147	0.180	0.219	0.262	0.305
2	0	5	1	3	2945	0.553	0.432	0.349	0.293	0.255	0.231	0.215
2	1	3	0	3	7067	0.663	0.464	0.351	0.285	0.247	0.223	0.209
2	1	6	2	3	3820	0.285	0.266	0.249	0.234	0.222	0.211	0.204
3	2	4	3	1	18696	0.102	0.120	0.146	0.178	0.216	0.258	0.298
4	3	5	4	3	40512	0.063	0.078	0.102	0.133	0.174	0.222	0.271

Table 7.5: Effective flux (in units of erg cm^3/s) of the λ4472 line for the data in Table 7.4.

N_e cm^{-3}	Temperature in K						
	20000	10000	5000	2500	1250	625	312.5
10^6	2.930-26	6.133-26	1.198-25	2.224-25	4.039-25	7.475-25	1.512-24
10^4	2.923-26	6.090-26	1.176-25	2.126-25	3.667-25	6.171-25	1.044-24
10^2	2.922-26	6.081-26	1.170-25	2.102-25	3.570-25	5.830-25	9.313-25

We also tested the sensitivity of the model to a change in the recombination coefficients by running the codes using the values of α_{nl} tabulated by Robbins (1968, 1970). These values of α_{nl} were calculated using the tables of Peach (1967) rather than the QDM which we used. The relative intensities of these results were compared with our calculations and with those of Brocklehurst (1972). The differences found were much smaller than the differences between the recombination rates of the various models. This demonstrates that the calculated intensities are not particularly sensitive to the radiative recombination rates. The n = 3 level shows the largest sensitivity.

Table 7.6: Case A (upper) and Case B (lower) fluxes relative to λ4472 for lines produced by collisional excitation from the metastable levels. In all cases $N_{HeII} = 0.1N_e$.

λ Å	$N_e = 10^6$ cm^{-3} Temperature in K			$N_e = 10^4$ cm^{-3} Temperature in K			$N_e = 10^2$ cm^{-3} Temperature in K		
	20000	10000	5000	20000	10000	5000	20000	10000	5000
7067	1.590	0.606	0.062	1.378	0.473	0.038	0.098	0.021	0.001
7283	0.174	0.072	0.006	0.150	0.056	0.004	0.011	0.003	0.000
3889	1.603	0.497	0.034	1.388	0.388	0.021	0.099	0.017	0.001
5876	2.014	0.396	0.016	1.746	0.310	0.010	0.124	0.014	0.000
6681	0.178	0.052	0.003	0.152	0.040	0.002	0.011	0.002	0.000
5017	0.000	0.000	0.000	0.000	0.000	0.000	0.000	0.000	0.000
7067	1.594	0.607	0.062	1.378	0.473	0.038	0.098	0.021	0.001
7283	0.177	0.073	0.006	0.151	0.057	0.004	0.011	0.003	0.000
3889	1.606	0.498	0.034	1.388	0.388	0.021	0.099	0.017	0.001
5876	2.018	0.397	0.016	1.746	0.310	0.010	0.124	0.014	0.000
6681	0.181	0.053	0.003	0.152	0.040	0.002	0.011	0.002	0.000
5017	0.122	0.036	0.002	0.104	0.028	0.001	0.007	0.001	0.000

7.4 Complex Atoms

The model for complex atoms relies heavily on hydrogenic rates for its upper levels. Non-hydrogenic values have been used in the CNO calculations only for those terms for which empirical data were available. The accuracy of this approximation has been tested using helium data. In the HeI model described above we used extrapolated quantum defects for determining A-values with n > 20 and scaled recombination coefficients from n = 13 up to n = 50. By using empirical data up to some specific principal quantum number, n_s say, and hydrogenic values for all higher n, we can get some idea of the errors involved in applying the hydrogenic approximation. The HeI atomic rates most probably deviate less from hydrogenic values than those of other atoms so these uncertainties are really a lower limit to what can be achieved. In the models for HI and HeI rates for radiative processes can be calculated more accurately than in the models for complex atoms. Another source of error in our complex atom computations is the use of LS coupling. We have no way of determining the errors introduced by this approximation.

We ran helium models using $n_s = 12$ and $n_s = 6$, and compared the results with the data in Table 7.4. The n = 12 results deviated from the exact model by two percent at most. When $n_s = 6$ the triplet series had errors of less than 5%, but the singlet series errors were slightly larger. For complex atoms the uncertainties in the atomic rates are larger than for HeI. Errors of 10% – 20% could be expected in the effective fluxes, while even the relative fluxes might contain similar inaccuracies because of errors in the A-values.

The effective fluxes of some of the stronger and more important lines in the spectra of C, N and O in various stages of ionization are listed in Table 7.7. Only those lines with wavelengths longer than 1200Å have been listed, and then only the strongest lines from any particular wavelength band. Although these results necessarily contain larger uncertainties than the results for either HI or HeI, they should nevertheless provide some idea of the relative fluxes of lines that could be expected in recombination conditions. Dielectronic recombination contributions to the populations have not been included in any of these calculations but the importance of this process to the various lines will be discussed with the spectrum of each atom individually. In all cases we have used the dielectronic recombination coefficients determined by Nussbaumer & Storey (1984b). Note that there are also a number of strong lines that can arise from transitions between excited core configurations. We have not considered any of these lines unless tabulated A-values were available because our routines are unreliable when dealing with these configurations.

The fluxes we have determined are based on term values and are therefore multiplet averages. The lines in some multiplets span quite a large range of wavelengths. In high dispersion spectra most of these multiplets can be resolved but in objects such as nova shells which have a low surface-brightness

the resolution is limited to $\sim$ 10Å. Although the line flux distribution is not always correctly represented in our model, the total integrated line flux should be correct (subject to the accuracy of the A-value). We have assumed that the levels in each term are statistically populated. When the energy separation between the levels is small this approximation is often used because the inter-level collision rates are large. However, the collisional processes have to be faster than the spontaneous decay rates to allow for redistribution before decay. As we have no way of estimating these inter-level collision rates, however, we cannot check when this condition is valid. In the case of HI we showed that the n-method is inappropriate, specially for levels with small n and l. The same could be true for these atoms, particularly for the lower energy levels which have large A-values. Another possible source of error has been introduced by the exclusion of any processes involving groundstate or metastable levels. Besides optical depth effects, collisional excitation out of these terms can be important at higher temperatures. For HeI we have shown that collisional excitation from the 2^3S metastable level is not important below temperatures of $\sim$ 2500 K. This same condition should apply to the ions of C, N, and O, and so line fluxes should not have been seriously affected by the exclusion of these levels when the level populations were determined. The process of charge exchange can also populated excited levels and could prolduce line fluxes in disagreement with our recombination models.

The line fluxes of forbidden transitions out of the metastable levels can become quite large if no other processes are emptying the levels. We can set an upper limit on the flux of these lines by assuming that the only mechanism by which these metastable levels are depopulated is via a forbidden spontaneous transition. In our model we determined the filling rates for these levels, so it is a straight forward procedure to determine the maximum possible effective flux of these lines. The filling rates for the groundstate and metastable levels of CNO atoms in various stages of ionization are presented in Table 7.8. The filling rates as listed do not contain any contributions from forbidden transitions. The effective fluxes of the forbidden lines at a temperature of 625 K and $N_e = 10^2$ cm^{-3} are listed in Table 7.9. These parameters were chosen because they should most closely resemble the conditions believed to exist in nova shells. Many of these forbidden lines occur in multiplets and have fixed line flux ratios. We have only listed the stronger transition in the cases where the wavelength separation is large enough for these lines to be easily resolved. The A-values and the energy level data were taken from Mendoza (1983), who has also listed collision strengths. Collision rates for the lowest temperature listed were determined in each case. We found that the spontaneous transition rate is always larger than the collisional deexcitation rate provided $N_e \leq 10^4$ cm^{-3}. Even though many of the forbidden transitions cascade into the groundstate, they suffer less from radiative absorption than the allowed transitions because their radiative absorption cross sections are

much smaller than those of the allowed transitions.

Modelled spectra of neutral C, N and O emit their strongest fluxes in either the UV or near infrared, but have only weak lines in the optical band. Many of the UV lines with large fluxes have wavelengths longer than the HI ionization limit at $\lambda 912$, so that if these lines are present in astronomical plasmas they should not be excessively absorbed by the ISM. Of course, if the ISM contains large column densities of CNO along the line of sight to the nebulae, then lines produced by transitions to the groundstate are likely to be scattered out of the beam. Dielectronic recombination to all listed lines of the neutral atoms make insignificant contributions to the fluxes and can be ignored. The same is not true for the ground and metastable terms, however. The only neutral atom multiplet listed in Table 7.7 that shows any significant line dispersion is NI $\lambda 8694$. About two thirds of the flux is centered around $\lambda 8682$, the rest is above $\lambda 8700$.

CI : The strongest UV lines are all caused by transitions to the groundstate and are therefore susceptible to scattering. The IR line $\lambda 7089$ is the strongest line not involving the groundstate configuration. Intercombination transitions were iteratively included in this model but it was found that they made very little difference to the populations. The strongest forbidden transition produces $\lambda 9840$ radiation but is weaker than the allowed line $\lambda 7089$ and therefore is not a good indicator of the presence of CI. The largest and only significant dielectronic recombination rate is that to the metastable ^{1}D term whose filling rate is enhanced by $\sim$ 1% at 1250 K but by $\sim$ 25% at 2500 K.

NI : This spectrum is similar to CI in that all the strong UV lines are produced by cascades to the groundstate configuration while the strongest IR line $\lambda 8694$ is due to a transition between excited levels. The $\lambda 5201$ forbidden line is stronger than the $\lambda 1493$ line if the contribution from [NI] $\lambda 10405$ is included in the filling rate of $2p^2\ ^2$D. Even so, it has the largest optical flux in the NI spectrum. The multiplet consists of two lines separated by 3Å so it is unlikely that they will be resolved if the signal is weak (as in nova shell spectra). Dielectronic recombination is significant to both metastable levels, particularly $^2D^0$.

OI : This spectrum differs slightly from CI and NI in that the groundstate belongs to the lower multiplicitly (triplet) of the two polyads formed from the $^4S^0$ core. Lines of a higher multiplicity are usually stronger because of their larger statistical weights but, as in HeI, transitions to the groundstate dominate the spectrum even if this term belongs to the lower multiplicity. The strongest line, $\lambda 1026$, in the OI spectrum is due to a triplet transition to the groundstate but this wavelength cannot be detected by the present

generation of satellite detectors. The next line, λ7775, is due to a transition between quintet terms and is in an easily observable range for ground-based telescopes. The lower level of this cascade is metastable, though, so optical depth effects could limit the flux. Forbidden transitions between groundstate configurations of OI include the well known auroral lines λ6300, λ6363 and λ5577 which have singlet terms for their upper level. The auroral lines are usually difficult to identify in astronomical nebulae because of contamination by atmospheric emissions. There is also an intercombination line from $3s\ ^5S^0 \rightarrow 2p^4\ ^3P$ at λ1355, which is fed by λ7775 amongst others. This line will be the strongest in the spectrum by nearly an order of magnitude if no other factors come into play to influence the population of the metastable quintet term. The filling rate of the groundstate is increased by $\sim$ 10% at 2500 K due to dielectronic recombinations.

The singly ionized atoms CII, NII and OII produce their strongest line fluxes in the wavelength region shortward of the HI Lyman continuum edge and are hence of little observational value. However, a few UV lines longward of the 912Å limit are also produced, as well as a number of strong optical transitions. The effective fluxes of these optical lines are, typically, stronger than the neutral atom UV lines. The transitions producing these lines are generally between excited levels, so that they do not suffer self-absorption. There should be essentially no radiative absorption of these lines by the ISM, although extinction by dust is always possible.

CII : The CII doublet series produces only two usable lines in its spectrum, namely λ1335 and λ4268. The next lines above λ1200 in the recombination spectrum have significantly smaller fluxes. The dielectronic recombination rate to the upper level of the λ1335 transition exceeds the radiative recombination rate for T > 400 K (FWL), and increases rapidly as the temperature rises. The effective flux of λ1335 is, therefore, strongly dependent on the temperature. There are no important forbidden transitions in the CII doublet series, but there is an intercombination transition from the metastable $2p^2\ ^4P$ term to the groundstate with λ2363 emission. The groundstate filling rate is also substantially affected by dielectronic recombinations, both directly and via cascades from other levels.

We cannot use our models to get any quantitative line fluxes for CII quartets but we can use comparisons with other spectra to make some qualitative assessment of the spectrum. The intercombination line λ2326 should be one of the stronger lines because all quartet recombinations cascade to the metastable 2s2p term which is the upper level of the λ2326 transition. In the spectra of CII, NII, and OII 4f $\rightarrow$ 3d transitions are strong and we expect, therefore, the same in the CII quartet spectrum. In decreasing order of strength, we anticipate lines at λ3877, λ4076, and λ4373. Succesive cascades after the λ3877 transition give rise to lines at λ7119 and λ6786,

both of which should have larger fluxes than F(3877) because there are no alternative decay channels for the levels involved. Note, though, that the CII quartet polyad is formed from a CIII 2s2p $^3P^0$ core and if this species is not abundant in the plasma then quartet recombinations will be undetectable.

NII : This spectrum could have large uncertainties in its predicted fluxes because of the limited A-value data we had available for our model. There are a number of optical lines with strong effective fluxes, mostly formed by transitions within the triplet series. In practice the lines of these multiplets may be quite dispersed because many of the levels have large energy separations. In particular, the λ5681 multiplet has lines at λ5667, λ5676, λ5680, λ5686, and λ5711, while the λ4436 multiplet has about two thirds of its flux around λ4433, and the rest is at λ4442. Dielectronic recombination is not an important process for any of the NII lines of interest to us. The forbidden NII lines λ6584 and λ6548 are found in numerous astronomical plasmas. Normally they are formed by collisional excitation from the groundstate of NII but in a low temperature environment they could be formed entirely by recombination and cascades within the singlet series. Tables 7.7 and 7.8 show that the λ6584 forbidden line has a recombination effective flux comparable to that of λ5006. The λ6548 line has a flux about one third that of λ6584 but it is usually blended with Hα in nova shell spectra. Dielectronic recombination to the groundstate is significant, but to the metastable levels it is unimportant.

OII : The OII recombination spectrum contains a number of strong optical lines, but unfortunately many of them have large dispersions. The λ4653 multiplet has the largest effective flux but λ4076 has its lines spread over a much smaller wavelength range. The flux of λ4095 is distributed fairly evenly between lines at λ4088 and another set at λ4096, and likewise, λ4113 has equal concentrations at λ4105 and λ4120. The former line will be blended with Hδ if the resolution is low. The λ4294 multiplet has a peak emission at λ4304 but the rest of the flux is distributed between λ4295, λ4289, and λ4282. The strongest doublet line, λ4343, will be blended with Hγ in low resolution spectra. The [OII] λ3727 line is the strongest in the optical spectrum when formed by recombination in a low temperature environment. Its ubiquitous presence in nebulae, though, is, like the [NII] lines, due to collisional excitation. The filling rates of the metastable levels get significant contributions from dielectronic recombinations, particularly the $^2D^0$ term.

Doubly ionized atoms of CNO also have a number of strong UV and optical recombination lines in their spectra. Many of these lines are produced by transitions from upper levels with n = 4 or 5. Most of the flux from the recombination spectrum of these ions, however, is in the extreme-UV

band. Note that in Table 7.7 the L quantum numbers for the CIII and OIII transitions 5g → 4f have been left out. The reason for this is that we have used hydrogenic values for these terms and have summed over the degenerate L terms. In the case of NIII because of the ^{1}S core the L and l quantum numbers are the same.

CIII : The CIII spectrum will be identified best by the strong λ1923 line in the UV. There are also a number of optical lines in the spectrum but they coincide with lines of other atoms. The optical lines are λ4650 and λ4069 which could be confused with OII, although the relative fluxes are different, and λ3889 which would be blended with Hξ + HeI. There is only one groundstate term in CIII, namely $2s^2\ ^1$S, but the CIII triplet series terminates on $2s2p\ ^3P^0$ which is metastable. The intercombination transition from the triplet metastable level to the singlet groundstate has a wavelength of λ1909 and in pure recombination has a larger flux than λ1923.

NIII : A number of strong optical and UV lines are produced in the recombination spectrum of this ion. The λ4380 line is convenient to use for abundance determinations because it is unaffected by dielectronic recombination, fluorescence or optical depth effects. The λ4640 line, which is quite weak in pure recombination, is enhanced by all three of these processes in certain situations, and can become one of the stronger lines in an emission spectrum. NIII is isoelectronic to CII and, like CII, has a quartet series for which our algorithms produce unreliable calculations. There are no NIII doublet metastable levels and dielectronic recombination is not an important process for any of the listed NIII lines. However, many of the UV lines with wavelengths less than λ1200 do have large dielectronic recombination rates, as does the groundstate term at high temperatures.

OIII : The data set for OIII was limited to terms on or below n = 6 and extrapolations of the series did not seem reliable. Our algorithms require empirical term values up to n = 8 for calculations at temperatures of 312.5 K, so populations for this temperature were not determined. Extrapolations of the existing tables to 312.5 K should be more accurate than calculating coefficients based on extrapolated quantum defects. The OIII spectrum has a number of strong lines, all with very similar effective fluxes. The λ3763 line is the strongest and has the advantage of lying in the optical band so that it can be detected using ground-based telescopes. The [OIII] lines λ5006 and λ4959, like the NII and OII forbidden lines, are found in many astronomical nebulae. These two lines have relative fluxes of 3:1 and both originate on the $2p^2\ ^1$D level, their flux ratio being determined entirely by the A-values. Dielectronic recombination is not an important contributor to the filling rate

of the metastable levels, but it contributes about 10% to the groundstate filling rate at 2500 K. At 1250 K it has fallen to unimportant levels, though.

The population levels of the groundstate and metastable levels of these ions depends on the processes that are emptying them and at what rate this happens. We have compiled a list of filling rates for these levels, based entirely on the recombination model. No dielectronic recombination contributions are included, neither are the contributions of forbidden transtions from energetically higher metastable level. For example, the ^{1}D term of NII does not have any contribution from [NII] λ5756 transitions included in its filling rate, nor does the ^{3}P term have either λ3067 or λ6585 included in its filling rate. These results cover the usual range of temperatures and densities that are of interest to us and are listed in Table 7.8. Collisional excitations should be too small at these temperatures to affect the populations by collisional excitation but at densities above about 10^3 – 10^4 cm^{-3} collisional deexcitation empties most of the metastable levels faster than the forbidden decays do.

Table 7.7: Effective fluxes for some selected lines of the modelled spectra of carbon, nitrogen, and oxygen in the first three stages of ionization. In all cases $N_H = 0.9\times N_e$. The columns, from the left, are N_e, the multiplicity M = 2S +1, the n, l, and L quantum numbers of the upper state and the lower state, the wavelength of the transition in Angstroms, and the effective fluxes in erg cm^3/s for temperatures of 2500, 1250, 625, and 312.5 K.

CI

N_e								λ	Temperature in K			
cm^{-3}	M	n_u	l_u	L_u	n_l	l_l	L_l	Å	2500	1250	625	312.5
	3	3	0	1	2	1	1	1657	2.446-24	4.555-24	8.767-24	1.849-23
	3	3	2	2	2	1	1	1277	1.297-24	2.508-24	4.951-24	1.065-23
10^6	3	3	2	3	2	1	2	7089	6.737-25	1.299-24	2.564-24	5.515-24
	1	3	2	3	2	1	2	1463	4.496-25	8.821-25	1.758-24	3.809-24
	3	4	2	3	2	1	2	5088	3.702-25	6.611-25	1.226-24	2.503-24
	3	3	0	1	2	1	1	1657	2.344-24	4.165-24	7.295-24	1.289-23
	3	3	2	2	2	1	1	1277	1.263-24	2.350-24	4.256-24	7.650-24
10^4	3	3	2	3	2	1	2	7089	6.552-25	1.216-24	2.198-24	3.944-24
	1	3	2	3	2	1	2	1463	4.405-25	8.340-25	1.530-24	2.776-24
	3	4	2	3	2	1	2	5088	3.501-25	5.898-25	9.795-25	1.654-24
	3	3	0	1	2	1	1	1657	2.326-24	4.084-24	6.986-24	1.178-23
	3	3	2	2	2	1	1	1277	1.262-24	2.333-24	4.160-24	7.217-24
10^2	3	3	2	3	2	1	2	7089	6.547-25	1.207-24	2.146-24	3.720-24
	1	3	2	3	2	1	2	1463	4.415-25	8.310-25	1.503-24	2.637-24
	3	4	2	3	2	1	2	5088	3.449-25	5.710-25	9.169-25	1.455-24

NI

N_e								λ	Temperature in K			
cm^{-3}	M	n_u	l_u	L_u	n_l	l_l	L_l	Å	2500	1250	625	312.5
	4	3	0	1	2	1	0	1200	5.848-24	1.087-23	2.106-23	4.521-23
10^6	2	3	0	1	2	1	2	1493	5.437-25	1.211-24	5.559-24	3.065-22
	4	3	1	2	3	0	1	8694	4.570-25	8.557-25	1.661-24	3.523-24
	4	3	2	2	2	1	1	5927	3.783-25	7.368-25	1.475-24	3.182-24
	4	3	0	1	2	1	0	1200	5.628-24	1.004-23	1.767-23	3.189-23
10^4	2	3	0	1	2	1	2	1493	5.181-25	1.107-24	4.744-24	2.351-22
	4	3	1	2	3	0	1	8694	4.422-25	7.963-25	1.405-24	2.501-24
	4	3	2	2	2	1	1	5927	3.710-25	7.002-25	1.279-24	2.310-24
	4	3	0	1	2	1	0	1200	5.593-24	9.871-24	1.701-23	2.939-23
10^2	2	3	0	1	2	1	2	1493	5.128-25	1.083-24	4.533-24	2.148-22
	4	3	1	2	3	0	1	8694	4.402-25	7.853-25	1.359-24	2.321-24
	4	3	2	2	2	1	1	5927	3.717-25	6.972-25	1.255-24	2.194-24

OI

N_e cm^{-3}	M	n_u	l_u	L_u	n_l	l_l	L_l	λ Å	Temperature in K 2500	1250	625	312.5
	5	3	1	1	3	0	0	7775	9.299-25	1.792-24	3.321-24	7.287-24
10^6	5	3	2	2	3	1	1	9266	4.363-25	8.936-25	1.683-24	3.844-24
	3	3	0	0	2	1	1	1302	6.351-25	1.213-24	2.358-24	5.025-24
	5	4	2	2	3	1	1	6159	1.061-25	1.973-25	3.679-25	7.950-25
	5	3	1	1	3	0	0	7775	8.841-25	1.586-24	2.792-24	4.967-24
10^4	5	3	2	2	3	1	1	9266	4.192-25	7.942-25	1.460-24	2.674-24
	3	3	0	0	2	1	1	1302	6.166-25	1.137-24	2.054-24	3.710-24
	5	4	2	2	3	1	1	6159	9.892-26	1.710-25	2.898-25	5.010-25
	5	3	1	1	3	0	0	7775	8.761-25	1.554-24	2.675-24	4.529-24
10^2	5	3	2	2	3	1	1	9266	4.176-25	7.848-25	1.419-24	2.494-24
	3	3	0	0	2	1	1	1302	6.149-25	1.123-24	1.990-24	3.453-24
	5	4	2	2	3	1	1	6159	9.710-26	1.647-25	2.695-25	4.342-25

OII

N_e cm^{-3}	M	n_u	l_u	L_u	n_l	l_l	L_l	λ Å	Temperature in K 2500	1250	625	312.5
	4	3	1	2	3	0	1	4653	5.118-24	9.128-24	1.752-23	3.764-23
	4	3	2	3	3	1	2	4076	4.381-24	7.846-24	1.506-23	3.224-23
	4	4	3	4	3	2	3	4095	1.842-24	3.453-24	6.865-24	1.490-23
10^6	4	3	2	2	3	1	1	4113	2.198-24	3.937-24	7.564-24	1.621-23
	2	4	3	4	3	2	3	4343	8.518-25	1.600-24	3.189-24	6.839-24
	4	4	3	2	3	2	1	4295	8.037-25	1.507-24	3.000-24	6.512-24
	4	3	2	2	3	1	2	3868	9.095-25	1.630-24	3.130-24	6.707-24
	2	4	3	3	3	2	2	4608	5.387-25	1.012-24	2.017-24	4.324-24
	4	3	1	2	3	0	1	4653	4.928-24	8.409-24	1.430-23	2.443-23
	4	3	2	3	3	1	2	4076	4.237-24	7.281-24	1.241-23	2.109-23
	4	4	3	4	3	2	3	4095	1.864-24	3.428-24	6.106-24	1.053-23
10^4	4	3	2	2	3	1	1	4113	2.128-24	3.660-24	6.246-24	1.064-23
	2	4	3	4	3	2	3	4343	8.630-25	1.591-24	2.840-24	4.902-24
	4	4	3	2	3	2	1	4295	8.133-25	1.497-24	2.669-24	4.605-24
	4	3	2	2	3	1	2	3868	8.805-25	1.515-24	2.585-24	4.402-24
	2	4	3	3	3	2	2	4608	5.462-25	1.008-24	1.799-24	3.105-24
	4	3	1	2	3	0	1	4653	4.857-24	8.183-24	1.360-23	2.253-23
	4	3	2	3	3	1	2	4076	4.183-24	7.109-24	1.187-23	1.970-23
	4	4	3	4	3	2	3	4095	1.852-24	3.392-24	5.993-24	1.036-23
10^2	4	3	2	2	3	1	1	4113	2.099-24	3.572-24	5.970-24	9.925-24
	2	4	3	4	3	2	3	4343	8.576-25	1.576-24	2.790-24	4.831-24
	4	4	3	2	3	2	1	4295	8.083-25	1.482-24	2.620-24	4.533-24
	4	3	2	2	3	1	2	3868	8.688-25	1.478-24	2.471-24	4.107-24
	2	4	3	3	3	2	2	4608	5.429-25	9.978-25	1.768-24	3.062-24

CII

N_e cm^{-3}	M	n_u	l_u	L_u	n_l	l_l	L_l	λ Å	Temperature in K 2500	1250	625	312.5
	2	2	1	2	2	1	1	1335	2.442-23	3.579-23	5.353-23	8.381-23
10^6	2	4	3	3	3	2	2	4268	5.401-24	1.013-23	2.032-23	4.388-23
	2	2	1	2	2	1	2	1324	4.944-24	7.048-24	1.001-23	1.418-23
	2	2	1	2	2	1	1	1335	2.432-23	3.541-23	5.172-23	7.616-23
10^4	2	4	3	3	3	2	2	4268	5.482-24	1.014-23	1.814-23	3.127-23
	2	2	1	2	2	1	2	1324	4.944-24	7.048-24	1.001-23	1.418-23
	2	2	1	2	2	1	1	1335	2.427-23	3.523-23	5.117-23	7.456-23
10^2	2	4	3	3	3	2	2	4268	5.451-24	1.005-23	1.788-23	3.102-23
	2	2	1	2	2	1	2	1324	4.944-24	7.048-24	1.001-23	1.418-23

NII

N_e cm^{-3}	M	n_u	l_u	L_u	n_l	l_l	L_l	λ Å	Temperature in K 2500	1250	625	312.5
	3	3	1	2	3	0	1	5681	3.978-24	7.047-24	1.345-23	2.873-23
	3	3	2	3	3	1	2	5006	3.418-24	6.158-24	1.188-23	2.542-23
10^6	3	4	3	4	3	2	3	4042	2.087-24	3.911-24	7.779-24	1.666-23
	3	4	3	3	3	2	2	4243	1.358-24	2.548-24	5.072-24	1.087-23
	3	4	3	2	3	2	1	4436	8.519-25	1.600-24	3.187-24	6.826-24
	1	4	3	4	3	2	3	4544	6.100-25	1.146-24	2.283-24	4.891-24
	3	3	1	2	3	0	1	5681	3.826-24	6.479-24	1.096-23	1.867-23
	3	3	2	3	3	1	2	5006	3.317-24	5.744-24	9.838-24	1.677-23
10^4	3	4	3	4	3	2	3	4042	2.113-24	3.887-24	6.929-24	1.195-23
	3	4	3	3	3	2	2	4243	1.374-24	2.530-24	4.513-24	7.783-24
	3	4	3	2	3	2	1	4436	8.639-25	1.593-24	2.844-24	4.909-24
	1	4	3	4	3	2	3	4544	6.182-25	1.140-24	2.035-24	3.512-24
	3	3	1	2	3	0	1	5681	3.771-24	6.303-24	1.041-23	1.717-23
	3	3	2	3	3	1	2	5006	3.278-24	5.612-24	9.426-24	1.572-23
10^2	3	4	3	4	3	2	3	4042	2.100-24	3.847-24	6.803-24	1.176-23
	3	4	3	3	3	2	2	4243	1.366-24	2.504-24	4.430-24	7.662-24
	3	4	3	2	3	2	1	4436	8.588-25	1.578-24	2.795-24	4.839-24
	1	4	3	4	3	2	3	4544	6.144-25	1.129-24	2.001-24	3.461-24

CIII

N_e cm^{-3}	M	n_u	l_u	L_u	n_l	l_l	L_l	λ Å	Temperature in K 2500	1250	625	312.5
	3	4	3	3	3	2	2	1923	2.875-23	5.228-23	9.963-23	2.058-22
	1	4	3	3	3	2	2	2164	8.612-24	1.558-23	2.984-23	5.931-23
	3	5	3	3	3	2	2	1296	1.031-23	1.824-23	3.489-23	7.336-23
10^6	3	5	4		4	3		4069	8.105-24	1.499-23	2.848-23	5.400-23
	1	2	1	2	2	1	1	2298	4.873-24	7.070-24	1.048-23	1.622-23
	3	3	1	1	3	0	0	4650	3.568-24	5.799-24	1.046-23	2.141-23
	3	5	3	3	4	2	2	3888	1.219-24	2.158-24	4.126-24	8.676-24
	3	4	3	3	3	2	2	1923	2.898-23	5.172-23	9.021-23	1.483-22
	1	4	3	3	3	2	2	2164	8.663-24	1.547-23	2.694-23	4.430-23
	3	5	3	3	3	2	2	1296	9.582-24	1.582-23	2.638-23	4.566-23
10^4	3	5	4		4	3		4069	8.598-24	1.603-23	2.860-23	4.583-23
	1	2	1	2	2	1	1	2298	4.829-24	6.927-24	9.987-24	1.459-23
	3	3	1	1	3	0	0	4650	3.358-24	5.102-24	8.052-24	1.359-23
	3	5	3	3	4	2	2	3888	1.133-24	1.871-24	3.120-24	5.400-24
	3	4	3	3	3	2	2	1923	2.836-23	4.989-23	8.537-23	1.442-22
	1	4	3	3	3	2	2	2164	8.488-24	1.491-23	2.551-23	4.303-23
	3	5	3	3	3	2	2	1296	9.374-24	1.513-23	2.414-23	3.890-23
10^2	3	5	4		4	3		4069	8.432-24	1.554-23	2.751-23	4.744-23
	1	2	1	2	2	1	1	2298	4.819-24	6.889-24	9.862-24	1.417-23
	3	3	1	1	3	0	0	4650	3.304-24	4.920-24	7.447-24	1.158-23
	3	5	3	3	4	2	2	3888	1.109-24	1.789-24	2.855-24	4.601-24

OIII

N_e cm^{-3}	M	n_u	l_u	L_u	n_l	l_l	L_l	λ Å	Temperature in K 2500	1250	625	312.5
	3	4	3	4	3	2	3	1761	1.464-23	2.652-23	4.996-23	0.000-00
	3	3	1	2	3	0	1	3763	1.606-23	2.793-23	5.234-23	
10^6	3	3	2	3	3	1	2	3267	1.441-23	2.536-23	4.763-23	
	3	4	3	3	3	2	2	1846	9.587-24	1.737-23	3.274-23	
	3	5	4		4	3		4500	7.293-24	1.347-23	2.503-23	
	3	4	3	4	3	2	3	1761	1.596-23	2.706-23	5.023-23	
	3	3	1	2	3	0	1	3763	1.577-23	2.629-23	4.567-23	
10^4	3	3	2	3	3	1	2	3267	1.455-23	2.427-23	4.288-23	
	3	4	3	3	3	2	2	1846	1.046-23	1.774-23	3.294-23	
	3	5	4		4	3		4500	8.810-24	1.518-23	2.975-23	
	3	4	3	4	3	2	3	1761	1.393-23	2.544-23	4.842-23	
	3	3	1	2	3	0	1	3763	1.449-23	2.495-23	4.421-23	
10^2	3	3	2	3	3	1	2	3267	1.316-23	2.299-23	4.145-23	
	3	4	3	3	3	2	2	1846	9.127-24	1.668-23	3.175-23	
	3	5	4		4	3		4500	7.405-24	1.419-23	2.863-23	

NIII

N_e								λ	Temperature in K			
cm^{-3}	M	n_u	l_u	L_u	n_l	l_l	L_l	Å	2500	1250	625	312.5
	2	4	3	3	3	2	2	1885	3.870-23	7.011-23	1.342-22	2.776-22
	2	3	0	0	2	1	1	1327	3.016-23	5.074-23	9.696-23	2.118-22
	2	5	4		4	3		4380	1.002-23	1.843-23	3.526-23	7.213-23
	2	5	3	3	3	2	2	1324	1.280-23	2.265-23	4.338-23	9.131-23
10^6	2	6	5		5	4		8239	3.292-24	6.083-24	1.157-23	2.331-23
	2	4	2	2	3	1	1	1387	2.292-24	3.855-24	7.132-24	1.471-23
	2	5	3	3	4	2	2	4003	1.907-24	3.374-24	6.463-24	1.360-23
	2	3	1	1	3	0	0	4101	5.998-25	9.858-25	1.804-24	3.740-24
	2	3	2	2	3	1	1	4640	3.578-25	6.305-25	1.194-24	2.475-24
	2	4	3	3	3	2	2	1885	3.907-23	6.978-23	1.216-22	2.003-22
	2	3	0	0	2	1	1	1327	2.792-23	4.317-23	7.036-23	1.245-22
	2	5	4		4	3		4380	1.065-23	1.985-23	3.532-23	5.673-23
	2	5	3	3	3	2	2	1324	1.189-23	1.962-23	3.269-23	5.662-23
10^4	2	6	5		5	4		8239	3.693-24	7.142-24	1.293-23	2.005-23
	2	4	2	2	3	1	1	1387	2.129-24	3.338-24	5.366-24	9.124-24
	2	5	3	3	4	2	2	4003	1.771-24	2.923-24	4.870-24	8.435-24
	2	3	1	1	3	0	0	4101	5.642-25	8.667-25	1.383-24	2.351-24
	2	3	2	2	3	1	1	4640	3.483-25	5.919-25	1.003-24	1.675-24
	2	4	3	3	3	2	2	1885	3.828-23	6.736-23	1.153-22	1.949-22
	2	3	0	0	2	1	1	1327	2.730-23	4.109-23	6.347-23	1.015-22
	2	5	4		4	3		4380	1.044-23	1.924-23	3.407-23	5.876-23
	2	5	3	3	3	2	2	1324	1.163-23	1.875-23	2.992-23	4.822-23
10^2	2	6	5		5	4		8239	3.632-24	6.982-24	1.274-23	2.239-23
	2	4	2	2	3	1	1	1387	2.090-24	3.210-24	4.952-24	7.788-24
	2	5	3	3	4	2	2	4003	1.732-24	2.794-24	4.458-24	7.183-24
	2	3	1	1	3	0	0	4101	5.540-25	8.339-25	1.276-24	2.003-24
	2	3	2	2	3	1	1	4640	3.415-25	5.705-25	9.409-25	1.552-24

Table 7.8: Filling rates per N_eN_i for the groundstate and metastable levels of CNO atoms for N_e of 10^6, 10^4, and 10^2 cm^{-3}. The particular ion is listed at the top of each table. The columns, from the left, are n, l, the multiplicity M = 2S + 1, L, parity P where even=0 and odd=1, the term value in cm^{-1}, and the filling rates per N_eN_i in cm^3s^{-1} for temperatures of 2500, 1250, 625, and 312.5 K.

CI

N_e cm^{-3}	n l M L P	Term cm^{-1}	Temperature in K 2500	1250	625	312.5
	2 1 3 1 0	0	8.294-13	1.362-12	2.334-12	4.377-12
10^6	2 1 1 2 0	10163	2.526-13	4.097-13	6.981-13	1.306-12
	2 1 1 0 0	21618	3.648-14	5.970-14	1.032-13	1.977-13
	2 1 3 1 0	0	8.126-13	1.296-12	2.078-12	3.393-12
10^4	2 1 1 2 0	10163	2.471-13	3.889-13	6.200-13	1.009-12
	2 1 1 0 0	21618	3.554-14	5.619-14	9.026-14	1.490-13
	2 1 3 1 0	0	8.100-13	1.283-12	2.030-12	3.211-12
10^2	2 1 1 2 0	10163	2.463-13	3.853-13	6.055-13	9.550-13
	2 1 1 0 0	21618	3.540-14	5.560-14	8.793-14	1.403-13

NI

N_e cm^{-3}	n l M L P	Term cm^{-1}	Temperature in K 2500	1250	625	312.5
	2 1 4 0 1	0	5.652-13	9.782-13	1.781-12	3.607-12
10^6	2 1 2 2 1	19228	2.357-13	4.098-13	1.050-12	3.258-11
	2 1 2 1 1	28839	1.286-13	2.233-13	5.019-13	1.048-11
	2 1 4 0 1	0	5.504-13	9.208-13	1.545-12	2.669-12
10^4	2 1 2 2 1	19228	2.304-13	3.885-13	9.210-13	2.502-11
	2 1 2 1 1	28839	1.256-13	2.112-13	4.382-13	8.031-12
	2 1 4 0 1	0	5.479-13	9.092-13	1.499-12	2.497-12
10^2	2 1 2 2 1	19228	2.295-13	3.842-13	8.918-13	2.289-11
	2 1 2 1 1	28839	1.252-13	2.090-13	4.254-13	7.356-12

OI

N_e cm^{-3}	n l M L P	Term cm^{-1}	Temperature in K 2500	1250	625	312.5
10^6	2 1 3 1 0	0	3.876-13	6.457-13	1.123-12	2.146-12
	3 0 5 0 1	73768	3.740-13	7.188-13	1.331-12	2.915-12
10^4	2 1 3 1 0	0	3.750-13	6.020-13	9.741-13	1.603-12
	3 0 5 0 1	73768	3.554-13	6.364-13	1.118-12	1.986-12
10^2	2 1 3 1 0	0	3.735-13	5.954-13	9.484-13	1.510-12
	3 0 5 0 1	73768	3.521-13	6.231-13	1.071-12	1.810-12

CII

N_e cm^{-3}	n l M L P	Term cm^{-1}	Temperature in K 2500	1250	625	312.5
10^6	2 1 2 1 1	0	8.230-12	1.297-11	2.164-11	3.978-11
10^4	2 1 2 1 1	0	8.064-12	1.239-11	1.918-11	3.010-11
10^2	2 1 2 1 1	00000	8.009-12	1.221-11	1.863-11	2.860-11

NII

N_e cm^{-3}	n l M L P	Term cm^{-1}	Temperature in K 2500	1250	625	312.5
	2 1 3 1 0	0	4.631-12	7.567-12	1.321-11	2.573-11
10^6	2 1 1 2 0	15227	1.510-12	2.414-12	4.106-12	7.758-12
	2 1 1 0 0	32600	2.774-13	4.526-13	7.885-13	1.530-12
	2 1 3 1 0	0	4.509-12	7.125-12	1.135-11	1.835-11
10^4	2 1 1 2 0	15227	1.476-12	2.291-12	3.592-12	5.720-12
	2 1 1 0 0	32600	2.704-13	4.269-13	6.792-13	1.095-12
	2 1 3 1 0	0	4.467-12	6.990-12	1.092-11	1.717-11
10^2	2 1 1 2 0	15227	1.464-12	2.254-12	3.473-12	5.388-12
	2 1 1 0 0	32600	2.679-13	4.190-13	6.542-13	1.027-12

OII

N_e cm^{-3}	n l M L P	Term cm^{-1}	Temperature in K 2500	1250	625	312.5
	2 1 4 0 1	0	3.311-12	5.584-12	1.012-11	2.061-11
10^6	2 1 2 2 1	26817	1.466-12	2.342-12	3.981-12	7.524-12
	2 1 2 1 1	40467	8.350-13	1.358-12	2.358-12	4.568-12
	2 1 4 0 1	0	3.202-12	5.190-12	8.469-12	1.402-11
10^4	2 1 2 2 1	26817	1.434-12	2.223-12	3.481-12	5.547-12
	2 1 2 1 1	40467	8.137-13	1.281-12	2.033-12	3.274-12
	2 1 4 0 1	0	3.165-12	5.070-12	8.088-12	1.297-11
10^2	2 1 2 2 1	26817	1.422-12	2.186-12	3.366-12	5.223-12
	2 1 2 1 1	40467	8.065-13	1.257-12	1.959-12	3.072-12

CIII

N_e cm^{-3}	n l M L P	Term cm^{-1}	Temperature in K 2500	1250	625	312.5
10^6	2 0 1 0 0	0	3.762-12	6.153-12	1.084-11	2.087-11
	2 1 3 1 1	52419	1.147-11	1.869-11	3.271-11	6.320-11
10^4	2 0 1 0 0	0	3.647-12	5.751-12	9.192-12	1.493-11
	2 1 3 1 1	52419	1.112-11	1.747-11	2.780-11	4.490-11
10^2	2 0 1 0 0	0	3.598-12	5.593-12	8.715-12	1.374-11
	2 1 3 1 1	52419	1.098-11	1.700-11	2.638-11	4.138-11

NIII

N_e cm^{-3}	n l M L P	Term cm^{-1}	Temperature in K 2500	1250	625	312.5
10^6	2 1 2 1 1	0	2.181-11	3.413-11	5.670-11	1.029-10
10^4	2 1 2 1 1	0	2.135-11	3.253-11	5.014-11	7.842-11
10^2	2 1 2 1 1	00000	2.116-11	3.191-11	4.827-11	7.372-11

OIII

N_e cm^{-3}	n l M L P	Term cm^{-1}	Temperature in K 2500	1250	625	312.5
	2 1 3 1 0	0	1.126-11	1.857-11	3.289-11	0.000-00
10^6	2 1 1 2 0	20063	3.481-12	5.635-12	9.753-12	
	2 1 1 0 0	42975	7.098-13	1.177-12	2.096-12	
	2 1 3 1 0	0	1.102-11	1.761-11	2.909-11	
10^4	2 1 1 2 0	20063	3.414-12	5.372-12	8.718-12	
	2 1 1 0 0	42975	6.965-13	1.118-12	1.860-12	
	2 1 3 1 0	0	1.040-11	1.694-11	2.836-11	
10^2	2 1 1 2 0	20063	3.249-12	5.192-12	8.523-12	
	2 1 1 0 0	42975	6.552-13	1.074-12	1.812-12	

Table 7.9: Effective fluxes for some forbidden and intercombination lines at a temperature of 625 K and $N_e = 10^2$ cm^{-3}. The last column is the total effective flux of the given line including the contibution from forbidden transitions into the level.

Atom	Term	λ Å	eff. flux erg cm^3/s	Total erg cm^3/s
CI	$2p^2\ ^1S$	4626	3.777-25	
		8730	2.000-25	
	$2p^2\ ^1D$	9840	1.222-24	1.399-24
NI	$2p^3\ ^2P$	3468	1.374-25	
		10405	7.661-25	
	$2p^3\ ^2D$	5201	3.405-24	4.938-24
OI	$3s^1\ ^5S$	1356	1.569-23	
NII	$2p^2\ ^1S$	3067	1.245-25	
		5756	2.198-24	
	$2p^2\ ^1D$	6585	7.830-24	9.266-24
OII	$2p^3\ ^2P$	2471	3.272-24	
		7326	4.208-24	
	$2p^3\ ^2D$	3727	1.794-23	2.622-23
CIII	$2s2p\ ^3P$	1909	2.744-22	
OIII	$2p^2\ ^1S$	2327	1.728-24	
		4364	7.339-24	
	$2p^2\ ^1D$	5007	2.519-23	2.996-23

Chapter 8

Abundance Determinations

8.1 Introduction

In this chapter we use the effective fluxes generated by our models to check the line identifications in the observed spectra of nova shells, and to determine the abundances of the various ionic components of these nebulae. In the discussion that follows unless otherwise stated we shall use the flux measurements of Ferland et al. (1984), Williams (1982) and Gallagher et al. (1980) for the shells of DQ Her, CP Pup and T Aur respectively. Hereafter we shall refer to these papers as FWL, WIL and GHK, and the Williams et al. (1978) paper will be referred to as WWH.

Since the initial analyses on the shells of CP Pup and T Aur no further observations have been reported. This makes it rather difficult to assess the accuracy of these flux measurements. However, multiple observations do exist for the cool shell of DQ Her, but the results show large scatter. Both UV and optical observations have been repeated. UV measurements of the DQ Her shell were reported by Hartmann & Raymond (1981), who detected CII λ1335 and CIII λ1909], and by FWL who only detected λ1335. The fluxes derived for the CII line differed by a factor of two between the two sets of measurements, and the λ1909 strength reported by Hartmann & Raymond (1981) was below the sensitivity limit of FWL's equipment and has therefore not been independently confirmed. Optical spectra of the DQ Her shell were initially made by WWH who found the ratios $F_{Bac}/F_{H\beta} = 2.5$ and F(4267)/F(4239)/F(4651)/F(Hβ) = 5/2/4/10. The flux measurements of FWL, after correction for an assumed reddening of $A_v = 0.35$, were reported to be $F_{Bac}/F_{H\beta} = 1.55$ and F(4267)/F(Hβ) = 2.9/10. Although they should have been detectable according to the fluxes recorded by WWH, the two other lines for which WWH gave fluxes, NII λ4239 and OII λ4651, were not reported by FWL.

The uncertainties that exist in the observed spectra of these nebulae are due in part to the difficulty of observing such low surface-brightness objects. The line flux variations could be due entirely to observational and instrumental effects. They could also, however, be due partly to a time dependence in the emissions from the nebula. More regular observations would be useful in reducing the observational uncertainties and determining whether there is any noticeable time dependence (on a time scale of years) in the spectra. The T Aur shell in particular is nearly a hundred years old and likely to fade into obscurity within the next few years. Similarly, the rapid rate of expansion of the CP Pup shell will limit its observable lifetime.

In the following sections we re-examine the line identifications given to the features in the spectra of the shells of DQ Her, T Aur, and CP Pup. The

conditions appropriate to the formation of these lines are discussed and the ionic abundances are determined using our modelled effective fluxes. Based on our interpretations of the data we make some predictions regarding other lines that should be observable in various regions of the spectrum.

8.2 DQ Her

Spectra from four regions of the DQ Her shell were obtained by WWH and are shown in their Figs. 2 and 3. Traces A and C are from the ends of the major axis of the ellipsoidal shell, and B and D are from the ends of the minor axis (see their Fig. 1 for the orientation). Unfortunately, because different aperture sizes and integration times were used for each of the scans, the signal-to-noise ratios of the scans vary. Furthermore, direct comparisons of their Figs. 2 and 3 are not possible because they have used different scales for the ordinates of their red and blue spectra.

Since we believe the lines of hydrogen and helium can be modelled with good accuracy, it is disturbing to note that there are such large discrepancies between the predicted and observed fluxes. The line identifications seem to be correct but their intensities are not always what would be expected. This might be an indication that the gas is more inhomogeneous than previously expected rather than that the physics is not understood. It is also possible that the observations are unreliable considering the low surface-brightness of this shell. However, with these caveats in mind, we now go on to look at the CNO lines that are predicted for this shell, and compare them with the observations. Atomic data for CNO ions are much less reliable than those for H and He and the models are subject to more uncertainty. It is therefore comforting to see that our predicted spectra show many features of the observations. In this shell lines of CII, NII, and OII were identified in the optical and near UV bands. The strongest predicted CII lines are λ1335 and λ4267 both of which were seen. The λ1335 line was only just detectable by IUE and it is quite expected that λ1324 was not detected since its flux is $\sim$5 times weaker. For NII, in decreasing order of intensity, lines were observed at λ5006, λ4041, and λ4239. Together with λ5678 these correspond to the strongest predicted lines. The absence of λ5678 in the observed spectra is a mystery. OII idetifications were given by WIL to lines at λ4651, λ4075, λ4294, and λ4607. With the exception of λ4607 these identifications agree with our model predictions. Other predicted lines such as λ4095, λ4113, and λ4343 could be present, but would not be apparent because of blending with other lines.

Neutral atoms are predicted to have relatively weak effective fluxes and would have to be present in large quantities to produce observable fluxes. Their null detection is consistent with the results from photoionization models that the gas is in a fairly high state of ionization. Triply ionized atoms on the other hand are predicted to have significant effective fluxes. The null

detection of any lines from CIII, NIII, or OIII has been used to constrain photoionization models. Once again, our modelled fluxes for these ions are consistent with the results from photoionization models in predicting that the recombination lines of these ions will be below threshold.

The model for HI is thought to be the most reliable, so we start our analyses by examining the hydrogen lines found in the shell of DQ Her. We have already mentioned the problems experienced in trying to fit modelled HI spectra to the observed Balmer decrement in DQ Her. The observed ratios Hα/Hβ/Hγ were 1.64/1.00/0.62, or 1.46/1.00/0.65 after correcting for reddening with an A_v of 0.35 (FWL). The total integrated Balmer continuum flux relative to Hβ was 1.55. Note, though, that WWH reported a ratio of 2.5 but did not correct for reddening, which would increase this ratio. The Balmer decrement is too flat to be fitted by any of the modelled low temperature spectra; nor can the Balmer continuum intensity be reconciled with the modelled emissivities. For a 625 K plasma with $N_e = 10^2$ cm^{-3} the case A flux ratios would be 4.07/1.00/0.42 while for case B they would be 3.86/1.00/0.424. The Balmer continuum fluxes (relative to Hβ) would be 2.64 and 1.98 respectively. Increasing the temperature flattens the Balmer decrement but increases the F(Bac)/F(Hβ) ratio. Increasing N_e flattens both the Balmer decrement and the continuum to Hβ flux ratio, but densities in excess of 10^6 cm^{-3} would be required to explain the measured fluxes. Neither of these options provide an acceptable explanation for the observations.

Some of the Balmer lines could be enhanced due to blending with lines from other ions with similar wavelengths. For example, the λ3889 line is a mixture of Hζ and HeI. There are also OII λ4343 and λ4105 lines which will overlap with Hγ and Hδ respectively. CIII has a transition which produces λ3889 emission, and there is an NIII line at λ4101. There are probably many more coincidences, but the ones we have mentioned have the strongest recombination lines. While this would explain why the higher members of the Balmer series are too strong, it does not account for Hα being too weak. Absorption of flux, increasing towards the red end of the spectrum, i.e. dereddening, is necessary to account for this behaviour.

The matter ejected by DQ Her went through a period of grain formation. This dust could still be present in the shell. The behaviour of the spectrum is contrary to that expected of dust, however. Dust scatters blue light more than red light, producing the familiar reddening observed in stellar bodies. If large quantities of dust were present in the nebula, the light curve would be reddened rather than dereddened. The possibility of the shell emissions being formed by scattering of the central stellar system's light off dust can also be excluded: the spectra of the central stars (Williams 1983) and the nova shell (WWH) are quite different.

Another possibility is that the Balmer lines are affected by radiative transfer effects. If the Lyman lines are optically thick, however, then the Hα/Hβ

ratio should be steeper than in case B conditions (Osterbrock 1974). The reason is that Hα is merely scattered, whereas some of the Hβ that is absorbed is converted to Hα plus Pα. This increases Hα/Hβ and decreases Hβ/Hγ. On the other hand, if the nebula is optically thin to Lyman lines then Balmer absorptions from 2S fill nP levels, from which transitions to the groundstate occur in preference to returning to 2S. The nett effect of this process is that for each Balmer photon absorbed a Lyman photon is emitted, thereby reducing the number of Balmer photons. The largest effect would be on the Hα line. For the Lyman lines to be optically thin while the Balmer lines are optically thick requires that the groundstate of HI be emptied much faster than the 2S level. However, the emptying process cannot be absorption of Lyman line radiation because the Lyman lines would become optically thick. It must rather occur via photoionization or charge exchange. Photoionization models (see Chp. 9) predict that hydrogen should be predominantly in an ionized state in this shell, which would make it possible for the Lyman lines to be optically thin.

The possibility of two regions of different temperatures should also be considered. The Balmer continuum feature must come exclusively from the cool region, and its integrated flux can be used with a suitable model to determine the fluxes of the Balmer lines. The differences between the measured and the estimated line fluxes of the cool region will yield the warm region fluxes. At present, however there is no convincing explanation for the hydrogen line spectrum in this gas. Density and temperature inhomogeneities seem like the most plausible explanation and should be investigated further. To this end it would be useful to image the shell in the light of Hα, Hβ, Hγ, and the Balmer continuum feature.

The spectral lines attributed to HeI by WWH are at λ5876, λ4472 and λ3889. The λ3889 line is seen as a blend with Hζ — the flux at this wavelength is too large to be due to hydrogen alone. Modelled flux ratios for the HeI lines λ10830/λ5876/λ6681/λ3889/λ4472 in a plasma with $N_e = 10^2$ cm^{-3} and T = 625 K are 4.1/4.0/1.2/1.2/1.0, and at a density of 10^4 cm^{-3} and T = 2500 K they are 4.6/3.2/0.94/1.4/1.0. Note that F(5876)/F(6681) = 3.4 over a broad range of temperature and density. Optical depth effects are not included in the model calculations so the fluxes of λ10830 and λ3889 represent upper limits. The flux of λ3889 relative to both λ5876 and λ4472 increases as either the temperature or density increases, and can, in principle, be used to estimate the gas temperature.

Based on these results, we expect to find F(6681) = F(5876)/3.4. FWL measured F(5876)/F(Hβ) = 26/100 and set a limit of < 5 on OI λ6300. The predicted flux of λ6681 according to our model is about 7.6. A flux this size should have been detectable by FWL, unless their instrument response had fallen off at this wavelength. The spectrum presented by WWH is notably flat in the wavelength region of λ6681, although it is possible that F(6681)

is too small to be discerned on the scale of their Fig. 3. Since λ6681 was not detected, although λ4472 was, the indications are that the latter line has the stronger flux, and hence that the temperature is higher than 625 K. This implies that the HeI lines are formed in a hotter region of the gas than the Balmer continuum feature. Unfortunately, no flux measurements have been reported for λ3889 or λ4472 so temperature determinations using these lines are not possible. However, an enhancement of F(3889) relative to F(4472) of more than 1.2 does not seem unreasonable from the WWH spectra, so a higher temperature region for the HeI lines is quite plausible. In fact, dereddening these traces would further enhance the λ3889 line, as would any corrections for optical depth effects. On the other hand, an increased temperature leads to a flux ratio of 3.2 for λ5876 relative to λ4472, which means that FWL should have seen the latter line with a relative flux of 8. This might have been too small for them to have unambiguously identified above the noise. Once again, the temperature and density distributions could be inhomogeneous so that no single set of parameters is able to adequately describe the conditions.

One of the weaker lines in the observed spectrum is at λ4686 and was suggested by WWH as being due to HeII. They also pointed out that the λ4686/λ4472 intensity ratio is larger than one would expect given the fact that no CIII, NIII, or OIII is observed in the shell, and that this identification could therefore be incorrect. However, there are no obvious alternative identifications to HeII. FWL measured fluxes of 26 for λ5876 and 18 for λ4686 relative to Hβ. At a temperature of 625 K and density of 10^2 cm^{-3} the abundances (by number) of He^+ and He^{++} relative to H^+ in case A conditions are 0.081 and 0.0071 respectively. At T = 2500 K these abundances go up to 0.101 and 0.0086, and there would be a further increase at both temperatures if the case B hydrogen results were used. Note that for HeII we used the case A results. If the helium recombination lines are formed in the same region as the Balmer continuum band then its abundance is essentially solar. On the other hand, if they are formed in a warmer region then the abundance is slightly larger than solar.

The two strongest observable lines in the CII doublet spectrum are λ1335 and λ4268. A λ4268 line was seen very clearly in the spectra from all four regions of the DQ Her shell and was taken to be CII. In fact, it was the only allowed, non-hydrogenic line clearly visible in the B and D spectra. Confidence in this identification has been provided by the observation of λ1335 (FWL). The flux ratio F(1335)/F(4268) = 9.3 reported by FWL contains large uncertainties. Their measured flux of λ1335 was twice that of Hartmann & Raymond (1981) and they estimated errors of up to a factor of three in the UV to optical flux ratio. According to our model, for pure recombination F(1335)/F(4268) = 2.9 at 625 K but increases to 3.5 at 1250 K. At this temperature the flux of λ1335 will be noticeably increased by dielectronic

recombinations so our figure is an underestimate. Using the values given by Nussbaumer & Storey (1984b) for dielectronic recombination together with our results at 1250 K, we get F(1335)/F(4268) = 8.8. At 2500 K this ratio has increased to 27.3. The measured value of 9.3 supports a cool gas interpretation, but at a temperature of $\sim$ 1300 K rather than 500 K. Note that the value we predict for F(1335)/F(4268) is about half that quoted by FWL. More precise temperature determinations are unreliable with these data because of the large observational uncertainties.

WWH suggested that a λ4075 line observed in their spectra is formed partly by CII emissions. There is a quartet line at this wavelength which is the result of a 4f $\rightarrow$ 3d transition but we have no quantitative measure of line intensities with this multiplicity. In the B trace the CII λ4268 is very weak and there is no sign of any λ4075 emission. In the D trace, however, the λ4268 line is quite prominent and there is a definite bump in the wing of the Hδ line in the region of λ4075. This suggests that at least some of the λ4075 emission could be due to CII. Note, though, that there are some other quartet transitions that produce optical photons which are quite clearly absent from the spectra. For example, the flux of λ3877 should be stronger than the CII λ4075 flux but is not present in WWH's Fig. 2, and similarly, F(6786) should be larger than F(4076). This last line may be too weak to be seen on the scale of WWH's Fig. 3. However, we shall henceforth ignore the CII identification and assume that F(4076) is due entirely to OII.

A number of lines in the DQ Her shell spectra were suggested as being due to allowed NII transitions formed by recombination in the cool plasma. In particular, because there is no [OIII] λ4959, which must appear at one third the strength of λ5005, an [OIII] identification for λ5005 was rejected. Lines in the DQ Her shell identified as permitted recombination lines of NII were λ5005, λ4239 and λ4041 (WWH) in decreasing order of strength. The flux for λ5005 was given as 0.3 by FWL and for λ4239 as 0.2 by WWH. These results can not be compared directly but they do provide some measure of the relative fluxes. The calculated effective fluxes for these lines are in the ratios 9.4/6.8/4.4, while the next predicted line is λ4436 with a flux (on the same scale) of 2.8. However, the strongest optical line in our model of NII, λ5678, is not seen in the spectra. Unfortunately, the red and blue scans of WWH cannot be compared so we are not able to set a limit on F(5678). As pointed out in chapter 7, the lines in the λ5678 multiplet are quite widely spaced so we expect this multiplet to appear as a broad feature with a peak amplitude of about half the predicted flux. In fact, there is a broad, shallow bump in the A and C traces (WWH, Fig. 3) which could be due to this multiplet.

The absence of λ4436 in the observed spectra might be due to an overestimate in our model of any of the atomic rates, in particular the A-value, associated with this transition. This multiplet also has a line separation of

about 9Å so the flux will be dispersed and have a lower peak. The strongest singlet line is λ4544 with an estimated intensity $\sim 1/5$ that of λ5005, and λ4123 is next with a slightly lower effective flux. There are bumps in the A and C traces of WWH which could be due to these lines, although they are slightly smaller than predicted by the model. However, in spite of the non-detection of λ5678, the NII identifications in DQ Her are quite reasonable, considering that a 10 - 20% error margin is expected for the modelled spectra.

OII identifications were given by WWH to lines at λ4651, λ4076, λ4607 and λ4294 in decreasing order of strength. F(4294) is very weak and only visible in the A and B traces of WWH Fig. 2. These fluxes show a marked deviation from our modelled values. For example, in the observed spectra F(4607) is stronger than F(4294) and F(3868), and the λ4095 and λ4113 lines are not even identified. Lines at λ4343 and λ4607 belong to the doublet series; all the others are quartets. In our model the λ4095 line has a predicted flux of half that of F(4075) and a line dispersion of $\sim$ 8Å. The high bridge between OII λ4075 and Hδ λ4101 in WWH Fig. 2 could be explained by the presence of λ4095. The λ4113 multiplet can be resolved into two lines with equal fluxes at λ4105 and λ4120. The λ4105 component will be blended with Hδ in WWH's spectra, and, although it is slightly smaller than predicted the λ4120 component could be the signal in the wing of the Hδ line. The λ4343 line will most probably be blended with Hγ and could be partly responsible for the flat Balmer decrement.

Although we do not have flux measurements and so cannot quantify the assessment, the λ4607 line appears to be significantly stronger than predicted. Contrary to our model predictions, its observed flux is larger than either F(4294) or F(3868). The flux of OII λ4607 should be weaker than the doublet line OII λ4343, but since this line is blended with Hγ we cannot check this. There are no reasonable alternatives to an OII identification. The suggestion of NIV for a line at λ4607 in the CP Pup shell is quite feasible, as an NIII λ4379 line has been identified (WIL): in the DQ Her shell an NIV identification would be inconsistent.

This essentially takes care of all the allowed recombination lines in the spectrum. The optical spectra reported by FWL omitted many of the lines seen by WWH. For example, OII λ4651 and λ4076 are missing, as well as NII λ4042 and λ4239. The OII lines might not have been present in the section of the shell observed by FWL, but the NII lines should be seen if the λ5005 identification is correct.

The forbidden lines of nitrogen and oxygen, [NII] λ6584 and [OII] λ3727, are also seen in the spectra. In most nebulae these lines dominate the spectrum, whereas in these spectra they have intensities comparable with the allowed recombination line intensities. It has been suggested (WWH, WIL) that these lines are formed by recombination. All NII singlet and OII dou-

blet recombinations cascade down into their lowest levels, from which the only radiative transitions to the groundstate are via [NII] $\lambda\lambda$6548, 6584 or [OII] λ3727. We can check this idea using our model. In Table 7.9 we have listed the effective fluxes of the forbidden lines of various ions. Because we have assumed that no processes besides the forbidden transitions empty each metastable term, these fluxes are the maximum possible under recombination conditions. In practice, charge exchange and photoionization might also play a significant role. According to Table 7.9, for NII F(5756)/F(6584) $\sim$ 1/4 in pure recombination, and F(6584) $\approx$ F(5005). No λ5756 emissions were identified by either FWL or WWH in any of their spectra. Furthermore, the flux of [NII] λ6584 is smaller in the A and C traces of WWH's Fig. 3 than in the B and D traces, and yet F(5005) was only found in the former spectra. This is contrary to the requirements that the forbidden lines be formed by recombination. The [OII] λ3727 emission displays a similar inconsistency in WWH's data in that the OII λ4650 flux is seen only in the A and C traces, while the forbidden line appears with essentially equal strengths in all four spectra. FWL do not list any flux measurements for OII λ4650. According to the modelled recombination results, F(4650) = F(3727)/2, and therefore OII λ4650 should have been one of the stronger lines in their spectrum. The fact that it was not mentioned indicates that F(4650) is quite weak.

8.3 Discussion

CNO lines identified in the spectra were CII λ1335 and λ4267, NII λ5005, λ4041 and λ4243, and OII λ4653, λ4076, λ4608 and possibly also λ4295, where the lines of each ion are listed in order of intensity from the strongest to the weakest. Our model calculations for CNO at low temperatures predict the same lines in the same order except that NII λ5678 is the strongest line in the modelled NII spectrum, and the OII λ4608 flux is one of the weaker lines in the modelled OII spectrum. An OII λ4095 line was not identified by WWH in their spectra of the DQ Her shell but we suggest that it is present with a flux in good agreement with our model predictions. The identifications given by WWH to the lines of CNO in the shell spectra of DQ Her appear to be quite reasonable and support the idea that they are formed by recombination in a cool gas. The agreement with our calculations also confirms our model. The hydrogen Balmer lines are still not understood in terms of either a case A or case B recombination model.

An unusual feature of these spectra is that the allowed recombination lines are only seen along the shell's major axis, but the forbidden [NII] and [OII] lines appear with essentially equal strengths in all regions of the nebula. There are no reasonable alternative identifications to [OII] and [NII] for the λ3727 and λ6584 emissions. It appears that they are not formed by recombination in a cool plasma, so other possibilities must be considered. As the abundance of NI and OI was found to be quite small, population of the

metastable levels by photoionization of NI and OI seems unlikely. The most obvious condition is that suggested by WWH — these lines are formed in a warmer region of the nebula than the recombination lines. The forbidden lines would be formed by collisional excitations in the warm portions of the shell and the allowed recombination lines of CNO in the cool regions. In the warm regions nitrogen and oxygen must then be predominantly in the form of NII and OII (since no [OIII] is found), but in the cool region they must be in the form of NIII and OIII to account for the recombination spectrum. This leads to the seemingly paradoxical situation that the cool region of the gas is in a higher state of ionization than the hot region.

There is another problem. The spectra show that the Balmer continuum feature is similar in all four regions of the shell. The temperature, therefore, appears to be the same throughout. It has been shown that a cool plasma can be formed if there is a much larger than solar abundance of oxygen present in the form of OIII (FWL; §9.3). Collisional excitation of its groundstate fine-structure lines can cool the gas to the estimated values. However, along the minor axis (trace B and D) there are no observable OII lines, and hence also less OIII there, so what cools the plasma?

It is quite clear from the spectra of WWH that neither NIII λ4380 nor OIII λ3763 emissions are present above a limit of $\sim$ 0.1F(Hβ). The flux measurements of FWL for NII λ5005 set a limit of $N(N^{++})/N(N^{+}) < 0.1$. FWL did not give any OII fluxes but we estimate a similar ratio for $N(O^{++})/N(O^{+})$. The CIII optical lines λ4069 and λ4650 coincide with OII emissions, so we cannot determine if there is any CIII contribution to them. The low fluxes of NIII and OIII lines, however, suggest that CIII emissions will also be very small. This is supported by the absence of CIII λ1923 in the IUE data of FWL. Although Hartmann & Raymond (1981) claimed a detection of the CIII] λ1909 intercombination line at a flux level of 0.13 with respect to F(Hβ), it was not seen in the UV data of FWL. The model results in Tables 7.7 and 7.9 show that in pure recombination the CIII] λ1909 emission should be a factor of ten larger than CIII λ4069 and about three times larger than λ1923. Because charge exchange and photoionization will be competing with spontaneous decay to empty this level, it is doubtful that pure recombination conditions apply. The non-detection of any CII quartet lines, which are formed at low temperatures by radiative capture of an electron onto a CIII $2s2p^2P^0$ ion, imply that the CIII $2s2p\ ^2P^0$ population is at least six times smaller than the CIII groundstate population. If this is the case then spontaneous decay is not the main depopulating mechanism for this level and CIII] λ1909 will not be a good indicator of the presence of CIV ions.

8.4 T Aur

The T Aur shell is very faint and the signal-to-noise ratios of its spectra were hence rather small. Sky-subtracted data in the range λ4500 to λ7000 were

collected using a Reticon device, and long-slit photographic spectra were also made. Only the first two Balmer lines of the HI series fall in the range of the Reticon data, but both were readily detectable. They had an observed ratio of F(Hα)/F(Hβ) $\sim$ 7, which is very large, and is in strong contrast to the DQ Her shell spectra. This led GAL to suggest that T Aur suffers substantial extinction. They adopted a value of 3.3 for this ratio based on an extrapolation to a temperature of 1000 K of the Brocklehurst (1971) case B calculations. Relative line intensities corrected for this amount of extinction were used in their analyses. Whereas low density case A conditions are usually regarded as being appropriate to nova shells, our calculations show that a value of 3.3 for Hα/Hβ is relevant to a case B hydrogen plasma with an $N_e \sim 10^5$ cm^{-3}. In case A with $N_e = 10^2$ cm^{-3} the Balmer ratio at 1250 K would be 3.7, increasing to 4.1 as the temperature drops to 625 K. The case B Balmer ratios at these temperatures and an electron density of 10^2 cm^{-3} are 3.5 and 3.9 respectively. Unfortunately, no accurate temperature determination can be made, but the value of 3.3 adopted for the Hα/Hβ flux is possibly a bit low. Note that because of the large extinction, observations at wavelengths shorter than λ4500 might give a poor return. The long-slit spectra did show the presence of [OII] λ3727 emissions.

The only HeI identification made by GAL in the T Aur shell spectrum was a line at λ5876. The lack of any detectable λ6681 emission above the noise is to be expected considering how weak F(5876) is. Similarly, both λ4472 and λ3889 would be too weak to be seen at low temperatures. Effective fluxes for a variety of models, all with $N_e = 100$ cm^{-3}, were used by us with the observed fluxes to determine the He^+ abundance. The lowest abundance, 11% HeII relative to HII, was obtained with a case A hydrogen model at 625 K, and the highest, 16%, with case B at 1250 K. These values would be even higher if a lower extinction was used. We therefore support the findings of GAL that the helium abundance is enhanced with respect to the solar value, but propose a value of $N(He^+)/N(H^+) \sim$ 13%.

No HeII emission was identified in this shell, although there was quite a broad feature in the vicinity of λ4650, which was attributed to OII λ4651 rather than HeII λ4686. In DQ Her a fairly weak λ4686 line was found which was assumed to be HeII. In view of the large HeI abundance, some HeII lines could be expected in this plasma. Since the λ4650 line is so broad and the signal so weak, we suggest that this emission could be a blend of OII λ4650 and HeII λ4686. Unfortunately, this makes it very difficult to determine the abundance of either species.

NII identifications were given to lines at λ5005 and λ5678 (GAL). In light of the non-detection of NII λ5678 in the DQ Her shell, but the good agreement between models and observation of the other NII lines, we do not fully understand the relationship between F(5005) and F(5678). We cannot, therefore, use F(5678) to determine the NII abundance, but neither

is F(5005) suitable because of the possibilty that this line is blended with [OIII] emission. Because the λ4959 line of the multiplet lies below the noise level, a limit can be set on the [OIII] flux. [OIII] λ5005 must be less than three times the noise level. The modelled flux ratio of λ5678/λ5005 is 1.1 over quite a broad range of temperature and density. Taking the relative flux of λ5678 to be 24 (FWL) implies an NII λ5005 flux of 22, an [OIII] λ5007 flux of 18 and an [OIII] λ4959 flux of 6. These would not be inconsistent with the data. These fluxes yield an N^{2+} abundance of $N(N^{2+})/N(H^{+}) = 0.018$ for HI case A and 0.024 for case B. These values vary very little as the temperature changes. If we use a relative flux of 40 for NII λ5005 then these values are just under two times larger.

All the allowed lines in the spectrum are accounted for so we now turn our attention to the forbidden lines. [NII] λ6584 and [OII] λ3727 were both seen in the long-slit spectra (GAL), but flux measurements are only available for the [NII] line. Comparison of its flux with Hα is convenient because of their close proximity (in wavelength). GAL measured their fluxes to be $F(6584)/F(H\alpha) = 23/70 \approx 1/3$. This is close to the value of $\sim 1/4$ found for the ratio of these lines in the DQ Her shell. No [NII] λ 5756 line was detected in the spectra and F(5678) was much smaller than F(6584). Both of these facts indicate that most of the [NII] emission is not formed by recombination in a low temperature plasma.

8.5 Discussion

The faintness of this old nova shell has made observation of it very difficult. Furthermore, there are indications of substantial reddening to this object so that the blue end of its spectrum is heavily extinguished. Sky-subtracted spectra of the shell only extend to λ4500 (GAL), although a line at λ3727, identified as [OII], was seen in long-slit photographic spectra. This means that the [OII] line must be very strong. The lack of the blue end of the spectrum is an unfortunate restriction: cross-checks on some of the line identifications cannot now be made. For example, F(4042) or F(4239) detections might have helped to clarify the situation with the NII lines. Similarly, a slightly smaller flux of λ4076 emission relative to F(4650) would confirm the OII identification, while a stronger flux at λ4069 would indicate a CIII identification. An OII rather than a CIII identification is favoured for this nebula because, by comparison with DQ Her, the HeI/HeII line ratios indicate that lower stages of ionization are more favoured. The strongest carbon emissions would most probably have come from CII, but the CII λ4268 line is outside the observed wavelength range. We therefore have no measure of the carbon content of this shell.

The measured flux of the λ4650 feature is about three times larger than the OII λ4650 line in DQ Her. It is much broader than the other spectral lines, which could be due to it being blended with HeII λ4686. Unfortunately,

we cannot determine the individual contributions to this line, so the best we can say is that the OII flux is less than 102 and that the total helium content of the shell is higher than previously determined. The presence of some HeII in this plasma is not unexpected, and is consistent with our earlier comments regarding the state of ionization of this gas. DQ Her, for example, had some HeII and its spectra only had lines from singly ionized CNO. The NIII λ4380 line would be a good indicator of the presence of higher stages of ionization, but once again it is out of range. The T Aur spectrum is far too noisy in the region of the OIII line λ4583 for any meaningful detection to be made, so we have no definitive indication of any doubly ionized atoms. Even the amount of [OIII] λ5007 is uncertain.

During its decline, nova T Aurigae's light curve underwent a period of sudden dimming similar to the behaviour of the DQ Her light curve. This phenomenon has been noted in most slow novae and is believed to be due to the formation of dust in the shell. Precisely what happens to this dust is not clear. Reflection nebulae, which appear as blue regions on photographs, are formed when starlight is scattered by dust. GAL pointed out that the spectral features of this shell cannot be due to scattered light from the central stellar system. Besides the fact that the shell appears heavily reddened rather than dereddened, the T Aur stellar system has only weak emission lines and the HeII λ4686 line is about 10% stronger than the λ4650 blend in the star's spectrum.

The spectra of DQ Her and T Aur are similar in many respects. Lines of HeI, NII, and OII are present in both spectra, as well as the forbidden lines [NII] λ6584 and [OII] λ3727. The flux ratio of [NII] λ6584 to Hα is $38/146 \approx 1/4$ in DQ Her and $23/70 \approx 1/3$ in T Aur. Because no [NII] λ5756 line is present, and F(6584) is much larger than F(5678), the [NII] emission does not appear to be formed by recombination. Similarly, the [OII] λ3727 line has a larger flux than would be expected in low temperature recombination conditions. However, the same arguments pertain to the [NII] and [OII] emissions in the DQ Her shell.

The λ4650 line was attributed to OII but it is broader than any other line and could easily have some HeII λ4686. There might also be some [OIII] λ5007 present in T Aur which was definitely absent in the DQ Her shell. Unfortunately we have no measure of the carbon abundance in this shell, but it appears that OII and HeI are slightly enhanced with respect to DQ Her values. One significantly different feature of these two shells is the Hα/Hβ flux ratio. T Aur appears to be substantially reddened, whereas DQ Her appears heavily dereddened. If this is due to internal processes in the nebulae then their physical parameters must be quite different. If, however, this effect is caused by external influences, then these two shells could after all be very similar.

8.6 CP Pup

The shell spectrum of CP Pup differs quite markedly from those of DQ Her and T Aur. Only lines of H, He, and N in various stages of ionization have been identified by WIL. The line fluxes indicate a high excitation nebula. Lines identified as the Balmer series of HI were prominent and fit the model calculations for a low temperature case A situation reasonably well (Martin 1988). This is in strong contrast to the other two shells which both show large deviations from modelled HI spectra. Low optical depth for the HI lines is implied by the case A condition. For a fast nova such as CP Pup, large velocity gradients are to be expected so that this is a credible result.

Lines at λ5876 and λ3889 (blended with Hζ) were identified by WIL as HeI. The relative flux of λ5876 is 19, and the Hζ + HeI blend has a flux of 20. The Hζ contribution cannot be more than 12 (because Hϵ = 13), which leaves 8 units of flux over from other sources. The predicted fluxes of λ6681 and λ3889 in an 800 K plasma are less than 6, so that λ6681 should be below the noise level. As we pointed out earlier, the F(5876)/F(3889) ratio is temperature dependent, the measured value of 8/19 corresponding to a temperature close to 2500 K. On the other hand, if Hϵ is under-estimated then Hζ could be larger and the extra λ3889 flux could consistently be due to HeI at low temperatures. The λ4472 line is not seen, although with an estimated flux of less than 5 this is not surprising. The original abundance determination of He^+ in the CP Pup shell was based on extrapolated effective recombination coefficients for λ5876 (cf. WIL equation 1). Using our Hβ case A effective fluxes, we get an He^+ abundance at 625 K by number of 0.059 and at 2500 K of 0.079 relative to H^+. These values are both lower than $N(He^+)/N(H^+)$ determined by WIL.

A strong emission at λ4686 was identified as HeII. The flux of this line relative to λ5876 was measured to be 92/19. This enhancement of HeII over HeI indicates that this plasma is capable of supporting a higher stage of ionization than either of the previous two nebulae discussed. Two other lines, λ5411 and λ6233, have also been suggested as being HeII emissions. The λ5411 identification seems quite reasonable. It arises from a $7 \rightarrow 4$ transition in HeII and has $F(4868)/F(5411) = 92/7 \sim 13$. Scaling the zero-density capture-cascade results for HI to apply to HeII at a temperature of 625 K, we get a predicted flux ratio of 21 for both case A and B. At higher temperatures and densities this ratio is slightly smaller; for example, at T = 2500 K we get a value of 16 for this ratio. Observational uncertainties do limit the accuracy of these measurements and the fluxes in the red scan ($\lambda > 5300$Å) have been arbitrarily normalized so that $F(H\alpha)/F(H\beta) = 3$. Our calculations for hydrogen give a value of 4 for this ratio under the relevant conditions, which increases the λ5411 flux and hence lowers the observed ratio of F(4686) /F(5411). This, in turn, leads to higher temperature estimates. However, even as they stand, the measurements suggest that HeII emissions

are produced in a warmer region of the nebula than the Balmer continuum feature.

The λ6233 line has a significant flux; F(5876)/F(6233) = 19/23. In the light of modelled spectra, it is difficult to reconcile the λ6233 identification as being from HeII. Its line flux would have to be less than that of λ5411. In HeII it arises from a $17 \rightarrow 5$ transition, but has a smaller branching ratio than the $17 \rightarrow 4$ transition which produces λ3859 photons. There is an unmarked feature to the left of the λ3889 line in WIL's Fig. 2 but it appears to be more than 30Å shortward of the Hζ + HeI blend and has a flux less than that of the λ6233 line. It seems unlikely that it is due to HeII λ3859. For λ6233 to be an HeII line, the n = 17 level would have to be filled by some mechanism such as resonant pumping, and the transitions to levels below n = 5 would have to be optically thick. This is inconsistent with the other HeII lines. We therefore reject this identification but have no alternative explanation at this stage.

Analysis of the CP Pup shell by WIL indicated a large abundance of nitrogen in the gas. Many of the observed lines were identified as those of nitrogen in various stages of ionization. However, only two lines, λ5005 and λ5678, were attributed to NII. Their flux ratio was measured to be 44/9 which is much higher than our model predicts. However, the other allowed NII lines predicted by our model and observed in DQ Her, λ4239 and λ4041, were absent from the spectra of the CP Pup shell. The intensity of the λ5005 line was sufficiently strong that, if it was due to NII, the other lines should have been quite noticeable in the spectrum. Dielectronic recombination does not contribute much to the flux of NII lines, so that even if the gas was at a higher temperature it should not cause an enhanced λ5005 line flux. This calls into question the assignment of an NII transition to this line. The only alternative appears to be [OIII]. There is a perturbation in the spectrum around λ4959 which could be the other component of the [OIII] multiplet. Considering that a number of NIII transitions and one NIV transition have been suggested for some of the other lines, if there is any oxygen present in the plasma it would not be unreasonable to find it in a triply ionized state. Also, the presence of strong HeII fluxes indicates that the gas is in a higher stage of ionization than the DQ Her shell. The same arguments applied to nitrogen argue against large fluxes of NII lines, and hence that the λ5005 line is due mainly to [OIII]. In this case, the only line that can be used to determine the NIII abundance is NII λ5678. Using our calculated effective fluxes at a temperature of 625 K, an N_e of 10^2 cm^{-3}, and the case A model for hydrogen, we get $N(NIII)/N(HII) = 6.4 \times 10^{-3}$.

WIL suggested that the three lines λ4099, λ4379, and λ4640, are due to allowed NIII transitions. The NIII λ4379 line is produced by a $5g \rightarrow 4f$ transition and is an expected strong recombination line (WIL). Our model calculations for a recombination plasma predict that it should have the largest

flux by more than an order of magnitude of all the allowed optical NIII lines. Because it is not likely to be affected by optical depth effects or fluorescence, and can hence be modelled reasonably well in recombination conditions, it is a convenient line to use to determine the NIV abundance. Of the three suggested NIII identifications, the only one listed in Wiese et al. (1966) is λ4099. It appears in the observed spectrum (WIL, Fig. 2) as a blend with Hδ around λ4100. The measured flux of this line is about 7 – 9/19 relative to F(4379), whereas the predicted flux is less than 10% of F(4379). Similarly, NIII λ4640 is predicted by our model to be weaker than λ4101 and yet its measured flux is larger even than F(4379). A line at λ4003 due to an NIII 5f $\rightarrow$ 4d transition is predicted to be stronger than both λ4101 and λ4640 in recombination, but is not seen in the observed spectrum. However, the modelled flux of λ4003 with respect to λ4379 is so small that it would not be expected to be seen above the noise in WIL's spectrum. These two lines are essentially formed entirely by recombination so their relative strengths are as predicted, whereas if the λ4101 and λ4640 lines are due to NIII transitions some other mechanism must be responsible for enhancing their fluxes.

OII λ4653 and CIII λ4650 can be rejected as candidates for producing the λ4640 feature because of the absence of any detectable emissions in the region of λ4076 or λ4069 which these ions would produce. There would also be the problem of explaining why the measured wavelength is displaced by 10Å from its expected position. In fact, there is a good reason for accepting the NIII identification: the NIII λ4640 multiplet has lines at λ4634, λ4641, and λ4642 which would account for the broad nature of this feature in the observed spectrum.

Because the upper level of the NIII λ4640 transition, 3d ^{2}D, can decay directly to the groundstate, F(4640) is expected to be very weak in ordinary recombination conditions. In fact, the 3d $\rightarrow$ 2p transition has the largest A-value of all NIII transitions and gives rise to the strongest line (λ374) in the spectrum. However, the brightest emission lines observed in the spectra of the optical counterparts of galactic X-ray sources are often NIII λ4640 and HeII λ4686 (McClintock et al. 1975). In particular, in most X-ray binaries the NIII λ4640 line is prominent (Deguchi 1985). This line is interpreted as being produced by the Bowen fluorescence mechanism. In this mechanism, as a result of coincidence in the frequencies, HeII Lα photons are absorbed by OIII. A fraction of the OIII photons which are created by cascade through the OIII energy ladder are absorbed again by NIII and produce the NIII emission lines. Because of a coincidental OIII transition which produces λ374 photons, resonance pumping of NIII occurs via the 2p – 3d transition.

CP Pup was reported to be an X-ray source (Becker & Marshall 1981), but there are some problems in applying the fluorescence mechanism to nova shells. Firstly, Deguchi (1980) found it necessary to have densities of $\sim 10^8$ cm^{-3} for this mechanism to work efficiently, particularly when there were sub-

stantial velocity gradients. Secondly, fluorescence cannot explain the λ4099 flux. Note that Kallman & McCray (1980) gave the λ4099 line a branching ratio of 0.25 but they left out the 3p $^2P^0 \rightarrow 2p^2\ ^2P$ transition in their calculations of this value. It is the strongest transition out of 3p (Nussbaumer 1971), and, if included, reduces the λ4099 branching ratio to ~ 0.1. In fact, in Of stars NIII λ4640 appears in emission but λ4099 in absorption. This occurs because the filling rate of the 3p $^2P^0$ term is enhanced by dielectronic recombination while transitions to the groundstate are optically thick. This means that 3p $^2P^0$ is emptied via the λ4640 transition rather than by the λ374 transition. Because of the case B conditions, the lower term of the λ4099 transition, which normally cascades to the groundstate, develops a large population. Its upper level is filled by the λ4640 transitions but the branching ratio to λ4099 is so small that more photons are absorped than emitted. This clearly demonstrates that enhancing the λ4640 line does not automatically imply that the λ4099 emission is enhanced, rather the reverse. Finally, it is not clear that there is sufficient (if any) OIII in the CP Pup shell to pump NIII.

At low temperatures dielectronic recombination will not contribute much to the 3p $^2P^0$ filling rate. However, by running our NIII model under case B conditions, (i.e. by excluding transitions to the groundstate) we find that the λ4640 line flux is significantly enhanced even at low temperatures. The λ4101 flux, as expected, does not change by much. Every alternate HeII Brackett line has a wavelength that corresponds closely to an HI Balmer line. However, there is no reason to expect the HeII $12 \rightarrow 4$ cascade, which emits λ4101 photons, to be enhanced relative to the other lines in the series. We can, therefore, exclude any HeII contributions to this line.

The line identified as NIV λ4606 is also not listed in Wiese et al. (1966), but it too is a reasonable identification. WIL has discussed at some length which transitions are likely to produce the strongest optical lines in the recombination spectra of each of the five lowest ionization stages of the elements carbon, nitrogen, and oxygen. Where comparisons are possible, our model calculations agree with these assessments. There is, therefore, good reason to expect that NIV λ4606 is a strong line in the NIV recombination spectrum, but without detailed modelling we can say nothing about any other NIV lines.

WIL did not make any OIII identifications in the CP Pup shell but we see from Table 7.7 that there are two optical lines with large effective fluxes in the recombination spectrum of this ion. They are at λ3763 and λ4583 and have relative fluxes of 1.5 – 2 depending on the temperature. The wavelength scale in WIL's Fig. 2 is not aligned accurately with the identified lines so it is difficult to determine the wavelengths of unmarked features. However, there is a peak less than 50Å longward of the [OII] λ3727 identification which could be OIII λ3763. This is at least some evidence of the presence in this shell

of OIII. FWL have suggested that OIII is responsible for cooling the DQ Her shell and, presumably, the same mechanism applies to this nebula. This feature was not identified by WIL but neither λ3763 nor λ4583 were listed in his table of strongest optical recombination lines. For CIII and NIII he lists the 4f – 5g transitions but for OIII only the 3p – 3d λ3266 transition. λ3763 emissions are produced by the cascade 3p $\rightarrow$ 3s which follows this and should, therefore, be stronger. We should mention, though, that OIII is isoelectronic to NII and the λ3266 and λ3763 lines in OIII are equivalent to NII λ5005 and λ5678 whose relative fluxes have been a source of confusion. OIII produces λ4583 photons from 5g $\rightarrow$ 4f cascades which have an effective flux smaller than, but comparable to, those of NIII λ4379 and CIII λ4069. There is certainly no obvious feature at λ4583 in WIL's spectrum, but there could be a signal in the wing of the NIV λ4606 line. However, F(3763)/F(4583) will not necessarily have a ratio of 2 because F(3763) can be enhanced by various mechanisms. If the lines produced by transitions to the groundstate of OIII are optically thick then F(3763) will be enhanced. Alternatively, if Bowen fluorescence is occuring, an enhancement will also occur. If case B conditions apply to OIII then not only will the Bowen lines be enhanced but so will some of the other lines such as λ3363 and λ3017. The λ3266 line should not be affected by either mechanism.

It would be a worthwhile exercise to look for some other OIII lines so that its presence in this nebula can be confirmed. The relative strengths of the various lines would also help to determine what atomic processes are important in this gas. If there is no OIII in the shell then NIII λ4640 is not being resonantly pumped via the Bowen mechanism, and some alternative cooling agent to the OIII fine structure lines will need to be found.

If there is any significant Bowen fluorescence of OIII in this nebula we would expect λ3763 to be enhanced with respect to λ4583. Hence, even if a λ4583 line is not present, an OIII identification for the feature next to λ3727 is still quite feasible. The contributions of Bowen fluorescence to the OIII spectrum could be checked by looking for lines such as λ3133 (3p ^{3}S – 3d ^{3}P) or λ3444. They have weak recombination fluxes but are dramatically enhanced relative to λ3763 by fluorescence. If we assume pure recombination then the abundance can be approximated by comparison with NIII λ4380. Letting F(3763) = 1 – 1.5 $\times$ F(4380) gives an N(OIV) of 0.75 – 1.0 $\times$ N(NIV).

8.7 Discussion

The spectrum of the CP Pup shell differs quite markedly from that of DQ Her and T Aur. One of the stronger features in this spectrum is the line at λ4686 which has a flux only slightly smaller than F(Hβ). This line is almost certainly due to HeII and, since it is so much stronger than HeI λ5876, indicates that this plasma is in a higher state of ionization than those in the other two shells. This contention is supported by the identification of lines

of NIII and NIV in the gas, in contrast to the other shells which have only CII, NII, and OII lines.

Besides the λ4686 and λ5411 lines, modelled HeII spectra indicate that some other helium lines with measurable fluxes should be produced by this nebula. There is an HeII Brackett line at λ6560 but this will be swamped by Hα. However, the $5 \rightarrow 3$ and $5 \rightarrow 4$ transitions have wavelengths of λ3203 and λ10123 respectively, and should both be stronger than λ5411. Their calculated flux ratios at a temperature of 625 K are 0.35 for F(10123) and 0.24 for F(3203) with respect to F(4686). Although their ratio is model dependent, flux measurements of these two lines could be used to determine the reddening to CP Pup. Finally, there is the $3 \rightarrow 2$ transition which produces emissions at λ1640. HeII case A calculations yield fluxes for this line relative to F(4868) of 4.32 and 3.87 at temperatures of 2500 K and 625 K respectively. Because there is no λ3859 line with a larger flux than F(6233)and because we cannot find a suitable mechanism that would lead to an enhancement of the HeII λ6233 line, we have rejected the identification. If it is an HeII line then neither case A nor case B models are appropriate and the helium abundance would have to be much larger than quoted to account for the opacities of some of the other lines which are not observed.

WIL suggested that the [OII] λ3727 emission is formed in the ISM rather than in the nova shell. His reasons were that there is a large component of λ3727 emission in all the sky spectra, and the fact that this line is much narrower than all the other lines which are supposedly formed in the nova shell. Our analysis supports the idea that this line is formed in a different region to the recombination lines. Because there is no OII λ4650 emission at half the flux of F(3727), the [OII] λ3727 line could not have been formed by recombination at low temperatures so it appears that the bulk of the gas in this shell is in a higher stage of ionization than doubly ionized. This latter condition eliminates formation of [OII] lines either by recombination from OIII or collisional excitation from the OII groundstate.

An NIV recombination line, λ4606, was identified in the spectrum, and as the above analysis shows that nitrogen and oxygen both appear in this gas with similar properties, the possibility of OIV recombination lines should also be considered. WIL suggested that OIV λ4633 would be one of the stronger lines expected in these conditions. There could be some contribution from OIV λ4633 in the broad λ4640 feature, in which case its flux would be very similar to that of the NIV λ4606 line.

8.8 Summary

We present a summary of the line identifications and the ionic abundances determined from our models in Table 8.1. The upper section uses effective fluxes at a temperature of 625 K, and the lower section uses the results from models run at a temperature of 1250 K.

Table 8.1: Observed relative line fluxes and deduced abundances for the shells of DQ Her, T Aur and CP Pup at temperatures of 625 K (upper panel) and 1250 K (lower panel). A ? indicates a possible identification but no flux determination and a - indicates that the line was not observed.

ion	λ Å	eff. flux erg cm^3/s	DQ Her rel. flux	DQ Her abund. wrt HI	T Aur rel. flux	T Aur abund. wrt HI	CP Pup rel. flux	CP Pup abund. wrt HI
Hα	6560	2.998-24	146		330		300	
Hβ	4861	7.363-25	100		100		100	
HeI	5876	2.361-24	26	0.081	35	0.11	19	0.059
HeII	4868	1.870-23	18	0.007	?		92	0.036
CII	4267	1.788-23	29	0.012	-		<5	
NII	5678	1.041-23	-		24	0.017	9	0.006
NII	5005	9.426-24	29	0.023	40	0.031	44	0.034
OII	4650	1.360-23	30	0.016	102	0.055	-	
NIII	4380	3.407-23	<10	0.0022	-		19	0.004
OIII	3763	4.421-23	<10	0.0017	-		?	
[NII]	6584	9.266-24	38	0.030	110	0.087	200	0.159
[OII]	3727	2.622-23	100	0.028	?		21	0.0059
[OIII]	5007	2.996-23	-		18	0.0044	36	0.0088
Hα	6560	1.699-24	146		330		300	
Hβ	4861	4.521-25	100		100		100	
HeI	5876	1.306-24	26	0.090	35	0.12	19	0.066
HeII	4868	1.048-23	18	0.008	?		92	0.040
CII	4267	1.005-23	29	0.013	-		-	
NII	5678	6.303-24	-		24	0.017	9	0.0065
NII	5005	5.612-24	29	0.023	40	0.032	44	0.035
OII	4650	8.183-24	30	0.017	102	0.056	-	
NIII	4380	1.924-23	-		-		19	0.004
[NII]	6584	6.002-24	38	0.028	110	0.083	200	0.151
[OII]	3727	1.835-23	100	0.027	?		21	0.0056
[OIII]	5007	1.817-23	-		18	0.0045	36	0.0090

A check on the HeI lines can be made by looking for the λ10830 line. The flux of this line relative to F(5876) can in principle provide a crude estimate of the temperature, but in practice its flux is probably altered by optical depth effects. Another feature that should be looked for is the 2^3P continuum "line" which has a threshold wavelength at λ3422. At low temperatures its recombination coefficient is about 3/4 that of the HI Balmer coefficient, and its shape should be similar to the λ3644 feature. The total integrated flux of this line at a temperature of 625 K is $\sim 9.0 \times 10^{-25}$ erg cm^3/s which is larger than the HeI λ3889 flux. If N(HeII) is too small this line may be lost in the noise. Detection of the HeI continuum line would show how similar the HI and HeI line forming regions are, and provide a model-independent method of determining the HeII abundance.

In principle, because F(1335) has a strong temperature dependent contribution from dielectronic recombination, the CII F(1335)/F(4268) ratio can be used to determine the temperature. However, instrument calibration and other observational constraints introduce large uncertainties into the measured fluxes so this procedure had limited application. The dielectronic recombination coefficient below 1000 K is also only poorly known.

We cannot make any quantitative predictions regarding the CII quartet series but we would expect λ3877 to be one of the stronger lines. This is far enough removed from λ3889 not to be blended with it. In the higher temperatures characteristic of nebulae the [OIII] multiplet is usually formed by collisional excitation from the groundstate. However, strong forbidden lines can also arise due to recombination in cool plasmas, so that some of the λ5005 flux could be from [OIII] if the λ4959 component is lost in the noise.

Because it has been identified in the shells of CP Pup and T Aur the absence of the NII λ5678 line from the DQ Her spectra is embarrassing. In these shells, contrary to the model predictions, F(5005) has been found to be larger than F(5678), but this could be due to enhancement of λ5005 by [OIII]. The problem with the non-detection of the λ5678 line is that it is produced by the only transition emptying 3p ^{3}D, so that changing the A-value in our model would not alter the predicted flux. Furthermore, it is fed by NII λ5005 and should, therefore, be stronger than λ5005. Other spontaneous transition channels which could empty 3p ^{3}D go via excited-core configurations and involve two-electron transitions. The A-values for these decays are usually low, a fact amply supported by the non-detection of these lines in laboratory plasmas. An alternative explanation for the weakness of λ5678 is that the upper level 3p ^{3}D lies energetically close to 3p ^{1}P and their orbitals could overlap significantly. The singlet level 3p term decays to 3s emitting a λ6428 photon. This is not one of the predicted stronger singlet lines. To empty the upper level of λ5678 efficiently, the flux of λ6428 would have to be significantly enhanced, but there is no indication of any feature at this wavelength in the spectra. Hence, this explanation can also be discarded.

The sources of the forbidden line fluxes remain unresolved. Their fluxes relative to the allowed lines are too large for them to have been formed entirely by recombination, besides which lines such as [NII] λ5756, which should be present in the recombination spectrum were, not observed. If these lines are formed by collisional excitation then a hot gas with a low state of ionization must be present.

Chapter 9

Photoionization Models

9.1 Introduction

The temperature of a plasma is determined by the balance between the energy it gains and the energy it loses. In most astronomical plasmas the energy input comes from a flux of UV radiation which photoionizes the ions and in the process imparts kinetic energy to the ionized components. In supernovae, and possibly also in the early stages of nova shell evolution, fission of radioactive nuclei provides a source of energy. The main energy-loss mechanism in nebulae is radiation. Forbidden line emission from collisionally excited levels is the dominant process, but recombination and free-free emissions also contribute to the energy-loss. If sufficient dust is present in a gas then the shorter wavelength radiation is absorbed and the energy is reemitted by the heated gas. This radiation, which in low density plasmas such as planetary nebulae and nova shells has a blackbody spectrum at a temperature of a few hundred Kelvin, peaks in the IR.

The unusually low temperatures of some nova shells indicate that the energy-loss mechanisms are enhanced with respect to the energy-gain processes in these nebulae, compared to plasmas of similar densities, such as planetary nebulae (PN) or HII regions. High metal abundances have been found in nova shells (Williams et al. 1978; Gallagher et al. 1980; Williams 1982) so it is possible that the chemical abundance is responsible in some way for the low temperatures. Ferland et al. (1984) showed that the fine-structure lines in OIII, if it is present in sufficient concentrations, can efficiently cool a plasma to temperatures below 1000 K while the gas remains in a high state of ionization. The time-scale on which the shell cools is also of interest, i.e. whether this occurs gradually over decades, or rapidly at some particular epoch in its evolution. The question arises whether other ions could also cool the gas and on what time scale this would occur. The shells of DQ Her and CP Pup, for example, have noticeably different compositions and yet both have low temperatures.

To investigate the energy budget in nova shells and to trace their evolution from outburst, we have constructed a photoionization model. This type of model has been successfully used to interpret the line emissions observed in objects such as PN and HII regions (Harrington 1968; Harrington et al. 1982; Keyes & Aller 1978), supernova remnants excited by synchrotron radiation (Williams 1967), and Seyfert galaxy nuclei and QSOs (MacAlpine 1972; Kwan & Krolik 1981). A perfect fit between observations and modelling is an unrealistic goal. Besides the inhomogeneous nature of the shell, there are many uncertainties in the atomic physics incorporated in the model. For example, recombination coefficients of complex atoms and charge-exchange

cross sections are poorly known, particularly at low temperatures. However, by including all known reactions it is possible to ascertain the relative importance of the various processes and, hopefully, to understand the general physics governing these plasmas.

Our model is similar to those mentioned above. In PN and HII regions densities are low (typically $< 10^6$ cm^{-3}) and the gas is cooled by forbidden line emission from collisionally excited levels. However, the plasmas of these objects do not appear to be illuminated by strong X-ray fluxes so these models do not need to include radiation much above 100 eV. AGNs and Seyfert galaxies, on the other hand, have densities in excess of 10^9 cm^{-3} and strong X-ray fluxes so that in models it is necessary to include a photoionizing continuum up to 5 keV and the appropriate atomic physics. Nova shells appear to have a combination of properties from these objects. Their densities are low, typical of PN or HII regions, but their ionizing flux appears to have a significant X-ray component. Theoretical modelling of accretion onto white dwarfs predicts X-ray generation (King 1989), and, although only 8 out of 24 classical novae looked at in X-rays have been detected (Becker 1989), this might be an effect of the geometry of the systems or their distance from us. When X-radiation has been detected it has been found to be hard, where the hardness is quantified by comparing the ratio of counts above 0.5 keV to those below 0.5 keV. This ratio exceeds 2 in almost all cases. Studies of DQ Her by Ferland & Truran (1981) and Martin (1989) have used models with significant X-radiation even though DQ Her was not found to be an X-ray source. CP Pup, another classical nova which has an observed low temperature shell, has a strong X-ray flux (Becker & Marshall 1981).

In the next section we describe our model and the method of solution used, and in the following section we give details of the atomic data used. A discussion of some test results follows and then we go on to look at applications to nova shells.

9.2 The Model

Our photoionization model was parameterized by the luminosity and shape of the ionizing continuum, by the chemical composition, total mass and rate of expansion of the gas, and by the separation of the shell from the radiation source. We assumed that the nebula was spherically symmetric, with an inner radius R_i and an outer radius R_o. This region was subdivided into 100 concentric shells, each of equal thickness. At any given time after the outburst, R_i and R_o were determined from their expansion rates and, hence, the volume of the shell calculated. The density of each component was determined from the total density using the given abundances and assuming atomic masses of 1, 4, 12, 14, and 16 for H, He, C, N, and O respectively. Spatial inhomogeneities of density and composition are difficult to model, so in the interests of simplifying the problem they were left out. Similarly,

dust was not included in the model. In each shell the state of ionization was fixed by balancing photoionization with recombination, and simultaneously requiring thermal equilibrium by equating energy gains and losses within the gas. All known charge exchange and dielectronic reactions were included in the model, as well as photoionization by X-rays.

9.2.1 The Radiation Field

The radiation field was divided into stellar J^s and diffuse J^d components and solved on different frequency grids. Thus $J = J^s + J^d$. The stellar component was given by

$$J^s_\nu = \pi F_\nu \left(\frac{R_*}{R}\right)^2 \exp(-\tau_\nu(R))$$

where πF_ν is the flux emitted by each cm^2 of stellar surface, R_* is the stellar radius, R the distance to the central star and τ_ν the optical depth of the intervening material. The optical depth was calculated using all the components in the gas. We divided the stellar radiation field on the range from 11.6 eV (the ionization threshold of CI) to 5 keV into 85 intervals which were bounded in most cases by the ionization thresholds of the ions considered. The integration over each of the 85 intervals was carried out using Gaussian quadrature, with two frequency points per interval. The sources of the diffuse component were recombination to the groundstates of HI, HeI and HeII, recombinations to the $n \geq 2$ level of HeII, two-photon decays from HeII 2s and HeI 2^1S, and the HeII Lα line. A mesh of 50 frequency points was used to span the relevant continuum intervals from each ionization threshold, and 20 frequency points were used for each of the 2-photon continua.

Sufficiently energetic photons in the X-ray band can ionize CNO ions by interacting with either their valence electron or their K-shell electrons. K-shell photoionization of these ions is followed in $\sim$ 98% of the cases by the production of an Auger electron. The atom therefore undergoes a double ionization. We have followed the treatment of Weisheit & Dalgarno (1972) for determing the equilibrium conditions when K-shell photoionization is occurring by assuming that double ionization was produced in every instance. In view of the large ionized fractions of the elements in our models we assumed that all K-shell ionizations go into heating the gas (Shull 1979).

Given the stellar radiation field, the density distribution in the nebula and its chemical composition, an initial model was constructed using a modified on-the-spot approximation. In each shell we first set the diffuse radiation to zero, solved for N_e, T and all N_{ij} , where N_{ij} represents the number density of a j-times ionized atom of element i, and then computed the volume emission coefficients j_ν for the diffuse radiation and the volume absorption coefficients $\kappa_\nu = \sum N\sigma(\nu)$. We then assumed some fraction f of this diffuse radiation was absorbed on-the-spot by setting $J^d_\nu = f j_\nu/\kappa_\nu$. We used a value of $f = 0.1$. This solution was iterated until N_e, T and J^d_ν were constant from one iteration

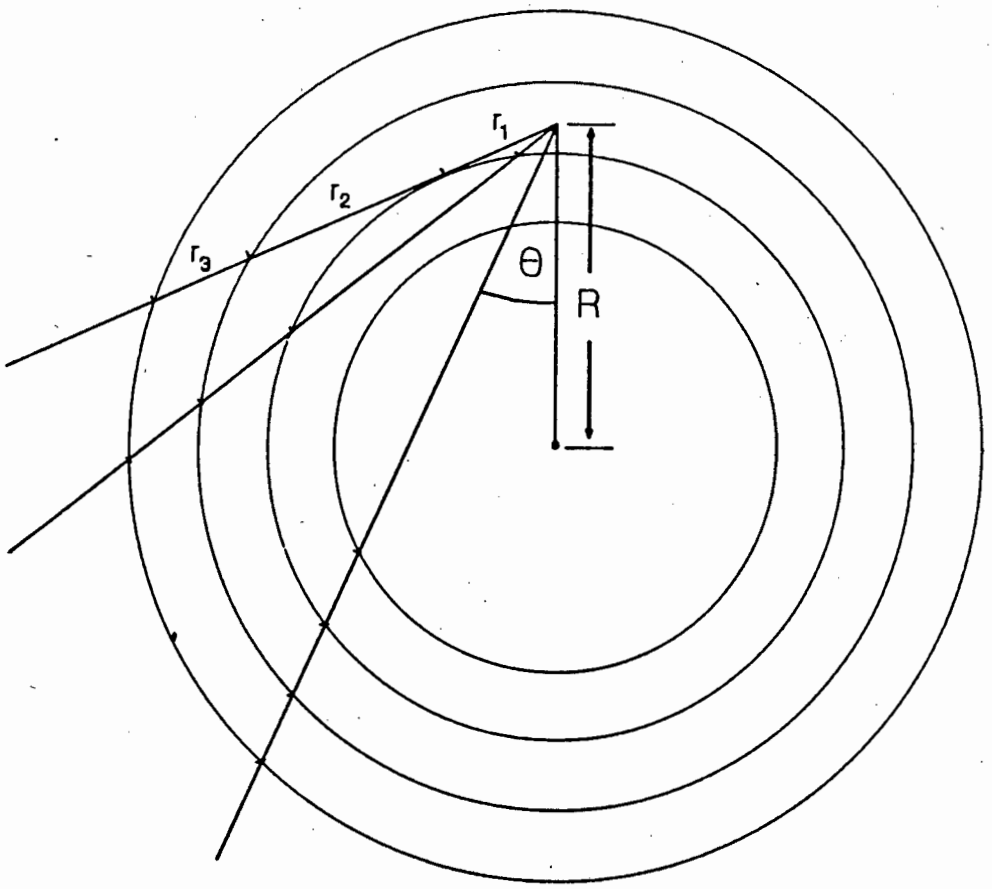

Figure 9.1: The geometrical configuration used in our model to calculate the equilibrium conditions in the shell. The reference point is a distance R from the central star and r_1, r_2, ... are the path lengths through each shell.

to the next. The outward integration of the optical depth, which included contributions from all ions, was carried out using the trapezoidal rule.

We then used the results of the on-the-spot model to calculate J_ν^d in each shell using

$$J_\nu^d = \int j_\nu(r)\, \exp(-\tau_\nu)\, dV$$

where the integration extends over the volume of the shell and the optical depth between the point of emission r and the reference point R is $\tau_\nu = \int \kappa_\nu\, dr$. The geometry used in the model is shown in Fig. 9.1. The integration over the volume, which was evaluated numerically, was performed in spherical coordinates. 10 discrete angles were used for θ which was integrated with a Gaussian scheme. Due to the symmetry of the system, the integration over ϕ is simply 2π. The integration in the radial direction had to take into account the path length through each shell and the optical depth from the reference point to the relevant shell. A new ionization model was then constructed using the J_ν^d from this computation and the whole process iterated to convergence in each shell. The shell parameters thus obtained were then

used to calculate J_ν^d again and the whole process repeated until convergence from one complete set of parameters to the next was obtained. We found that four or five iterations were generally sufficient to produce convergence.

9.2.2 Atomic Data

We used a mixture of H, He, C, N, and O in our model. Although other elements such as Ne, Mg, Si, and S have also been observed in nova shell ejecta, their abundances appear to be essentially solar in many cases. These elements do not have much influence on the conditions in the plasma compared to the effects produced by the over-abundant metals, and we have hence not included them in our model. Modelling of neon-enriched plasmas is discussed in Chp. 10. For each element energy levels, electron collision rates and spontaneous transitions for terms within $\sim$ 80000 cm^{-1} of the groundstate of the various ionization stages were taken from the compilation of Mendoza (1983). These data have been supplemented by the following values: NI A-values from Butler & Zeippen (1984), OII A-values from Zeippen (1987), CII collision strengths from Hayes & Nussbaumer (1984), the OIII collision strengths of Aggarwal (1983b), the OIV A-values and collision strengths of Nussbaumer & Storey (1982) and Hayes & Nussbaumer (1983) respectively, the HI collision strengths of Giovanardi & Palla (1989), and the HeI collision strengths from Berrington & Kingston (1987). The populations of the n = 2 levels of HeI, which lie above 80000 cm^{-1} of the HeI groundstate and are populated predominantly by recombination, were based on the results of our recombination model (Chp. 5), which were then linearly interpolated to the required temperature and density. We treated the OI, NII, OIII and OIV atoms as having 5 levels and CI, CII, NI and OII as atoms with 3 levels and solved them by matrix inversion. The fine-structure levels in CII and NIII were treated as 2 level atoms, as were CIII, CIV, NIII, NIV, NV, OV, and OVI. Neutral hydrogen was treated using its 6 lowest terms but it was never an important coolant in the plasma. For HeI the results from our recombination model as described in Chp. 5 were used.

For each ion the recombination rates and associated energy loss rates from all levels except the groundstate configuration were determined using the hydrogenic formulae of Seaton (1959a). The data of Henry (1970) were used to calculate the corresponding values for the groundstate terms, as well as the photoionization cross sections. K-shell photoionization cross sections were taken from Daltabuit & Cox (1972). The kinetic energy of the Auger electron produced by these ionizations contributes to the energy input to the gas. We used the values given by Shull (1979). The two-photon transition probabilities for decay of HeII 2S to the groundstate were scaled from the hydrogenic values of Spitzer & Greenstein (1951), and those for the decay of the 2^1S metastable level of HeI were from Dalgarno (1966).

Rates for the dielectronic recombination process discussed by Burgess

(1964), which involves transitions between optically allowed levels, were taken from Shull & Van Steenberg (1982). At nebular temperatures the dielectronic process involving levels connected by forbidden transitions is far more important. We used the values of Nussbaumer & Storey (1983) for this process, extrapolating the rates for all ions except OIV when the temperature of the plasma was below the range of fit of their formulae. For OIV we used $\alpha^{di}(T < 1000) = \alpha^{di}(1000)$. This probably grossly underestimates the dielectronic recombination rate to this ion at low temperatures. No estimates of the rate of energy lost from the electron gas by this recombination process were found in the literature, so it has not been included in the determination of the equilibrium temperature. In general, energy losses via recombination are not important compared to the cooling produced by the collisional excitation of forbidden lines, so the temperature estimates should not be too sensitive to this exclusion.

Charge exchange reactions involving H and He with ions of CNO up to the triply ionized stage were included in the models. Most of the charge exchange reactions we used were exothermic and, since they leave the products in excited states which rapidly decay, were only important in the forward direction. Their effect was to ionize H, He, or He^+ and to lower the degree of ionization of CNO. The rates we used came from Brown (1972), Butler & Dalgarno (1979), McCarroll & Valiron (1979), Watson & Christensen (1979), Butler & Dalgarno (1980), Butler et al. (1980), Heil et al. (1981), and Gargaud et al. (1989). Only reactions of N^+ and O^+ with H, and C^{+2} with He were treated in both the forward and reverse direction, since these are the only reactions that involve groundstate terms before and after interaction. The rates were linearly interpolated with respect to log(T), and in some cases extrapolated to low temperatures. No results were found for reactions involving two heavy elements. In most situations the low abundance of metal ions compared to H and He makes such reaction channels insignificant compared to those involving H and He. In environments such as nova shells, however, which have high CNO concentrations, these types of reaction could be important.

9.3 Results

To test our codes we ran them using the parameters of Harrington's (1969) homogeneous model and compared the results. The central source consisted of a 10^5 K blackbody with a radius of $0.236 R_\odot$. The nebula had inner and outer radii of 0.029 and 0.072 pc respectively and had a uniform distribution of H at a density of 2×10^3 atoms/cm^3. The abundances of He, C, N, O and Ne relative to H were 0.16, 2.0×10^{-4}, 1.5×10^{-4}, 4.5×10^{-4}, and 5.5×10^{-5} per cm^3. Our model did not contain any Ne so we increased the O abundance to 5.0×10^{-4} cm^{-3}. In Figs. 9.2 and 9.3 we show the results of running our codes using the above data. The ionization structure of

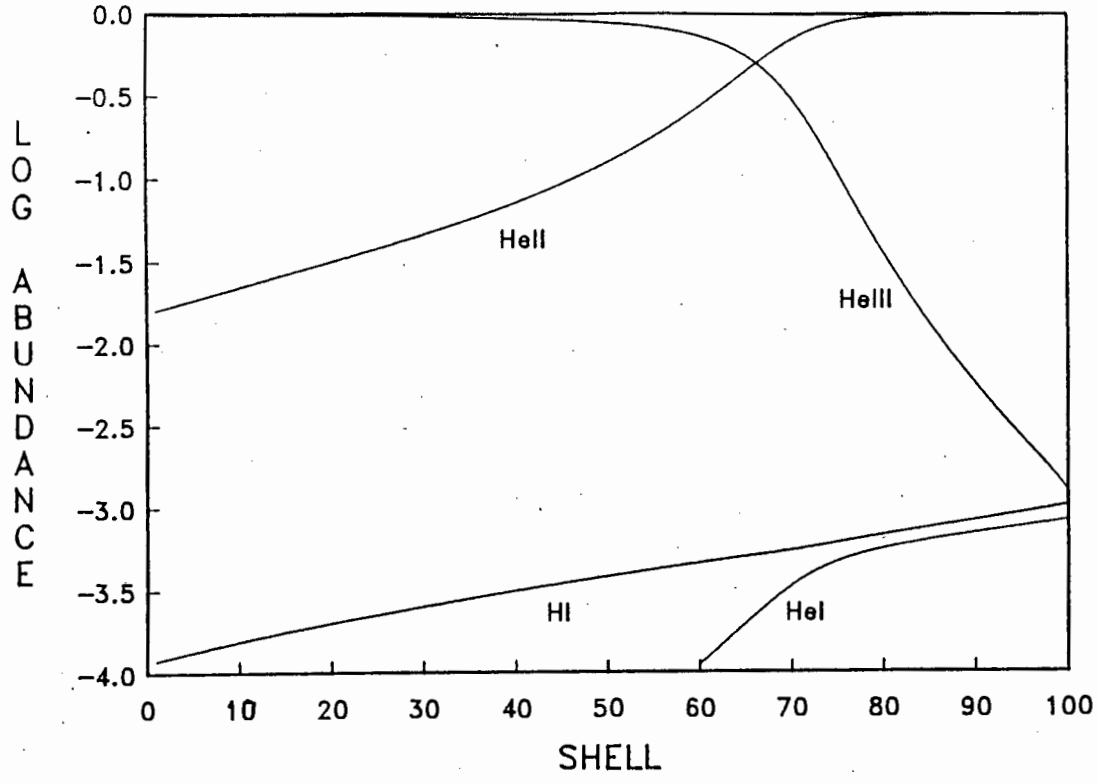

Figure 9.2: The ionization structure of hydrogen and helium for Harrington's (1969) homogeneous model computed using our photoionization codes. Shell numbers 1 and 100 correspond to distances from the central star of 0.029 pc and 0.072 pc respectively.

hydrogen and helium shown in Fig. 9.2 can be compared with the relevant traces in Fig. 2 of Harrington (1969). The agreement is excellent. Although we do not show the CNO ionization structure for our model, it is also very similar to that shown in Harrington's Fig. 2. The temperature profile is more sensitive than the state of ionization to the processes included in the model and the atomic data used, as can be seen by comparing the traces in Fig. 9.3 with Fig. 1 of Harrington (1969). The inclusion of dielectronic recombination and charge exchange in the model noticeably lowered the temperature of the gas in the inner regions (dashed line of Fig. 9.3) of the nebula. Harrington (1969) did not include these processes in his model so the solid line is more appropriate for comparison with his graph. Some differences are apparent, notwithstanding the distortion introduced by the disparate lengths of the axes. In particular our maximum temperature is lower than that of Harrington's model. Although there are a number of differences between our models, such as the numerical techniques employed and the frequency grids used, the overall agreement is very good. The most important differences concern the atomic data used. The data set of available rates has expanded since Harrington's work, and many of the rates he used have been recalcu-

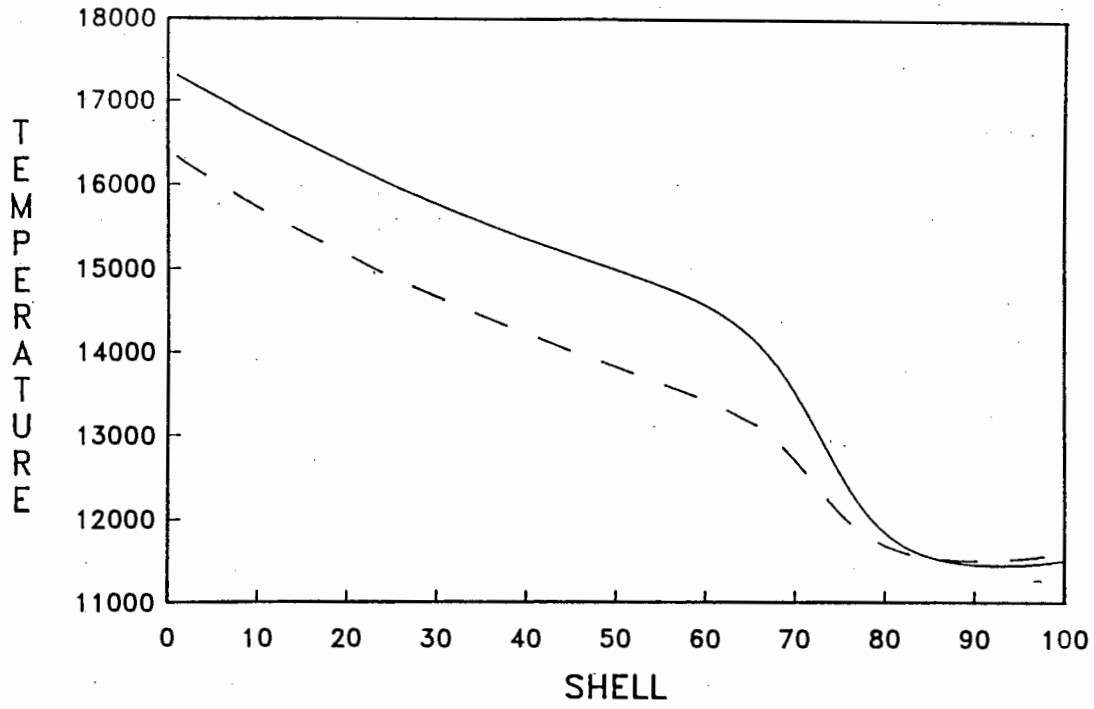

Figure 9.3: The temperature structure versus shell number for Harrington's (1969) homogeneous model as calculated using our codes. The solid line is for a model without dielectronic recombination or charge exchange processes, and the dashed line for a model which includes these processes.

lated. The nett effect of these changes was that the temperature in our model was slightly lower than that in Harrington's.

Since nova shells have been reported to have overabundances of He and CNO in various proportions, we have used our model to investigate the effects of increasing the abundance of each element while keeping all other parameters fixed. These results are instructive to consider since, with the hindsight provided by the model, it is easy to describe the effects produced, but it is not so easy to see *a priori* what will happen. The reason is that many effects are produced but it is not always clear which is dominant.

In what follows we shall refer to the model with dielectronic recombination and charge exchange described above as HAR. We have used this result as our baseline for discussing all the changes that occured. As our first example we look at the effect of doubling the helium abundance, i.e. we set N(He)/N(H) = 0.32. This has a noticeable effect on the temperature structure of the nebula, as can be seen from the curve labelled He2 in Fig. 9.4. The enhanced helium abundance absorbs more of the UV flux in the inner region of the nebula and raises the temperature of the gas. Around shell number 40, however, the $He^+ \rightarrow He^{2+}$ ionizing photons have all been absorbed and the edge of the He^{2+} Strömgren sphere is reached. The energy input to the gas is drastically reduced and the temperature falls rather rapidly by $\sim$ 3000 K. The cooling

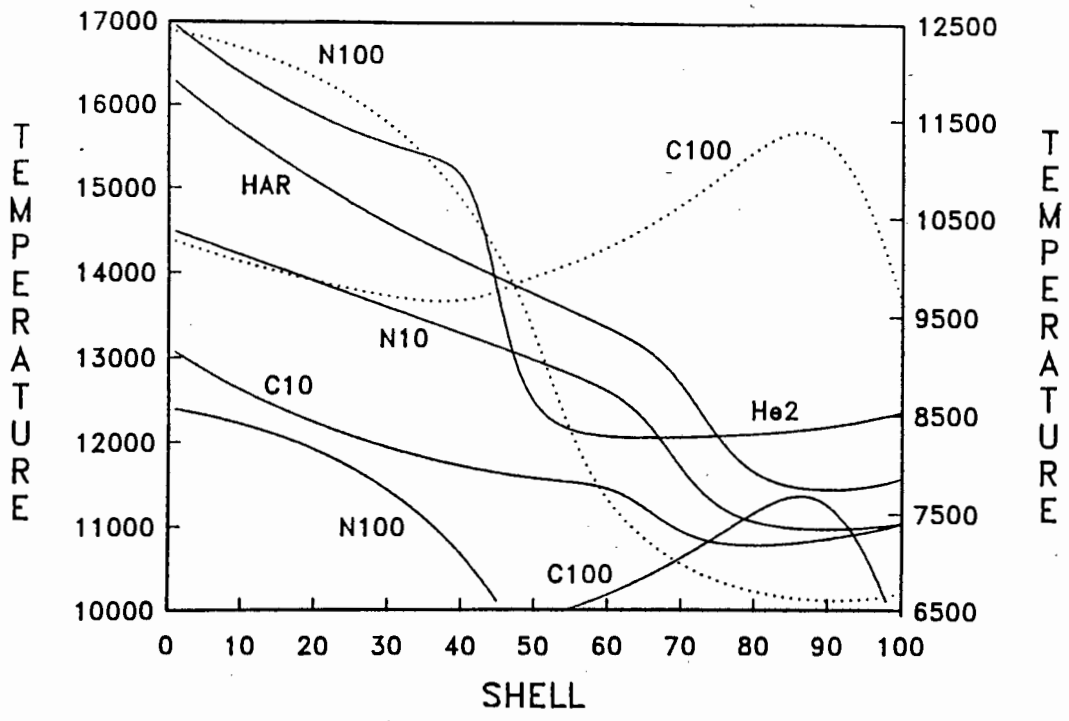

Figure 9.4: Temperature profiles for models with twice the helium abundance (He2) and 10 and 100 times the carbon (C10 and C100) and nitrogen (N10 and N100) abundance. For comparison the Harrington model temperature profile (HAR) is also shown. The solid lines use the left-hand axis and the dotted curves the right-hand axis.

in the inner region is predominantly due to OIV 25.9μm, CIV λ1549 and [OIII] $\lambda\lambda$5007, 4969. The OIV and CIV abundances fall off beyond shell 40, leaving the [OIII] lines to cool the gas.

Increasing either the carbon or nitrogen abundance by a factor of 10 lowers the temperature throughout the shell due to an increase in the cooling that can be achieved, but has very little effect on the ionic distribution. An increase in either of these components by a factor of 100 over HAR has a more pronounced effect on the thermal structure, as can be seen from Fig. 9.4. The cooling for the carbon model is produced by CIV λ1549 and OIV 25.9μm at the inner edge, but as the state of ionization of the gas decreases radially outwards, CIII λ1907 becomes the dominant cooling line. The forbidden OIII lines are also quite strong. In the nitrogen enriched model NIV λ1485, OIV 25.9μm, and NV λ1240 have the strongest fluxes at the inner edge, but as the ionization decreases radially, the NIII fine-structure line at 57.3μm becomes important. At the outer edge of the nebula the forbidden NII lines $\lambda\lambda$6584, 6548 produce the second strongest fluxes after NIII 57.3μm.

An increase in the oxygen abundance has a far more dramatic effect than those discussed thus far. Admittedly the oxygen abundance in HAR is higher than either the carbon or nitrogen abundance and a tenfold increase in its

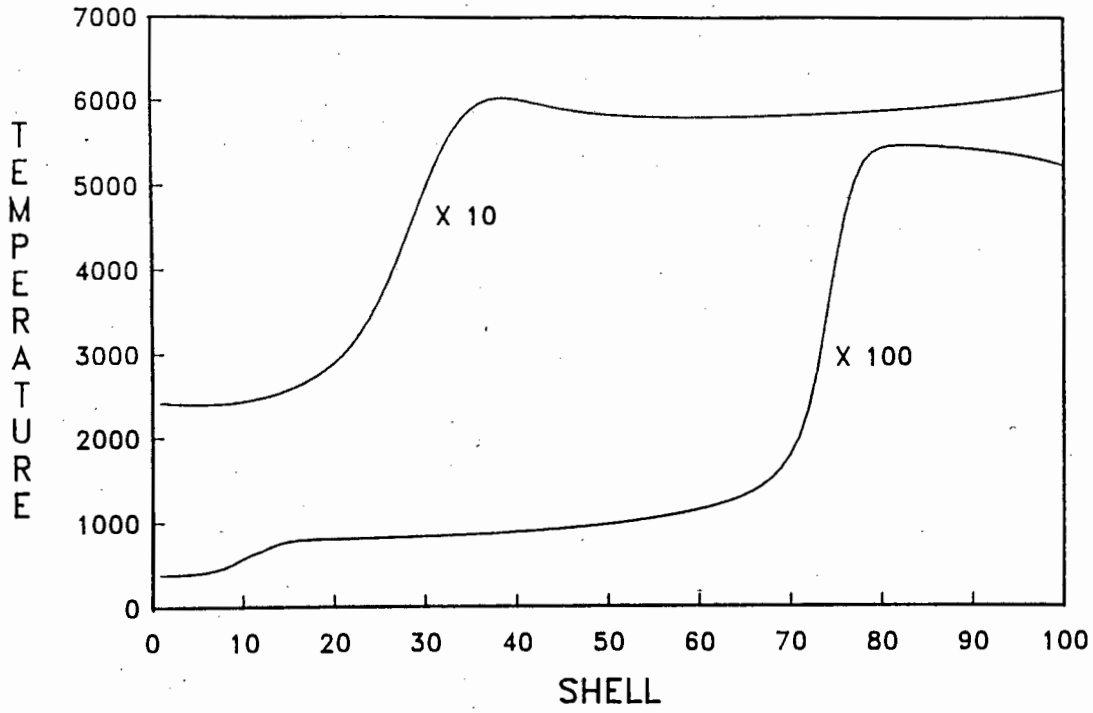

Figure 9.5: Temperature profiles for the Harrington model with the oxygen abundance increased by factors of 10 and 100.

abundance therefore represents a much bigger change than if either of the other two elements are increased by a similar factor. However, even if we increase the C or N abundances to the same concentration that we used for O, the effects are not as remarkable. Fig. 9.5 shows the modelled temperature in the nebula if the oxygen abundance is increased by factors of 10 and 100. The fascinating feature about these models is that the inner region of the nebula has a lower temperature than the outer region. Furthermore, the gas is in a higher state of ionization in the inner region where the temperature is low than in the outer, warmer region. In the ten times enhanced model OIV 25.9μm provides most of the cooling up to $\sim$ shell 35, beyond which OIII lines are responsible for the cooling. The forbidden and fine-structure lines of OIII contribute approximately equal amounts to the total flux radiated by these ions. In the case of a hundred-fold enhancement of oxygen the temperature at the inner radius is $\sim$ 350 K, due predominantly to the cooling efficiency of the OIV 25.9μm line. There is a rise in temperature as the OIV abundance decreases (around shell 10), but the OIII fine-structure lines are also efficient coolants and maintain the gas temperature around 1000 K. The slow rise in temperature from $\sim$ 700 K at shell 15 to $\sim$ 1200 K at shell 70 is due to a gradual decrease in the OIII abundance, and hence a decrease in the cooling. Around shell 70 the OIII abundance starts to fall off and there is a rapid rise in the temperature to $\sim$ 5400 K. The [OII] λ3727 line then becomes the dominant coolant.

Decreasing the temperature of the central blackbody source reduces the number of available ionizing photons and hence reduces the heating source of the gas. This results in a lowering of the temperature in the nebula, and a decrease in the size of the Strömgren sphere for each species of ion.

9.4 Non-uniform density distribution

All the photoionization models for nova shells described in the literature have used a constant density throughout the nebula. On the other hand, most of the models used to fit radio data consist of a spherically symmetric shell with a density gradient. In many cases a $1/R^2$ form provides a good fit to the data for novae (Seaquist 1989). Furthermore, assuming, as a first approximation, a steady outflow of gas during a nova eruption, the density of the ejecta will have a $1/R^2$ dependence.

We have run some tests using our photoionization codes to see what effect a $1/R^2$ density gradient has on the temperature and ionization structure of a nova shell. The DQ Her shell has been modelled previously and is therefore a good candidate to study. We used the abundances and shell parameters of Ferland et al. (1984). The chemical composition was H, He, C, N, and O with relative abundances of 1.0, 0.30, 0.0223, 0.0682, and 0.0249. By comparison, Martin (1989) used abundances of 1.0, 0.25, 0.015, 0.030, and 0.040. The inner and outer radii were $3.7 \times 10^{16}(t/47.4)$ cm and $5.1 \times 10^{16}(t/47.4)$ cm where t was the time since outburst in years, a shell mass of $4.8 \times 10^{-5} M_{\odot}$ and a volume filling factor of 0.3. For the ionizing source we used the parameters given by Martin (1989), namely a total luminosity of 10^{34} erg/s due to an accretion rate of 10^{17} g/s onto a $0.6 M_{\odot}$ white dwarf with a radius of 8.7×10^{8} cm. This luminosity was produced by two blackbodies of equal luminosity at temperatures of 3×10^4 K and 10^5 K. Ferland et al. (1984) used a different source for their model but the total luminosity was also 10^{34} erg/s. They have in fact pointed our that the shape of the source is not particularly important, rather that the number of available ionizing photons matters.

We ran two sets of models, one with a constant density and one with a $1/R^2$ density. The composition, shell mass, filling factor and shell volume (i.e. the inner and outer radii of the shell) were the same in both models. The temperature profiles through the shell at epochs 15.4, 22.0, 30.0, and 47.4 years after outburst are shown in Fig. 9.6. Clearly, the largest difference in the temperature profiles occurs at epoch 22.0.

The relative abundances of the H, He, and C ions were almost identical in the two models at all stages of the shell's evolution. The nitrogen and oxygen ionic abundances deviated the most in the early years but showed progressively less deviation as time progressed. Fig. 9.7 shows the logarithm of the relative oxygen ion abundances through the shell for year 15.4. The curves for nitrogen look very similar to those shown for oxygen. The mean

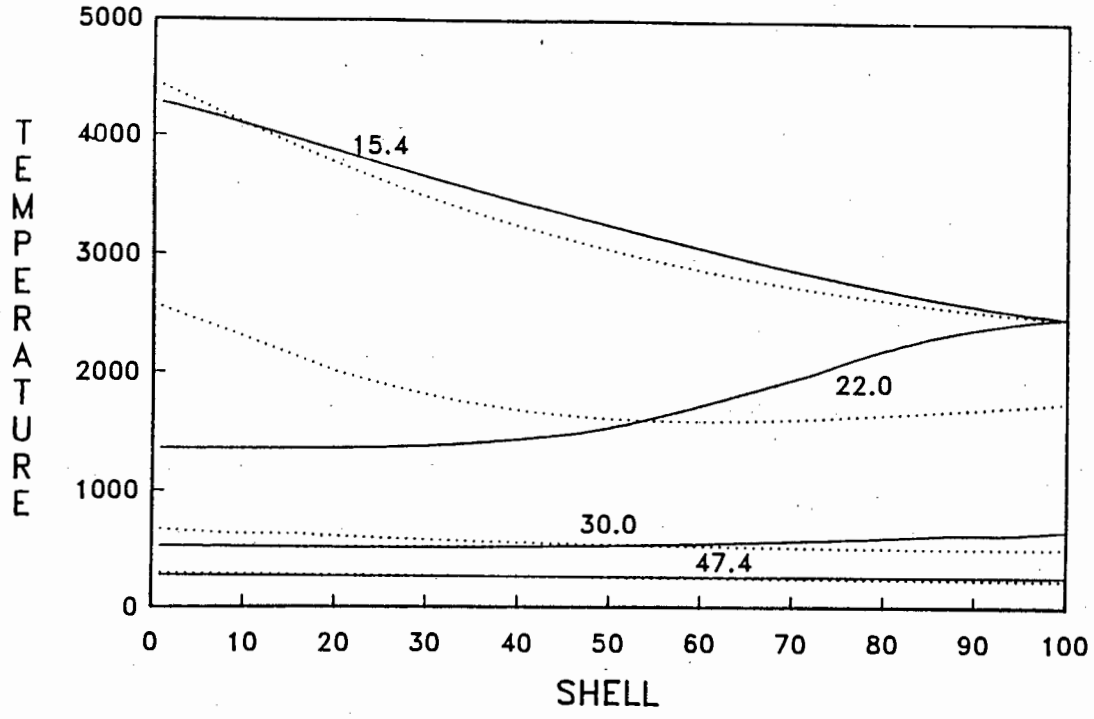

Figure 9.6: Temperature profiles for DQ Her nova shell models using constant density (solid line) and $1/R^2$ density (dotted line) distributions. The numbers indicate the year after outburst for which the calculations were made.

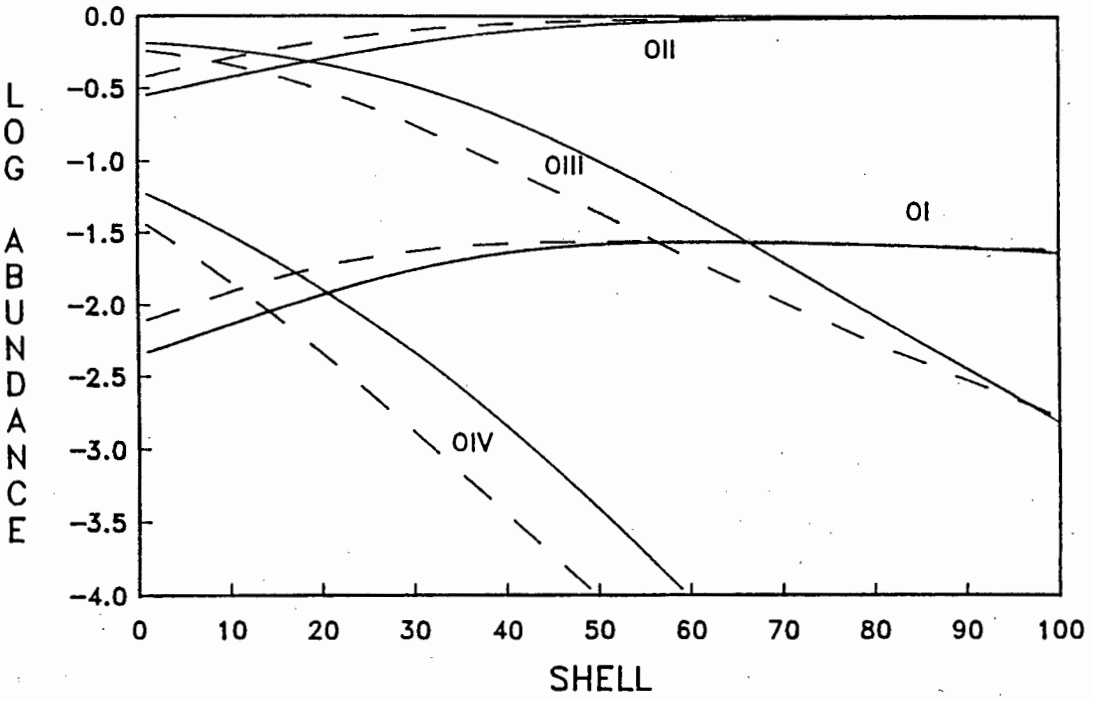

Figure 9.7: The ionization structure of oxygen in the constant density (solid line) and $1/R^2$ density (dashed line) models of DQ Her 15.4 years after outburst.

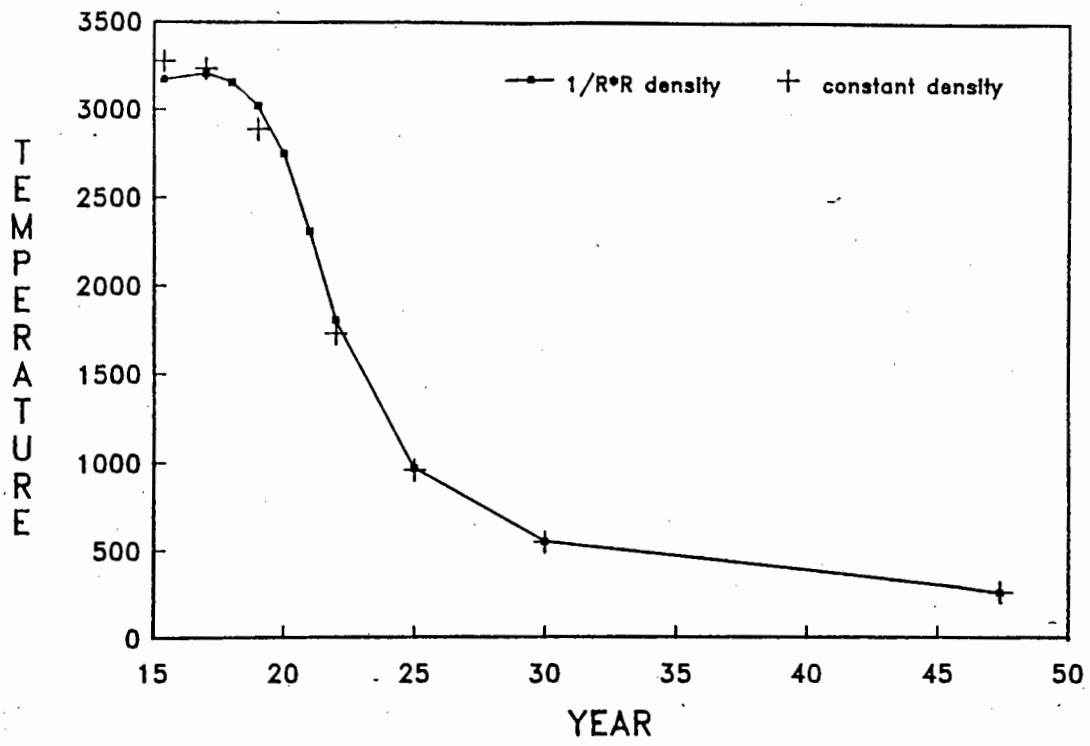

Figure 9.8: A comparison of the mean temperature (in Kelvin) of the DQ Her shell for a $1/R^2$ density model and a constant density model as a function of years since outburst. Because the two data sets are very similar, fewer points have been plotted for the constant density model so as not to clutter the diagram.

temperature of the shell

$$< T >= \frac{\int_{R_i}^{R_o} T(R)\, dR}{R_o - R_i}$$

differed very little between the two models, as can be seen from Fig. 9.8. Although a $1/R^2$ density model might be a more realistic representation of the conditions in nova shells, it appears that the results are not significantly different to a constant density model, and hence there should be no major differences in the physics occurring in shells with non-uniform densities. However, from an observational point of view there can be some significant differences. If radiative transfer effects are neglected, the measured line fluxes will be the emission per unit volume integrated along the line of sight. As an example we consider the [OIII] $\lambda\lambda$ 5007, 4959 lines in year 22.0. Most of this emission will come from the higher temperature region of the shell which, in the case of the constant density model, is the outer region. In the inverse squared distribution it is in the inner region. The density is much higher in this region compared to the constant density model, so the total flux emitted in these lines will be much higher in the $1/R^2$ model. Fig. 9.9 illustrates this difference for the [OIII] λ5007 line. Note that a log scale has been used for

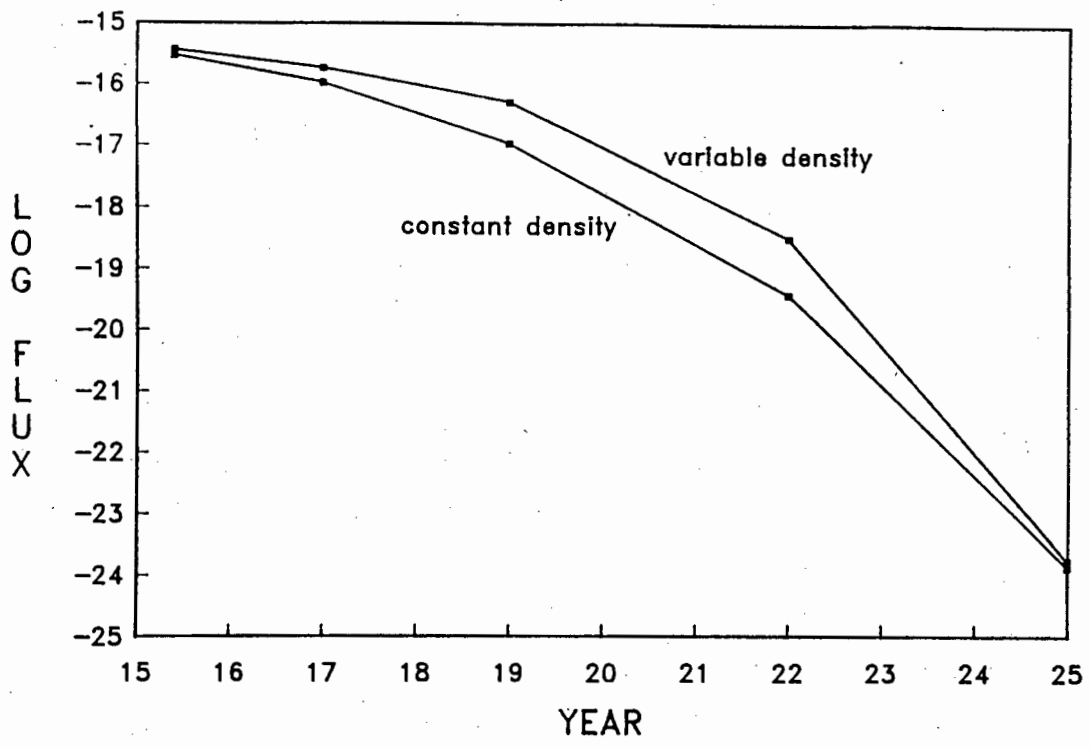

Figure 9.9: Flux of the [OIII] λ5007 line versus year since outburst for the constant and $1/R^2$ density models.

the ordinate axis so that between years 19 and 22 there is about an order of magnitude difference between the fluxes for the two models. After year 25 the difference becomes insignificant. Actually, what happens is that the temperature becomes too low for these lines to be collisionally excited after year 25 and the flux of these lines rapidly tends to zero.

Chapter 10

Nova Shells — Case Studies

10.1 Introduction

In this chapter we examine the old nova CP Pup 1942 and look at the newly discovered class of novae that occur from neon white dwarfs. In particular, we shall be using our photoionization codes to study the ionic element abundances and temperature structure within the shells of these novae as they evolve from outburst. In attempting to model the gaseous shells of novae using our photoionization codes we need to include a source of ionizing radiation from the central stellar system. It appears that the shape of this continuum is not important, but the total number of ionizing photons it produces is. Because this radiation is as capable of ionizing the ISM as the nebula, any radiation that is not absorbed by the shell is absorbed on its path through the ISM. The column density of interstellar space is sufficiently large to ensure that no meaningful signal at wavelengths shorter than the ionization threshold of HI reaches our telescopes. As we cannot measure this radiation, we have to rely on theoretical arguments to determine its spectrum. Our models of the nebulae impose certain constraints on this radiation and so, to an extent, we are able to verify its form. Before looking at specific cases of nova shells, we examine the predicted shape and intensity of the stellar continuum radiation. We use parameters from the CP Pup system to derive quantitative values for the continuum flux, but the parameters are often poorly determined so we have used "typical" values. The results we obtain are therefore fairly general and are applicable to many other systems.

10.2 The Ionizing Radiation

Most of the luminosity of cataclysmic variables comes from the accretion process and not from the stellar components. Matter falling onto the degenerate primary star gives up its binding energy to radiation, with a resulting luminosity of

$$L_{acc} = \frac{GM_1\dot{M}}{R_1} \quad \text{erg/s}$$

where M_1 and R_1 are the mass and radius of the primary star. In degenerate stars these are dependent quantities: for white dwarfs the mass-radius relation is given approximately by $R_1/R_\odot = 0.007(M_1/M_\odot)^{-0.8}$ (Hamada & Salpeter 1961). A $1M_\odot$ white dwarf has a radius $R_1 \simeq 5 \times 10^8$ cm.

In systems with weak or no magnetic fields an accretion disk and boundary layer are formed. About half of the accretion luminosity is radiated by

the disk itself so that

$$L_{disk} = 6.5 \times 10^{32} \dot{M}_{16} M_1 / R_9$$

where we have parameterized $\dot{M}$ in units of 10^{16} g/s, M_1 in $M_\odot$ and R_9 in 10^9 cm. For frequencies ν such that $h\nu \approx kT_{max}$, this flux has the form $F_\nu \propto \nu^{\frac{1}{3}} \exp(-h\nu/kT_{max})$ where

$$T_{max} = 1.7 \times 10^5 (\dot{M}_{18})^{\frac{1}{4}} (M/M_\odot)^{\frac{1}{4}} (R/R_9)^{-\frac{3}{4}} \text{ K.}$$

At long wavelengths the whole disk is a Rayleigh-Jeans emitter so $F_\nu \propto \nu^2$. For typical values of the parameters for classical novae the long wavelengths lie below the ionization limit of CI and are of no interest to our photoionization calculations. Models of the accretion flow onto the surface of a white dwarf (Pringle 1977, Pringle & Savonije 1979) predict a boundary layer emitting a luminosity equal to L_{disk} as a blackbody with temperature

$$T_{BL} = 8.6 \times 10^5 \dot{M}_{18}^{\frac{2}{9}} M_1^{\frac{1}{3}} R_9^{\frac{7}{9}} \text{ K.}$$

The effective radius R_{eff} of this source of radiation is given by

$$L_{disk} = L_{BL} = 4\pi R_{eff}^2 \sigma T_{BL}^4$$

where σ is the Stefan-Boltzmann constant.

If the primary has a sufficiently strong magnetic field then accretion flow is channelled along the field lines onto the primary's surface, creating a stand-off shock above the surface. Depending on the strength of the field and the accretion rate, the accretion can occur either directly as in the AM Her systems, or via a partial accretion disk as in the intermediate polars. The emitted radiation consists of (Lamb & Masters 1979): (1) a blackbody-limited UV cyclotron component; (2) a hard X-ray bremsstrahlung component; (3) a soft X-ray or hard UV blackbody component due to the absorption and reemission of (1) and (2) from the stellar surface; and (4) secondary radiation from infalling matter above the shock or, possibly, from the stellar surface around the emission region. No polarized optical emission has been detected in the CP Pup nova remnant (Stockman et al. 1988; Kaluzny & Chlebowski 1988), but a hard X-ray blackbody bremsstrahlung component has been found (Becker & Marshall 1981). The UV/soft X-ray blackbody component should be very similar in both the magnetic and non-magnetic systems. Since this component is the main contributor to the ionizing flux, it is unlikely that photoionization models will be able to distinguish between the different sources. Therefore, we used the flux distribution curves for a non-magnetic source, but added in an X-ray component that matched the observations.

We need to determine values for the parameters $\dot{M}$ and M_1 or R_1 to be able to apply these models. There is no direct method for measuring the

accretion rate in CVs. The best general method (Patterson 1984) seems to be to find the absolute visual magnitude M_v and then to use theoretical disk models to find what $\dot{M}$ is required to produce M_v. M_v can be determined if the distance and interstellar extinction to the CV are known, but these quantities are usually subject to some uncertainty. Patterson & Raymond (1985a) have used a distance of 700pc to determine M_v from the observed m_v =15.5 for CP Pup, and have then interpolated Table 1 of Tylenda (1981) to estimate $\dot{M}$. This table has been calculated assuming the accretion takes place on a $1M_\odot$ white dwarf. For CP Pup they obtain $\dot{M} = 10^{16.8}$ g/s =6.3×10^{16} g/s. For a $1M_\odot$ white dwarf this gives a bolometric luminosity of $L_{bol} = 1.6 \times 10^{34}$ erg/s. The continuum spectrum for these parameters has T_{max} = 50000 K and a blackbody temperature of 2.7×10^5 K. A third source of continuum radiation in CP Pup has been detected by Becker & Marshall (1981) in their *Einstein* observations of old novae. They found a hard continuum with a 0.2 – 4.0 keV luminosity of 1.3×10^{33} erg/s (Patterson & Raymond 1985a). This has been interpreted as an optically thin 10 keV bremsstrahlung spectrum (Cordova et al. 1981).

10.3 CP Pup

Unlike nova DQ Her, which has been extensively studied over a broad range of wavelengths and subjected to a number of analyses (see Bode & Evans 1989 for references to previous work as well as some original analyses), the CP Pup system has not received nearly as much publicity. Although similar in some respects, there are also many differences between these two novae. Typical of fast novae, CP Pup never went through a phase of dust formation which is generally believed to have been responsible for the large minimum in the DQ Her light curve. Besides their diverse outburst characteristics, the CP Pup and DQ Her shells differ in chemical composition and state of ionization. CP Pup has a strong X-ray flux and its shell spectrum has characteristics resembling those of high excitation PN, i.e. strong HeII λ4686 emission and lines of NIII and NIV. The Bowen fluorescence mechanism involving He and OIII is responsible for enhancing the NIII emissions in PN, but no OIII has yet been detected in the CP Pup nebula. This indicates that the nitrogen abundance in the shell must be quite large. The OIII fine-structure lines are responsible for most of the cooling in the DQ Her shell, but, as no oxygen has been observed in this gas, it is not clear that there is enough OIII present to provide the necessary radiative emission from its fine-structure lines to cool the gas to the low temperature that has been measured.

We have used our photoionization model to see if the NIII 57 μm fine-structure line can provide the required cooling and to set limits on the oxygen and carbon abundances. Although the photoionization model is not very sensitive to the shape of the ionizing spectrum, we are still able to learn something about the central source from our results.

The problem of distance determination to this system is addressed first, as there appear to be some conflicting results in the literature.

10.3.1 Distance to CP Pup

Distances to novae are often poorly known, but the expansion parallax method applied to nova shells provides one of the more accurate techniques of distance determination. Non-spherical shells introduce a degree of uncertainty into the estimates, as does the fact that the size of the shell is usually measured in the light of Hα, whereas the expansion velocity is determined from other lines such as Hβ, Hγ, HeII λ4686 and [OIII] $\lambda\lambda$5007, 4959. Measured line fluxes, usually Hβ, can be used together with the distance to determine the density in the shell. Methods normally employed to determine densities in nebulae do not work in the peculiar conditions found in cool nova shells.

In the literature a factor of two difference between values for the distance to CP Pup can be found, most probably due to the use of an incorrect value of v_{exp}. The initial detection and distance determination of a shell around CP Pup was made by Zwicky in 1955 and reported by Bowen (1956). A distance of $\sim$ 1500 pc was determined from the measured angular radius of 2".78 and v_{exp} = 1600 km/s taken from spectrograms of the nova shortly after maximum light. Following this announcement, Sanford & Greenstein (1957) reported a distance determination based on some spectroscopic measurements of the expansion velocity from line widths made in 1956. Unfortunately, this report contains an error. They estimated the expansion velocity to be $\sim$ 700 km/s from the width of the N_1, N_2, Hβ, and HeII λ4686 emission lines in the shell but they took Zwicky's measured angular parallax to be the *diameter* rather than radius of the shell. This gave them a distance similar to that reported by Zwicky. This error was corrected by Greenstein et al. (1957) who then suggested a distance of 700pc and $M_v \sim -9.4$. Note that this report has not been included in the bibliographies of either Duerbeck (1987a) or Bode et al. (1989). The expansion velocity of 1600 km/s used by Zwicky has been attributed to a shell of a transient nature seen only in the early stages of the nova, while the value of 700 km/s has been observed more than once at widely spaced intervals. In a review of novae, McLaughlin (1960) used these values, which have subsequently been quoted extensively. More recently Cohen & Rosenthal (1983) have measured the expansion velocity of the CP Pup shell, obtaining v_{exp} = 710 km/s in good agreement with Greenstein et al. (1957).

Unfortunately, the incorrect value of 1600 km/s for v_{exp} still permeates the literature and the distance to CP Pup is often falsely given as $\sim$ 1.5 kpc. For example, Duerbeck (1981) quotes a distance of 1500pc based on observations of the shell he made in 1979. Williams (1982), in his analysis of the shell spectrum, measured the angular radius of the envelope to be 7".0 from a photograph taken in the light of Hα 37.3 years after outburst. He also used v_{exp} = 1600 km/s and hence claimed a distance of 1.6 kpc for CP

Pup. Reporting on *Einstein* X-ray observations of novae, Becker & Marshall (1981) used a distance of 700 pc (from McLaughlin 1960), but Becker (1989) has changed this to 1500 pc to calculate the absolute X-ray flux emitted by CP Pup. At this distance it is the brightest X-ray source amongst the classical novae, whereas at 700 pc its X-ray flux is more in line with those of other fast nova and no longer the strongest source.

If we use v_{exp} = 710 km/s (Cohen & Rosenthal 1983) and an angular shell radius of 7".0 at year 37.3 (Williams 1982) then we get a distance of 800 pc to CP Pup. For m_v(max) = 0.4 and A_v = 0.3 Cohen & Rosenthal (1983) obtained M_v(max) = -9.55, which corresponds to a distance of 850 pc. It is not clear what value they used for the time since outburst, but for a period of 40 years we obtained this same value. The M_v versus rate of decline relationship given by Cohen (1985) yields M_v(max) = -9.0 for a t_2 of 5 days, which implies a distance of 660 pc to CP Pup for A_v = 0.3, while for A_v = 0.8 (Duerbeck 1981) we get 525 pc. The ISM appears to be relatively inhomogeneous in the direction of Puppis (Deutschman et al. 1976) so that determinations of A_v to CP Pup are somewhat uncertain. We shall henceforth adopt a value of 800 pc to the nova.

10.3.2 The model

A theoretical continuum source for use with CP Pup was described in §10.2. Modifications to this flux, required to match our results with the observations, will be described shortly. Parameters used for the gaseous shell were as follows. The outer and inner radii of the shell have been scaled from the photograph of the shell taken 37.3 years after outburst (Williams 1982) and were estimated to be $R_o = 2.24\times10^{15}$t cm, where t is the time in years since outburst, and $R_i = \frac{2}{3}R_o$. This corresponds to an expansion velocity v_{exp} = 710 km/s at 800 pc. We assumed a volume filling factor of 0.3, and, based on the Hβ flux reported by Williams (1982), used a shell mass of 2×10^{-5} $M_\odot$.

We also needed to include abundances of H, He, C, N, and O in our model. The values in Table 8.1 were used as a guide. The helium abundance should be reliable because the effective fluxes of its lines could be modelled quite accurately. We used an N(He)/N(H) ratio of 0.1 based on our interpretation of the spectrum given in chapter 8. The HeI to HeII line intensities were used as a guide to the relative abundances of HeII and HeIII. Because the effective fluxes for CNO ions are so uncertain, abundances could not be determined nearly so accurately, and it was thus necessary to vary them until a reasonable solution was obtained. The presence of lines of nitrogen and the absence of carbon and oxygen lines requires the nitrogen abundance to be a factor of at least a few times larger than either carbon or oxygen.

The model as described above was reasonably successful in describing some of the features seen in the CP Pup shell at year 37.3, but some tuning of the parameters was necessary. The abundances we used in our final model

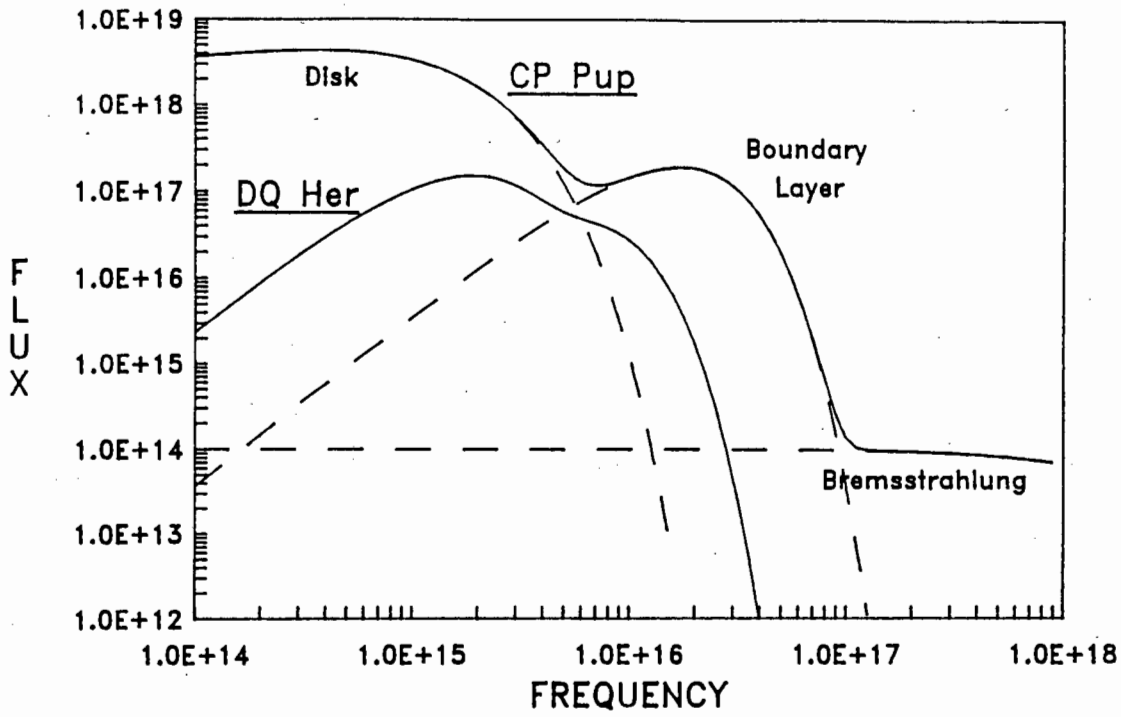

Figure 10.1: The total flux used for CP Pup and the contributions from the disk, the boundary layer and Bremsstrahlung. Also shown is the flux distribution used for the DQ Her model in §9.4.

are listed in Table 10.1. The ionizing radiation was very similar to the theoretical models, except that we found it necessary to increase the blackbody temperature to 2.8×10^5 K and its total flux by a factor of 1.5 to produce the necessary ionization. The total luminosity consisted of 8.2×10^{33} erg/s from the disc, 5×10^{32} erg/s from Bremsstrahlung, and 9.7×10^{33} erg/s from the boundary layer. The total flux and its contributors are plotted in Fig. 10.1. However, this model is at odds with the observations. The *Einstein* IPC observations should have detected the upper edge of the blackbody emission in the low energy end of its detector. This problem is not unique to CP Pup: a similar missing flux was reported for V603 Aql (see Figure 1 and the discussion in §II of Patterson & Raymond 1985b).

Table 10.1: Abundances used in CP Pup model.

H	He	C	N	O
1.0	0.1	0.002	0.01	0.002

There are a number of important observed features in the CP Pup shell that our model for year 37.3 was able to reproduce. The mean temperature of the modelled shell was $\sim$ 760 K which compares very well with the measured value of 800 K. The ionizing flux was adjusted so that the HeII/HeIII ratio

in our model was about 1.6. The predicted HeI λ5678 and HeII λ4686 line intensities due to recombination closely match the measured values. The carbon and oxygen abundances were sufficiently small that no observable emission could be expected from them. The abundances of the nitrogen ions NII/NIII/NIV/NV were in the ratio 16.7/47.9/9.0/0.9 so that the relative intensity of NII λ5005 with respect to NIII λ4380 was 1.4 while the NI line intensities were very small. We have not explicitly calculated effective fluxes for the NIV ion but hydrogenic calculations can be scaled to account for a charge of Z = 3. For the 6h $\rightarrow$ 5g transition in a triply charged hydrogenic ion we get an effective flux of 1.8×10^{-23} erg cm^3/s. Using the NV abundance from our model, this implies an NIV λ4606 flux that would be 20 times weaker than NIII λ4380. This is clearly at odds with the observations if an NIV assignment for the λ4606 feature is correct. The largest line flux from this nebula was produced by the NIII 57μm fine-structure transition, followed by the OIII 88μm, the NII 205μm, the OIII 52μm and NII 122μm lines. The NIII line flux was more than an order of magnitude larger than the OIII 88 μm line flux, and was $\sim$ 230 times larger than the Hβ flux. The NIII 57μm line produced $\sim$80% of the radiative flux from the nebula and was therefore the dominant coolant in the gas.

The [OII] λ3727 line flux from our model would be insufficient to explain the measured flux of this line. However, if we accept the suggestion of Williams (1982) that this line is formed by photoionization of neutral oxygen in a surrounding interstellar cloud, then our model is still consistent. The biggest problem we have with our model is to explain the large observed [NII] λ6584 emission. Forbidden lines can be formed under recombination conditions but our calculations (see Table 7.9) indicated that [NII] λ6584 should have a flux about equal to NII λ5005. Furthermore, in recombination conditions [NII] λ5756 should be present with a flux of F(5756) $\approx \frac{1}{5}$F(6584), which would make it one of the stronger lines in the spectrum. Since it was not seen it seems more likely that the [NII] λ6584 emission was formed in a warm gas, possibly in the same region as the [OII] λ3727 line. The nova shell is not radiation bounded so there is a source of photons to ionize any surrounding clouds. Even in gases with enhanced CNO, if the electron density is low enough the gas temperature will increase to nebular temperatures. The high velocity gas (v = 1600 km/s) detected during the early development of the nova could be in a cloud of a sufficiently low density that the cooling is not very efficient so that nebular temperatures prevail. This cloud could be responsible for the [NII] and [OII] emission.

If the shell emissions have not already faded to levels below the limits of detectability, there are a number of emission lines that should be looked for. We have already indicated the possible existence of OIII λ3760 as an unmarked feature in Williams's (1982) spectrum. Another OIII line that might be detectable is λ3133. Under pure recombination conditions this line

has a weak flux — our calculations show it to be $\sim$ 200 times weaker than F(3726). However, in many gaseous nebulae the Bowen fluorescence mechanism pumps this line to become one of the stronger lines in the spectrum. Although the column density in nova shells is low, the enhanced nitrogen abundance might produce enough resonant line flux for the Bowen process to become important, and hence to generate observable fluxes of λ3133. Because NIV λ4380 has been detected, the NIV λ3484 line should be looked for as it is fed by λ4380 and should therefore have a larger flux. The HeII lines λ3203 and λ10123 are also likely to be quite strong, particularly the former line. UV lines of CNO falling in the range of the *IUE* detectors should be too weak to be observed and similarly only the NIII 57μm line (and perhaps also the OIII and NII fine-structure lines) should have enough flux to be detectable in the IR.

10.3.3 Evolution of the Shell

The fluxes and abundances determined for year 37.3 can be used to trace the evolution of the shell over the period in which the ionizing flux was a constant. Unfortunately there is not much observational material in this period. This lack of data from the earlier years is a serious drawback to our modelling, since we have no way of checking the validity of the results we obtain. We also cannot tell when the shell became optically thin or at what epoch the ionizing source stabilized. Nevertheless, we can use our model to compare the theoretical cooling curve for CP Pup with that of the well-studied DQ Her system which has different abundances and ionizing source. We can also make predictions as to how the shell will evolve in later years, and these results can be used to check the model if suitable observations can be obtained.

A number of spectroscopic studies of CP Pup were made in the five years following outburst (see Bode et al. 1989 for a list of references). These spectra are of little use to us since line fluxes were not determined and modelling of the shell is not particularly instructive. The basic method used to match theory and observations from this stage of a nova's outburst is to assume the ionizing source is a spherical blackbody and the temperature and radius are then varied until reasonable agreement is obtained between the calculations and the measurements. Abundance determinations from this phase of novae have been notoriously unreliable in the past! Note also that the ejected matter is far more likely to be clumpy during the early phases, making our symmetrical models inappropriate. As can be seen from the following data, during the nebular phase the shell was hot and radiation bounded. Poor quality spectra taken on 7 January 1947 revealed the presence of only [OIII] $\lambda\lambda$ 5007, 4959 but the observations were made in a restricted wavelength interval. However, on the night of 15 March 1946 lines, in decreasing order of strength, of [OIII] $\lambda\lambda$5007, 4959, the Balmer series, [OIII] λ4363, HeII

λ4686, [OI] $\lambda\lambda$ 5577, 6300 and a few other allowed and forbidden lines of nitrogen ions amongst others were observed. Clearly, the shell must have been radiation bounded for sufficient quantities of both OIII and OI to be present simultaneously at this epoch to produce the observed lines, and the temperature must have been a few thousand Kelvin to produce the [OIII] lines.

From 1947 until 1980, when Williams (1982) observed the shell, the only other spectroscopy we know of was that carried out by Sanford & Greenstein (1957). This set of observations on the spatially-resolved shell was made 13 years after outburst. The widths of the lines of HeII λ4686, Hβ, and [OIII] $\lambda\lambda$5007, 4959 were used to determine an expansion velocity for the shell, but no intensities for any lines were reported. These were certainly some of the stronger lines in the spectrum, probably only Hα and [NII] $\lambda\lambda$6584, 6548 were stronger. The [OII] λ3727 line might also have been quite strong at this time, but unfortunately there are no data available to check this. The shell was almost certainly density bounded. Because the [OIII] lines were present in the spectrum with such large intensities, the shell temperature must have been of the order of a few thousand Kelvin.

Once accretion becomes the dominant source of luminosity, the visual magnitude of a nova essentially remains constant. CP Pup has had m_v = 15.5 for a number of years but it is not certain when it reached this stable state. On March 15, 1946 it had m_v = 10.8 and on January 9, 1947 it had a value of 11.3. If this rate of decline was maintained, the constant luminosity phase would only have been reached after about another 10 years, i.e. in year 14. We ran our constant density model for a variety of times since outburst and in each case determined the mean temperature of the shell. A plot of the mean shell temperature versus year since outburst is shown in Fig. 10.2. We assumed that the ionizing radiation was constant over this period and had the form described for year 37.3. This constant luminosity model was totally inadequate for describing conditions in the shell at year 5. For example, our model was density bounded, whereas [OI] and [OIII] were both seen in the spectrum at this time, which meant that the nebula was radiation bounded. Although we have plotted the curve from year 5 it is only appropriate around year 14. The arrow indicates the time at which Sanford & Greenstein (1957) obtained the first known spectrum of the shell.

The shape of the cooling curves for CP Pup and DQ Her determined from our models show very similar cooling rates. If we define the cooling time as the interval in years that it takes for the shell to fall from maximum to $\frac{1}{3}$ of maximum, then for DQ Her we obtain a cooling time of $\sim$ 8 years and for CP Pup we get $\sim$ 14 years. The CP Pup shell was initially much warmer ($T_e \sim$ 5500 K) than the DQ Her shell ($T_e \sim$ 3200 K) so cooling rates of about 260 - 270 K/year are obtained. As there are a number of factors contributing to this quantity it is most probably coincidental that

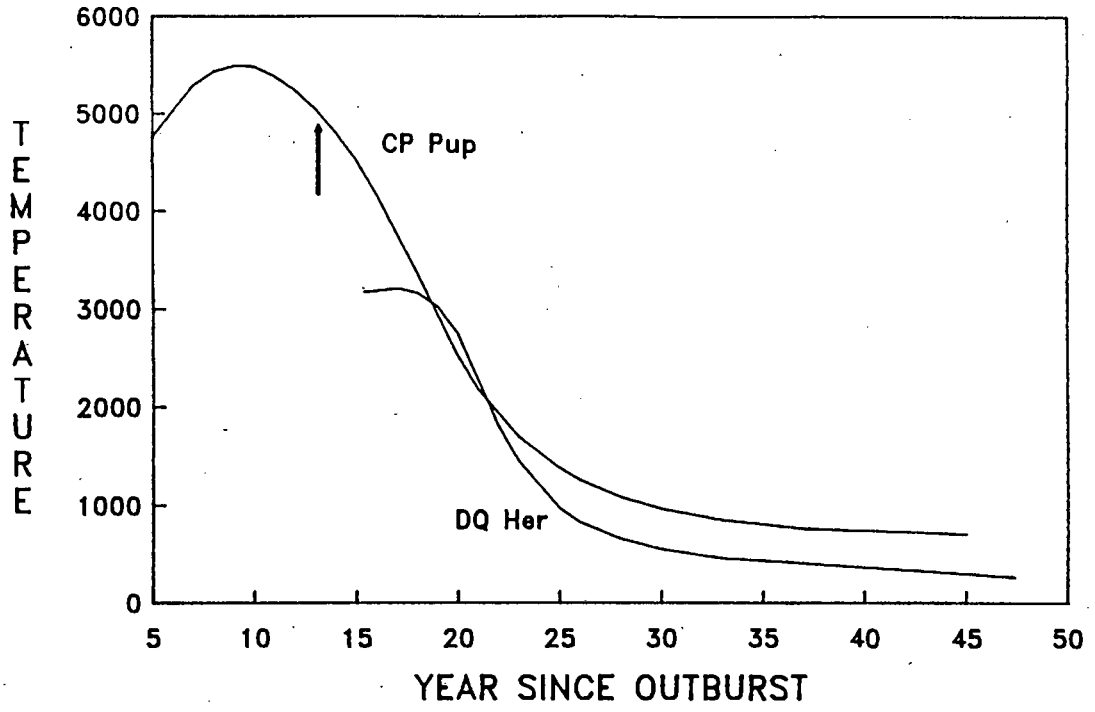

Figure 10.2: The modelled mean temperature (in Kelvin) of the CP Pup and DQ Her shells as a function of years since outburst. The arrow indicates when the CP Pup shell was first observed.

their rates are so similar. The cooling rate depends on parameters intrinsic to the shell such as its chemical composition and its density, as well as on external factors such as the ionizing continuum. This radiation determines the electron density via the ionic abundances and also which atomic levels are available to cool the gas radiatively. Each shell needs to be studied on a case-by-case basis, while regular monitoring of shell spectra over as broad a wavelength range as possible, particularly within the first 20 years following outburst, would greatly help modelling attempts.

In year 13 the modelled temperature through the shell decreased approximately linearly from 5400 K to 4750 K as a function of the radius from the central source. The mean temperature was 5051 K. Using a $1/R^2$ density model the range of temperatures was reduced. We used the computed ionic abundances to calculate the total flux of the strongest emission lines produced by the gas. The line fluxes, normalized with respect to F(Hβ), are listed in Table 10.2. The [NII] λ6584 line had the largest flux, dwarfing even Hα. [OIII] λ5007, Hβ and HeII λ4686 were all strong, HeI λ5768 was $\sim$ 6 times weaker than HeII and [OIII] λ4363 was very weak. These results agree very well with the observations of Sanford & Greenstein (1957). According to our calculations, the [OII] λ3727 line was also one of the stronger lines but we have no way of checking this result. The [NII] λ5756 line has a flux equal to that of HeII λ4686 which should have been detected. The fact that

Table 10.2: Relative line fluxes.

Line	Flux
Hα λ6566	3.00
Hβ λ4861	1.00
HeII λ4686	0.77
HeI λ5876	0.13
NII λ5678	0.10
[NII] λ5756	0.77
[NII] λ6585	18.7
[OII] λ3727	0.55
[OIII] λ5007	1.47
[NII] 122μm	1.47
[OIII] 88μm	2.06
[OIII] 52μm	5.32

it was not commented on must mean that it was not present with a flux as large as we have calculated. We might have too much nitrogen in our model, but if we reduce its abundance we need some other ion to cool the gas radiatively. In later sections we shall consider the inclusion of neon with larger abundances than solar. We have also listed some of the fine-structure line fluxes to demonstrate how large these can be, and hence to encourage observation of them. The strongest CNO recombination line according to our model was NII λ5678 which was even weaker than HeI λ5867.

We have already pointed out that the NIII fine-structure line provided the dominant source of cooling in the gas in year 37. Calculations for other post-outburst times showed that the flux of NIII 57μm has been the strongest emission from the shell for most of the time since outburst. OIII and NII fine-structure lines were the next largest contributors to the total radiative energy from the plasma, but their contribution amounted to less than 20%. In Fig. 10.3 we have plotted the relative fluxes of the stronger forbidden and fine-structure lines produced by the shell as a function of time. The OIIIfs curve is a sum of the 88μm and 52μm fluxes and the NIIfs curve a sum of the 205μm and 122μm fluxes. Similarly, the [NII] and [OIII] curves are the total forbidden-line fluxes, consisting of $\lambda\lambda$ 6585, 6550 and $\lambda\lambda$ 5007, 4959 emissions respectively. The [NII] λ5756 flux, not shown on the graph, lies between [OII] and [OIII]. The [OII] curve is for the λ3727 line flux only. Clearly, the NIII 57μm emission was responsible for most of the cooling in the shell from about year 13 onwards.

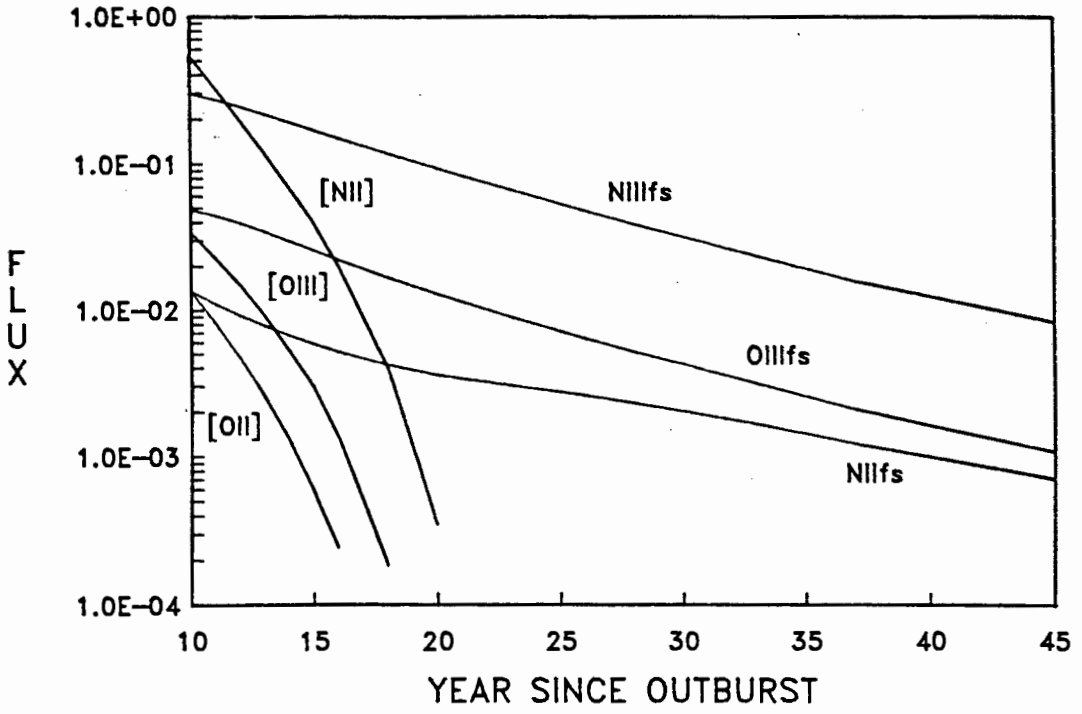

Figure 10.3: Relative fluxes of the stronger forbidden and fine-structure lines as a function of year since outburst. The OIIIfs curve is a sum of the 88μm and 52μm fluxes and the NIIfs curve a sum of the 205μm and 122μm fluxes. Similarly, the [NII] and [OIII] curves are the total forbidden-line fluxes, consisting of $\lambda\lambda$ 6584, 6548 and $\lambda\lambda$ 5007, 4959 emissions respectively. The [OII] curve is for the λ3727 line flux only.

10.4 Neon Novae

Determinations of heavy-element abundances in the ejecta of recent classical novae have been based upon emission-line analyses of spectra obtained during decline. While most novae show overabundances by factors of $\sim$ 100 with respect to solar values of at least one of C, N or O, and He is often enhanced by a few percent, some novae have also been found to have very large (factors of up to 10^3) overabundances of neon. In particular, V693 CrA (Nova CrA 1981) (Williams et al. 1985), V1307 Aql (Nova Aql 1982) (Snijders et al. 1984, 1987) and QU Vul (Nova Vul 1984 Number 2) (Gehrz et al. 1985) have this property, as well as having larger (than solar) abundances of at least one of Na, Al, Mg, or Si. The most plausible explanation for these abundance anomalies appears to be that the nova outbursts occurred on O-Ne-Mg white dwarfs, rather than on the more familiar C-O degenerate stars (Williams et al. 1985). In fact, Law & Ritter (1983) predicted that such a nova would manifest itself via its peculiar chemical composition. Although only a relatively small fraction of cataclysmic variable systems should contain O-Ne-Mg white dwarfs, selection effects act to insure that $\approx \frac{1}{3}$ of observed outbursts occur on these systems (Truran & Livio 1986). Note that the ejecta

of V1500 Cyg also have an Ne enhancement, but only by a modest factor of $\sim$10 over the solar value (Lance et al. 1988), whereas its CNO enhancements relative to solar values are much larger. We shall concentrate our attention for the present on the other three novae since they have significantly larger neon enhancements.

10.4.1 Properties of Neon Novae

In this section we present a summary of the principal features observed in the three neon novae mentioned above and then look at the properties of this type of nova predicted by theoretical modelling.

Nova V693 CrA was a fast nova ($t_3 = 12$ days) which reached a peak of $m_v = 7$ and lies at a distance of $\approx 8-9$ kpc. This nova was systematically observed over a period of seven months with the *IUE* satellite (Williams et al. 1985). The initial evolution of the UV spectrum was similar to other novae observed in the UV, but after several months high ionization forbidden lines of Na, Mg, Al, and Si appeared. The abundances of He/C/N/O/Ne were determined from *IUE* spectra to be 1.0/0.0053/0.075/0.097/0.109 which represent large enhancements compared to solar values. Na, Al, Si, and Mg also have substantial enhancements over solar abundances. An optical spectrum taken a few days after outburst was typical of novae at this stage of their development — broad emission lines of H, He, N and O were present. No Ne lines were observed.

Nova Aql 1982 was only discovered after maximum light in a direction close to the sun. The nova lies at a distance of 3 - 8 kpc. The results discussed here are based on the detailed analysis of UV, optical, IR and radio data presented by Snijders et al. (1987). The V band light curve initially ($\leq$ 15 days) had a fast exponential decline, giving $t_3 \approx 13$ days, but thereafter had a much slower (exponential) decline. Both the UV and the optical light curves underwent dips (minima at 77 and 55 days respectively) while the dominant contribution to the total flux came from infrared emissions. It appears that dust internal to the nova shell absorped the shorter wavelength radiation and re-emitted it in the IR region. From day 156 onwards the optical emissions were affected very little by dust.

Three velocity components were identified in the nova remnant. A high velocity gas with v $\leq$ 10000 km/s was seen in UV absorption line spectra on days 29 and 36 after outburst but has subsequently vanished. A component of medium velocity with v$\leq$ 3000 km/s was deduced from the broad width of all lines in the optical spectra. [NeIII] and [NeV] lines were the strongest and hence used to determine the line profile. OIII lines had weak, broad components suggesting depletions of oxygen with respect to neon in this part of the gas. Lines of HI, HeI and HeII had strong narrow components with FWHM of 200 km/s. These narrow widths were also seen in some forbidden lines such as [OIII] but not in the strong forbidden neon lines. The only

optical absorption feature seen was NaI on day 73 blueshifted by $\sim$ 2000 km/s. This absorption presumably occurred in a cold, dense region where dust condensation could be expected. Many discrete "clouds" of gas appear to have been present giving a wide range of temperatures and densities in the nova shell. Gas-phase element abundances are dependent on the values chosen for T_e and N_e, and may hence show large variability. Recommended abundances for H/He/C/N/O/Ne are 1.0/0.445/0.059/0.21/0.065/0.53, and for C/O/Mg/Si/Fe in the grains are 0.9/1.6/0.14/0.16/0.16. The total abundances for H/He/C/N/O/Ne are then 1.0/0.45/1.0/0.21/1.7/0.53. The H/He abundance ratio in nova Aql 1982 is very unusual. The heavy element abundances are less certain, but nevertheless also peculiar. The gas-phase abundances of many heavy elements are severely depleted due to grain formation. The prominence of [NeIII] and [NeV] lines and the large neon abundance deduced are a consequence of neon being an inert rare-gas which does not condense into grains.

The mass of the gas was estimated to be 7×10^{-6} $M_\odot$ with a volume filling factor of 2.5×10^{-5}. The dust was composed of silicate and metallic grains and of carbon smokes and had a mass of at least 4×10^{-6} $M_\odot$ but was possibly as high as 2×10^{-5} $M_\odot$. Radio data for this nova are fragmentary and cannot be fitted to a simple model that consistently explains the observations.

QU Vul has been very well studied over a broad range of wavelengths and has been found to have a number of interesting features. Lying about 3.6 kpc away, it was a fast nova (t_3 = 40 days) that reached a maximum of m_v = 5.7. Gehrz et al. (1985) observed strong [NeII] 12.8 μm emission 140 days after outburst. This flux represented a significant fraction of the total shell luminosity. The physical conditions which enable significant population of, and efficient cooling through, the 12.8μm line may be quite rare (Gehrz et al. 1985). The FWHM for this line and the Brα line implied expansion velocities of 5000 – 7000 km/s for the ejecta. P Cygni absorption components with terminal velocities of $\sim$ 5000 km/s were also found in *IUE* spectra (Ögelman & Krauter 1985). Andrillat (1985) found a low velocity expansion component with a terminal velocity of $\sim$1000 km/s. On day 240 after outburst Gehrz et al. (1986) detected 10 μm and 20 μm emission lines in the infrared spectrum. These have been attributed to the formation of silicate grains in the ejecta. They are believed to form in the slow moving gas and indicate an oxygen-rich environment. Near-infrared observations by Greenhouse et al. (1988) found emission lines from high ionization states of Al, Si, Ca, Mg, and Ne which are formed by photoionization. The line profiles suggest that the material is clumpy and that the dust has formed inside these clumps. QU Vul is also a radio nova. Based on their radio observations, Taylor et al. (1988) suggested a $1/R^2$ density distribution for the shell, and measured velocities of 880 and 1010 km/s respectively for the inner and outer radii of the shell.

Finally, we look at the properties of neon novae predicted by theoretical

models of the outburst. The accretion of hydrogen-rich material on to the surface of a $1.25M_{\odot}$ O-Ne-Mg white dwarf was found to lead to a nova outburst (Starrfield et al. 1986). Hydrodynamic modelling of these eruptions showed them to be more violent than thermonuclear runaways on C-O white dwarfs, and they could eject the entire accreted envelope plus core material at high velocities. The ejecta should be rich in Ne and Mg and other post-Ne elements on the periodic table, such as Al, Si, Na, and S. These numerical calculations are in good agreement with observation. For example, all novae with neon enhancements have been either fast (QU Vul) or very fast, while V1370 Aql showed evidence of gas ejection up to 10000 km/s and QU Vul had velocity components of 5000 – 7000 km/s.

10.4.2 Old Neon Novae

Three out of about twelve novae that occurred this decade have been identified from UV or IR observations as being neon-rich. If, as theory suggests, about $\frac{1}{3}$ of all novae occur on O-Ne-Mg white dwarfs, then many of the novae observed before 1980 should have occurred on degenerate neon stars. We want to check this assertion, but to do so we need to be able to identify these objects. In this section we look for features that are characteristic of neon novae and see whether any of the data from old classical nova outbursts can be interpreted in terms of this type of event.

Because properties such as white dwarf mass, accretion rate and envelope composition are different in every system, each nova has unique behaviour. As we cannot do statistics with only 3 events it is difficult to determine what is "typical" for neon novae. However, it appears from the available data and theoretical models that these novae have violent outbursts that eject matter at high velocities. If this is a necessary feature then, because the high ejection velocities measured in V1370 Aql and QU Vul are unprecedented in nova outbursts, these must be the first neon novae seen. Measured values of ejection velocities in classical novae characteristically fall in the range $250 < v[km/s] < 2500$ (Cohen 1985). Clearly, if high ejection velocities are a requirement of neon novae then none of the observed old classical novae are from this class. If they occur as frequently as predicted then our position in space or time must be special for us not to have seen any prior to 1980. Alternatively, not all neon novae are as violent as the 3 events discussed above suggest.

Stellar evolution calculations predict that O-Ne-Mg white dwarfs should be more massive than their C-O counterparts at the start of their nova phase. Theoretical modelling of a 1.25 $M_{\odot}$ white dwarf with an oxygen-enriched envelope showed that outbursts occurred more frequently and more violently than on C-O white dwarfs (Starrfield et al. 1986). The mass ejected decreases as the white dwarf mass increases but there is a nett mass loss from a massive degenerate star as a result of an outburst. A nova that has undergone many

outbursts should have lost mass according to the above arguments, and hence have less frequent and less violent outbursts than when it started its nova phase. Nova eruptions on old neon systems would then be less extreme than on new systems, although still more violent than on a C-O white dwarf of the same mass. If neon novae are not always extremely violent, we need to be able to identify these events from other sources, such as the spectroscopic data.

Although many recent novae have been observed over a broad range of wavelengths including the optical band, old classical novae were observed only in the optical band. If some of these occurred on neon white dwarfs, and hence had oxygen and neon enhanced ejecta, this characteristic was not discerned from their spectra. This is not altogether surprising if one considers that CNO overabundances in nova ejecta were only realised from spectral analyses of their spatially-resolved shells and not from their outburst spectra. The presence of neon, usually identified from [NeIII] $\lambda\lambda$ 3868, 3976 or [NeIV] λ4720 lines, is not uncommon in the spectra of novae during decline (for examples see Payne-Gaposchkin 1957). In V1370 Aql, besides the [NeIII] and [NeIV] lines, [NeV] $\lambda\lambda$ 3346, 3426 were also seen, whereas the [NeIII] lines alone were seen in V1500 Cyg. Only one optical spectrum was obtained of V693 CrA and it had no neon lines. Had optical spectra been taken at other stages of its decline, it is quite likely that the presence of neon would have been detected.

Recombination lines of H and He are ubiquitous in nova spectra, and allowed CNO lines are also common. V693 CrA had optical recombination lines of NII and NIII and V1370 Aql had NIII and CIII lines. Recombination lines of neon ions have not been detected in declining novae, but with regular monitoring, particularly of the neon-rich gasses, they might show up. A guide to the strongest neon recombination lines can be obtained from Kaler's (1976) catalogue of spectral lines observed in planetary and diffuse nebulae. A search through the entries revealed that only NeI λ4169 (which overlaps an OII line) and a few lines of NeII — λ3694 and λ4392 were the strongest lines — have been seen in these objects. Lines at λ6506 and λ6402 should be quite strong in the spectrum of neutral neon but have not been detected. In most nebulae neon has a nearly solar abundance and is hence not particularly plentiful, which partly explains why so few lines have been seen. That no neon recombination lines have been seen in the spectra of novae might be because neon was not greatly enhanced in any of these events. However, even in the known neon novae no recombination lines of neon were seen, although the optical coverage of these eruptions was particularly poor. Unfortunately the optical NeIII and NeIV lines come from higher levels than the CNO lines of the same ionization stage, and are therefore intrinsically weaker.

If the optical spectra from the nova's period of decline are not a reliable indicator of the presence of neon, then what of nova shells? The spatially-

resolved shells that have been examined have not shown any neon excesses, and therefore appear to have C-O progenitors. But what would old neon-rich nova shells look like and can we unambiguously say that none of the systems examined to date arose from neon stars? In an attempt to answer these questions we have modelled the shells of neon novae.

10.4.3 Models with Neon

The inclusion of neon in our codes was straight forward and did not require any major modifications. Most of the rates we used for the various atomic processes involving neon ions came from the same references as those used for the CNO ions. Additional data used were the dielectronic recombination rates of Nussbaumer & Storey (1987), the collision strengths for [NeII] 12.8μm from Bayes et al. (1985), and the energy levels of [NeIII] from Butler & Mendoza (1984). Although Pradhan (1980) has made some more accurate calculations than those of Henry (1970) for the cross section of Ne ions at threshold, we have used the latter data. Pradhan has only calculated the threshold value whereas we need the cross section at all energies. The shape of the cross section curve determined using Pradhan's method will not necessarily be the same as Henry's, so we can not simply use the alternative threshold value. Furthermore, Henry's cross sections integrated over a flux or velocity distribution may not have such large errors as the threshold values.

We once again tested our codes and investigated the effects of neon enhancements using the parameters of Harrington (1969). The temperature profile in the gas for the Harrington model with a neon abundance of 5.5×10^{-5} with respect to hydrogen is shown by the solid line labelled HAR in Fig. 10.4. The results from the same model but without the processes of charge exchange and dielectronic recombination included are labelled CEDI. The dashed lines are for the models without any neon. These two sets of results do not differ much from each other so the conclusions we drew earlier for differences with Harrington's results apply here too. The ionization structure through the shell is similar, but not identical to, that shown in Harrington (1969) Fig. 2. For example, there is more Ne^{+} in the inner part of the nebula in our model, and our Ne^{2+} never exceeds an abundance of 0.8 whereas in Harrington's model it goes up to 1.0. These differences are most probably due to the atomic data we used which have undergone some significant revisions in the past few years.

A comparison of the cooling efficiency of oxygen and neon is provided by the curve labelled NeO in Fig. 10.4. In the run that generated this curve we exchanged the O and Ne abundances, i.e. we set the O abundance to 5.5×10^{-5} and Ne to 4.5×10^{-4}. It is interesting to note that this change has very little effect on the ionization structure in the shell, even that of neon and oxygen. The logarithm of the relative neon ion abundances for HAR (solid line) and NeO (dashed line) are shown in Fig. 10.5. In both

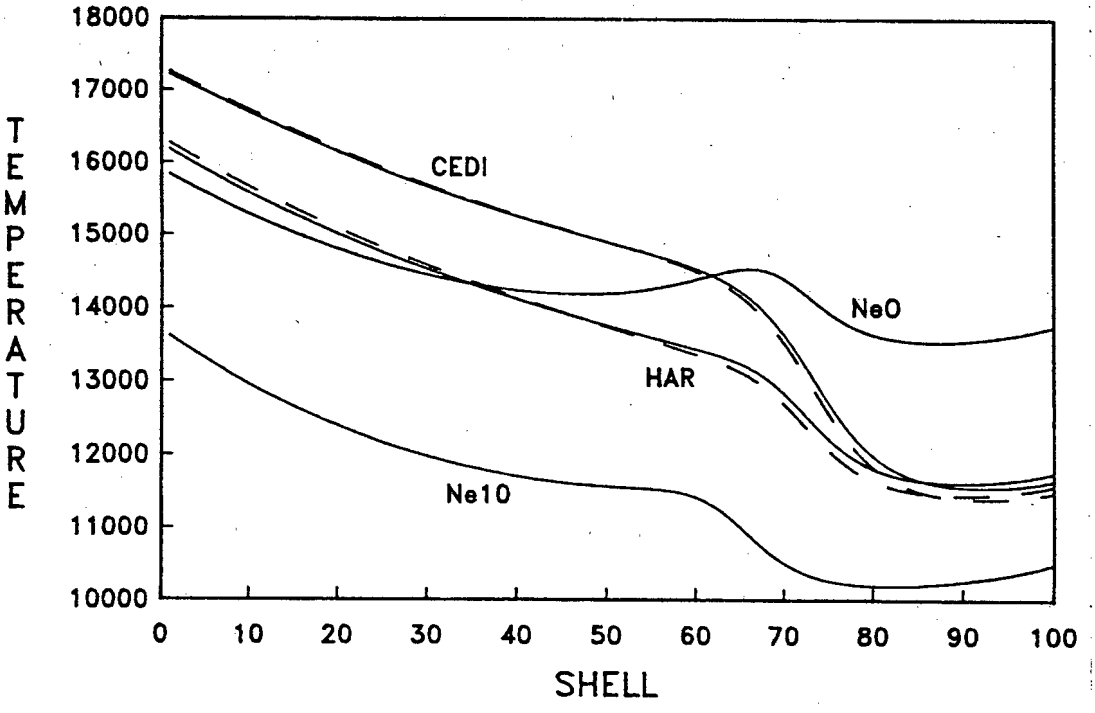

Figure 10.4: Temperature profiles versus shell number for various models. HAR is the Harrington model described in the text and CEDI is the same model without the processes of charge exchange and dielectronic recombination. The dashed lines are for models without any neon. NeO has the oxygen and neon abundances exchanged and Ne10 has a neon enhancement of 10 with respect to HAR.

these shells the NeIII ion is dominant throughout the gas, whereas the OIV ion dominates in the inner region but gets replaced by OIII at the outer edge. The increase in the abundance of OIII is responsible for the dip that occurs in the HAR model temperature profile around shell 70, and for the minimum in the same region of the NeO model. In the neon-enriched gas (NeO), NeIII lines (forbidden and fine-structure) are responsible for most of the cooling with NeIV and, to a lesser extent, OIV contributing as well. The temperature rise in the NeO model occurs as the NeIV abundance decreases and the cooling is left to the NeIII ion. When OIII becomes abundant the temperature again drops because the collisionally excited lines of this ion are very efficient coolants.

In Fig. 10.4 we have also plotted the temperature profile of a gas with a neon enhancement of 10 over HAR (labelled Ne10). The neon and oxygen abundances are very similar in this case. The effect of this enrichment is to lower the state of ionization of the gas (with respect to HAR) so that NeIII, OIII, NeII and OII increase at the expense of NeIV, OIV, NeV and OV. Most of the cooling at the inner edge of the nebula was produced by NeIII and OIV. As the OIV abundance decreased and OIII increased, the OIII ion took

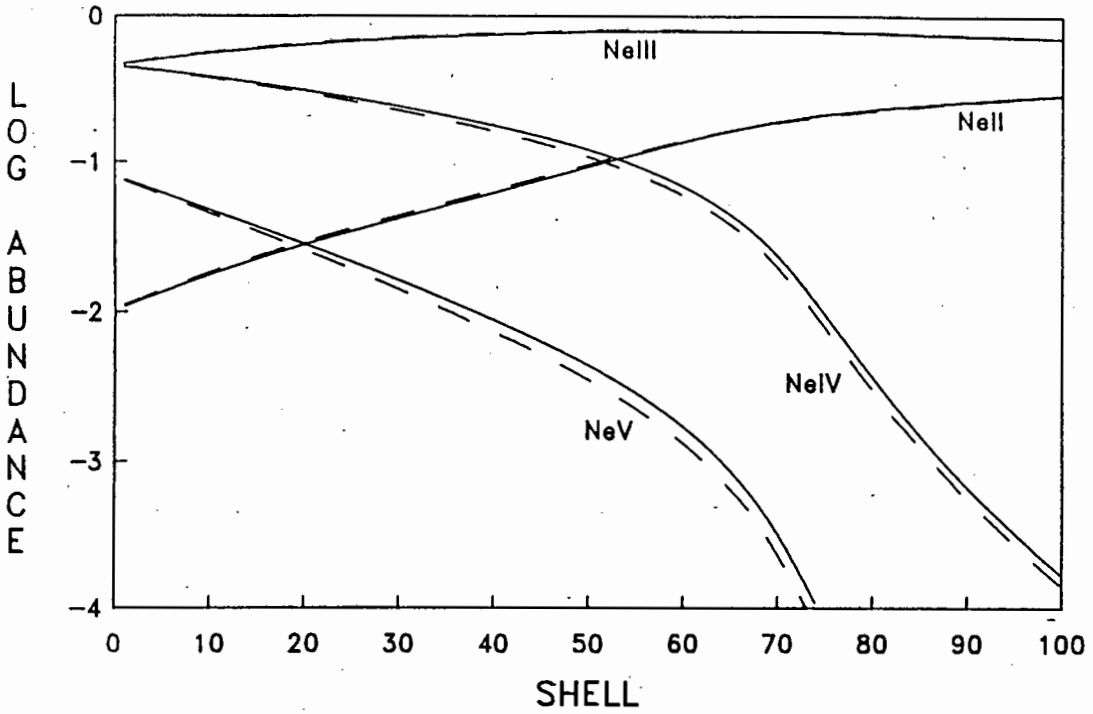

Figure 10.5: Relative abundances of neon ions versus shell number for HAR (solid line) and NeO (dashed line).

over from NeIII as the dominant coolant. The radiative cooling contribution from OIII increased throughout the shell. The change from the HAR model is easy to understand — NeIII helps to cool the gas and hence lowers the temperature, in addition to which the increased OIII abundance results in more efficient cooling.

As in the case for oxygen, large neon enhancements have a significant effect on the ionization structure and temperature profile through the shell. Fig. 10.6 shows the results of running the model with Ne enhancements of 100, 200 and 500 times. Because neon is nearly 10 times less abundant than oxygen, an increase in its abundance by a factor of 100 corresponds to an oxygen enhancement of only 10 times. Observations of neon novae indicate that enhancements of Ne by factors of 1000 over solar values occur. An interesting feature of the temperature profiles for the neon-enriched models is that the temperature is at a minimum in the middle of the shell rather than on the outside as in normal nebulae, or on the inside as in the oxygen-enhanced shells. The reason for this behaviour is that the NeIII fine-structure lines are more efficient coolants than either the NeII 12.8μm line or the NeIV lines. We shall discuss the shape of the curves in Fig. 10.6 in terms of the Ne100 model, since it has the most dramatic shape. Fine-structure emissions from NeIII and NeII accounted for $\approx$ 90% of the energy radiated by the plasma. The initial temperature drop was caused by an increase in the NeIII abundance at the expense of NeIV and NeV, which led to more efficient energy losses.

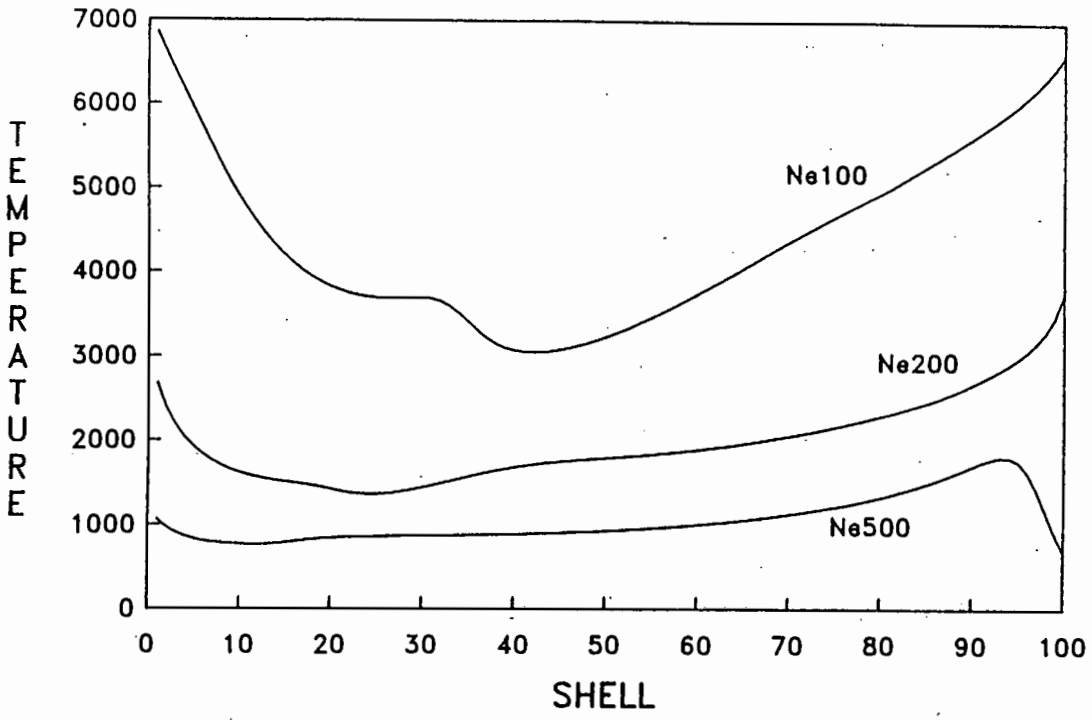

Figure 10.6: Temperature profiles for models with neon enhancements of 100 (Ne100), 200 (Ne200) and 500 (Ne500) times the abundance in HAR.

There was another drop in temperature around shell 30 due to the edge of the He^{2+} Strömgren sphere being reached. From this shell outwards there were essentially no more photons with energies above the He^{2+} ionization limit, so the energy input to the gas decreased, producing a concomitant drop in temperature. The increase in temperature from shell 40 outwards was due to the fact that for the density in this nebula ($N_e \sim 2300$ cm^{-3}) the NeII 12.8μm line emits about an order of magnitude less flux than the NeIII fine-structure lines. The NeIII abundance decreased from shell 20 to the edge of the nebula while the NeII abundance increased monotonically from the inner edge to the outer edge. These ions had equal abundances around shell 50. Because NeII is so inefficient as a coolant compared to NeIII, the gas temperature increased as the NeIII abundance decreased.

The Ne500 curve has a further temperature decrease beyond shell 94. This was caused by the nebula becoming radiation bounded. The electron density drops from 2000 cm^{-3} at shell 94 to 860 cm^{-3} at shell 100, with a corresponding decrease in abundance of ionic species. The energy input to the gas dropped rapidly as the source of ionizing radiation was reduced. A neon enhancement of 1000 led to a nebula that was completely radiation bounded around shell 80.

10.4.4 Neon Nova Shells

We have demonstrated that neon enrichment of a plasma provides for more efficient cooling of the gas and hence, with sufficient enhancement, to conditions of low temperatures, i.e. $T_e \approx 1000$ K. However, large neon abundances lowered the state of ionization of the gas and led to our test nebula becoming radiation bounded. Conditions in nova shells differ markedly from our test nebula, however, so different behaviour can be expected. The results of tests run on nova shells are discussed in this section.

Two methods were used to investigate the behaviour of neon nova shells. In one method we used the shell parameters in our models determined from observations of the known neon novae. The results provide a guide as to how we expect these nova shells to evolve and can be checked by observations. They also indicate what features old neon nova shells should have and hence suggest ways of checking whether any of the known old classical novae belong to this class. It is unfortunate that V693 CrA, V1370 Aql and QU Vul are so distant because by the time their shells become spatially-resolvable (from groundbased observatories) their surface brightness will be very low and most probably undetectable. However, the finer resolution of the Hubble Space Telescope may afford an opportunity to observe these shells. In the second method, we modified our existing model of CP Pup, which provided a reasonable description of the shell evolution, to include varying amounts of neon. These results demonstrate the effects of moderate neon enhancements on nova shell evolution.

Of the 3 neon novae discussed in §10.4.2, the data for V1370 Aql are the most comprehensive. Abundances but no other shell parameters have been determined for V693 CrA, while for QU Vul, even though it has been extensively observed, the only published quantitative parameters of use to us are those for the shell velocities. In Table 10.3 the available information on each shell is summarized. The data for CrA, Aql 82 and QU Vul are from Williams et al. (1985), Snijders et al. (1987) and Taylor et al. (1988) respectively. Note that V1370 Aql has undergone a phase of dust formation so that the shell consists of grains and gas. The abundances in Table 10.3 are for the gaseous phase only. In our models we assumed that the grains did not evaporate when the shell thinned, and the grains therefore did not contribute to the abundances in the gaseous phase during the shell's evolution. Dust grains have also been reported for QU Vul based on IR observations (Gehrz et al. 1986).

Our main interest was in the behaviour of these shells during their constant-luminosity phase, which occurs when the principal source of radiative energy is produced by accretion processes. These novae have yet to reach this state so the accretion rates are an unknown factor. However, typical rates for classical novae and nova-like variables, i.e. $10^{16} - 10^{18}$ g/s, seem applicable (Starrfield et al. 1986). We therefore used the continuum sources

Table 10.3: Shell parameters for observed and modelled neon novae.

	Aql 82	CrA	QU Vul	Model 1	Model 2	Model 3
H	1.0			5.0	1.0	1.0
He	0.445	1.0		1.0	0.445	0.445
C	0.059	0.0053		0.0053	0.059	0.059
N	0.21	0.075		0.075	0.21	0.21
O	0.065	0.097		0.097	0.065	0.065
Ne	0.53	0.109		0.109	0.53	0.53
v_i			880	880	2640	2640
v_o	3000		1010	1010	3030	3030
M_s	7×10^{-6}		3.6×10^{-4}	1×10^{-5}	7×10^{-6}	7×10^{-6}
ϵ	2.5×10^{-5}			0.1	2.5×10^{-2}	2.5×10^{-4}

from our DQ Her model (§9.4) and CP Pup model (§10.3.3). The parameters for 3 models tested are listed in Table 10.3. Based on the observations of QU Vul by Taylor et al. (1988), a $1/R^2$ density distribution was used for all models. Model 1 used the abundances from V693 CrA, the shell velocities from QU Vul and a "canonical" shell mass of 1×10^{-5} $M_\odot$. The value of 3.6×10^{-4} $M_\odot$ quoted by Taylor et al. (1988) is high, even for C-O nova outbursts. The volume filling factor, ϵ, was arbitrarily taken to be 0.1, giving an environment that was more clumpy than those of our other models, which had $\epsilon = 0.3$. The abundances determined for V693 CrA did not include the hydrogen abundance or the He/H ratio. We adopted a value of 0.20 for this ratio which is close to the mean value of He/H in nova shells (Truran & Livio 1986). Helium is believed to be quite significantly enhanced in neon novae — in V1370 Aql, for example, He/H was measured to be 0.45, although this appears to be an extreme value. The parameters for Models 2 and 3 were based on the data from V1370 Aql and differ only in their value of ϵ, which determines the density in the shell. The velocities of the shells were taken to be 3 times the values measured for the QU Vul envelope. The value of v_i was not particularly important as it was used with v_o to determine the volume of the shell, which together with the mass determined the density of the gas. As the density was being varied over a broad range of values by changing ϵ, the precise value of v_i was not significant.

Model 1 was run for years 5, 10 and 20 after outburst using the DQ Her source for the ionizing flux. Mean shell temperatures of 450, 641 and 311 K respectively were obtained. When the CP Pup source was used the gas temperature increased, but even so the maximum temperature achieved in year 10 was only 1030 K, and the mean temperature was 900 K. The maximum temperature this gas achieved (with either source) was that around year 10, decreasing steadily thereafter. Novae normally reach their constant-luminosity phase between about 10 and 15 years after outburst, but in our

previous models temperatures of a few thousand Kelvin existed in the shells at this stage. The large metal abundance in this model cooled the gas so effectively that the temperatures were low at all stages. A plasma with the low temperature predicted by this model would have strong recombination lines, as well as strong fluxes from the fine-structure lines of NeII, NIII and OIII. The NeII 12.8 μm line flux was responsible for about 80% of the radiated energy, followed by NIII 57μm and then the OIII 52μm and 88μm lines. It is interesting to see that under the conditions used here, the NIII 57μm flux was larger than the sum of the OIII lines, even though the nitrogen abundance was lower than that of oxygen.

The metal abundances in models 2 and 3 were even more extreme than in model 1, producing correspondingly more extreme results. The temperature in both these shells was under 200 K in year 10 — model 2 had a mean temperature of 107 K and model 3 179 K. Because of its smaller volume filling factor, model 3 had a higher density than model 2. This clearly had an effect on the plasma, but it is unlikely that such small filling factors would persist when the gas expands into the surrounding ISM. This density was much larger than that in any of our other models. The temperature in the shell decreased as the time since outburst increased, but because many of the atomic rates have been extrapolated or are undetermined at these low temperatures, our models are not particularly accurate. Furthermore, the small value of ϵ implies that the matter is in the form of dense clumps. As the shell evolves these clumps should expand and the gas should become more uniformly distributed. This would lower the gas temperature. Our model is not really applicable in the asymmetric conditions produced by small values of ϵ. If the metal abundances are as extreme as the analyses have suggested, then as the temperature and radius of the central sources of these systems decrease towards a condition in which accretion energy dominates their flux output, the temperature of the shell should decrease to values of a few hundred Kelvin.

The dominant sources of radiative flux in models 2 and 3 were produced by the fine-structure lines of NIII, NII and OIII. Surprisingly, the neon ions, in particular NeII which was the dominant form of Ne in model 2, contributed very little to the energy output of the gas. In model 3 the neon was essentially all neutral and therefore had no effect on the cooling or heating of the gas. This was confirmed by running a model using the same parameters as in model 3, but without any neon. We obtained temperature and abundance profiles almost identical to those of model 3; the only real difference was in the electron density which increased by a factor of $\sim$2.5. The reason for this was that both models had the same shell mass from which the number density of each species was calculated. By removing the large contribution of neon to the mass the number density of all the other species increased. CNO recombination lines were also present in the optical spectrum. CIII was

the dominant form of carbon in models 2 and 3 so CII λ4268 was present. NII, NIII, OII and OIII had very similar abundances so the flux of the lines of NII and OII were stronger than those of NI and OI. Because of the large nitrogen abundance, the lines of NII dominated the optical spectrum. Neon was predominantly in the form of NeII (model 2) or NeI (model 3) so lines of NeI should be present in model 2. Unfortunately, we have not modelled any neon ions yet so we can not quantify the fluxes.

Even if the shells of neon novae have temperatures as low as our models indicated, they should still be able to be detected. The rate of recombination increases as the temperature decreases so that for a given gas density, recombination line fluxes will be stronger at low temperatures than at high temperatures. The Balmer lines of hydrogen and HeII λ4686 are recombination lines and would hence be more prominent in a low temperature gas than if the gas had nebular temperatures. HeI λ5876 is enhanced by collisional excitations from the metastable 2s ^{3}S level if $T_e > 5000$ K, but at low temperatures it is formed purely by recombination and will be enhanced as the temperature decreases. Hydrogen appears to be under-abundant in neon nova shells, so Hα, which is usually the strongest recombination line, was not as prominent in these models as in our other models. Furthermore, the gas in these nebulae was not very highly ionized. For example, in model 1 helium was only $\approx$ 90% ionized and less than 1% was in the form of HeIII so the lines of HeII were very weak. Only about 95% of the hydrogen was ionized. Our calculations for the effective fluxes of hydrogen and helium show HeIλ5876 to be smaller than Hα but larger than Hβ. The gain in recombination flux due to the low temperatures is offset to some extent by the low number density in neon nova shells. It was shown theoretically (see discussion in §10.4.1) that the shell mass was smaller and the heavy metal enhancements larger for shells from neon novae than from C-O novae. Both of these factors reduce the number density of ions in the shell and hence the amount of flux emitted by the nebula. If nova shells do exist with such large metal abundances, the surface brightness of these objects would be very low and it would be difficult to detect them. Furthermore, if our models are correct and the hydrogen and helium are not fully ionized then there is a further reduction in the amount of recombination radiation produced, in addition to which these shells seem to form dust which would further reduce their optical output.

The above considerations do not present a very optimistic outlook for finding neon nova shells from their optical emissions. This might in fact be a key to finding this type of shell — novae whose shells can not be detected 2 or 3 decades after outburst could have low number densities because most of the shell mass is in over-abundant heavy metals, a large dust content that reduces their optical emission, and low levels of ionization. The optical recombination lines did not have the strongest fluxes in our models, however. The fine-structure lines of nitrogen and oxygen, and sometimes neon, were

stronger than the optical recombination lines. In view of the large neon abundances expected in the shells of neon novae, one way of searching for these novae would possibly be to look for NeII 12.8μm emissions from the surrounding medium.

10.4.5 CP Pup revisited

Precisely what constitutes a neon nova has yet to be decided. It has been suggested that V1500 Cyg belongs to this class (Livio & Truran 1986), and yet it has a modest neon enhancement (factor of 10 larger than solar). Its ejecta showed fairly normal values of CNO enrichment for novae and its abundances are certainly far less extreme than those of the other 3 neon novae discussed (Lance et al. 1988). CP Pup has a number of properties similar to those of neon novae. It was a very fast nova with high ejection velocities and its maximum and minimum magnitudes covered a large range, all of which are indicative of a violent outburst. One of the features found in models of thermonuclear runaways on O-Ne-Mg white dwarfs was that their eruptions were more violent than on C-O stars (Starrfield et al. 1986). Of course, this does not exclude CP Pup from having been a violent outburst on a C-O white dwarf. The enhanced nitrogen abundance in the old shell of CP Pup is not understood in terms of element synthesis by thermonuclear runaway on any type of progenitor, but carbon and oxygen deficiencies have also been noted in V1370 Aql. In this instance, the carbon and oxygen are believed to have formed into dust grains, thereby reducing their gaseous phase abundances. No dips were observed in the CP Pup light curve, however, from which it was concluded that dust did not form. If the dust formed slowly over a number of years then it could explain the unusual nitrogen excess. This explanation does not necessarily require a neon progenitor, though, unless the dust formed preferrentially in the presence of Si, Al and Mg which would presumably be enriched if the progenitor was an O-Ne-Mg star. Finally, forbidden neon lines were observed in the spectrum at an earlier stage of its decline than is normal for novae, even compared to other fast novae such as V603 Aql. This could be an indicator of a neon excess, but, on the other hand, it could also just be one of the peculiarities of this nova.

Our CP Pup model, as described in §10.3.3, was modified to include neon and initially run with a neon abundance of N(Ne)/N(H) = 10^{-4}, which is slightly larger than the solar abundance. This change had essentially no effect on either the temperature or the ionic abundances within the gas at any stage of its constant-luminosity phase. In fact, increasing the abundance to 10^{-3} had only a slight effect on the temperature of the plasma, causing changes of $\sim$ 300 K in year 10 and $\sim$ 25 K in year 37. Changes to the ionic abundances were hardly noticeable. However, increasing the neon/hydrogen ratio in the model to 10^{-2} had a pronounced effect on the temperature of the gas. In year 10 there was a temperature decrease of $\sim$ 3300 K through the

shell, and in year 37 a drop of $\sim$ 150 K. There was a slight lowering of the state of ionization of the gas in year 37 but it hardly altered our earlier line fluxes. For example, N(HeII)/N(HeIII) averaged over the shell was 1.62 in the model with an Ne abundance of 10^{-4} and 1.67 with an Ne abundance of 10^{-2}. The dominant ionic species of neon was NeII. The change in the ionization state was far more noticeable in the results for year 10 — for example, the N(HeII)/N(HeIII) ratio was doubled by changing the Ne abundance from 10^{-4} to 10^{-2}. The flux of the HeII lines was halved compared to our original model, and, because the temperature was only $\approx$ 2000 K, there were no [OIII] lines emitted by the gas. This model is obviously inadequate at describing the CP Pup shell.

The temperature in the 100 times neon-enriched CP Pup shell model was too low. One method we tried of increasing the temperature in year 37 was to lower the shell mass. Halving the shell mass, i.e. using 1×10^{-5} $M_{\odot}$, increased the temperature in year 37 to 890 K but also affected the ionic abundances. The HeII/HeIII ratio was only 0.7, whereas observations require a value of 1.6. Furthermore, because the density is higher in year 10 than in year 37, the temperature decreased rather than increased. This method clearly did not resolve the problem. Instead we tried lowering the CNO abundances by a factor of 0.9. In year 37 both the temperature and ionization structure were almost the same as in the original model. In year 10 the ionization structure was similar to the model without any neon but the the gas was cooled to a temperature of $\sim$2300 K. A temperature this low is too cold to form [OIII] lines, so this model was incapable of explaining the shell observations of Sanford & Greenstein (1957).

It appears then that a neon abundance of less than 100 times but more than 10 times the solar value could be present in the CP Pup shell. There certainly was some neon in the ejecta because forbidden lines were seen in the spectra during the nova's decline. Recombination lines from neon would have been too weak to be detected in the emission spectrum at any stage of its evolution, but fine-structure lines from NeII and NeIII may well have been observable at some stage. In fact, NeII 12.8μm emission might be detectable in the shell at the present time, depending on its abundance. Our calculations have shown that the shell could have quite substantial quantities of neon and yet this would not have been detected in the normal course of events. For example, [NeIII] λ3868 would most probably not have been seen in many of the early spectra because these lines were too far towards the blue end of the spectrum for them to have been detected. Note that V1500 Cyg has a 10 times solar abundance of neon (Lance et al. 1988) and has sometimes been classified as a neon nova. It could be that a neon enhancement is a necessary requirement to produce very fast novae like CP Pup and V1500 Cyg.

Chapter 11

Near-Infrared Observations of three Southern Nova Shells

11.1 Introduction

In this chapter we present some spectroscopic observations made in the near-IR region on the nova shells of CP Pup, RR Pic and T Pyx. The main motivation for observing the CP Pup shell in the near-IR was to look for the Paschen continuum. This would provide a means of confirming the Balmer continuum identification, and for measuring the temperature of the shell more accurately. There are also a few lines from CNO ions that occur in this region of the spectrum. The shells surrounding the old nova RR Pic (1925) and the recurrent nova T Pyx (1966) show characteristics more akin to those of planetary nebulae (Williams & Gallagher 1979; Williams 1982), namely temperatures of $\geq 10^4$ K and approximately solar abundances. Although our observations produced a null result, it is possible that other nova shells might be bright enough to have detectable emissions at these wavelengths. We have investigated which lines are most likely to be seen in this spectral region, and provide some graphs for determining the temperature from the width of the Paschen continuum. We know of no other near-IR spectroscopic observations on spatially-resolved nova shells.

The temperature of the CP Pup shell has been determined from the width of the Balmer continuum which, because of the low temperature, appears as a broad emission line (Williams 1982). This identification is not certain, but extensive observations on the DQ Her shell (Williams et al. 1978, Ferland et al. 1984), which displays a similar feature, tend to confirm that the temperature of the DQ Her shell is anomalously low compared to other emission line objects. It is, therefore, reasonable to expect CP Pup to have a low temperature as well. Another way of checking the Balmer continuum identification is to look for the Paschen continuum. The shape of continuum bands is proportional to $\exp(-h\nu/kT)$ and, since frequencies in the Paschen series are smaller than those of the Balmer series, the continuum will be wider than the Balmer continuum. In principle, the width of the Paschen continuum can provide a more accurate measure of the temperature. Unfortunately the cost of looking at the broader Paschen continuum emission is that its flux is smaller than that of the Balmer continuum by more than an order of magnitude, and hence more difficult to detect.

Many lines have been found in the near-IR spectra of emission line objects such as planetary nebulae (Kaler 1976; Morris & Ward 1984) and active galaxies (Morris & Ward 1985), the observations always being made on the brighter objects in these categories. The low surface brightness of nova shells

does not bode well for IR observations, so the null result is not at all surprising, but there have been enough surprises from the spectra of nova shells to warrant some caution in anticipating their behaviour.

11.2 Observations and Data Reduction

The data were collected on the CTIO 1.5 m telescope using the CCD spectrometer on the nights 29/30 and 30/31 January 1988 under excellent seeing conditions. The CCD detector was a GEC array (Epi #6) with a 385 $\times$576 pixel format. A red corrector was included to prevent any contamination of the signal from the second order blue spectrum. The spectrograph dispersion was oriented in the 576 pixel direction. The chip was preflashed for 0.1 ms to improve the charge transfer characteristics. A slit width of 4″ was used together with a grating that gave a wavelength coverage from λ7250 to λ9100 centered near λ8200. The Paschen continuum starts at λ8208 and for a plasma at a temperature of 800 K the theoretical shape has a half-width of $\sim$350Å. The exposures were restricted to 2700s (45 mins) to prevent excessive contamination of the spectra by cosmic rays.

The slit was oriented east-west and positioned so that its centre lay about 6″ north or south of the central star. This range allows for any expansion of the shells since the previous measurements were made. The recent CCD image of CP Pup made by Duerbeck (1987b) is consistent with the expansion rate determined by Williams (1982). The observations combined over the two nights were as follows: 2.25 hrs on the southern part of CP Pup, 5.25 hrs on the northern part of CP Pup, 3.75 hrs on the northern part of T Pyx and 1.5 hrs on the southern section of RR Pic.

On the evening of 31 January 1988 an unsuccessful attempt was made to measure the spectrum in the wavelength region of the Balmer continuum. The failure was due to the presence of a nearly-full moon creating a sky background that swamped any signal from the nova shells. It was therefore not possible to confirm the presence of the broad emission feature around λ3640 which is interpreted as the Balmer continuum formed in a low temperature plasma.

Initial data reduction was carried out on the CTIO computer at La Serena using the IRAF data reduction package. The following stages of reduction were performed:

i) cosmic ray removal

ii) subtraction of DC bias and division by flat field

iii) sky background subtraction

iv) correction for atmospheric extinction

v) wavelength calibration

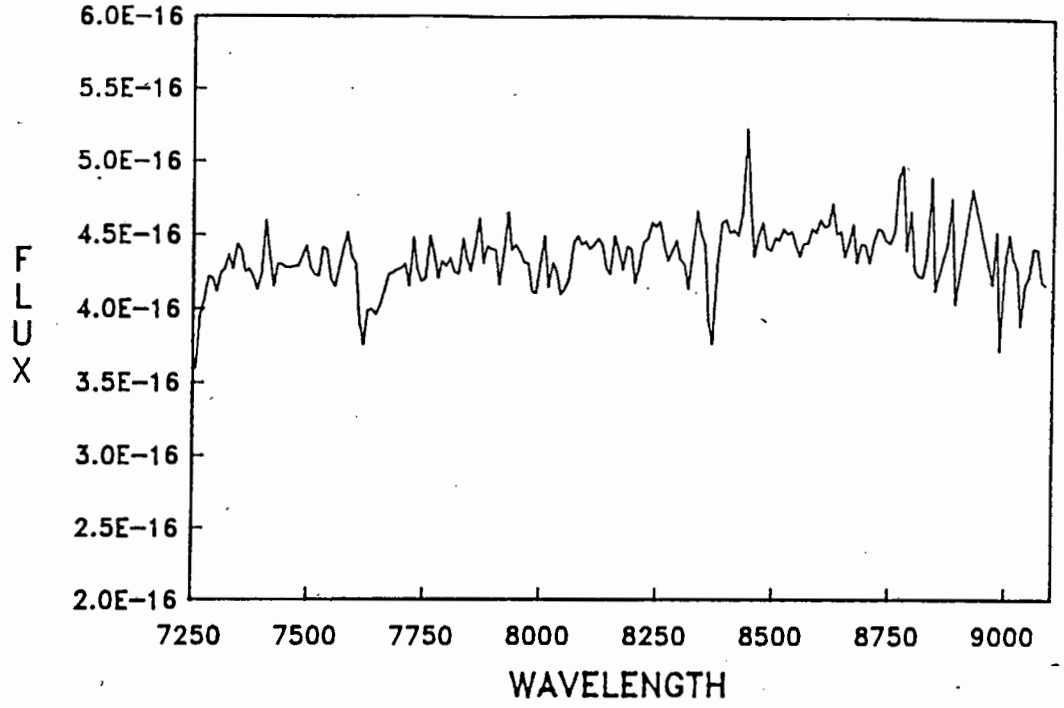

Figure 11.1: A typical spectrum of our near-IR observations of nova shells.

vi) flux calibration

Wavelength calibration was obtained from a He-Ne-Ar comparison lamp, and absolute fluxes were derived from observations of spectrophotometric standard stars. The calibration of the standard stars in the near-IR region is not as secure as in the visible. Small scale fluctuations in the spatial response of the CCD were calibrated by observing flat fields in the dome. As the signal we were looking at was very weak, various methods were tried to improve the signal-to-noise ratio. Each CCD frame was analyzed separately and the reduced frames from each area were then added together. We also added the frames from the same area prior to reductions.

The data were filtered using a variable length box-car averaging process to reduce the noise level. An example of the data filtered using a 7-point box-car average is shown in Fig. 11.1. The data is the sum of all the frames of the northern part of the CP Pup shell, and is representative of all the frames.

11.3 Results and Discussion

It is clear from Fig. 11.1 that neither the Paschen continuum nor any emission lines are present in our data, which covered the wavelength range λ7250 to λ9100. A few emission lines have been detected in planetary nebulae (Kaler 1976; Morris & Ward 1984; Cyzac & Aller 1979) and also in some Seyfert galaxies (Morris & Ward 1984). These objects are generally much hotter and denser than nova shells and most of the observed lines are formed by

collisional processes or, in the case of OI λ8446, by beta fluorescence (Grandi 1980). We also searched through Wiese et al. (1966) for possible transitions in ions of H, He, C, N and O in the range of our observations. However, as we discuss below, the null observations reported here are to be expected from the low surface-brightness nova shells.

HI lines in the Paschen series with $n \geq 10$ occur in this range. Many of these lines can be seen in bright planetary nebulae but are unlikely to be seen in nova shells since the much stronger Balmer series was only observed up to $n = 6$. Similarly, some HeII lines in the Pfund series fall in this range and have been detected in planetary nebulae. However, these lines will have fluxes more than an order of magnitude smaller than those of the λ4686 line. These signals will be swamped by noise. The HeII Brackett line at λ10123, which was outside our range, should be stronger than the Pfund lines and is a line that should be looked for. The strongest near infra-red HeI lines occur at λ10830 due to a $2^3P \rightarrow 2^3S$ transition, and at λ7065 and λ7281 due to $3s \rightarrow 2p$ transitions in the singlet and triplet series respectively. The λ10830 and λ7065 lines were outside our range. The HeI λ5876 line will be stronger than either λ7065 or λ7281 in a recombination spectrum and, since the optical line is so weak, neither of these near-IR lines can be expected. The λ10830 line should have a flux comparable to that of the λ5876 line, and is therefore a good candidate to look for. However, J-band photometry of the CP Pup shell did not reveal any noticeable signal above the sky background (Whitelock, private communication).

During the early phases of a nova's evolution, lines from neutral CNO are prominent in the spectra. Because the shells are radiation bounded at this stage, the outer layers are in a low state of ionization. By the time the shells become spatially resolved, however, the gas has become density bounded, with fairly uniform conditions existing throughout the shell. Because no lines of neutral CNO have been detected (in the optical) it can be concluded that a relatively high state of ionization exists in the gas. Photoionization models have confirmed that neutral ions are only present in very low abundances, and hence none of the neutral CNO near-IR lines can be expected in the spectrum. The absence of CII λ4268 from the optical spectrum precludes the detection of any CII lines in the near-IR. The IR lines of NII are so weak that they have not even been detected in planetary nebulae. Triply and higher ionized species of CNO only produce near-IR lines from transitions out of levels with large principal quantum numbers and these lines are always weaker than the optical and UV lines. Because of the small amplitude of the optical lines, IR lines will be below the noise level.

Of the heavy metals, OII is the most likely ion to be observed in this spectral region. There is a doublet forbidden OII transition at λ7319 and λ7330 often only detected as a blend at λ7325. This line is found in many planetary nebula spectra. Although the [OII] λ3727 doublet line was seen

in the spectrum of the CP Pup shell, Williams (1982) attributed it to the ISM because it is narrower than the other lines, and appears prominently in all the sky spectra. Regardless of where the line originates, it is not at all clear how it is formed. It is usually the result of collisional excitation out of the groundstate of OII, but an excited OII ion can also be produced by photoionization of OI, by charge exchange of H or He with OIII, or by recombination. The data we have available indicate that λ3727 will always be stronger than λ7327 no matter which mechanism is responsible for its production. The λ7327 flux will have to be determined on an individual basis. In NGC7009 it appears that F(7327)/F(3727) is less than 0.20 (Cyzak & Aller 1979).

Other lines that have been observed in astronomical objects in this range of wavelengths come from ClII, ClIV, ArIII, ArIV, FeII, SI, SII and SIII, and are collisionally excited forbidden lines. None of these ions has been detected in cool nova shells yet, most probably because their abundances are solar and their emissions are therefore too weak to be detected.

Observations of the shells of T Pyx and RR Pic also displayed no signs of any emission lines in this spectral region. These shells both appear to have characteristics similar to those of planetary nebulae, and in view of their weak optical emissions, their IR emissions must be below the noise level.

Williams & Gallagher (1979) found the RR Pic shell to have possible He, N and Ne enhancements but normal O and Fe abundances. The gas is hot, T $\sim$ 15000 K, giving rise mainly to lines of FeV, NeIII and OIII, along a NE-SW line. The Paschen continuum will be spread out over a broad range of wavelengths at these temperatures and its peak flux will be too small to be detected. Helium is overabundant and predominantly in the form of HeIII, so that recombination lines of HeII could be expected. However, although λ4686 is strong, no other HeII lines appear in the optical spectrum, so HeII λ8236 is most probably also too weak to be seen. The HeII λ10123 line, on the other hand, should be quite strong and would be worth looking for. The [OIII] lines were quite strong but no [OII] λ3727 was seen, indicating that the shell is in a high state of ionization. The λ7327 line will not be found under these conditions. Similarly, in the T Pyx shell the temperature is too high for any Paschen continuum to be expected, and the optical HeI and HeII emissions preclude any detectable IR signals. [OII] λ3727 was found, but only rather weakly, and the [OII] λ7327 should, therefore, also be too weak to be detected in the IR.

Finally, we present some graphs that can be used to interpret cool nova shell spectra. We define the width of the continuum to be the wavelength interval for the flux to fall to 1/e of its peak (threshold) value. The width in Ångstroms for the Balmer and Paschen continua are shown as functions of T_e by the dashed lines in Fig. 11.2. The scale is shown on the right hand axis. These lines can be described by the equations W(Bac) = $0.093 \times T_e$

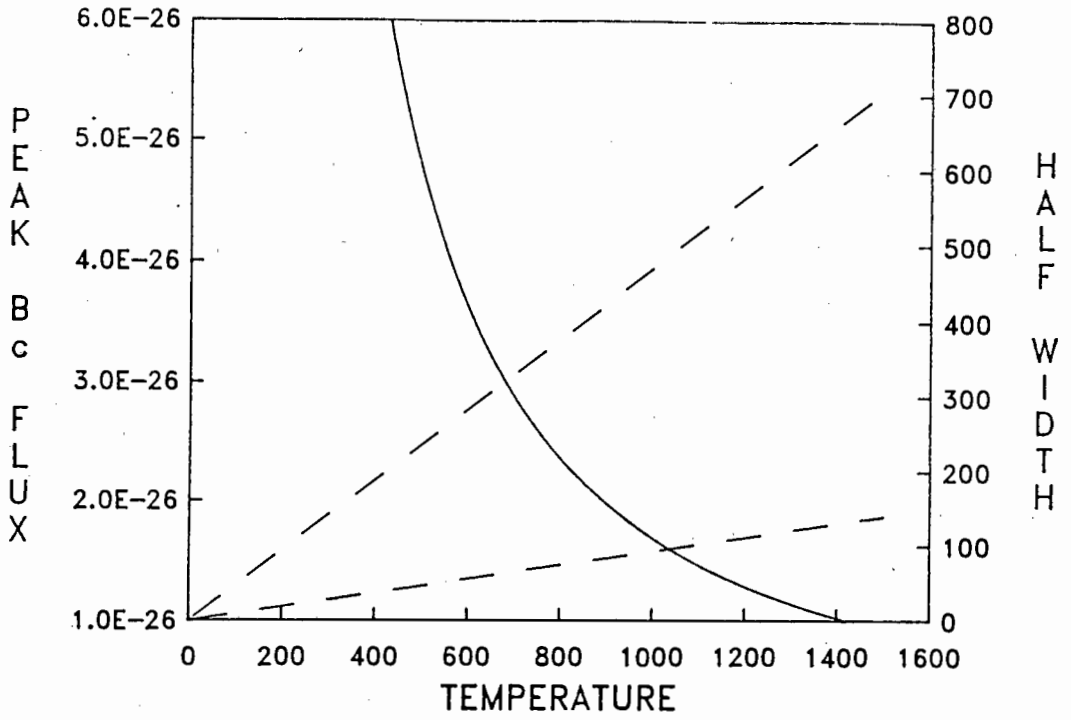

Figure 11.2: The flux (per $N_e N_p$) of the Balmer continuum at threshold is shown as a function of temperature by the solid line. The scale is shown on the left-hand axis. Also shown, by dashed lines, are the e-folding widths of the Balmer and Paschen continua as functions of temperature. The scale for these traces, in units of Å, is on the right-hand axis.

and W(Pac) = $0.472 \times T_e$. The solid line in Fig. 11.2 shows the variation with temperature of the peak Balmer continuum flux per $N_e N_p$. The cross section for recombination at the Paschen edge is 0.13 times smaller than at the Balmer threshold, and, because the wavelength is longer, the peak flux of the Paschen continuum is 0.058 times smaller than the Balmer flux.

The null result reported for these nova shells should not deter futher attempts at near-IR observations. Brighter objects, such as DQ Her, may well have detectable signals. The most likely emissions should be the Paschen continuum, the HeI λ10831, λ7065 and λ7281 lines, the HeII λ10123 line and the [OII] λ7325 line.

References

Aggarwal, K.M., 1983a. Mon. Not. R. astr. Soc., **202**, 15P.

Aggarwal. K.M., 1983b. Astrophys. J. Suppl., **52**, 387.

Aggarwal, K.M., Baluja, K.L. & Tully, J.A., 1982. Mon. Not. R. astr. Soc., **201**, 923.

Aldrovandi, S.M.V. & Pequignot, D., 1973. Astr. Astrophys., **25**, 137. Errata, 1976 Astr. Astrophys., **47**, 321.

Andrillat, Y., 1985. IAU Circ., 4026.

Baker, J.G. & Menzel, D.H., 1938. Astrophys. J., **88**, 52.

Bates, D.R. & Damgaard, A., 1949. Phil. Trans. Roy. Soc., **A242**, 101.

Bath, G.T. & Shaviv, G., 1976. Mon. Not. R. astr. Soc., **175**, 305.

Bayes, F.A., Saraph, H.E. & Seaton, M.J., 1985. Mon. Not. R. astr. Soc., **215**, 85P.

Becker, R.H., 1989. In "Classical Novae", ed. Bode & Evans. John Wiley & Sons Ltd.

Becker, R.H. & Marshall, R.E., 1981. Astrophys. J. Lett., **244**, L93.

Beigman, I.L. & Chichkov, B.N., 1980. J. Phys. B Atom. Molec. Phys., **13**, 565.

Berrington, K.A., Fon, W.C. & Kingston, A.E., 1982. Mon. Not. R. astr. Soc., **200**, 347.

Berrington, K.A. & Kingston, A.E., 1987. J. Phys. B Atom. Molec. Phys., **20**, 6631.

Bhatia, A.K., Doschek, G.A. & Feldman, U., 1979. Astr. Astrophys., **76**, 359.

Bode, M.F. & Evans, A., 1983. Quart. Jnl. Roy. Astr. Soc., **24**, 83.

Bode, M.F. & Evans, A., 1989. "Classical Novae", John Wiley & Sons Ltd.

Bode, M.F., Duerbeck H.W. & Evans A., 1989. In "Classical Novae", ed. Bode & Evans. John Wiley & Sons Ltd.

Bohm, D. & Aller, L.H., 1947. Astrophys. J., **105**, 1.

Bowen, I.S., 1956. Astron. J., **61**, 338.

Brocklehurst, M., 1970. Mon. Not. R. astr. Soc., **148**, 417.

Brodklehurst, M., 1971. Mon. Not. R. astr. Soc., **153**, 471.

Brocklehurst, M., 1972. Mon. Not. R. astr. Soc., **157**, 211.

Brooks, N.H., Rohrlich, D. & Smith, W.H., 1977. Astrophys. J., **214**, 328.

Brown, R.L., 1972. Astrophys. J., **174**, 511.

Burgess, A., 1964. Astrophys. J., **139**, 776 (Lett.).

Burgess, A., 1965a. Mem. R. astr. Soc., **69**, 1.

Burgess, A., 1965b. Astrophys. J., **141**, 1588 (Lett.).

Burgess, A. & Seaton, M.J., 1960. Mon. Not. R. astr. Soc., **120**, 121.

Burgess, A. & Summers, H.P., 1969. Astrophys. J., **157**, 1007.

Burgess, A. & Summers, H.P., 1976. Mon. Not. R. astr. Soc., **174**, 345.

Burke, P.G. & Taylor, K.T., 1979. J. Phys. B Atom. Molec. Phys., **12**, 2971.

Butler, S.E. & Dalgarno, A., 1979. Astrophys. J., **234**, 765.

Butler, S.E. & Dalgarno, A., 1980. Astrophys. J., **241**, 838.

Butler, S.E., Heil, T.G. & Dalgarno, A., 1980. Astrophys. J., **241**, 442.

Butler, K. & Zeippen, C.J., 1984. Astr. Astrophys., **141**, 274.

Butler, K. & Mendoza, C., 1984. Mon. Not. R. astr. Soc., **208**, 17P.

Callus, C.M., Evans, A., Albinson, J.S., Mitchell, R.M., Bode, M.F., Jameson, R.F., King, A.R. & Sherrington, M., 1987. Mon. Not. R. astr. Soc., **229**, 539.

Catchpole, R., 1969. Mon. Not. R. astr. Soc., **142**, 119.

Chang, M-W., 1977. Astrophys. J., **211**, 300.

Clegg, R.E.S., 1987. Mon. Not. R. astr. Soc., **229**, 31P.

Cohen, J.G., 1985. Astrophys. J., **292**, 90.

Cohen, J.G. & Rosenthal, A.J., 1983. Astrophys. J., **268**, 689.

Cordova, F.A., Mason, K.O. & Nelson, J.E., 1981. Astrophys. J., **245**, 609.

Cruise, A.M., 1977. Nature, **267**, 685 (Lett.).

Cyzak, S.J. & Aller, L.H., 1979. Mon. Not. R. astr. Soc., **188**, 229.

Dalgarno, A., 1962. Adv. Phys., **11**, 281.

Dalgarno, A., 1966. Mon. Not. R. astr. Soc., **131**, 311.

Daltabuit, E. & Cox, D.P., 1972. Astrophys. J., **177**, 855.

Deguchi, S., 1985. Astrophys. J., **291**, 492.

Deutschman, W.A., Davis, R.J. & Schild, R.E., 1976. Astrophys. J. Suppl., **30**, 97.

Dinerstein, H.L., 1986. Astron. J., **92**, 1381.

Dinerstein, H.L. & Robinson, E.L., 1986. In "Light on Dark Matter", Proc. 1st IRAS Conference, ed. F.P. Israel, p. 145.

Drew, J.E. & Storey, P.J., 1982. J. Phys. B Atom. Molec. Phys., **15**, 2357.

Duerbeck, H.W., 1981. Publ. Astr. Soc. Pacific, **93**, 165.

Duerbeck, H.W., 1987a. Space Sci. Reviews, **45**, 1.

Duerbeck, H.W., 1987b. The Messenger, No. **50**, p. 8.

Edlén, B., 1964. Atomic Spectra, Handbuch der Physik, **XXVIII**.

Fawcett, B.C., 1987. Atom. Data Nuc. Data Tables, **37**, 411.

Ferland, G.J., 1980a. Observatory, **100**, 166.

Ferland, G.J., 1980b. Publ. Astr. Soc. Pacific, **92**, 596.

Ferland, G.J. & Shields, G.A., 1978. Astrophys. J., **226**, 172.

Ferland, G.J. & Truran, J.W., 1980. Astrophys. J., **240**, 608.

Ferland, G.J. & Truran, J.W., 1981. Astrophys. J., **244**, 1022.

Ferland, G.J., Williams, R.E., Lambert, D.L., Shields, G.A., Slovak, M. Gondhalekar, P.M. & Truran, J.W., 1984. Astrophys. J., **281**, 194.

Gallagher, J.S., 1977. Astron. J., **82**, 209.

Gallagher, J.S. & Holm, A.V., 1974. Astrophys. J. Lett., **189**, L123.

Gallagher, J.S. & Starrfield, S., 1978. Ann. Rev. Astr. & Astrophys., **16**, 171.

Gallagher, J.S., Hege, E.K., Kopriva, D.A., Williams, R.E. & Butcher, H.R., 1980. Astrophys. J., **237**, 55.

Gaposchkin, S., 1946. Harvard Bull. No. 918.

Gargaud, M., McCarroll, R. & Opradolce, L., 1989. Astr. Astrophys., **208**, 251.

Gee, C.S., Percival, I.C., Lodge, J. & Richards, D., 1976. Mon. Not. R. astr. Soc., **175**, 209.

Gehrz, R.D., Grasdalen, G.L. & Hackwell, J.A., 1985. Astrophys. J. Lett., **298**, L47. Erratum Astrophys. J. Lett., **306**, L49.

Gehrz, R.D., Grasdalen, G.L., Greenhouse, M., Hackwell, J.A., Hayward, T., & Bentley, A.F., 1986. Astrophys. J. Lett., **308**, L63.

Geisel, S.L., Kleinmann, D.E. & Low, F.L., 1970. Astrophys. J., **161**, L101.

Giovanardi, C., Natta, A. & Palla, F., 1987. Astr. Astrophys. Suppl., **70**, 269.

Giovanardi, C. & Palla, F., 1989. Astr. Astrophys. Suppl., **77**, 157.

Goldbach, C. & Nollez, G., 1987. Astr. Astrophys., **181**, 203.

Gordon, W., 1929. Ann. Phys., **2**, 1031.

Gould, R.J., 1978. Astrophys. J., **219**, 250.

Grandi, S.A., 1976. Astrophys. J., **206**, 658.

Grandi, S.A., 1980. Astrophys. J., **238**, 10.

Gratton, L., 1953. Astrophys. J., **118**, 568.

Greenhouse, M., Grasdalen, Hayward, T.L., Gehrz, R.D., & Jones, T.J., 1988. Astron. J., **95**, 172.

Greenstein, J.L., Sanford, R.F. & Zwicky, F., 1957. Publ. Astr. Soc. Pacific, **69**, 352.

Grotrian, H. 1937. Z. Astrophys., **13**, 215.

Haefner, R. & Metz, K., 1982. Astr. Astrophys., **109**, 171.

Hamada, T. & Salpeter, E.E., 1961. Astrophys. J., **134**, 683.

Harrington, J.P., 1968. Astrophys. J., **152**, 943.

Harrington, J.P., 1969. Astrophys. J., **156**, 903.

Harrington, J.P., Seaton, M.J., Adams, S. & Lutz, J.H., 1982. Mon. Not. R. astr. Soc., **199**, 517.

Hartmann, L. & Raymond, J., 1981. In "The Universe of Ultraviolet Wavelengths", NASA Conf. Publ. 2171 ed. R.D. Chapman, p. 495.

Hayes, M.A. & Nussbaumer, H., 1983. Astr. Astrophys., **124**, 279.

Hayes, M.A. & Nussbaumer, H., 1984. Astr. Astrophys., **134**, 193.

Heil, T.G., Butler, S.E. & Dalgarno, A., 1981. Phys. Rev. A, **23**, 1100.

Henry, R.J.W., 1970. Astrophys. J., **161**, 1153.

Hey, J.D., 1987. South African J. Phys., **10**, 118.

Ho, Y.K. & Henry, R.J.W., 1984. J. Quantit. Spectrosc. Radiat. Transfer, **31**, 57.

Hoffman, J.A, Lewin, W.H.G., Brecher, K., Buff, J., Clark, G.W., Joss, P.C. & Matilsky, T., 1976. Nature, **261**, 208.

Hoffmann, H., Saha, H.P. & Trefftz, E., 1983. Astr. Astrophys., **126**, 415.

Hummer, D.G. & Storey, P.J., 1987. Mon. Not. R. astr. Soc., **224**, 801.

Hummer, D.G. & Norcross, D.W., 1974. Mon. Not. R. astr. Soc., **168**, 263.

Hutchings, J.B., 1972. Mon. Not. R. astr. Soc., **158**, 177.

Iitkawa, Y., Hara, S., Kato, T., Nakazaki, S., Pindzola, M.S., Crandall, D.H., 1985. Atm. Data & Nuc. Data Tables, **33**, 149.

Jacobs, V., 1971. Phys. Rev. A, **3**, 289.

Jacobs, V.L., 1974. Phys. Rev. A, **9**, 1938.

Johnson, L.C., 1972. Astrophys. J., **174**, 227.

Kaler, J.B., 1976. Astrophys. J. Suppl., **31**, 517.

Kallman, T. & McCray, R., 1980. Astrophys. J., **242**, 615.

Kaluzny, J. & Chlebowski, T., 1988. Astrophys. J., **332**, 287.

Karzas, W.J. & Latter, R., 1961. Astrophys. J. Suppl., **6**, 167.

Keenan, F.P., LenonN, D.J., Johnson, C.T. & Kingston, A.E., 1986. Mon. Not. R. astr. Soc., **220**, 571.

Keyes, C.D. & Aller, L.H., 1978. Astrophys. Space Science, **59**, 91.

King, A.R., 1989. In "Classical Novae" ed. Bode & Evans. John Wiley and Sons Ltd.

Krautter, J., Beuermann, K., Leitherer, E., Oliva, Moorwood, A.F.M., Duel, E., Wargau, W., Klare, G.,

Kohoutek, L., Van Paradijs, J. & Wolf, B., 1984. Astr. Astroph

Kurucz, R.L. & Peytremann, E., 1975. Smithsonian Astrophysical Observatory, Special Report 362.

Kwan, J. & Krolik, J.H., 1981. Astrophys. J., **250**, 478.

Lamb, D.Q. & Masters, A.R., 1979. Astrophys. J. Lett., **234**, L117.

Lance, C.M., McCall, M.L. & Uomoto, A.K., 1988. Astrophys. J. Suppl., **66**, 151.

Law, W.Y. & Ritter, H., 1983. Astr. Astrophys., **123**, 33.

Lugger, P.M., York, D.G., Blanchard, T. & Morton, D.C., 1978. Astrophys. J., **224**, 1059.

MacAlpine, G.M., 1972. Astrophys. J., **175**, 11.

Martin, P.G., 1988. Astrophys. J. Suppl., **66**, 125.

Martin, P.G., 1989. In "Classical Novae", ed. Bode & Evans. John Wiley and Sons Ltd.

McCarroll, R.W. & Valiron, P., 1979. Astr. Astrophys., **78**, 177.

McClintock, J.E., Conizares, C.R. & Tarter, C.B., 1975. Astrophys. J., **198**, 641.

McLaughlin, D.B., 1935. Publ. Am. Astr. Soc., **8**, 145.

McLaughlin, D.B., 1945. Publ. Astr. Soc. Pacific, **57**, 69.

McLaughlin, D.B., 1960. In "Stars and Stellar Systems", **6**, 585.

Mendoza, C., 1983. In "Planetary Nebulae", IAU Symposium No. 103, ed. D.R. Flower.

Moore, C.E., 1949. Atomic Energy Levels, N.B.S. Circular 467.

Morris, S.L. & Ward, M.J., 1984. Mon. Not. R. astr. Soc., **210**, 655.

Morris, S.L. & Ward, M.J., 1985. Mon. Not. R. astr. Soc., **215**, 57P.

Mühlethaler & Nussbaumer, H., 1976. Astr. Astrophys., **48**, 109.

Mustel, E.R. & Boyarchuk, A.A., 1970. Astrophys. Space Sci., **6**, 183.

Netzer, H., 1975. Mon. Not. R. astr. Soc., **171**, 395.

Ney, E.P. & Hatfield, B.F., 1978. Astrophys. J., **219**, L111.

Nussbaumer, H., 1971. Astrophys. J., **170**, 93.

Nussbaumer, H. & Storey, P.J., 1978. Astr. Astrophys., **64**, 139.

Nussbaumer, H. & Storey, P.J., 1981a. Astr. Astrophys., **96**, 91.

Nussbaumer, H. & Storey, P.J., 1981b. Astr. Astrophys., **99**, 177.

Nussbaumer, H. & Storey, P.J., 1982. Astr. Astrophys., **115**, 205.

Nussbaumer, H. & Storey, P.J., 1983. Astr. Astrophys., **126**, 75.

Nussbaumer, H. & Storey, P.J., 1984a. Astr. Astrophys., **140**, 383.

Nussbaumer, H. & Storey, P.J., 1984b. Astr. Astrophys. Suppl., **56**, 293.

Nussbaumer, H. & Storey, P.J., 1987. Astr. Astrophys. Suppl., **69**, 123.

O'Donoghue, D., Warner, B., Wargau, W. & Grauer, A.D., 1989. Mon. Not. R. astr. Soc., **240**, 41.

Ögelman, H., Beuermann, K. & Krautter, J., 1984. Astrophys. J. Lett., **287**, L31.

Ögelman, H. & Krautter, J., 1985. IAU Circ., 4065.

Osterbrock, D.E., 1974. Astrophysics of Gaseous Nebulae, W.H. Freeman and Company, San Francisco.

Patterson, J., 1984. Astrophys. J. Suppl., **54**, 443.

Patterson, J., Robinson, E.L. & Nather, R.E., 1978. Astrophys. J., **224**, 570.

Patterson, J. & Raymond, J.C., 1985a. Astrophys. J., **292**, 535.

Patterson, J. & Raymond, J.C., 1985b. Astrophys. J., **292**, 550.

Payne-Gaposchkin, C., 1957. The Galactic Novae.

Peach, G., 1965. Mon. Not. R. astr. Soc., **130**, 361.

Peach, G., 1967. Mem. Roy. astr. Soc., **71**, 13.

Peimbert, M., 1978. IAU Symposium No. 76, Planetary Nebulae, p. 215.

Pengelly, R.M., 1964. Mon. Not. R. astr. Soc., **127**, 145.

Pengelly, R.M. & Seaton, M.J., 1964. Mon. Not. R. astr. Soc., **127**, 165.

Pequignot, D. & Aldrovandi, S.M.V., 1976. Astr. Astrophys., **50**, 141.

Percival, I.C. & Richards, D., 1975. Adv. Atomic Mol. Phys., **11**, 1.

Percival, I.C. & Richards, D., 1978. Mon. Not. R. astr. Soc., **183**, 329.

Pradhan, A.K., 1980. Mon. Not. R. astr. Soc., **190**, 5P.

Pringle, J.E., 1977. Mon. Not. R. astr. Soc., **178**, 195.

Pringle, J.E. & Savonije, G.J., 1979. Mon. Not. R. astr. Soc., **187**, 777.

Reilman, R.F. & Manson, S.T., 1979. Astrophys. J. Suppl., **40**, 815.

Robbins, R.R., 1968. Astrophys. J., **151**, 497.

Robbins, R.R., 1970. Astrophys. J., **160**, 519.

Robbins, R.R. & Robinson, E.L., 1971. Astrophys. J., **167**, 249.

Roberge, W. & Dalgarno, A., 1982. Astrophys. J., **255**, 489.

Robinson, E.L., 1975. Astron. J., **80**, 515.

Robinson, E.L. & Nather, R.E., 1977. Publ. Astr. Soc. Pacific, **89**, 572.

Samson, J.A.R., 1976. Physics Reports, **28C**, 303.

Sanford, R.F., 1945. Astrophys. J., **102**, 357.

Sanford, R.F., 1947. Publ. Astr. Soc. Pacific, **59**, 334.

Sanford, R.F. & Greenstein, J.L., 1957. Publ. Astr. Soc. Pacific, **69**, 75.

Saraph, H.E., 1964. Proc. Physics Soc., **83**, 763.

Saraph, H.E. & Seaton, M.J., 1980. Mon. Not. R. astr. Soc., **193**, 617.

Sarazin, C.L., 1977. Astrophys. J., **217**, 772.

Schaefer, B.E., 1986. Publ. Astr. Soc. Pacific, **98**, 556.

Schaefer, B.E. & Patterson, J., 1983. Astrophys. J., **268**, 710.

Schneider, D.P. & Greenstein, J.L., 1979. Astrophys. J., **233**, 935.

Seaton, M.J., 1959a. Mon. Not. R. astr. Soc., **119**, 81.

Seaton, M.J., 1959b. Mon. Not. R. astr. Soc., **119**, 90.

Seaton, M.J., 1962. Proc. Phys. Soc., **79**, 1105.

Seaquist, E.R., 1989. In "Classical Novae", ed. Bode & Evans. John Wiley and Sons Ltd.

Shara, M.M., 1989. Publ. Astr. Soc. Pacific, **101**, 5.

Shara, M.M., Moffat, A.F.J., Williams, R.E., Cohen, J.G., 1988. Astrophys. J., **337**, 720.

Shull, J.M., 1979. Astrophys. J., **234**, 761.

Shull, M.J. & Van Steenberg, M., 1982. Astrophys. J. Suppl., **48**, 95.

Sneden, C. & Lambert, D.L., 1975. Mon. Not. R. astr. Soc., **170**, 533.

Snijders, M.A.J., Batt, T.J., Seaton, M.J., Blades, J.C. & Morton, D.C., 1984. Mon. Not. R. astr. Soc., **211**, 7P.

Snijders, M.A.J., Batt, T.J., Roche, T.J., Seaton, M.J., Morton, D.C., Spoelstra, T.A.T. & Blades, J.C., 1987. Mon. Not. R. astr. Soc., **228**, 329.

Soderblom, D., 1976. Publ. Astr. Soc. Pacific, 88, 517.

Sparks, W.M., 1969. Astrophys. J., **156**, 569.

Sparks, W.M., Starrfield, S. & Truran, J.W., 1976. Astrophys. J., **208**, 819.

Sparks, W.M., Starrfield, S. & Truran, J.W., 1978. Astrophys. J., **220**, 1063.

Spitzer, L., & Greenstein, J.L., 1951. Astrophys. J., **114**, 407.

Starrfield, S., Truran, J.W. & Sparks, W.M., 1978. Astrophys. J., **226**, 186.

Starrfield, S., Sparks, W.M. & Truran, J.W., 1986. Astrophys. J. Lett., **303**, L5.

Starrfield, S. & Sparks, W.M., 1987. Astrophys. Space Sci., **131**, 379.

Stewart, A.L., 1978. J. Phys. B Atom. Molec. Phys., **11**, 2449.

Stewart, A.L., 1979. J. Phys. B Atom. Molec. Phys., **12**, 401.

Stockman, H.S., Schmidt, G.D. & Lamb, D.Q., 1988. Astrophys. J., **332**, 282.

Storey, P.J., 1981. Mon. Not. R. astr. Soc., **195**, 27P.

Storey, P.J. & Hummer, D.G., 1988. Mon. Not. R. astr. Soc., **231**, 1139.

Summers, H.P., 1977. Mon. Not. R. astr. Soc., **178**, 101.

Taylor, A.R., Hjellming, R.M., Seaquist, E.R. & Gehrz, R.D., 1988. Nature **335**, 235.

Theodosiou, C.E., Inokuti, M., Mawson, S.T., 1986. Atm. Data & Nuc. Data Tables, **35**, 473.

Tozzi, G.P., Huber, M.C.E. & Pauls, U., 1983. Astr. Astrophys., **126**, 320.

Truran, J.W. & Livio, M., 1986. Astrophys. J., **308**, 721.

Tylenda, R., 1978. Acta Astr., **28**, 333.

Tylenda, R., 1981. Acta Astr., **31**, 127.

Van Regemorter, H., Hoang Binh, D.Y. & Prud'homme, M., 1979. J. Phys. B Atom. Molec. Phys., **12**, 1053.

Verbunt, F., 1987. Astr. Astrophyp. Suppl., **71**, 339.

Walker, M.F., 1954. Publ. Astr. Soc. of Pacific, **66**, 230.

Walling, R.S. & Weisheit, J.C., 1988. Physics Reports, **162**, 1.

Ward, M.J. & Morris, S.L., 1984. Mon. Not. R. astr. Soc., **207**, 867.

Warner, B., 1985. Mon. Not. R. astr. Soc., **217**, 1P.

Warner, B., 1986a. Mon. Not. R. astr. Soc., **219**, 751.

Warner, B., 1986b. Mon. Not. R. astr. Soc., **222**, 11.

Warner, B., 1987. Mon. Not. R. astr. Soc., **227**, 23.

Warner, B., Peters, W.L., Hubbard, W.B. & Nather, R.E., 1972. Mon. Not. R. astr. Soc., **159**, 321.

Watson, W.D. & Christensen, R.B., 1979. Astrophys. J., **231**, 627.

Weaver, H.F., 1974. In "Highlights of Astronomy", ed. G. Contopoulous (Dordrecht: Reidel), Vol. **3**, p. 509.

Webbink, R.F., Livio, M., Truran, J.W. & Orio, M., 1987. Astrophys. J., **314**, 653.

Weisheit, J.C., 1974. Astrophys. J., **190**, 735.

Weisheit, J.C. & Dalgarno, A., 1972. Astrophys. Letters, **12**, 103.

Westhaus, P. & Sinanoğlu, O., 1969. Phys. Rev., **183**, 56.

Whitelock, P.A., Carter, B.S., Feast, M.W., Glass, I.S., Laney, D., Menzies, J.W., Walsh, J. & Williams, P.M., 1984. Mon. Not. R. astr. Soc., **211**, 421.

Wiese, W.L., Smith, M.W. & Glennon, B.M., 1966. Atomic Transition Probabilities, Vol. **1** (NSRDS-NBS4).

Williams, G., 1983. Astrophys. J. Suppl., **53**, 523.

Williams, P.M. & Longmore, A.J., 1984. Mon. Not. R. astr. Soc., **207**, 139.

Williams, R.E., 1967. Astrophys. J., **147**, 556.

Williams, R.E., 1982. Astrophys. J., **261**, 170.

Williams, R.E., Woolf, N.J., Hege, E.K., Moore, R.L. & Kopriva, D.A., 1978. Astrophys. J., **224**, 171.

Williams, R.E. & Gallagher, J.S., 1979. Astrophys. J., **228**, 482.

Williams, R.E., Sparks, W.M., Gallagher, J.S., Ney, E.P., Starrfield, S.G. & Truran, J.W., 1981. Astrophys. J., **251**, 221.

Williams, R.E., Ney, E.P., Sparks, W.M., Starrfield, S.G., Wyckoff, S. & Truran, J.W., 1985. Mon. Not. R. astr. Soc., **212**, 753.

Wyckoff, S. & Wehinger, P.A., 1977. Proceedings IAU Coll. No. 42, ed. R. Kippenhahn, J. Rahe & W. Strohmeier.

Zeippen, C.J., 1982. Mon. Not. R. astr. Soc., **198**, 111.

Zeippen, C.J., 1987. Astr. Astrophys., **173**, 410.

Zeippen, C.J., Seaton, M.J. & Morton, D.C., 1977. Mon. Not. R. astr. Soc., **181**, 527.